TECHNISCHE UNIVERSITÄT MÜNCHEN

Fakultät für Chemie

Werner Siemens-Lehrstuhl für Synthetische Biotechnologie

Enhancing microalgae cultivation: Illumination effects and mutation procedures

Matthias Glemser

Vollständiger Abdruck der von der Fakultät für Chemie der Technischen Universität München zur Erlangung des akademischen Grades eines

Doktor der Naturwissenschaften (Dr. rer. nat.)

genehmigten Dissertation.

Vorsitzender:		Prof. Dr. Tom Nilges
Prüfer der Dissertation:	1.	Prof. Dr. Thomas Brück
	2.	Prof. Dr.-Ing. Dirk Weuster-Botz

Die Dissertation wurde am 16.04.2018 bei der Technischen Universität München eingereicht und durch die Fakultät für Chemie am 02.05.2019 angenommen.

1 Abstract

In this work microalgae cultivation was enhanced via novel LED illumination system and new methods for strain development were developed. In a bottom-lit shake flask cultivation system three microalgae strains, *Picochlorum* sp., *Dunaliella* sp. and *Microchloropsis salina*, were cultivated with varying growth parameters. The effect of four illumination levels between 50 µmol m^{-2} s^{-1} and 200 µmol m^{-2} s^{-1}, as well as illumination with blue, red, green and white light on growth, lipid formation and pigment composition was investigated. A special growth response on illumination with the green light LED was discovered for *Picochlorum* sp.. Novel pigment peaks could be detected via HPLC analysis in samples of the exponential growth phase. Scale-up studies and spectral modification of the illumination setup with glass filter plates were conducted. In an experimental approach in combination with High Resolution HPLC-MS and NMR analysis the structural identities of these newly discovered pigment spikes were resolved. The previously undocumented pigment variations were identified as Chlorophyll *a* and *b* versions with one and three additional double bonds. These additional double bonds are situated in the phytol-residue of the Chlorophyll.

Strain modifications via novel mechanisms for random mutagenesis were developed and tested for *Picochlorum* sp.. Atmospheric and Room Temperature Plasma (ARTP) and fast neutron bombardment treatment methods were used for a new approach towards generation of mutant strains. The mutagenic impact of several carrier gases, as well as treatment duration of the tested hand-held plasma-torch device Piezobrush by Relyon Plasma GmbH was evaluated and mutant strains were generated. The development of the plasma treatment procedure prepared the ground for plasma applications on microalgae in future work. Fast neutron beams with neutron-gamma radiation ratio of 2.2 – 2.7 D_n D_γ^{-1} were used in the Research Neutron Source Heinz Maier-Leibnitz (FRM II) facility of the Technical University of Munich in Garching, Germany for the evocation of random mutagenesis in microalgae. With dosage steps up to 500 Gy and a subsequent screening a model for exposure limits with a survival rate of 2% at 366.8 Gy neutron radiation was established for *Picochlorum* sp.. In a screening for faster growth of all tested mutagenesis methods first positive mutant strains could be identified.

In dieser Arbeit wurde die Kultivierung von Mikroalgen mittels einer neuartigen LED-Beleuchtungseinheit und neuen Methoden zur Stammentwicklung gesteigert. In einem von unten beleuchteten Schüttelkolben System wurden die drei Mikroalgen Stämme *Picochlorum* sp., *Dunaliella* sp. und *Microchloropsis salina* unter verschiedenen Wachstumsparametern kultiviert. Der Einfluss von vier Bestrahlungsintensitäten zwischen 50 µmol m^{-2} s^{-1} bis zu 200 µmol m^{-2} s^{-1}, sowie der Einfluss von verschiedenfarbiger Beleuchtung aus blauem, roten, grünen wund weißem LED Licht wurde anhand des Wachstums, der Bildung von Lipiden und der Pigmentzusammensetzung untersucht. Eine besondere Wachstumsreaktion von *Picochlorum* sp. auf die Beleuchtung mit grünem LED Licht konnte entdeckt werden. In Proben aus der exponentiellen Wachstumsphase konnten Spuren von neuartigen Pigmenten mittels HPLC Analyse entdeckt werden. In einem experimentellen Ansatz konnte durch Skalierungsversuche und die Modifikation des Beleuchtungsspektrums mittels Einsatz von Farbfiltern, in Kombination mit Hochauflösender HPLC Massenspektroskopie sowie NMR-Analysen, die strukturelle Aufklärung der neu entdeckten Pigmentspuren erreicht werden. Die bisher nicht beschriebenen Pigmentvariationen konnten als Versionen von Chlorophyll *a* und *b*, die je eine und drei zusätzliche Doppelbindungen in der Phytol-Seitenkette besitzen identifiziert werden.

Stammmodifikationen von *Picochlorum* sp. wurden durch neue Methoden zur Erzeugung von Zufallsmutationen entwickelt und getestet. Atmosphärisches und Raumtemperatur Plasma (ARTP) und Beschuss mit schnelle Neutronen wurden in einem neuartigen Ansatz zur Erzeugung von Mutantenstämmen verwendet. Mit dem Plasma-Flammen Handgerät Piezobrush PZ2 von der Relyon Plasma GmbH wurde der Einfluss verschiedener Trägergase, sowie die Behandlungsdauer zur Erzeugung von Mutantenstämmen untersucht. Die Entwicklung einer Methode zur Plasmabehandlung von Mikroalgen dient als Grundlage für weitere Anwendung in der Zukunft. Schnelle Neutronen mit einem Neutronen- zu-Gammastrahlen Verhältnis von 2.2 – 2.7 D_n D_γ^{-1} wurden in dem Forschungsreaktor Heinz Maier-Leibnitz (FRM II) der Universität München in Garching, Deutschland zur Erzeugung von Zufallsmutationen in Mikroalgen verwendet. Für *Picochlorum* sp. konnte mit Strahlungsdosen von bis zu 500 Gy und einem nachfolgenden Screening ein Modell der Bestrahlungswerte für eine Überlebensrate von 2 % bei 366.8 Gy Neutronenbestrahlung aufgestellt werden. In einem Screening nach schnell wachsenden Stämmen aller untersuchten Mutageneseverfahren konnten erste positive Mutantenstämme identifiziert werden.

2 Acknowledgements

An dieser Stelle möchte ich mich bei all denjenigen bedanken, die mich während meiner Dissertation unterstütz haben.

Zuerst gebührt mein Dank Prof. Dr. Thomas Brück, für die Möglichkeit diese Dissertation am IBK, bzw. dem jetzigen WSSB der TUM durchzuführen. Danke für ein stets offenes Ohr und Büro!

Vielen Dank an Prof. Dr. Tom Nilges und Prof. Dr. Dirk Weuster-Botz für die Bewertung und Prüfung meiner Arbeit.

Danke, Prof. Dr. Wolfgang Eisenreich für das Messen und die Hilfe bei den NMR Analysen zur Aufschlüsselung der Pigmente, sowie Franz Michael Wagner vom FRM II für die Möglichkeit meine Mikroalgen im Garchinger Forschungsreaktor bestrahlen zu können.

Bei Dr. Daniel Garbe möchte ich mich für die Betreuung meiner Arbeit und fachlichen Diskussionen, und bei Martina Haack für all die Hilfe bei Analysen und Messungen, sowie Diskussionen neuer Ergebnisse gerne bedanken.

Auch ein herzliches Dankeschön geht an alle Kollegen vom IBK, allen voran Johannes Schmidt, sowie auch den Projektpartnern vom BVT und den Studenten, die sich mit Abschlussarbeiten an meinen Algenthemen eingebracht haben. Mit euch hat man immer Spaß bei der Arbeit gehabt, konnte sich gut über fachliche Themen unterhalten und auch das Private ist dank euch nie zu kurz gekommen!

Abschließend möchte ich mich noch bei meiner Familie und vor allem bei meiner Frau Amelie für die Unterstützung und den Rückhalt bedanken.

I.   Contents

II. List of abbreviations

Table 1: List of abbreviations

Abbreviation	Description
ABS	Acrylonitrile butadiene styrene
APGDs	Atmospheric pressure glow discharges
ARTP	Atmospheric and Room Temperature Plasma
ATP	Adenosine triphosphate
BChl	Bacterial chlorophyll
BPF	Band-pass filter
CAP	Cold atmospheric plasma
CDW	Cell dry weight [g_{DW} L^{-1}]
Chl	Chlorophyll
CID	Collision induced dissociation
CO_2	Carbon dioxide
COSY	Correlation spectroscopy
dH_2O	Demineralized water
DEPT	Distortionless Enhancement by Polarization Transfer
DHGG	Dihydrogeranylgeranyl
DLP filter	Dichronic longpass filters
EMS	Ethyl methanesulfonate
EPSAG	Experimental Phycology and Culture Collection of Algae at Goettingen University
FACS	Fluorescence activated cell sorting
FAME	Fatty acid methyl ester
Fd	Ferredoxin
FSC	Forward scatter
FWHM	Full width at half maximum
FRET	fluorescence resonance energy transfer
GC-FID	Gas chromatography with flame ionization detector
GG	Geranylgeranyl
Gy	Gray
HPLC	High performance liquid chromatography
HR LC-MS/MS	High resolution LCMS with fragmentation MS
HSQC	Heteronuclear single quantum coherence
IBK	Professorship of Industrial Biocatalysis at the Technical University of Munich
IR	Infra red
LED	Light-emitting diode
LPF	Long-pass filter
MeV	Mega electronvolt
MS	Mass spectometry
MTP reader	Multi-titer plate reader
NADPH	Nicotinamide adenine dinucleotide phosphate
NMR	Nuclear magnetic resonance
O_2	Oxygen

Abbreviation	Description
O_3	Ozone
$OD_{750\ nm}$	Optical density at 750 nm, measured at the photometer
$OD^{PR}_{750\ nm}$	Optical density at 750 nm, measured at the plate reader
P_{680}	Reaction center of PS II
P_{700}	Reaction center of PS I
PAM	pulse-amplitude-modulated fluorescence
PAR	Photosynthetically active region
pC	Plastocyanine
Phe	Pheophytin
Phy	Phythyl
PMT	Photomultiplier tubes
PS	Polystyrene
PS I	Photosystem I
PS II	Photosystem II
PTFE	Polytetrafluoroethylene
Q	Plastochinone
QC	Quality control
RSQ	R-squared
RT	Retention time
SSC	Side scatter
SWW	Standard warm white LED
THGG	Tetrahydrogeranylgeranyl
U1 – U5	Unknown pigment peaks 1-5
UV	Ultraviolet
VIS	Visible light spectra
λ	Wavelength

III.   List of figures

IV. List of tables

3 Introduction

3.1 Light composition

Light beams coming from our sun are the source of life on earth. "Without the sun, earth would just be an icy rock in space." (Stern, 2006) "But what is light really? Is it a wave or a shower of photons? [..] It seems as though we must use sometimes the one theory and sometimes the other, while at times we may use either. [..] We have two contradictory pictures of reality; separately neither of them fully explains the phenomena of light, but together they do!" (Einstein and Infeld, 1938)

This quote of Albert Einstein describes the wave-particle dualism, in which light has been described as a particle and a wave.

Light is an electromagnetic radiation, which can be divided into several components. Figure 1 displays the various parts of this radiation. Very short wavelengths with 10^{-12} m up to 10^{-9} m are considered as gamma rays. Even shorter wavelengths, smaller than 10^{-12} m, occur only in cosmic rays. As the earth is shielded from them by its atmosphere they occur only rarely on its surface. The X-ray spectrum lies between 10^{-11} and 10^{-8} m, followed by the Ultraviolet (UV) ranging from 10^{-8} m to $4*10^{-7}$ m (400 nm). The human eye can only detect a very small light range between purple light at 380 nm and red light at 750 nm of the electromagnetic spectrum of the sun. This is why that range is called visible light spectrum (VIS). Wavelengths longer than $7*10^{-7}$ m are the so-called infrared radiation (IR). And radiation consisting of wavelengths longer than 10^{-3} m is defined and used as radio wave (Masojídek, Koblížek and Torzillo, 2003).
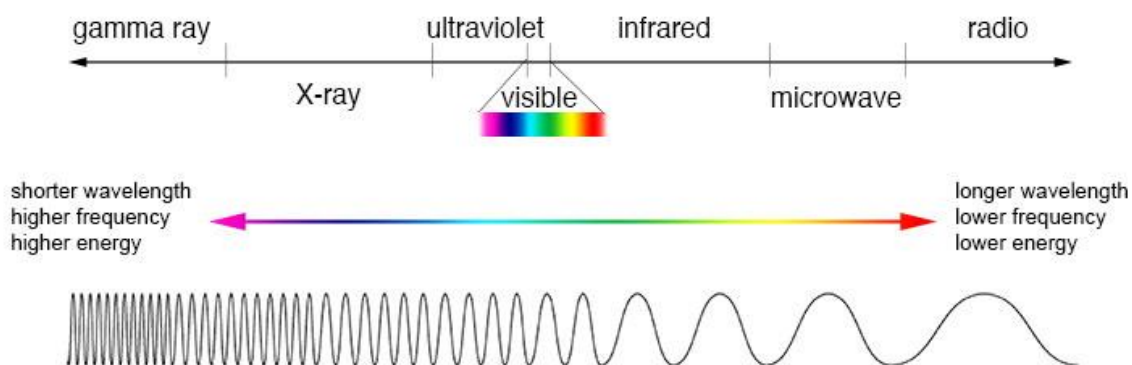
Figure 1: Correlation of electromagnetic radiation and wavelengths of the particles. (NASA, 2014)

With the wave-particle dualism the by sun delivered energy can be broken-down into single energy quanta, the so-called photons. The energy each photon contains depends on its

frequency (v) and the Planck constant ($h = 6.626 * 10^{-34}$ J s) and can be calculated via equation (1) (Masojídek, Koblížek and Torzillo, 2003). The photon frequency is depending on the speed of light (c = 29907920458 m s^{-1}) and wavelength (λ) of the photon.

$$E_{Photon} = hv = \frac{hc}{\lambda} \tag{1}$$

Einstein already discovered that the energy of a light quantum belonging to a homogeneous color decreases proportionally as the wavelength increases (Einstein and Infeld, 1938), meaning, a photon of blue light (400 nm) has a 75 % higher energy compared to a photon of red light (700 nm) (Zhu, Long and Ort, 2008).

The radiation spectrum emitted by the sun that reaches the earth is depending on the latitude and altitude. The ASTM Reference spectra (Gueymard, Myers and Emery, 2002) displayed in Figure 2 shows the averaged (over one year and of the 48 states of continental USA) daily solar irradiance in W m^{-2} nm^{-1}.
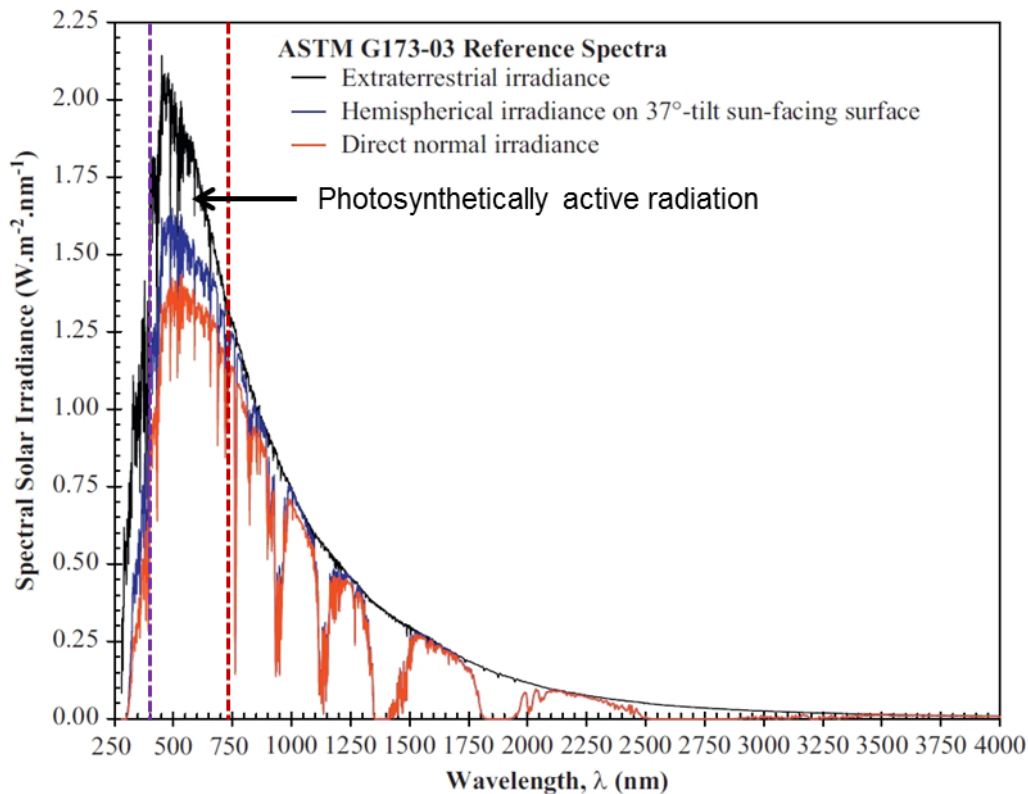
Figure 2 Averaged daily solar irradiance [W m^{-2} nm^{-1}] and photosynthetically active radiation between purple and dark red dashed lines. (Adapted from (Pilon, Berberoĝlu and Kandilian, 2011))

The effect of atmospheric gases like O_2, O_3, CO_2, H_2, methane and nitrous oxide which absorb radiant energy (especially strong in wavelength ranges 900 - 950 nm, 1100 - 1150 nm, 1350 - 1450 nm and 1800 - 1950 nm) can be seen via the gap between the black lined extraterrestrial and the red lined direct normal irradiance existing at sea level (Pilon, Berberoĝlu and Kandilian, 2011). Solar energy below 400 nm is mostly subducted by O_2 and

O_3 absorption. The area between the dashed purple and dashed red line is the region of photosynthetically active radiation (PAR) between 400 and 740 nm which can be used for photosynthesis whereas photons with longer wavelengths (above 740 nm) do not possess enough energy for photosynthesis. (Zhu, Long and Ort, 2008)

3.1.1 Photon energy

Photosynthetic live forms transfer the energy of the sun into chemical energy bound in form of stable chemical bonds through photosynthesis. The energy of each single photon, harvested by the pigments in the antenna complexes, provides a little portion of the energy used in photosynthesis. Chlorophyll molecules excited with a blue photon with 400 nm wavelength contain more energy compared to excitement by a red photon with 680 nm wavelength (see section 3.1). The photosynthetic reaction is finally driven only with the energy which a red photon contains. A charge separation within the photosystem II (PS II) needs approximately 176 kJ mol^{-1} which is equal to the energy of a red photon. Photons from the PAR region that can be absorbed might contain higher energy levels than the needed energy of the red photon. Higher excited stats with excessive energy incorporated by photons with wavelengths of 400 - 650 nm as for instance blue, green, yellow or orange light have more energy than need for the photosynthesis. However, this excessive energy, potentially incorporated within the blue photons is lost for photosynthesis as it cannot be utilized (Zhu, Long and Ort, 2008). This effect is displayed in Figure 3 where a blue photon absorbed by chlorophyll in the 400 - 500 nm region incorporates more energy than a red photon that is absorbed in the 650 -700 nm region.
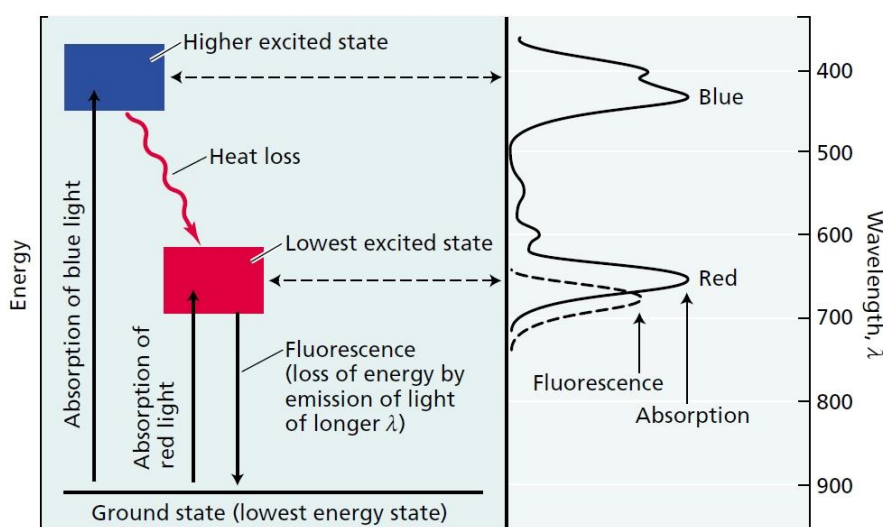
Figure 3: Energy level diagram for blue and red photons correlated to the absorption spectra of chlorophyll (Taiz and Zeiger, 2010)

With the blue photon energy the chlorophyll molecule is excited to the higher energy state, which is quickly changed to the lower excited (red-photon) state due to heat loss. Then it either gets back to ground state by re-emitting fluorescence with slightly longer wavelength, emitting heat or by transferring the incorporated energy to another molecule for instance to an acceptor within the photosystem.

3.2 Light and microorganisms

3.2.1 Microalgae

Microalgae are phototrophic microorganisms that are able to utilize light and CO_2 to build up biomass. Around 50% of the oxygen in the atmosphere is produced by marine algae (Borowitzka, 2013). The single celled microalgae with sizes up to few micrometers are the most important biomass producer on the planet and form the basis of the marine food chain (Posten and Walter, 2013). Microalgae were used by mankind directly as food additives for thousands of years, *Nostoc* sp. in China in times of famine or *Spirulina* sp. in Chad and Mexico (Spolaore *et al.*, 2006; Milledge, 2011). Of the estimated 500,000 algae species only about 220 macroalgae and less than 20 microalgae are currently commercially used (Posten and Walter, 2013). In recent years rising energy demands worldwide and the foreseeable decline of fossil energy brought microalgae in the focus as possible solution to these problems (Netravali and Chabba, 2003; Maness *et al.*, 2009; Shuba and Kifle, 2018). Microalgae show a high potential to solve these problems, as they have several advantages compared to other plants:

- Microalgae show fast growth with biomass double times once per 24 hours and produce 5-times more biomass than terrestrial crops (Chisti, 2007; Mata, Martins and Caetano, 2010)
- Utilization of sun and atmospheric CO_2 and little requirement of other fertilizers and no pesticides. Buildup of cheap and sustainable biomass is possible (Hu *et al.*, 2008; Satyanarayana, Mariano and Vargas, 2010).
- With little growth requirements biomass accumulation in non-agricultural environment is possible as there is no dependency on fertile land. Even growth in wastewater or seawater is possible. Arid areas not suitable for agriculture can be used.
- High lipid contents and high levels of other value products occur.

Microalgae growth can function as CO_2 sink as the algae typically consist of approximately 50% carbon which is mostly derived from atmospheric CO_2. In the process of production of 1 t microalgae biomass a total of 1.8 t CO_2 is processed (Sánchez Mirón *et al.*, 2003; Chisti,

2007). Microalgae form a sustainable biofuel product platform for products such as biodiesel, biogas, syngas, bioethanol or even biohydrogen (Raheem *et al.*, 2018; Shuba and Kifle, 2018) having oil yields tremendously higher than other lipid forming plants. A microalgae containing 30% lipid (by weight of dry biomass) comprises an oil yield of 58700 L ha^{-1} which is 340-fold higher than corn, 30-fold higher than jathropha and 10-fold higher than oil palm (Chisti, 2007). Whereas oil contents of 20 - 50% widely occur, some microalgae can even exceed 80% lipid content by weight of biomass. (Spolaore *et al.*, 2006) With the nitrogen fixation (Prasanna *et al.*, 2009) and even after oil extraction residual biomass can additionally be used as bio-fertilizers as it still contains a high nitrogen-phosphate ratio (Wang *et al.*, 2008). Aside Lipids that can be used as biofuels, microalgae can produce other high value products such as antioxidants, polysaccharides, triglycerides and fatty acids, vitamins pigments and β-carotene are of interest (Mata, Martins and Caetano, 2010). β-carotenes sell with prices between 300 and 3000 US$ kg^{-1} and are used as natural food colorant (orange juice coloring), as additive in animal feed products or in cosmetics (Del Campo *et al.*, 2000). The natural Astaxanthin sells for approximately US$ 2500 kg^{-1} with applications in salmon and trout feed industry, carp and chicken diets and is produced by *Haematococcus pluvialis* (Lorenz and Cysewski, 2000). Aside from the already mentioned applications there are also other biotechnological capabilities for microalgae. The usage in municipal or industrial wastewater treatment without the need of oxygen aeration such in the decomposition of volatile hazardous pollutants is promising (Muñoz and Guieysse, 2006). Extraction of heavy metals (Kalin, Wheeler and Meinrath, 2004) or rare earth metals from mining waste has also been reported (Palmieri, Garcia and Melnikov, 2000; Das and Das, 2013).

3.2.2 Photosynthesis

Photosynthesis in microalgae takes place at thylakoid membranes of the chloroplasts. And as in plants the five major complexes are involved: the light harvesting antennae complex, the photosystem II (PS II) and photosystem I (PS I), each with a reaction center, the cytochrome b$_6$/f and the ATP synthase. The latter two maintain the photosynthetic electron transport and the photophosphorylation (Masojidek *et al.*, 2013). Photons within the PAR range incorporate sufficient energy to be used for photosynthesis and are absorbed within the antennae complex (see Figure 4). The antennae complex consists of hundreds of pigment molecules, chlorophyll *a* and *b*, carotenoids and phycobilins, depending on the organism and the central reaction center. All pigment molecules are interlinked to the thylakoid membrane at the chloroplast. 20 - 30 pigment-clusters per reaction center occur in some bacteriochlorophylls, 200 – 300 chlorophylls per reaction center in higher plants and up to few thousands in some type of algae and bacteria. The photon energy is transferred

toward the reaction center highly efficiently with 95 - 99% via fluorescence resonance energy transfer (FRET). The average excitation transfer time from the Antenna subunits of the LHC to the PS I core in plants and algae systems was calculated to be 2 – 5 ps (Melih *et al.*, 2011). The nonradiative dipole–dipole coupling energy transfer between a donor and acceptor chromophore works only at a certain distance, as the process is inversely proportional to the sixth power of the distance (Masters, 2014). Therefore a highly conserved structural symmetry can be observed in all LHC-systems. After transferring the photon energy the excited electron in each molecule returns to its low-energy level which it had before the photon was absorbed. In this way, the energy of the photon and not an electron, is basically transferred towards the reaction center (Taiz and Zeiger, 2010). The specialized chlorophylls in the reaction centers of the PS II (P_{680}) and PS I (P_{700}) absorb the photon energy channeled toward them and use it to oxidize water to O_2. Here the electron energy of the photon is transferred into chemical energy. The proton of the oxidized water is released into the thylakoid lumen.
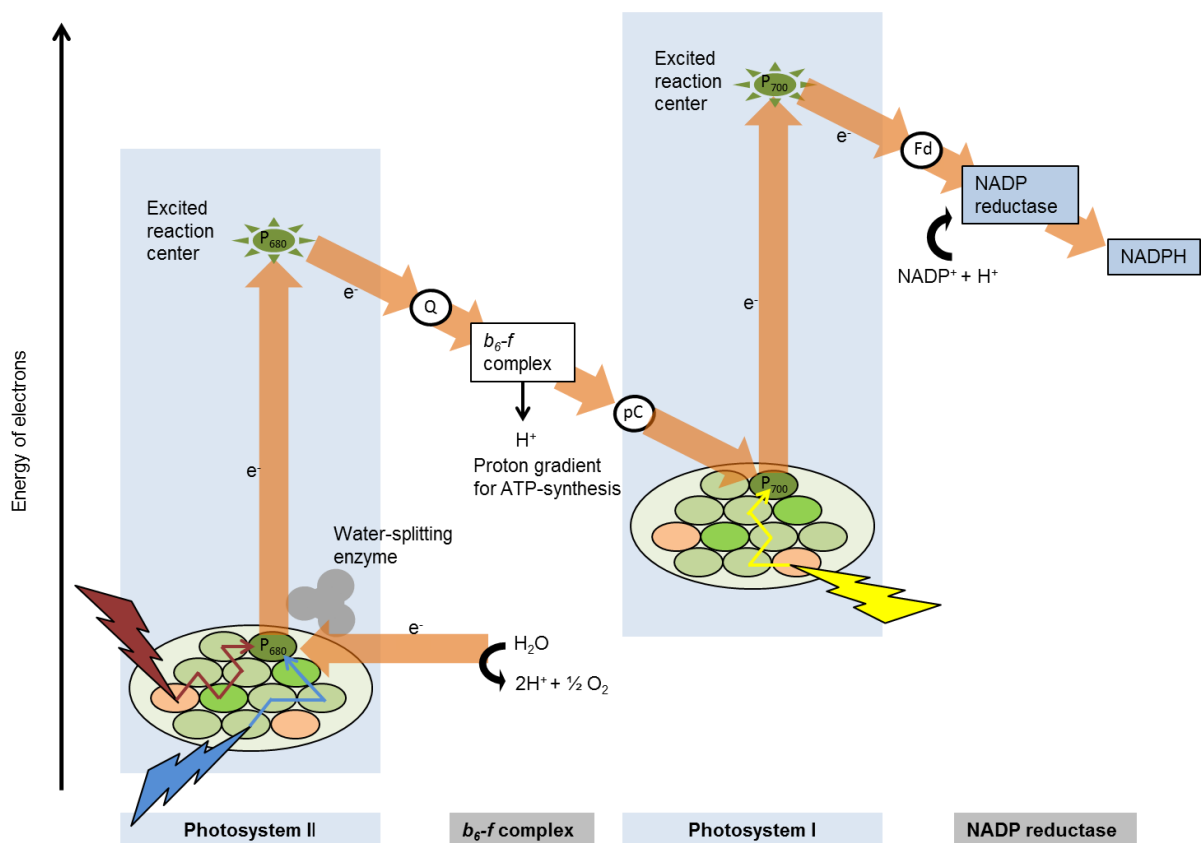
Figure 4: Z-scheme of photosystem I and II. Photons (blue, red or yellow) are captured by the antenna complex consistent of different chromophores (Chl *a* and *b*, carotenoids, phycobilins). Q = Plasto-quinone, pC = Plastocyanin, Fd = Ferredoxin. (Adapted from (Raven *et al.*, 2013)**).**

From the excited state of the P_{680} reaction center of the PS II the electrons are transferred by the reduced plastoquinone to cytochrome b_6f in the light reaction of the photosynthesis. The transmembrane protein as part of the electron transport chain works as a plastoquinone-

plastocyanin reductase and is building up the proton gradient later used to power the ATP synthase. Via plastocyanin the electrons are channeled further to the PS I. With the second excitation using photon energy at the P_{700} reaction center powered by further light harvesting complexes of the PS I ferredoxin is reduced. In the final step of the electron chain in the light reaction of photosynthesis $NADP^+$ is reduced to NADPH by the ferredoxin-$NADP^+$ reductase. The build –up proton gradient in the thylakoid lumen generated by the cytochrome b_6f complex and during the initial oxygen producing breakage of H_2O in the PS II is used by the ATP synthase enzyme to produce ATP, the other energy carrier in the organism (Raven *et al.*, 2013). The connection between the two photosystems PS II and PS I is very important as they work together in order to facilitate an efficient flow throughout the electron chain reaction and the creation of the proton gradient across the thylakoid membrane in the photosynthesis (Goldschmidt-Clermont and Bassi, 2015). Unbalances in the electron chain can occur due to illumination changes and differences in light quality, as the PS I is more sensitive for far-red light compared to the PS II, which is predominately excited at blue light (Longoni *et al.*, 2015). This could lead to the generation of reactive oxygen species and photooxidative damage with negative effect on the organism (Frenkel *et al.*, 2007). As a rapid regulation response to changing illumination properties, changes in light quality or a different metabolic demand the two photosystems can be phosphorylated by the algae. The phosphorylation of the antennae leads to a remodeling of the photosynthetic complexes thus altering its turnover. Via the antenna-phosphorylation of the light-harvesting proteins (LHCII) a relocation leads the dynamic allocation of light harvesting antennae between the two photosystems on the thylakoid membrane in order to balance the two photosystems (Goldschmidt-Clermont and Bassi, 2015). The kinase and phosphatase pair (STT7 and STN7) respond to the redox state of the electron transfer chain and are regulating the phosphorylation, thus affecting the redistribution of excitation energy (Bonardi *et al.*, 2005).

3.3 Pigments

3.3.1 Pigment structures

Pigments occur in three major groups, chlorophylls, carotenoids and phycobilins. All chlorophyll molecules have the same tetra-pyrrole ring structure as backbone which contains a central magnesium atom and a long-chain terpenoid alcohol, the phytol-sidechain. The polar head with the magnesium atom functions as the chromophore that captures the light photons. Chlorophyll *a* and *b* differ in just one sidechain with a methyl residue in Chl *a* and oxidized with the corresponding aldehyde residue in Chl *b*.
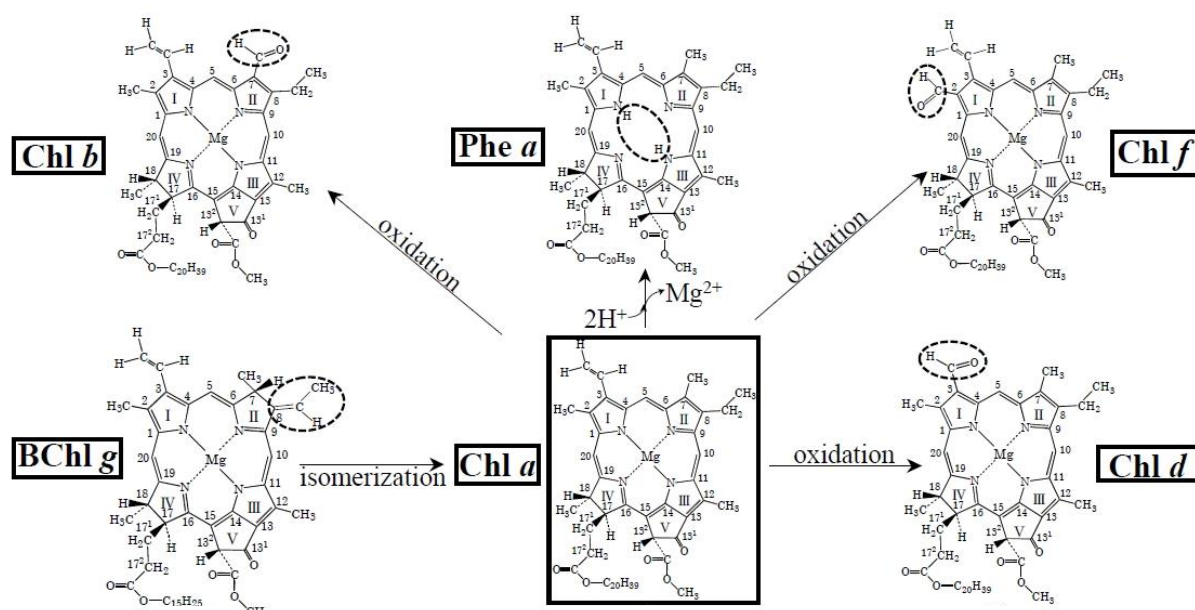
Figure 5: Different types of Chlorophylls and their differences (Kobayashi *et al.*, 2013)

The only exception to this basic chlorophyll structure is Chl *c*, which absorbs light in the 447-452 nm region and does not have the phytol sidechain (Garrido and Zapata, 1998; López-Rosales *et al.*, 2016). Figure 5 displays the possible evolution of Chlorophylls deviated from an ancestral bacterial Chlorophyll *g* (BChl *g*). Under mild conditions the *in vitro* isomerization takes place spontaneously (Kobayashi *et al.*, 1998). The rarely occurring Chl *f* has an absorption peak at about 706 nm and a maximum fluorescence emission at 722 nm and is thus the most red-shifted chlorophyll discovered jet. It was discovered in a filamentous cyanobacterium. (Chen *et al.*, 2012). A demetallated Chl *a* version, the pheophytin *a* (Phe *a*), was found in *Acaryochloris. marina* and works as electron acceptor of the PSII (Akiyama *et al.*, 2001; Ohashi *et al.*, 2010). All chlorophylls have the major absorption bands in the blue (450 - 475 nm) and the red area (630 - 675 nm), resulting in their characteristic green color. Chl *a* is part of the core and reaction center pigment-protein complex in all oxygenic photoautotrophs. The accessory antennae pigments Chl *b*, Chl *c* and Chl *d* widen the range of light absorption in the light harvesting complex (Masojidek *et al.*, 2013).

Carotenoids are a large group of chromophores which absorbs in the blue-green area (400 – 550 nm) and thus appear yellow orange. The structure consist, as shown for β-Carotene in Figure 6, a) of two hexa carbon rings that are connected via a 18 carbon chain with conjugated double-bonds. xanthophylls, such as Lutein, violaxanthin (shown in Figure 6, b)) or zeaxanthin are structurally very similar but consists of oxygenated hydrocarbons (Masojidek *et al.*, 2013). They are used by algae to protect the photosynthetic apparatus against excessive light by quenching poisonous free radicals and converting excess radiant energy to light (Kandilian, Lee and Pilon, 2013).

a   b
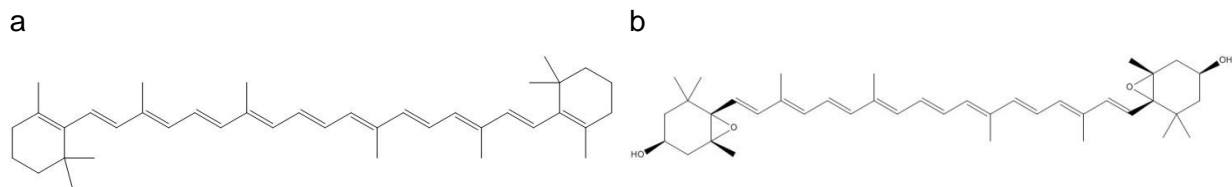
Figure 6: a) Structure of β-Carotene (*beta-beta*-Carotene), b) Structure of Violaxanthin. [generated with PerkinElmer ChemDraw Professional, V.16.0.1.4(77)]

Phycobilins are chromophores occurring in cyanobacteria, red algae and dome other smaller phylums but not in green algae or plants. They act as antioxidant, carbon and nitrogen storage and as accessory pigment within the antennae complex to capture and transfer photons to the active center chlorophyll (Markou, 2014).

3.3.2 Chlorophyll biosynthesis

The biosynthesis of chlorophyll contains numerous steps beginning with the formation of 5-aminolevulinic acid. Two 5-aminolevulinic acid molecules are condensed to form the porphobilinogen of which 4 units are linked to build up the precursor for the formation of the pyrrole ring. As displayed in Figure 7 the synthesis of the tetrapyrrole chain (hydroxy methyl bilane) and the formation of the tetra-pyrrole ring (Uroporphyrinogen III) follows. The removal of the acetate and propionate side chains and the development of the conjugated double bond system generates the protoporphyrin IX a precursor for chlorophyll. With the insertion of the magnesium ion, formation of ring V and synthesis of protochlorophyllide and followed by reduction the chlorophyllide is formed. The final chlorophyll is generated with the addition of the phytol-sidechain (Von Wettstein, Gough and Kannangara, 2010; Brzezowski, Richter and Grimm, 2015). Chlorophylls are anchored to the thylakoid membranes via the hydrocarbon phytol-chain. The phytol-residue comprises up to one third of the molecule mass and thus enhances the lipophilic character enabling interaction with the hydrophobic environment of the thylakoid membrane (Fiedor *et al.*, 2008). The porphyrin head forms the

photoactive domain. Depending on the side chain of the porphyrin ring with the centralized magnesium atom the absorption properties change (Raven *et al.*, 2013).
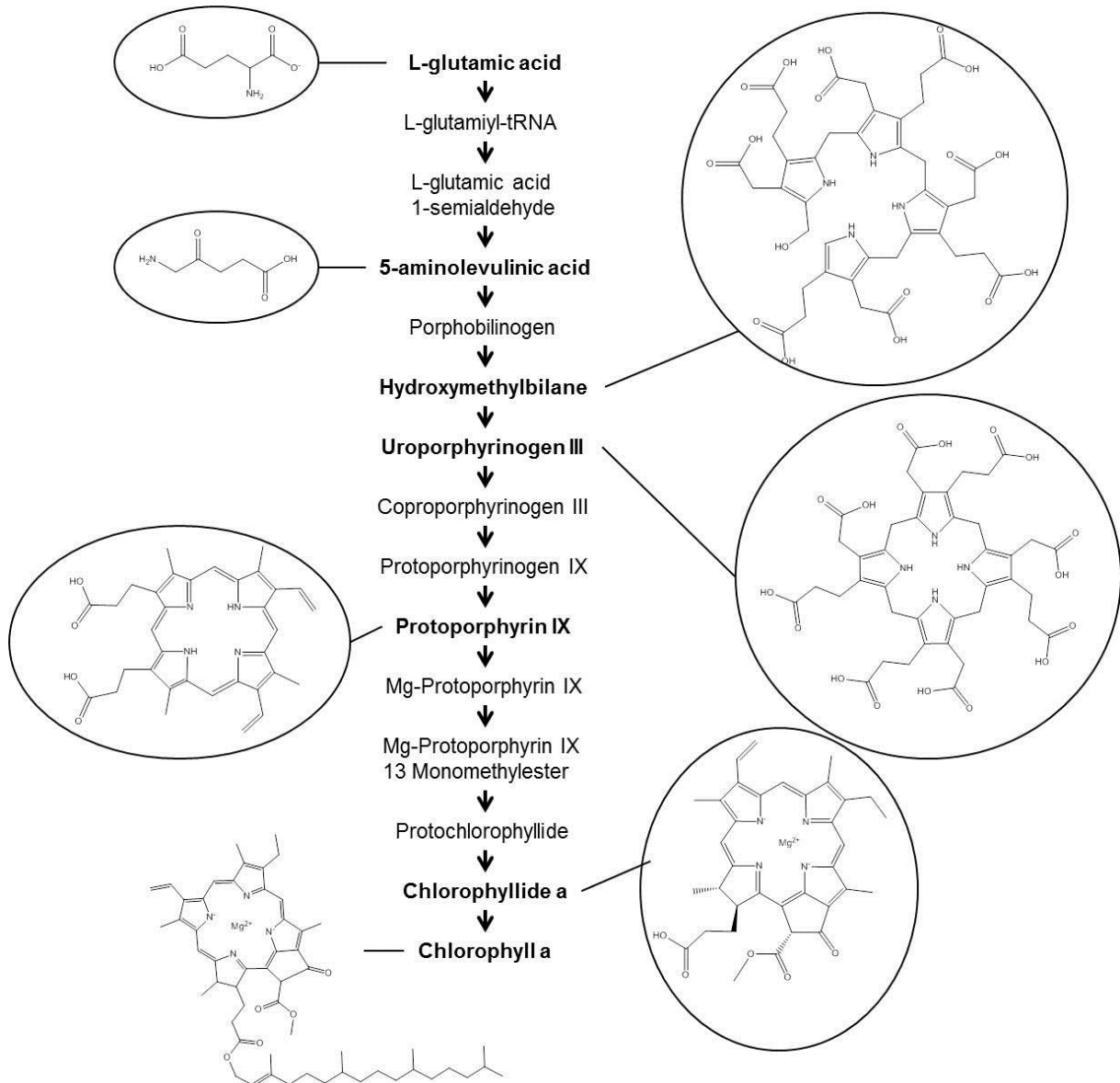
Figure 7: Chlorophyll *a* biosynthesis pathway. Bold names are intermediate-steps described in the text. [Generated with PerkinElmer ChemDraw Professional, V.16.0.1.4(77)] according (Brzezowski, Richter and Grimm, 2015)

3.4 Mutation Procedures

3.4.1 Traditional mutagenesis approaches for microalgae

Traditional mutagenic tools such as EMS treatment or UV irradiation have been widely used in microalgae with reports dating back several decades (Newton, Tyler and Slodki, 1979; Schneider *et al.*, 1995). Random mutagenesis with UV radiation has a deleterious effect on the DNA which leads to metabolic changes in microalgae (Hessen, De Lange and van Donk, 1997; Guihéneuf *et al.*, 2010). UV-C, compared to UV-A and UV–B, incorporates most energy, having the shortest wavelength and has therefore more effective on microalgae. (Sharma, Li and Schenk, 2014; Sivaramakrishnan and Incharoensakdi, 2017) Ethyl methanesulfonate (EMS) is a chemical mutagen that has also been applied to induce microalgae random mutagenesis. It induces many mutant alleles, (Bruggemann *et al.*, 1996) mostly in the form of point mutations via nucleotide substitution (Ahmad, Lin and Cashmore, 1995).

3.4.2 Genetic mutation via plasma

Cold atmospheric plasmas (CAP) or atmospheric pressure glow discharges (APGDs) were already described in 2009 mainly for the medicine and healthcare sector. The potential was already seen in the generation of reactive atoms and molecules enabled to interact with cell membranes and to modify the membrane permeability.
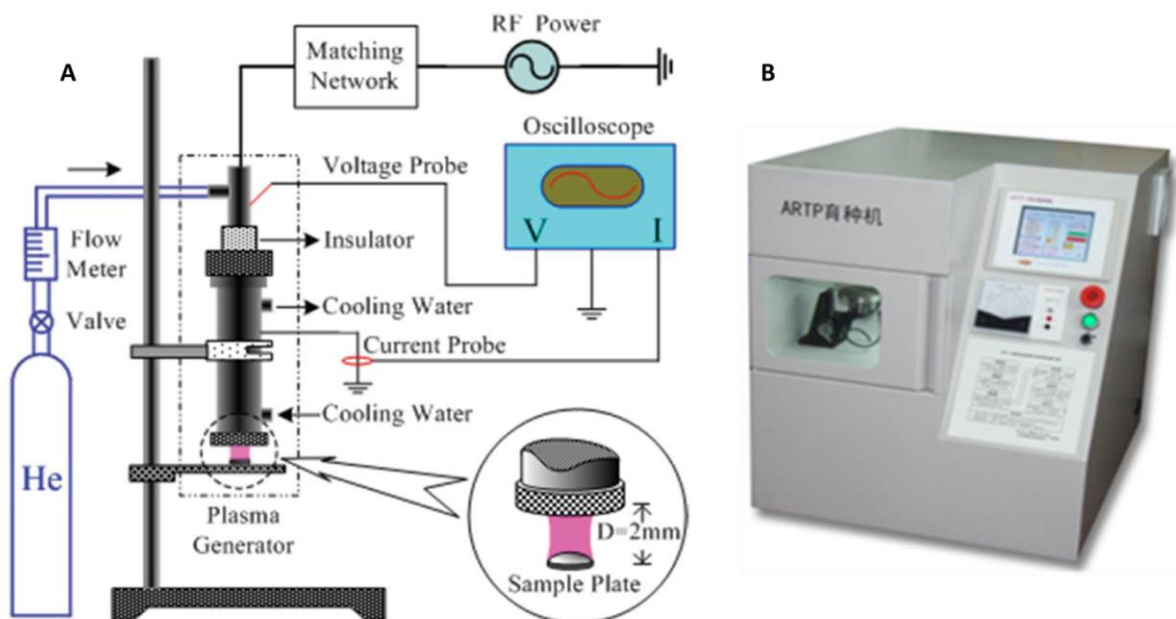
Figure 8: ARTP mutagenesis system developed by the Department of Chemical Engineering, Tsinghua University, Beijing, China (Fang *et al.*, 2013)

The production of ionic species close to or on living tissues and a delivery of plasma agents at atomic and molecular levels seemed promising once being able to produce these plasmas without the use of a vacuum chamber (Morfill, Kong and Zimmermann, 2009). An overview and practical example with radiofrequency atmospheric-pressure glow discharges (RF APGDs) was presented by Li et al. (Li *et al.*, 2012) describing a prototype called the atmospheric and room-temperature plasma (ARTP) mutation system, which was used to generate mutants of the bacteria *Methylosinus trichosporium.* The chemically reactive species in the helium RF APGD plasma jet could lead to the gradually break of the double chains of plasmid DNA depending on the composition of the plasma discharges. The plasma treatment therefore could be used similar to UV, X-ray or gamma radiation to insert random mutations within the genome of bacteria or plants (Arunyanart and Soontronyatara, 2002). The first use of plasma on microalgae was described for *Spirulina platensis* (Fang *et al.*, 2013)*.* The plasma treatment caused partial fragmentation of *S. platensis* and mutant strains could be identified in a 48-well plate screening showing up to 78% higher sugar contents than the wildtyp combined with improved genetic stability. Zhang et al. described the advantages of ARTP as a new mutagenesis tool for bacteria, fungi and microalgae. (Zhang *et al.*, 2014). The effects of helium plasma jets on biological samples was here described as a combination of UV radiation, heat, electromagnetic fields, neutral reactive species and charged particles. (Laroussi and Leipold, 2004). The effects of direct plasma treatment (in contrast to indirect treatment with the biological samples in direct surrounding of the plasma nozzle exit (Fridman *et al.*, 2007)) are very dependent on the plasma generating device, sample treatment procedures, the dosage and the distance to the nozzle exit. In Figure 8 the ARTP mutagenesis system developed by the Department of Chemical Engineering, Tsinghua University, Beijing, China is displayed. With this device the majority of published work with plasma mutation was performed. Overall ARTP possesses outstanding advantages, such as high efficiency, nontoxicity, zero pollution of the environment, and low operating costs (Wang et al., 2014) is therefore of high interest for mutation breeding of all kinds of microorganisms.

3.4.3 Fast neutron irradiation as mutagenesis tool for microalgae

Fast neutron irradiation or fast neutron bombardment consist of a high linear energy dosage of fast neutrons and a neutron flux of $3.2*10^8$ cm^{-2} s^{-1}. Secondary ionization and gene mutations are induced, which enable the possibility of mutant generation (Wang et al., 2015). Most common mutations are caused from base pair deletion in the DNA with the range of a few base pairs to several mega bases (Li et al., 2001).

Fast neutron bombardment has been widely used in many plant species for the generation of mutant strains such as *Arabidopsis thaliana* (Koornneef *et al.*, 1982; Li *et al.*, 2001), peanut plants (Wang *et al.*, 2015), *Solanum lycopersicon* (tomato plant) (Dor *et al.*, 2010), soybean (Bolon *et al.*, 2011; Hwang *et al.*, 2015), rice (Wu *et al.*, 2005), *Medicago truncatula* (Oldroyd and Long, 2003), barley (Zhang *et al.*, 2006) and *Lotus japonicas* (Hoffmann *et al.*, 2007). The identification of many phenotype-associated genes was obtained following fast neutron bombardment (Meinke, Sweeney and Muralla, 2009; Bolon *et al.*, 2011).

Despite these examples of fast neutron bombardment the data pool for neutron dosage estimation is very small, as the irradiation dosages have to be adapted for each species individually (Li and Zhang, 2002). Microalgae can be very radiation resistant as the discovery of a cyanobacteria (*Chroococcidiopsis* sp.) in the cooling water pool of a nuclear reactor with extremely high γ-radiation of up to 20.000 Gy demonstrates (Farhi *et al.*, 2008).

4 Scope of this work

The scope of this thesis is the enhancement of cultivation of microalgae as producers of biomass and metabolites that can ultimately be turned into high value products. Two of the aspects that need to be improved for microalgae to be used commercially are the microalgae's growth rate and the formation of pigments and lipids. Therefore, this thesis is divided into two parts, each of which covers one of these aspects.

In the first part, the effects of varying illumination setups on three microalgae strains are studied. With the application of artificial LED illumination the total irradiation is tested at four levels and with various colored LEDs. The effects on growth response and lipid formation of *Picochlorum* sp., *Dunaliella* sp. and *Microchloropsis salina* are investigated. In *Picochlorum* sp., the green light illumination setup has led to the discovery of new pigments the structures of which are elucidated by high resolution HPLC-MS and NMR techniques. For verification of the results, photo bioreactor scale-up experiments are performed where the formation of these new pigments can be observed through the course of the cultivation.

The second part covers method development for the generation of new, fast growing mutant strains of *Picochlorum* sp. via random mutagenesis. Standard methods such as UV-radiation and the chemical treatment with EMS have a reported effect on microalgae cells and can induce genetic mutations in the DNA. These applications are used as reference methods for the development and evaluation of novel methods for random mutagenesis. In a first approach a new device for atmospheric and room temperature plasma treatment is used. It generates plasma beams that can penetrate and change cellular structures. This led to the development of a new method for microalgae random mutagenesis. Secondly, highly energetic particles can easily penetrate the cell and cause changes within it. The feasibility of fast neutron bombardment for random mutagenesis is therefore investigated with the microalgae *Picochlorum* sp.

5 Material and methods

5.1 Strains and media composition

In this work three strains were used, the commercially available *Microchloropsis salina* (formerly known as *Nannochloropsis salina* (Fawley, Jameson and Fawley, 2015)) obtained from the IBK´s in-house strain collection and from the Experimental Phycology and Culture Collection of Algae at Goettingen University (EPSAG, 2017) respectively. Here the strain will be referred to as *M. salina*. The other two strains were halophilic microalgae strains that were obtained and isolated form two different habitats. *Dunaliella* sp. is an isolate from a salt lake in Australia (see Table 2) and was identified with 96% identity as *Dunaliella salina* strain KU11 on the NCBI database. The third strain is an IBK isolate from the Bahamas and was identified as *Picochlorum* sp. SENEW3.

Table 2: Name, origin and identity of microalgae strains used in this work.

Strain	Origin	Identity
Microchloropsis salina	IBK culture collection, EPSAG Göttingen	SAG 40.85
Dunaliella sp.	IBK isolate from Salt creek, SA, Australia (36°09'41.2"S, 139°38'50.0"E)	96% *Dunaliella salina* strain KU11, (NCBI Accession-No.: KF825549.1)
Picochlorum sp.	IBK isolate from Salt Lake Pond, San Salvador, Bahamas (24°01'40.7"N, 74°26'58.7"W)	99% *Picochlorum* sp. SENEW3 (NCBI Accession-No.: KF591594)

The media compositions of the strains used in this work are listed below in Table 3 (*M. salina*.), Table 4 (*Picochlorum* sp.) and Table 5 (*Dunalliella* sp.). These media compositions were used for precultures, shake flask experiments or fermentations. In some cases, such as growth analysis experiments, phosphate concentrations were increased to prevent early phosphate limitation. In this case the described experiments will be labeled accordingly

Fast neutron radiation procedures needed a special media composition to prevent long lasting radioactive isotopes. In these special media (for *Picochlorum* sp.) trace elements were neglected and NaCl was replaced with KCl.

Table 3: Components for *Microchloropsis salina* medium. Components in italics were added after autoclaving. Trace element solution was filter sterilized and stored at 4°C. CaCl$_2$ was autoclaved separately. pH set to 8.0 prior to autoclaving process.

Component	[g L^{-1}]	Trace Element solution	[mg L^{-1}]
NaCl	30	Na$_2$EDTA * 2 H$_2$O	3000
KNO$_3$	2.2	H$_3$BO$_3$	600
K$_2$HPO$_4$	0.05	FeSO$_4$ * 7 H$_2$O	200
MgSO$_4$ * 7 H$_2$O	1.2	MnSO$_4$ * 4 H$_2$O	140
*CaCl$_2$ * 2 H$_2$O*	0.8	ZnSO$_4$ * 7 H$_2$O	33
Trace element solution	1 mL L^{-1}	CoCl$_2$ * 6 H$_2$O	0.7
		CuSO$_4$ * 5 H$_2$O	0.2

Table 4: Components for *Picochlorum* sp. medium. Components in italics were added after autoclaving. Trace element solution was filter sterilized and stored at 4°C. pH set to 8.2 after the autoclaving.

Component	[g L^{-1}]	Trace Element solution	[mg L^{-1}]
NaCl	27	$ZnCl_2$	40
$MgSO_4 * 7 H_2O$	6.6	H_3BO_3	600
$CaCl_2 * 2 H_2O$	1.5	$CaCl_2 * 2 H_2O$	1.5
KNO_3	5	$CuCl_2 * 2 H_2O$	40
KH_2PO_4	0.07	$MnCl_2 * 4 H_2O$	628.7
$FeCl_3 * 6 H_2O$	0.014	$(NH_4)_6Mo_7O_{24} * 4 H_2O$	370
$Na_2EDTA * 2 H_2O$	0.021		
Trace element solution	1 mL L^{-1}		

Table 5: Components for *Dunaliella* sp. medium. Components in italics were added after autoclaving. Trace element solution was filter sterilized and stored at 4°C. pH set to 8.0 prior to the autoclaving.

Component	[g L^{-1}]	Trace Element solution	[mg L^{-1}]
NaCl	50	H_3BO_3	2860
$NaNO_3$	1.5	$MnSO_4 * 4 H_2O$	1810
K_2HPO_4	0.04	$ZnSO_4 * 7 H_2O$	222
$MgSO_4 * 7 H_2O$	0.075	$Na_2MoO_4 * 2 H_2O$	390
$CaCl_2 * 2 H_2O$	0.003	$CuSO_4 * 5 H_2O$	79
Citric Acid	0.006	$Co(NO_3)_2 * 6 H_2O$	49.4
Ammonium ferric citrate	0.006		
Na_2CO_3	0.02		
$Na_2EDTA * 2 H_2O$	0.001		
Trace element solution	1 mL L^{-1}		

5.2 Dry weight measurement

5.2.1 Lyophilization

To measure bio dry mass out of cultivation samples, volumes between 10 mL and 40 ml were taken. To reduce manual measuring errors, triplicates with 40 mL sample volume each were preferred for bioreactor cultivations. In cases of less biomass available, such as in shake flask cultivations, 10 or 25 mL volumes were obtained. For each dry weight determination, the optical density at the sample time point was measured to correlate dry mass to optical density. Samples were taken in a pre-weighted 50 mL falcon tube. After centrifugation (3214g, 10 min) the pellet was resuspended and washed with dH_2O. Once pelleted again (3214g, 10 min) the supernatant was removed thoroughly and the pellet was stored until lyophilization at -80°C. Lyophilization was acchieved using a Christ Alpha 1-2 LDplus lyophilizator for a minimum time of 48 h. Final sample weight was determined (m_2) and the empty vessel weight (m_1) was subtracted. Divided by the initial sample volume (V_s) the biomass dry weight was obtained.

$$m_{DW} [mg^*L^{-1}] = \frac{(m_2 [mg] - m_1 [mg])}{V_s [L]}$$ (2)

5.2.2 Infrared-balance

A second dry weight determination protocol was used in initial experiments using the infrared drying-balance MB25 by OHAUS. A pre-weighted (m_1) aluminum petry dish was filled with up to 10 mL (V_s) sample volume and placed inside the evaporation chamber. The balance was zeroed and the drying process started via the infrared-lamp with 105°C. The inbuilt balance checks sample evaporation until no further weight change is detectable. To increase accuracy, the aluminum tray was afterwards weighted at the fine balance to retrieve the dry-sample weight (m_2). Calculation of dry mass was performed according to equation (2).

5.3 Growth determination

5.3.1 Photometer

Growth determination of bioreactor and shake flask cultivations was performed using the photometer 8453 of Hewlett Packard. The full spectrum photometer detected a range of 300 – 800 nm. Samples were measured at 750 nm. 680 nm values were also recorded to monitor chlorophyll content. Media blank values were recorded at the start of each experiment and subtracted from subsequent measured values. Standard semi-micro cuvettes made of polystyrene (PS) were used with 900 – 1500 µL sample volume. Values were diluted with 3 % NaCl solution to stay within the linear range of the photometer between 0.05 and 0.5.

5.3.2 Plate reader

Large scale determination of optical densities with numerous samples was performed on the Microtiter Plate (MTP) Reader EnSpire2 by Perkin Elmer (Waltham, USA). 24-well-plates and 96-well plates (Sarstedt TC-Plate 24/96 Well Standard F) were used with a volume of 1 mL or 200 µL respectively. To ensure precise readings each sample was measured in triplicate. To stay within the border lines of the linear range (below 0.6) dilutions with 3 % NaCl solution were carried out and a blank reading of the used media was recorded. For growth analytic screenings in 24-well plates the plate needed to be manually shaken for 10 seconds prior the measurements to prevent cell settlement.

For each strain and color growth setup a correlation factor was established to convert OD-values measured on the plate reader to cell dry weight (CDW). Plate reader OD-values are indicated with a superscript "PR", for instance: $OD^{PR}_{750\ nm}$. Table 6 displays the correlation factors generated by color-illuminated shake flask experiments (Stage 1 experiments).

Table 6: Strain and color specific correlation factors between cell dry weight (CDW) and optical density of 96-well plate measurement at the plate reader ($OD^{PR}_{750\ nm}$)

$CDW/OD^{PR}_{750\ nm}$ correlation [$g_{DW}\ L^{-1}\ OD^{PR}_{750\ nm}{}^{-1}$]	*Picochlorum* sp.	*Dunaliella* sp.	*M. salina*
white	0.838 ± 0.034	1.275 ± 0.094	0.768 ± 0.051
blue	0.565 ± 0.032	1.235 ± 0.006	0.604 ± 0.028
green	0.826 ± 0.032	1.211 ± 0.035	0.773 ± 0.028
red	0.833 ± 0.005	1.372 ± 0.035	0.777 ± 0.053

5.3.3 Growth rate calculation

Growth analysis to determine maximum growth rates (μ_{max}) to assess differences of mutant strains concerning growth was carried out in early screening phases and thus based on the assumption of unlimited growth. Illumination with 50 µmol m^{-2} s^{-1} proofed to be sufficient for 1 mL cultivations in 24 well dimensions with culture thicknesses of less than 0.5 cm. Substrate availability was also provided, as for each new screening cycle at least 90% of the total volume in each well consisted of fresh media. Considering usual recultivation volumes the fresh media proportion consisted even up to 950 - 975 µL per 1 mL total volume. Aeration and CO_2 supply was ensured via venting the plates regularly every 48 hours.

Thus the exponential growth model in equation (3) was used.

$$y = y_0 * e^{(\mu * t)} \qquad (3)$$

The analysis of growth rates was calculated with an incremented growth rate determination of sample points via formulas in Microsoft Excel. Growth curves were divided into increments with a minimum of 4 sample points and with a minimum time-frame of 60 hours between the first and last sample of each increment. With the assumption of exponential growth the R-squared (RSQ) value was calculated for each increment with the natural logarithmic value of the y-values (RSQ(ln(known y´s));(known x´s)). If the result was equal or above RSQ = 0.95 the slope of the increment was calculated and exported (slope(ln(known y´s));(known x´s)). If not, a blank value was exported, signaling that the data points within the increment did not behave as expected. In these cases, a manual check of the data was carried out.

For a data set of 6 points three increments could be formed (1-4, 2-5 and 3-6) resulting in three RSQ-values and if they were above 0.95, three slope values or growth rates. In a final calculation the maximum slope value of a sample row was exported and used as maximum growth rate μ_{max} for the dataset. With this segmented data analysis a semi-automated growth analysis was possible ensuring comparable results and avoidance of manual errors.

5.3.4 Live-Dead screening

The dead or alive screening of *Picochlorum sp.* mutation procedures was carried out in 24-well microtiter plates. The plates were analyzed once a day via plate reader measurement. The sealed plates were also aerated to ensure no CO_2 limitation occurred. In case of strains or wells that showed a faster growth a well-specific dilution with fresh media was performed and the dilution steps noted correspondingly. Wells with OD-values above $OD^{PR}_{750\,nm}$ = 0.5 were also diluted with fresh media to prevent light or analysis limitations. The initial growth was monitored up to 14 days with several dilution steps per well if necessary. Survival rate was calculated according to equation (4)

$$Survival\ rate\ [\%] = \frac{OD^{PR}_{750\,nm}\ treated\ samples}{OD^{PR}_{750\,nm}\ control\ samples} * 100 \tag{4}$$

5.4 Phosphate/Nitrate analysis

5.4.1 Phosphate analysis

Phosphate analysis was adapted for plate reader dimensions by the protocol described by Schumann (Schumann, 2013). The detection method works with the formation of yellow colored phosphor molybdic acid out of phosphate ions and molybdate reagent solution (Sigma Aldrich 69888-100ML) in an acidic environment, which was reduced to blue colored molybdenum via ascorbic acid.

All samples were analyzed in triplicate in 96-well plates. Each well was filled with 100 µL filter sterilized samples and 10 µL molybdate reagent solution was added. A background measurement (absorption at 885 nm) was done and 5 µL 40 g L^{-1} ascorbic acid solution (max. 2 weeks old if stored at 4°C) was added. On an Eppendorf ThermoMixer® C the reaction was mixed at 800 rpm in darkness. The absorbance was measured at 885 nm on the MTP reader. A standard solution was measured with each 96-well plate. Standard solution was set up by using the media recipe of each strain (phosphate free) with 0 mg, 2.5 mg, 5 mg, 10 mg and 20 mg phosphate concentration.

5.4.2 Nitrate analysis

Nitrate concentration was analyzed via a colorimetric test developed and adapted for plate reader dimension (Peiffer and Pecher, 1997). Nitrate ions were reduced to nitrite-ions in an alkaline environment via zinc-power reduction and then form a diazonium compound when incubated with sulfanilic acid (4-aminobenzenesulfonic acid). A pink colored stain is formed via azo coupling, if 1-naphthylamine is added. The color intensity correlates with the nitrate concentration and can be measured photometrically in the plate reader.

As the color staining is a time-critical reaction a standard curve needs to be stablished to correlate the color intensity with nitrate concentrations for each 96-well measurement. For the standard curve the strain specific media recipe was used (nitrate free) and nitrate was added in 7 dilution steps (0 mg, 5 mg, 10 mg, 20 mg, 30 mg, 40 mg and 50 mg). The standard solution was stored in darkness at 4°C. A naphthyl reagent –solution was prepared beforehand and stored in darkness at 4°C. For the reagent 1 g sulfanilic acid and 5 g sodium acetate were solved in 50 mL dH$_2$O. 0.1 g 1-naphtylamine was solved in 100 mL 5 % (v/v) acetic acid and added to the sulfanilic acid solution and filled up to 200 mL.

Samples were analyzed in triplicate, for one sample 400 µL filter sterilized solution was transferred in a 2 mL Eppendorf tube and 20 µL 5M NaOH and 10 mg zinc powder were added. After 5 min vortex mixing at 400 rpm the zinc powder was sedimented via 1 min centrifugation (3000g). The supernatant was transferred in a 96-well plate with 100 µL per

each well. The full plate was measured once to obtain a blank value at 535 nm.

For the color reaction 25 µL glacial acetic acid was added in each well and mixed at 400 rpm for 5 min. 5 µL naphthyl reagent adding and mixing for another 5 min at 400 rpm started the color reaction. The plate reader measurement at 535 nm should detect values up to 1. For slow color changeover another 2 min mixing was added.

With the subtraction of the blank measurement a standard curve was established and the samples could be correlated to nitrate values.

5.5 Light measurement

The Ocean optics STS-VIS spectrometer was used for wavelength analysis and setpoint adjustment at the LED-shaker platform and the Illumination system of the Infors bioreactors. The range of 350 - 800 nm was detected with each measurement. Due to its small size the spectrometer could be mounted in a custom made positioning device for reproducible measurements and multi point calibrations. Before measurement the spectrometer was plugged in to warm up for 20 min. At the Ocean View Software (version 1.5.2) a predefined measurement file (setting the wavelength range, calculation via simpson's rule) was loaded and a snap-shot of the background in darkness was set. To prevent saturation of the sensor a medium light setting of the following measurements was chosen and integration time was auto-adapted. Each measurement was performed with 20 scans averaged. The output parameter "PAR uMoles/m²/sec:6090014" displayed the actual light intensity (in µmol m^{-2} s^{-1}) averaged for these 20 scans in the wavelength range of 400 - 800 nm.

5.6 Cultivation Systems

As the studies presented here are all working with microalgae, the cultivation of these organisms is a major factor to consider when comparing experiments and results. Different cultivation systems have been used, differing mostly in cultivation volume, but also illumination mechanics and reactor geometry.

5.6.1 Illuminated Incubation Shaker

For cultivation in Erlenmeyer flasks with size of 100 mL, 500 mL and 1 L (for volumes between 10 ml and 500 mL) as well as and in 24-well-plates (Sarstedt TC-Plate 24 Well Standard F) a New Brunswick Innova 44 shaker (Eppendorf) was used. The shaker was equipped with a temperature control unit, which was until otherwise stated set at 25°C and the platform was set to 120 rpm with a deflection of 5 cm. As lighting unit, the inbuilt lighting system by Eppendorf attached to shaker´s ceiling was used, consisting of warm-white halogen lamps to illuminate the bottom of the shaker with an average value of 50 µmol m^{-2}s^{-1}. The shaker unit was used for the working culture collection, precultures and small scale shake flask experiments. With custom made mounts for 24 well-plates the parallel cultivation of up to 20 plates was possible. Each plate was aerated every two days to ensure CO_2 availability. In between aeration steps the plates were sealed airtight.

5.6.2 LED-Shaker

Lighting experiments with specific wavelengths or illumination values were possible with the use of a prototype-LED-shaker (FUTURELED). The shaker unit consisted of a water-cooled platform with 18 LED-sockets that could be installed in the New Brunswick Innova 44 shaker. The LED-sockets allow a bottom-up illumination of a 500 mL shake flask. The advantage of this system is that no shading effects from lids or other installations interfere with the light path and the irradiation can be individually set, for each of the 18 sockets on the platform. Every socket is equipped with 8 types of different LEDs (each type mounted 2 or 3 times) covering the whole PAR region and thus being able to mimic sunlight both as in spectrum and intensity. The base of the socket is a square borosilicate glass plate with 70 mm * 70 mm size. The LEDs are mounted approximately 2 cm below that glass plate (see Figure 10). With the standard irradiation angle of 120° the manufacturer tried to achieve an evenly illuminated surface despite the unequally spread LEDs, which unfortunately was insufficient. Illumination intensities of the socket were therefore calculated via a 5-point calibration system, a center point plus one point in each corner. The median irradiation level was then used to set the desired irradiation values. Peak wavelengths, as well as bandwidth

of the 8 types of LEDs installed are shown in Table 7. The LEDs are named after the peak wavelength; the SWW LED is a standard warm white LED with a very wide bandwidth. The maximum irradiation at single LED illumination is also shown. These values derive from the previously explained 5-point calibration. Figure 9 shows the wavelength intensities of the four LEDs used for growth experiments, the blue 425 nm, green 510 nm, red 680 nm and warm white SWW LED. The shown data was obtained with the ocean optic spectrometer as described in section 5.5.

Two identical shaker units were available in total, enabling 36 parallel shake flasks experiments.

Table 7: LED properties of the installed LED in each socket. Bandwidth displays the width at the base of the peak. SWW is a standard warm white LED. Peak λ as labelled by manufacturer, peak λ*, FWHM and max irradiation determined via spectrometer.

peak λ [nm]	peak λ* [nm]	FWHM [nm]	max irradiation [$\mu mol\ m^{-2}\ s^{-1}$]
425	**422**	**17**	**473**
455	441	17	1033
470	468	22	921
510	**527**	**91**	**868**
565	532	107	922
SWW	**645**	**163**	**1764**
680	**679**	**20**	**776**
740	733	32	23
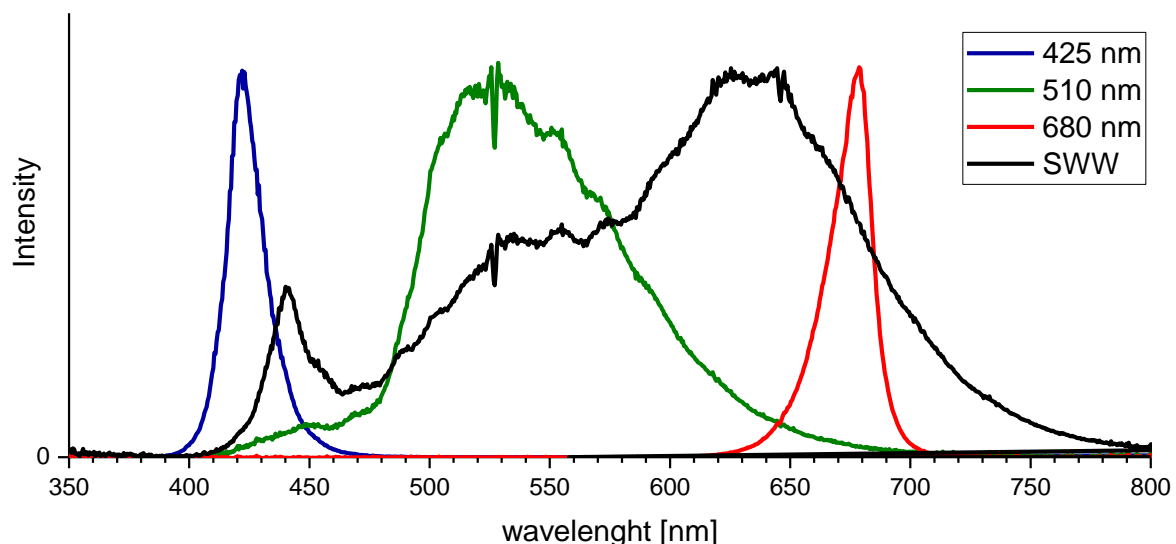
Figure 9: LED intensities (425 nm, 510nm, 680 nm and SWW) used for color growth experiments. Ocean optic spectrometer data normed to fit 425 nm peak.

5.6.3 Light setup and LED-shaker modifications for color experiments

Shaker aeration system

Shaker units equipped with the LED-platform were additionally improved with an aeration system powered by a DASGIP® MX4/4 mass-flow control unit. As shown in Figure 10 the aeration system was connected to the Erlenmeyer flasks.

.
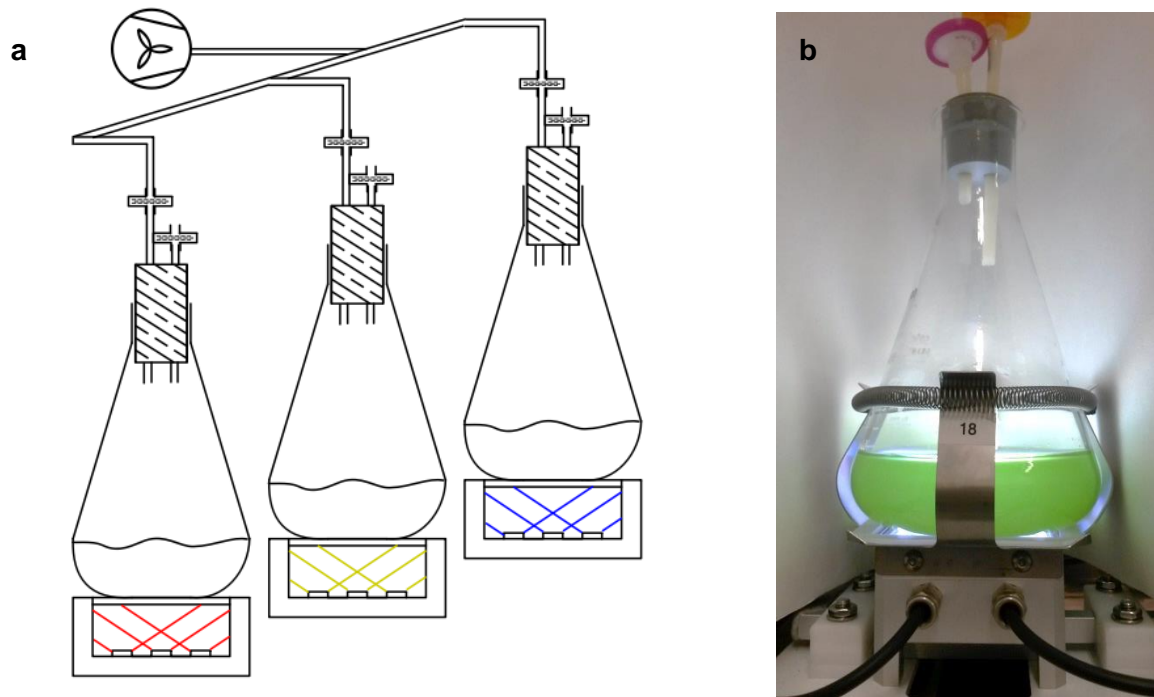
Figure 10: a) Graphical scheme of 3 individually illuminated LED-Sockets. Erlenmeyer flasks equipped with custom made, airtight stoppers equipped with sterile filters, attached to an aeration system (massflow control DASGIP® MX4/4), b) figure of one attached and illuminated flask

Each Erlenmeyer flask was sealed airtight with a custom made rubber-stopper where an air-inflow and exhaust-filter was attached. To ensure equal pressure and sterility, the air-distribution for the connected flasks used an air-inlet filter with a pore size of 0.45 µm, whereas the exhaust-filter only had 0.2 µm pores. The highest air-resistance appeared at the exhaust units (at the 0.2 µm pore-filter), ensuring equal distribution of the gas-mix system throughout all connected flasks. Nevertheless, for all experiments a maximum of 9 flasks were connected (usually just 6) to a single air-supply line. Figure 11 shows the installed air-distribution block which had two air-inlet sides (blue arrows at Figure 11 a). As air-supply line 1 and 5 are closer to the air inlet at the front and back than number 2 and 4, and accordingly outlet number 3, a growth analysis was conducted to evaluate any potential effects of unequal distributed air.

Figure 11 b shows the tremendous growth improvement of aeration compared to non-aerated flask with standard cotton caps (squares). The aerated flasks all showed very similar growth characteristics. All relative standard deviations of the individual curves are below 5 %. After combining all flasks, the maximum relative standard deviation of each time point

exceeds 5 % only thrice (at time point 1.7, 2.0 and 2.7) with a maximum of 8.34 %. After this short timeframe, relative standard deviation settles around 3.5 %. With this result an equal airflow throughout the 9 outlets was considered to be guaranteed.

a

b
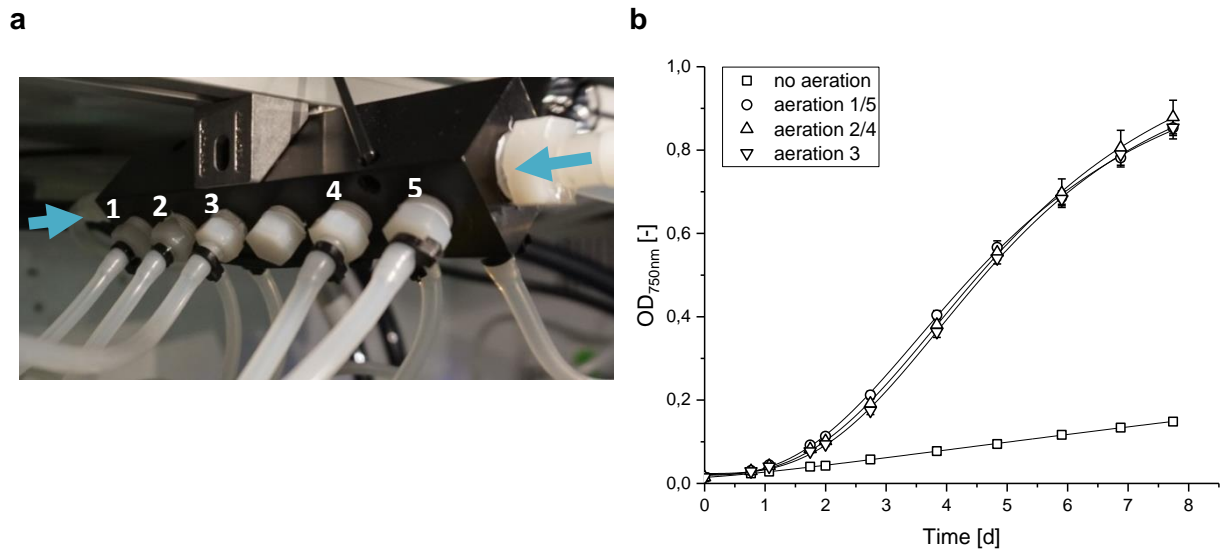
Figure 11: a) distribution system of the flask aeration system with 2 inlets (front and back, blue arrows) and 9 outlets total at both sides (5 visible on left side, 4 on the right side) b) growth comparison of aerated flasks (*Picochlorum* sp. at 120 rpm, 150 µmol m^{-2} s^{-1}, 31°C, aeration 6x headspace volume h^{-1} with 1% CO_2): aeration 1/5 (circles, n=8), aeration 2/4 (upward triangles, n=8), aeration 3 (downward triangles, n=2) and a non-aerated flask control (squares, n=1).

Aeration was set at all experiments at 1.8 nL h^{-1} per flask with 1 % CO_2-enriched air. This ensured a six-time air exchange per hour and flask. The setpoint of each air supply line was adjusted proportionally, depending on the number of flasks attached. At experiments performed in stage 2 the CO_2 –enrichment was set to 2 %.

Illumination system

To ensure that no cross-illumination occurred between different illuminated neighboring flasks, each flask was individually shaded by a black plastic-sleeve that was attached after installation on the LED-platform.

An overview of the color and irradiance-setup of the experiments performed with the LED-shaker is shown in Table 8. Stage 1 experiments were carried out with 3 irradiation intensities, 150, 100 and 50 µmol m^{-2} s^{-1}.

Table 8: Overview of LED-shaker experiments. Used illumination colors and irradiation intensities, strains and replicates for each experiment.

Setup	Stage 1	Stage 2	Stage 2	Stage 2
Colors	Blue, White, Green, Red	Blue, White, Green, Red	White, Green, Green+BPF, Green+LPF	White, Green, Green+BPF+LPF
Irradiation [µmol m^{-2} s^{-1}]	150, 100, 50	200	200	75

As illumination color the inbuilt blue 425 nm LEDs, white SWW LEDs, green 510 nm LEDs and red 680 nm LEDs were used. The properties of LEDs used for these experiments are shown in Figure 9 and Table 7. Stage 2 experiments focused on the illumination effects on *Picochlorum* sp.. Therefore additional alterations of the illumination systems were carried out. In order to reduce the wavelength width of the green 510 nm LED, two colored glass filter plates (LASER COMPONENTS GmbH, 2017) were attached to the LED-socket. The blue colored band-pass filter B 13 (BPF) and the orange colored long-pass filter O 540 (LPF) were sized 70 x 70 mm to fit on top of the LED-socket (shown in Figure 12 a). With a thickness of only 2 mm each, the plates were easy to attach with a negligible increase in distance between LEDs and bottom of the shake flask.
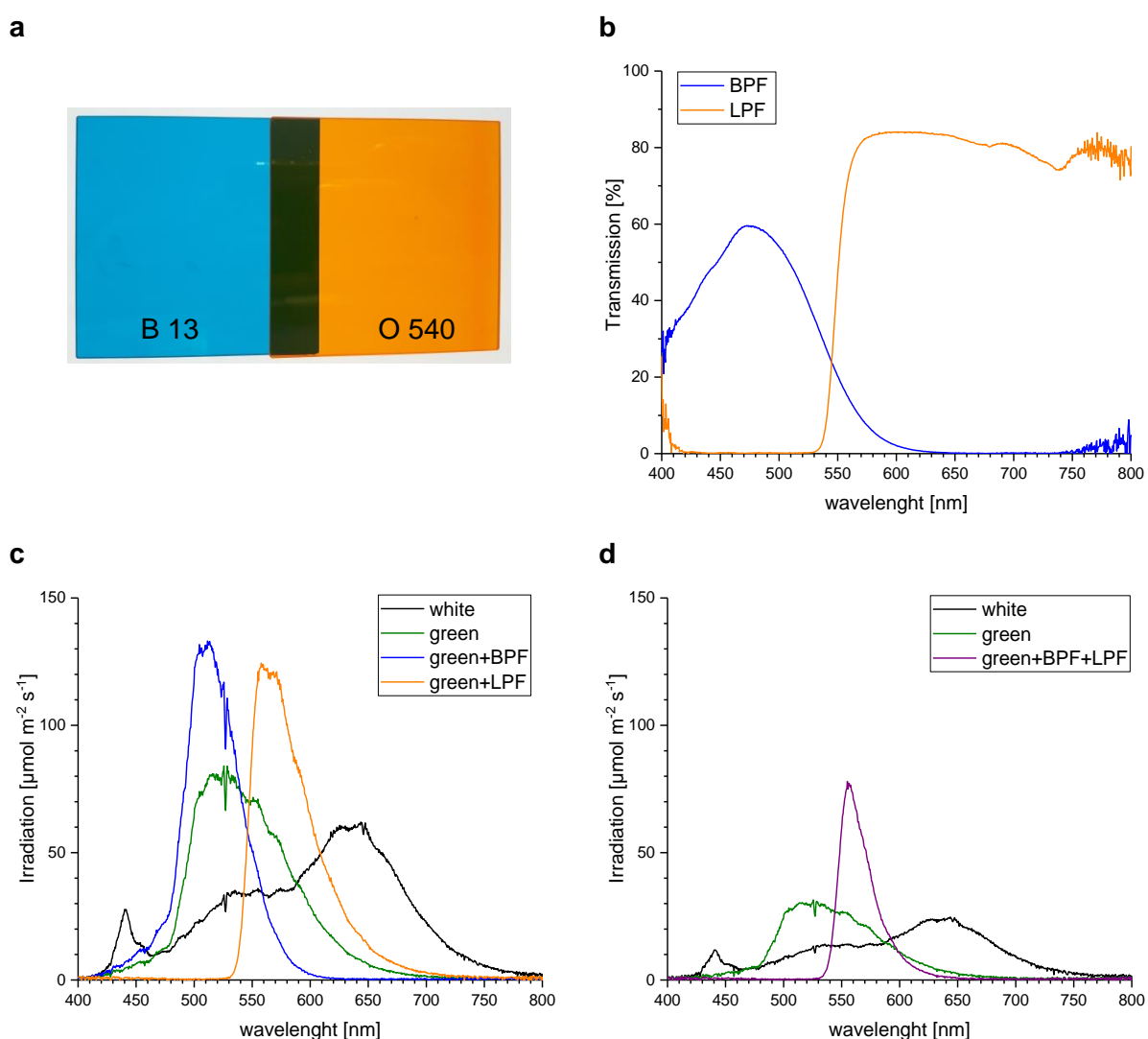
Figure 12: a) Colored glass filters: band-pass filter B 13 (BPF) and long-pass filter O 540 (LPF) (LASER COMPONENTS GmbH, 2017) **b) Transmission values of the BPF and LPF. Values obtained via warm-white LED illumination and ocean optic spectrometer measurement. c) Irradiation intensities of warm-white LED (SWW), green LED (510 nm), green LED with BPF and green LED with LPF at setpoint 200 µmol m^{-2} s^{-1}. d) Irradiation intensities of warm-white LED (SWW), green LED (510 nm) with BPF and LPF stacked at setpoint 75 µmol m^{-2} s^{-1}.**

Glass filter plates were chosen, because compared to interference filters the angle of incidence does not impair the performance. With the design of the LEDs in the socket (view

Figure 10 a) angles up to 60° occur on the bottom of the shake flask. The transmission efficiency of the glass filters is shown in b. Filters were chosen to limit transmission above 610 nm (BPF) and below 530 nm (LPF) in order to examine the wavelength-dependency of green illumination. In a combined experiment the two glass filter were stacked (view Figure 12 d) to obtain only illumination at wavelengths 530 – 610 nm. In this setup the warm-white LED (SWW), green 510 nm and green-yellow 565 nm LED had to turned on to maximum power to reach as high as possible irradiation levels. Irradiation levels were measured via the 5-point calibration described in section 5.6.2 and the resulting irradiation levels averaged at 75 µmol m^{-2} s^{-1}. This value was used to set the green (510 nm) and warm-white (SWW) LED.

5.6.4 Bioreactor system

Controlled environmental cultivations and upscale fermentations from shake flask experiments were done in Infors Labfors 5 Lux bioreactors (Figure 13). The stirred tank photo-bioreactor system is designed for algae, plant cells or cyanobacteria and could be used with a maximum culture volume of 2.5 L (for non-foaming cultures). Process control used the inbuilt touch panel or external software (Infors IRIS). Cultivations at high salinities (> 30 ppt) showed a tendency to block the aeration sparger within the first 4 days. A self-made Teflon sparger was used to circumvent changes of clogged sparger tubes. Standard cultivations were performed at temperature ranges between 21°C and 31°C and 150 rpm constant stirring speed was used.

Figure 13: The benchtop Labfors 5 Lux photobioreactor system by Infors. (Infors AG, 2017)

Fast settling algae strains or moss species were stirred with a reoccurring high velocity stirring interruption every hour (58 min at 150 rpm with 2 minutes at 800 rpm). Aeration was interlinked with pH regulation. A basic aeration of 0.5 vvm was achieved with pressured standard air via mass flow control units. Additional CO_2-aeration with a second mass flow control unit was added stepwise via an IRIS-process control software sequence. Exhaust air was cooled with 10°C water to prevent excessive evaporation and a BlueSense BlueInOne gas analyzer was used to measure O_2 and CO_2 levels leaving the reactor headspace. A sequence for a simple fermentation with 2.2 L reactor volume is shown in Table 9. More complex fermentations with day-night cycles (light and temperature) were also implemented via sequence control. In that case a mathematical formula, describing the diurnal changes for temperature and light intensities, need to be coupled with the setpoint regulation of the process control system.

Table 9: IRIS sequence for continuous fermentation with fixed setpoints on Infors stirred tank reactor.

IRIS sequence	functions
#0, Setup, 10	→ sequence repeat-time 10 sec
Light.sp=20	→ setpoint 20 = 100 µmol m^{-2} s^{-1}
Temp.sp=25	→ 25°C
pH.sp=8.00	→ pH = 8
Air_Flow.sp = 1.1	→ aeration 0.5 vvm = 1.1 nL min^{-1}
if(pH.v>pH.sp){CO2_Flow.sp=CO2_Flow.sp+2}	→ stepwise increase of CO2 in increments of 2 up to max. 100 mL min^{-1}
if(pH.v<=pH.sp){CO2_Flow.sp=0}	→ CO2 flow set back to 0 if pH value falls below setpoint

Two electrodes, one for pH measurement and one for dissolved oxygen were used, which needed a 2-point calibration prior to assembly (pH) and a 1-point calibration (dissolved oxygen) to 100% saturation before inoculation. The glass fermenter was fully assembled and autoclaved with all electrodes attached and media filled. Sterile sampling was ensured with a custom made sampling tube connected to a metal 3-way stopcock. Via an attached 0.45 µm PTFE sterile filter the sampling tube could be drained prior to sampling to avoid extraction of clogged biomass or unlighted media residues from within the immersion sampling-pipe. The stirred tank was surrounded by a cylindrical frame containing warm white LED-strips with a total irradiation intensity of up to 700 µmol*m^{-2}s^{-1}.

5.6.5 Illumination system for Infors bioreactors

Upscale experiments carried out with the LED-shaker system described in section 5.6.2 used the Infors bioreactor system as described in section 5.6.3. The equipped warm-white LED strips in the Infors system were insufficient for the upscale of single-wavelength experiments performed in the LED-shaking system. Therefore an external illumination system (see

Figure 14) was used. The system contained the same LEDs as the LED shaker (view Table 7). All LEDs were attached in six long strips in the inner cylinder. With all LEDs set to max level the water cooled illumination system reached illumination levels up to 8000 µmol m^{-2} s^{-1}.

a

b

c

Y=a + b*x	SWW	510 nm
a	89,390 ± 1,93	84,850 ± 1,56
b	0,745 ± 0,007	0,586 ± 0,006
RSQ	0,998	0,998
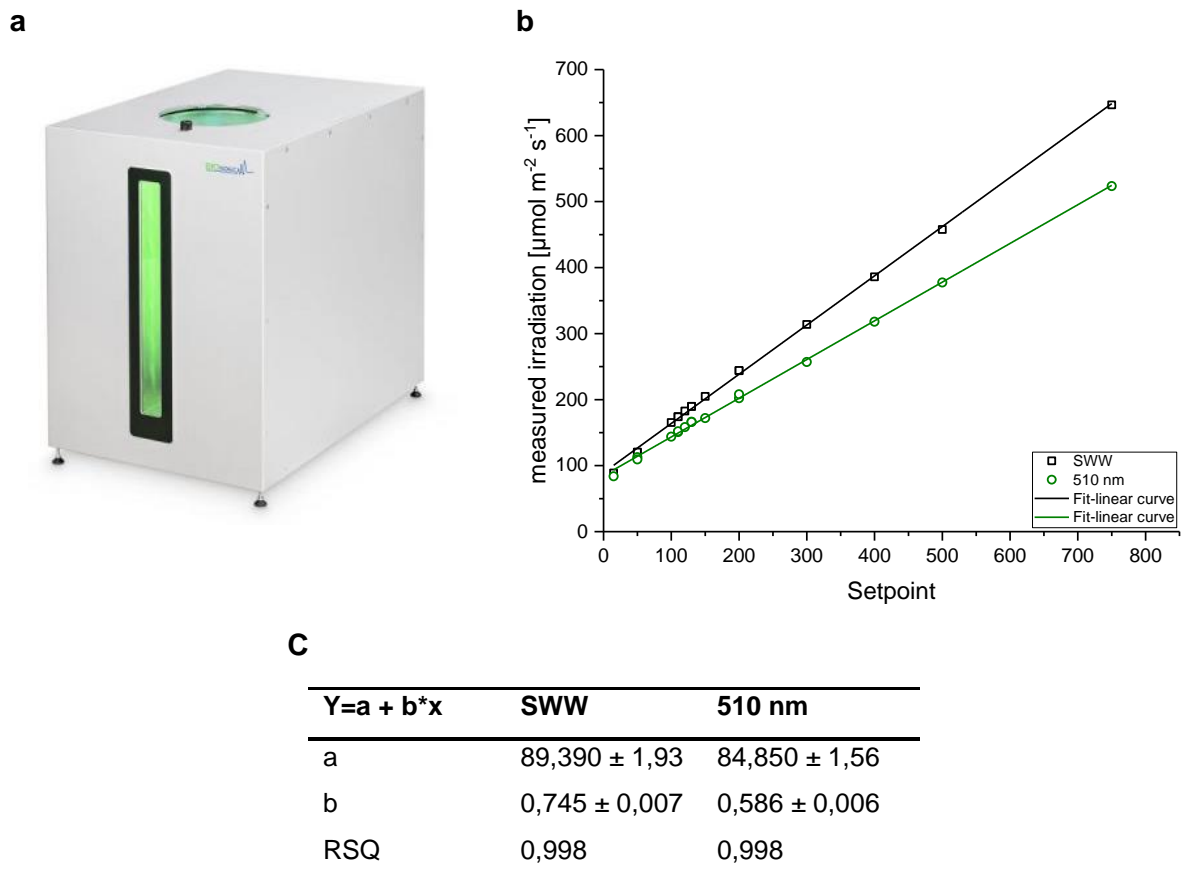
Figure 14: a)The retro fit-illumination system for stirred-tank bioreactors by biospec (BIOspec GmbH, 2017)**, b) calibration curve and line fit for the inbuilt warm white LED (SWW) and the green 510 nm LED, c) line fit data points and RSQ**

The basic control software allowed constant illumination or programmable ramps for day-night changes. For the single LED illumination a manual calibration of each LED-type was needed and conducted with the ocean optic spectrometer described in section 5.5. The calibration was conducted with an average of 20 scans and an integration time of 1007 ms. The spectrometer was placed inside the illumination cylinder and turned manually during the calibration measurement.

5.6.6 Bubble column system

For the generation of large biomass (up to 30 L) a larger scale bioreactor than the Infors system was needed.

An airlift bubble column was constructed for the low tech generation of biomass. A 200 mm acrylic glass cylinder (inner radius r_{1i} = 96 mm) with 4 mm thickness was connected to a bottom plate via a rubber-sealed connector tube to create the reaction vessel. With a total height of 1300 mm the disconnection possibility at the bottom plate enabled easy access to all inner surfaces for easy cleaning. An inner acrylic-glass cylinder with 150 mm diameter (inner radius r_{2i} = 72 mm) was chosen to function as air-flow riser. The ratio r_{BC} of riser and down-comer was chosen to be r_{BC} = 0.69 according to equation (5)

$$ r_{BC} = \frac{\pi * (r_{1i}{}^2 - r_2{}^2)}{\pi * r_{2i}{}^2} \qquad (5) $$
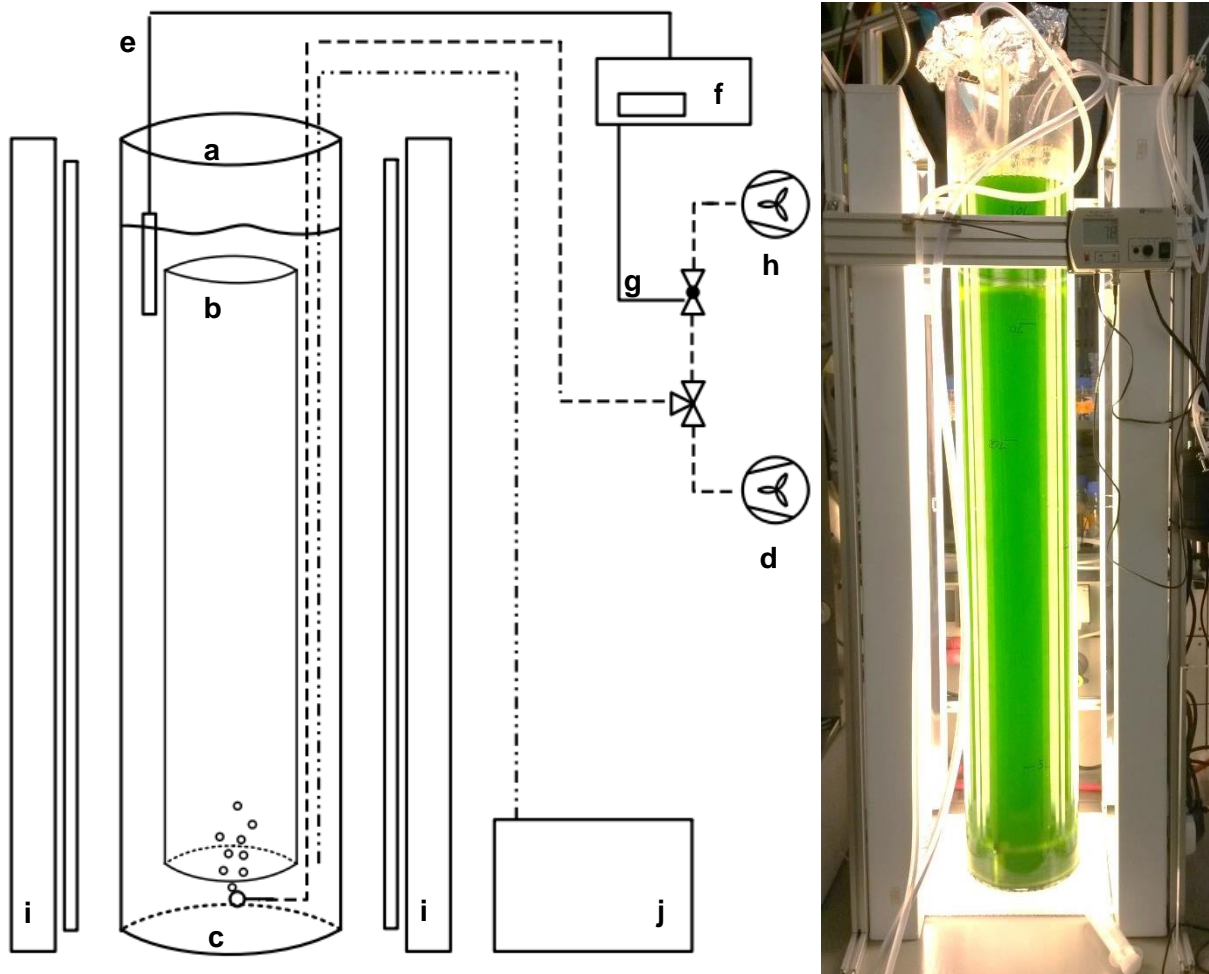
Figure 15: Controlled bubble column setup. a) outer column, b)inner column =riser, c) aeration nozzle, d) air pump, e) pH electrode, f) pH control unit, g) controlled solenoid valve, h) CO₂ supply i) lighting system, j)air-water cooling unit

With a 3D-printed ABS-support structure the inner cylinder was placed centered 100 mm above the bottom of the bubble column. The inner cylinder was placed in the outer cylinder with the use of 3 aluminum tubes that were used to fixate the 3D-printed support structure at the top and bottom of the inner cylinder. Two aluminum tubes were connected at the bottom to create a closed-loop temperature regulation system. The temperature setting was achieved via an air-water-cooling system with integrated water pump that could be set to temperatures between 10 and 30°C. The aluminum tubes allowed a good temperature transfer-rate between the culture volume and the cooling fluid. To compensate room temperature and the temperature influx of the lighting system, an empirically obtained setpoint of 20°C resulted in an average temperature of 25°C in the culture. The third aluminum tube was used as aeration tube for the attached sparger at the bottom center of the bubble column. For aeration an air pump (EHEIM Air 400) with 400 L h^{-1} airflow was used. pH regulation was achieved with the MC122 pH-Controller by Milwaukee. The sensor was placed at the top of the bubble column. The pH was set to 8.5. If the pH rose above the set value an attached solenoid valve opened and 100 % CO_2 was added to the airflow until the pH at the top of the column dropped. A system wise delay (CO_2 bubbles travel up inside the riser, gas-exchange, formation of HCO_3 and the resulting pH drop) at the pH sensor resulted in a pH-value of pH 8 - 8.5. The CO_2 flow was empirically reduced with a pressure valve to obtain the pH-range of just 0.5. Figure 15 shows the general setup. The constant illumination system was designed with eight 1.2 m halogen lamps. With this bubble column system and a cultivation volume of 30 L a biomass concentration of 1 g_{DW} L^{-1} could be cultivated within 10 days. At this point the culture was light limited and growth rates drastically declined. With better illuminations (such as inner illumination with lighting rod to reduce culture thickness) higher biomass concentrations were possible.

5.7 HPLC Analysis of Pigments

Working with pigments is a delicate task as they are light and temperature sensitive and even extracted and stored at 4°C the major pigments degrade an average of -0.7 % d^{-1} for acetone and -6.0 % d^{-1} for methanol as main solvent (Hooker *et al.*, 2005). Therefore, all work concerning pigments, beginning with the sample-extraction was performed on ice and in dark environment. Light-shielding was achieved by wrapping extraction tubes in aluminum foil, working with iceboxes with lids and dimming or shutting of the light during extraction steps.

5.7.1 Pigment sampling

Pigment extraction for HPLC determination was adapted from (*Phytoplankton Pigments: Characterization, Chemotaxonomy and Applications in Oceanography*, 2011).

For each sample 10 - 15 mg dry weight was utilized. Depending on the density of the culture this equals a culture volume of around 3 – 15 mL, therefore the standard sampling procedure was carried out in 15 ml falcon tubes. The samples were centrifuged (Eppendorf centrifuge 5810 R) at 10.000 rpm for 10 min. To remove any traces of salt, which might interfere with the HPLC analysis, the pellet was washed once with 10 mL dH$_2$O. After the complete removal of supernatant, the pellet was frozen and stored at -20°C in darkness.

5.7.2 Pigment extraction for HPLC Analysis

Samples taken for pigment extraction as described in section 5.7.1 were stored until timely HPLC analysis and only then freshly extracted. As before, all steps were carried out in darkness and on ice. The falcons were put on ice to thaw slowly for 30 min prior to extraction with 90 % (v/v) HPLC-grade acetone in dH$_2$O. Each pellet was resuspended with 2 mL acetone and promptly transferred in a precooled 10 mL glass-falcon tube with solvent proof screw-top lid. With further 2 mL acetone the falcon tube was washed to retrieve all from the pellet. Two 5 mm glass beads were added and in order to break open the cells the glass-falcon was vortex-mixed for 10 seconds. After 20 min of ultrasonic extraction in an ice-chilled waterbath the samples were vortex mixed again for 10 sec. Pigment extracts were stored over night at -20°C. After slowly thawing for 30 min on ice and another 10 sec shake on the vortex mixer the pigment extract was transferred in a 2 mL syringe and filtered through a 0.2 µm PTFE filter directly in GC-vials. The vials were transferred straight into the shaded HPLC autosampler with 4°C or wrapped light proof and stored temporarily at -20°C.

5.7.3 HPLC Measurements

The HPLC analysis protocol was adjusted from a tetrabutylammonium hydroxide-based method described by Van Heukelem (Van Heukelem and Thomas, 2001) due to its high separation efficiency for pigments. A YMC-Pack Pro C8 Column (250 mm * 4.6 mm I.D.) with 5 µm particle size was used in a HP Agilent 1100 HPLC-System equipped with a diode array detector (Agilent 1100) operating at 450 nm. The two buffer system, consisting of buffer A: 30:70 % (v/v) water / methanol (dH$_2$O and HPLC-grade methanol) and butter B: 100 % methanol, were set to the gradient shown in Figure 16. A flow of 1 mL min^{-1} and 10 µL injection volume was applied; oven temperature was set to 60°C and the shaded autosampler was kept at 4°C. Chromeleon 6.80 SR12 software (Thermo Fisher Scientific) was applied to control the HPLC system and for post-experimental analysis.
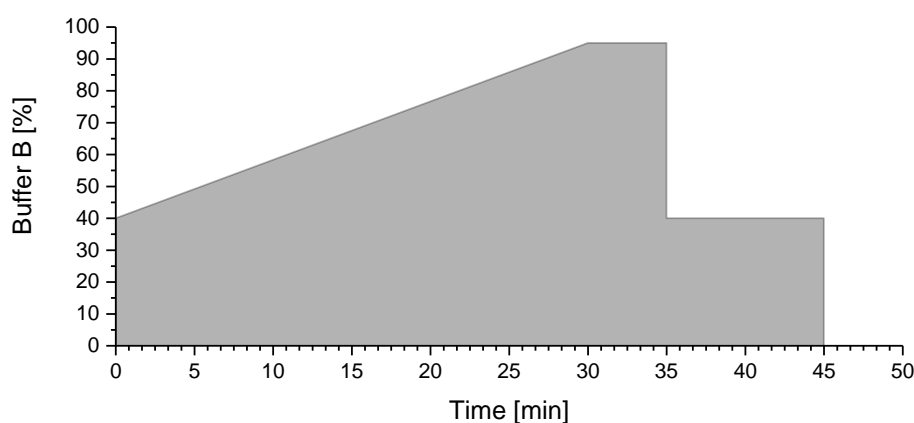
Figure 16: HPLC Gradient for pigment analysis. Proportion of buffer B (100 % methanol) during analytical cycle.

5.7.4 Pigment standards

Pigment standards were obtained from Carote*Nature* GmbH and Sigma-Aldrich Chemie GmbH in HPCL grade quality. The full details are shown in appendix VI at page 147 of this work. Table 10 shows the 10 pigment standards that were used for this work and the respective solvent they were dissolved in. The retention time refers to the HPLC method described in section 5.7.3

Table 10: Used pigment standards for this work, solvent and retention time and main absorption peaks in methanol (*Phytoplankton Pigments: Characterization, Chemotaxonomy and Applications in Oceanography*, 2011)

Pigment standard component	solvent	Retention time [min]	Main absorption λ_{max} [nm]
Neoxanthin	100 % ethanol	12.25	413, 438, 466
Violaxanthin	100 % ethanol	13.21	415, 436, 466
Astaxanthin	100 % acetone	13.82	470-472
Zeaxanthin	100 % ethanol	19.17	(429), 449, 475
Lutein	100 % ethanol	19.44	(422), 443, 470
Cantaxanthin	100 % ethanol	21.30	468
Chlorophyll *b*	90 % acetone	26.87	469, 603, 652
Chlorophyll *a*	90 % acetone	30.68	432, 618, 652, 665
γ-Carotene	100 % acetone	34.78	461, 491
β-Carotene	100 % acetone	36.15	449, 475

To identify pigment peaks single runs were carried out and compared to unknown pigment peaks via retention time and UV-VIS spectra. For quantification a pigment mix with defined standard concentrations was prepared and injected several times with various inoculation volumes. The resulting peak areas were normed to the injection volume and correlated to the inserted concentrations as shown in Table 11. As expected (Hooker *et al.*, 2005) the standard solutions degraded over time. Especially chlorophyll *b* degraded quickly and therefore the correlation factors were used to calculate actual pigment contents in the samples.

Table 11: Correlation factors for HPLC-Pigment quantification. The initial concentration used for the standard curve, the resulting area with standard deviation and the calculated correlation factor used for pigment analysis.

Standard component	Initial concentration [µg mL^{-1}]	Peak area [(mAU min) µL^{-1}]	Relative standard deviation	Correlation factor [ng (mAU min)$^{-1}$]
Neoxanthin	6.67	0.576 ± 0.013	2%	11.573
Violaxanthin	6.67	1.048 ± 0.041	4%	6.367
Astaxanthin	6.67	0.254 ± 0.010	4%	26.281
Zeaxanthin	10.00	0.487 ± 0.021	4%	20.527
Lutein	10.00	1.538 ± 0.039	3%	6.501
Cantaxanthin	66.67	1.766 ± 0.023	1%	37.759
Chlorophyll *b*	33.33	0.622 ± 0.030	5%	53.578
Chlorophyll *a*	6.67	0.108 ± 0.006	5%	61.616
γ-Carotene	6.67	0.360 ± 0.023	6%	18.539
β-Carotene	4.00	0.201 ± 0.014	7%	19.950

5.8 Pigment identification

Pigment identification was performed with a combination of different methods described in previous sections. As first step the HPLC analysis provided a number of pigment peaks that were correlated to commercially available standard components by matching retention time and UV-VIS spectra. Additionally, all pigments identified with this method were compared to literature data. Unknown peaks were fractioned and concentrated and analyzed with high resolution LC-MS/MS. The method allowed an allocation of the unknown pigment with a mass-structure. The UV-VIS spectra or absorption spectra allowed a broad classification towards possible pigment classes such as chlorophylls, xanthophylls or carotenes. The fragmentation in the MS and MS/MS mode allowed a more accurate outlook on the potential chemical backbone structure. NMR analysis was used to verify suspected pigment structures.

5.8.1 High resolution LC-MS/MS measurement and analysis

The extracts were vacuum-dried in a GeneVac Atlas Evaporator HT4 by GeneVac and resolved in small volumes of 100% acetonitrile (HPLC Grade) (e.g. 1.5 mL extract dissolved in 300 µL). To separate the pigments the previous described HPLC-method (see 5.7.3) was applied and the components of interest were collected manually. 100 µl of the resolved extracts were injected. The collected fractions were kept in darkness on ice. Pooled fractions were vacuum-dried and stored for further measurements in darkness at -20°C.

High resolution LC-MS/MS was performed at the central analytics Lab of the Department of Chemistry. A LTQ-FT mass spectrometer by Thermo Fisher Scientific with an UltiMate3000 HPLC-System was used to perform these experiments. The used solvents were for A water and for B 90 % (v/v) acetonitrile in dH_2O, both with 0.1 % formic acid. A flow of 1.1 ml min^{-1} of 80% B and 1 µl injection volume was applied. The autosampler was kept at 15 °C and the oven temperature was set to 22°C. No column was used; the injected sample was analyzed directly. The Full-scan mass spectra for a range of m/z 210 – 1500 were acquired in positive mode with a resolution of 100,000 (m/z 773.49). MS/MS analysis was obtained with CID (collision induced dissociation) using helium with a CE (collision energy) of 35 %. Xcalibur a Thermo Fisher Scientific Software for MS analyzes (software version 2.2.SP1.48) was used for the identification of the unknown pigments. For the peak identification process a range of potential atom types (such as carbon, oxygen, nitrogen, hydrogen and magnesium) and the quantity of these atoms was implemented. For Chlorophyll *a* with a mass formula of $C_{55}H_{72}MgN_4O_5$ the input parameters were used as shown in Table 12. The high resolution LC-MS/MS allowed working with a critical mass tolerance of 1 ppm. Peaks were identified with specific masses containing 5 decimal places whereof the first 3 were used to match. The software thus delivered the measured mass, combined with a possible elemental formula

within the previously set range (Table 12) and a conformity value in ppm. This conformity value describes the difference between the calculated molecular mass of the matched chemical formula and the actual measured mass. Any peak identification with lower probabilities of 1 ppm was considered a positive match.

Table 12: Input parameters of elemental composition for HR-LC-MS/MS analysis of Chlorophyll *a* ($C_{55}H_{72}MgN_4O_5$)

Isotope	Min	Max	Mass
14 N	4	6	14.003
16 O	4	6	15.995
12 C	52	58	12.000
1 H	70	76	1.008
24 Mg	0	2	23.985

5.8.2 NMR spectroscopy of unknown pigments

Nuclear magnetic resonance (NMR) spectroscopy was performed on a Bruker AV500 Avance-I with TopSpin 2.1 software at central analytics lab of the TUM department of chemistry. As solvent acetone-d_6 (99.9 atom % D) by Sigma-Aldrich was chosen to match results with recent literature publications (Kobayashi *et al.*, 2013). The same samples used for LC-MS/MS analytics (see section 5.8.1) were analyzed. Samples were placed on ice and the acetonitrile solvent was evaporated with nitrogen ventilation. Dried pigment samples were resuspended in 120 µL acetone-d_6 and transferred in a micro-NMR-tube. The NMR-measurement lasting up to 36 hours was possible without interference due to evaporation processes. The micro-NMR-tubes were sealed with the appropriate sample spinner and shaded until positioning inside the AV500. A minimum sample mass was supposed to be 1 mg$_{DW}$ or higher.

For all samples the ^{1}H (128 – 2048 scans) and COSY spectrum (16 – 128 scans) was recorded. Highly concentrated samples additionally allowed HSQC (128 – 196 scans) and HMBC (196 scans) analysis.

Figure 17 shows the chemical structure of chlorophyll *a*, and the section of chlorophyll *b* (Figure 17 b) where the two structures differ in the oxidized side chain at carbon atom number 7. Carbon atoms are numbered according to IUPAC system. The phytol sidechain is labeled P1-P16. Data analysis was performed with the MestReNova Software (version 11.0.3-18688). All data files were normed alongside the f1 axis to the acetone-d_6 peak at a shift of 2.050 ppm. An apodization or line correction was performed in the course of the Fourier transformantion with an exponential function set to 6.60 Hz in order to reduce noise. This was very useful for peak integration and comparison of runs. Nevertheless, for peak identification lower values around 0.10 - 1.30 Hz were used to identify multiplets or impurities.
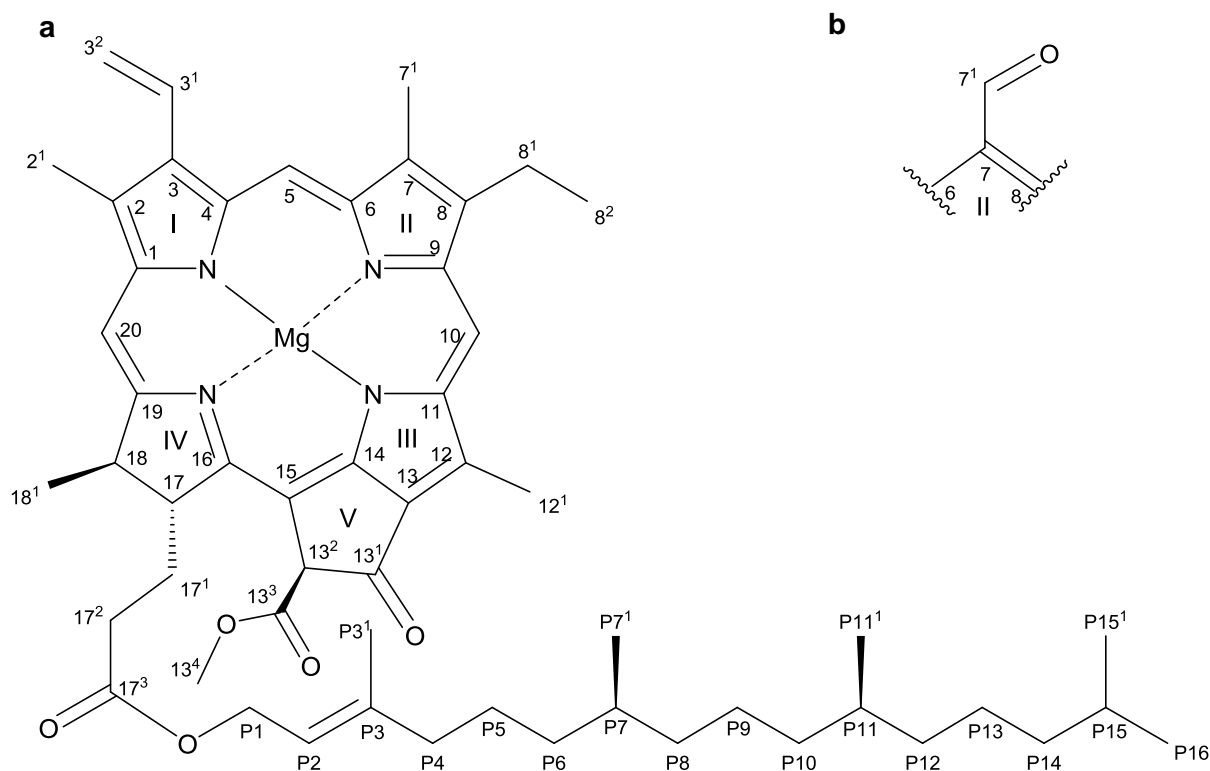
Figure 17: a) Chlorophyll *a* with IUPAC numbering of carbon atoms. b) Section of Chlorophyll *b* showing the oxidized residue at carbon atom 7[1] (Abraham and Rowan, 1991)

Multipoint-baseline correction was obtained manually to alter upfield values and identify peaks. The chemical shift in the ^{1}H spectra were correlated to literature data (Kobayashi *et al.*, 2013), starting from the known structural data of Chlorophyll *a* and *b*. For the unidentified peaks known to be similar to the chlorophyll *a* or *b* an integration of the distinguished downfield peaks 10, 5, 20 and 3[1] for chlorophyll *a*, respective 7[1], 5, 10, 20 and 3[1] for chlorophyll *b* were conducted. Comparison to the integrated peak area of the P2-shift allowed an estimation of additional double-bond numbers in the chemical structure. Although ^{13}C signals were very close to the limit of detection, beside COSY also HSQC data were used to confirm [1]H-chemical shifts if the signal was exploitable.

5.9 Lipid Analysis

5.9.1 Sample preparation

Lipid extraction was adapted from the protocol described by Griffith et al. (Griffiths, van Hille and Harrison, 2010). The protocol describes an alkaline and acidic transesterification and extraction of fatty acid methyl esters (FAME). Lipid samples were washed once with dH_2O and frozen for lyophilization (see section 5.2.1). 10 - 20 mg lyophilized biomass was weight in a screw-top glass tube. 500 µL C12-TAG-toluene solution (0.2 mg mL^{-1} glyceryl tridodecanoate in toluene used as internal standard for methylation and extraction) was added and thoroughly mixed. 1 mL of 0.5 M sodium methoxide/methanol solution was added and shaken at 900 rpm for 20 min. at 80°C (HLC Heating-ThermoMixer MHR 23 by Ditabis AG). Subsequently 1 mL of a 5 % (v/v) HCl in methanol was added and mixed again at 900 rpm for 20 min. at 80°C. For lipid extraction the tube was filled with 400 µL dH_2O, 400 µL hexane and vortex mixed. After phase separation 200 µL of the organic phase were transferred into gas-tight GC-vials. To reduce vapour pressure all steps were carried out on ice.

5.9.2 GC-FID

To analyze FAMEs a Shimadzu GC-2010 Plus gas chromatograph with flame ionization detector (FID) was used. 1 µL sample was injected via an AOC-20i auto injector (Shimadzu) on to a Phenomenex ZB-WAX column (length 30 m, 0.32 mm ID, 0.25 µm df). The injector and FID temperature was hold at 240°C and 245°C respectively. Initial column temperature was hold at 150°C for 1 min. With a linear temperature gradient the column was heated up with 5°C min^{-1} to 240°C maintained for 5 min. Hydrogen was used as carrier gas with a flow rate of 3 mL min^{-1} and constant flow compensation. Fatty acids were identified via comparison of retention times to FAME Marine Oil Mix Standard (Restek GmbH), containing 20 components from C14:0 up to C24:1.

5.9.3 GC-MS

The qualitative analysis of FAMEs was performed on a GC-MS (Thermo Fisher Scientific Trace GC Ultra equipped with a DSQII mass spectrometer). A Stabilwax-MS column (length 30 m, 0.25 mm ID, 0.25 µm film, Restek) was loaded with 1 µL sample volume. Initial column temperature was 50°C and maintained for 1 min increased via linear gradient (4°C min^{-1}) up to 250°C. The final temperature was maintained for 9 min. the Injector temperature was set to 250°C. MS data collection was carried out at 70 eV (EI) with an Ion source temperature of 250°C. The m/z range was recorded from 50 up to 650. The Marine Oil Standard Mix was also used as standard reference in addition with mass spectra correlation to NIST database.

5.10 FACS Cell Sorting

For fluorescence activated cell sorting (FACS) the Biorad S3 cell sorter was used. The sorter was equipped with a standard 488/6 nm laser and two detector filters at 588/24 nm (FL1) and 700/70 nm (FL2). The laser light was deflected via two dichronic longpass (DLP) filters, a 555 DLP and a 610 DLP. For each strain a specific protocol was established to ensure that the FACS scatter plot was within the range of detection. Via the photomultiplier tubes (PMT) adjustments of forward scatter (FSC), side scatter (SSC), as well as FL1 and FL2 were chosen. The threshold was adjusted after each startup to prevent detection of impurities in the system and ensure maximum cell detection. Therefor a test-run with water was carried out after the first setup run with biological samples. An extended startup with QC (quality control) via standardized sorter beads was carried out prior actual cell sorting steps. If the sorter was just used as analyzer to count cells, no QC was carried out.

For contamination checkups and strain purification work a specific sort-gate was set around the scatter plot. The contaminants or the desired cells within the scatter plot were then sorted in 1.5 mL eppendorf tubes or 96-well strips, filled with sterile media.

The cell sorter was also used for counting cells and preparation of precultures with a predefined cell concentration. Cellcounts within experiments delivered a second possibility to evaluate cell growth with better resolution and accuracy then optical density measurements. The drawback of this method was the higher time and effort for each sample point. All cellcount analysis was carried out in triplicates. The cell culture was diluted to an optical density between $OD_{750\ nm} = 0.5 - 2$ to prevent throttling of the cell sorter due to excessive counts per second in order to ensure a reasonable duration of less than 2 min for each sample. The cell-dilution was filtered with the standard filter caps and 100 µL were transferred in a clean and dry sample tube. The strain specific protocol was carried out with 40 – 80k counts per second until a bubble was detected in the sorter tube, indicating that all 100 µL were counted. Values were then multiplied by dilution factor and averaged to obtain the cellcount [cells mL^{-1}].

The same protocol was used in order to set up a specific cell concentration. Mutagenesis experiments were usually started with an initial count of $10^6 - 10^7$ cells mL^{-1}. A cultivation in exponential growth phase was used and the cellcount was analyzed in triplicate as described above. The required preculture volume was calculated as shown in equation (6) and the remaining volume was filled up with fresh media. A ratio of around 10% preculture in 90% fresh media was desired.

$$preculture\ volume[mL] = \frac{(desired\ conc.\,[cells\ mL^{-1}] * desired\ volume\,[mL])}{preculture\ cell\ count\,[cells\ mL^{-1}]} \quad (6)$$

5.11 Mutation procedures

New mutation procedures were tested and compared to traditional methods that have been reported for microalgae.

5.11.1 UV

Physical treatment of microalgae cells was performed with UV radiation as mutagenic agent. Several methods have been described in literature (Lanfaloni *et al.*, 1991; Manandhar-Shrestha and Hildebrand, 2013; Lim *et al.*, 2015) and were adapted for *Picochlorum* sp. Two UV-Lamps were tested ($UV_{254\,nm}$ and $UV_{366\,nm}$) with varying distances to the surface (20, 30 and 40 cm) and durations between 0 min and 60 min. Cellcounts between 10^5 and 10^7 cells mL^{-1} were altered, as well as cultivation vessel (96-well plate, 24-well plate, 6-well plate and 2 mL eppendorf tube) after treatment. Best results were obtained with the $UV_{254\,nm}$ lamp at a distance of 30 cm. Cell suspensions of 10^6 cells mL^{-1} (for some experiments 10^7 cells mL^{-1} were also used) were treated in 1 mL drops on a petri dish. After treatment all volume was extracted and transferred in 24-well plates and kept dark for 24 hours. Cultivation was executed at 150 rpm at 50 µmol m^{-2} s^{-1} irradiation with aeration steps every 2 -3 days. Growth rate determination was performed via OD-measurement at the plate reader or via cellcounting with the FACS cell sorter.

5.11.2 EMS

Ethyl methanesulfonate (EMS) mutagenesis was adapted for *Picochlorum* sp. from the protocol described for *N. salina* by Doan and Obbard. (Doan and Obbard, 2012). Cells in exponential growth phase (5 days) were set to a cell concentration of 10^7 cells mL^{-1} as described in section 5.10. Random mutagenesis was performed via exposure to different concentrations of EMS (0.0 M, 0.2 M, 0.4 M, 0.6 M, 0.8 M, 1.0 M and 1.2 M). Incubation lasted for 1 h in darkness at agitation of 300 rpm. After centrifugation (10 min at 8000 rpm) the pellet was washed thrice in sterile 10% (w/v) sodium thiosulfate solution. Following the last centrifugation step the pellet was resuspended in *Picochlorum* media (see section 5.1) and distributed in 1 mL aliquots and cultivated in 24-well plates.

5.11.3 ARTP Plasma

The novel use of atmospheric and room temperature plasma (ARTP) was shown with *Spirulina platensis* (Fang *et al.*, 2013) and has been described to work with bacteria and fungi (Zhang *et al.*, 2014). This method has never been tried with submerged cells in liquid phase, as the described methods worked with metal plates onto which the dried cells were

treated. The plasma tool used for these experiment, the Piezobrush PZ2 (2016 model) was provided by Relyon Plasma GmbH, Regensburg, Germany (see Figure 18). The handheld plasma tool was equipped with a multiple gas nozzle allowing the use of several carrier gases. The objective was to test several carrier gasses and treatment durations on the microalgae *Picochlorum* sp. and if successful screen for fast growing mutant strains.
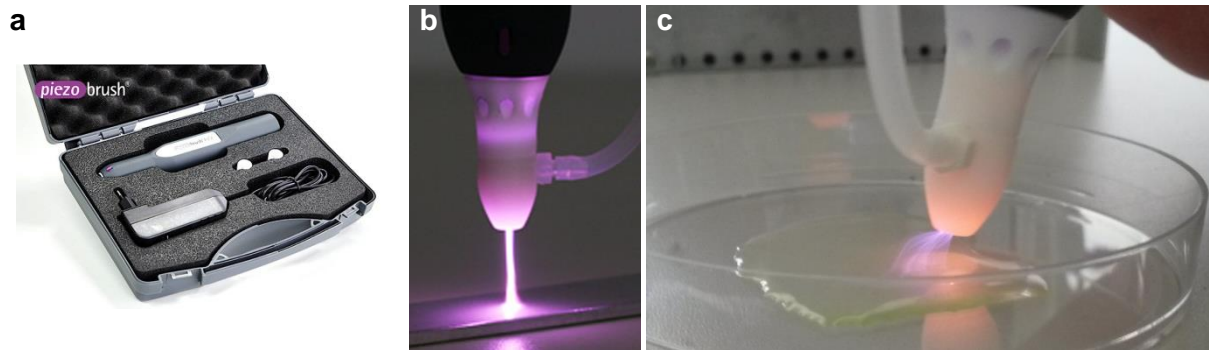
Figure 18: a) Piezobrush PZ2 (2016 model) by Relyon Plasma GmbH used for the ARTP treatment. b) multigas & needle nozzle (Relyon Plasma GmbH, 2017) c) plasma treatment of *Picochlorum* sp. on surface activated petri dish.

Plasma treatment was tested on 1 mL microalgae-solutions on surface activated petri dishes. To activate the surface, the plasma torch was moved evenly spread over the inside of a petri dish for one minute. Aside sterilization this surface activation led to reduced surface tension on which the 1 mL microalgae solution spread out thinly. Several carrier gasses were tested with various durations and flow rates (see Table 13). Microalgae cells (5 day culture) of *Picochlorum* sp. in exponential growth phase were set to a cellcount of 10^7 cells mL^{-1} via FACS counting. 1 mL culture was placed in the petri dish and the nozzle of the plasma torch was moved with a distance of a few millimeters evenly over the spread out cell solution for the assigned duration. In total 10 experiments were conducted and the cell solution was transferred in sterile Eppendorf tubes and kept in darkness for 24 h to prevent photo repair. Cell volumes were split up in 100 μL aliquots in a 24-well plate and filled up with 900 μL fresh media. Initial survival screening was carried out for 3 weeks.

Table 13: Variation of carrier gas, duration and flow used for plasma treatment of microalgae cells. Varigon®H2 = 98% argon + 2% helium

Carrier gas	Duration [min]	Flow [nL min^{-1}]
process air	0, 1, 2, 4, 6, 10, 15	1
Varigon®H2	2	1, 3
helium	2	1
process air	2 (on brass plate)	1

Screenings for fast growth were performed for 40 days with 3 recultivation steps and a follow-up screening of the 12 fastest growing mutant strains for an additional 21 days with one recultivation step in between.

5.11.4 Fast neutrons

Fast neutron mutagenesis experiments were conducted at the Research Neutron Source Heinz Maier-Leibnitz (FRM II) facility of the Technical University of Munich in Garching, Germany. The nuclear research reactor produces free neutrons through uranium fission that can be utilized for numerous scientific experiments. One meter from the reactor core a secondary source (converter facility, see Figure 19) consisting of two uranium plates produces very fast fission neutrons that are guided through beam tube number 10 (SR-10) to the MEDAPP instrument (FRMII, 2017). MEDAPP with a neutron flux density of approximately 3.2×10^8 cm^{-2} s^{-1} can be used for tumor treatment and physical and biological dosimetry.
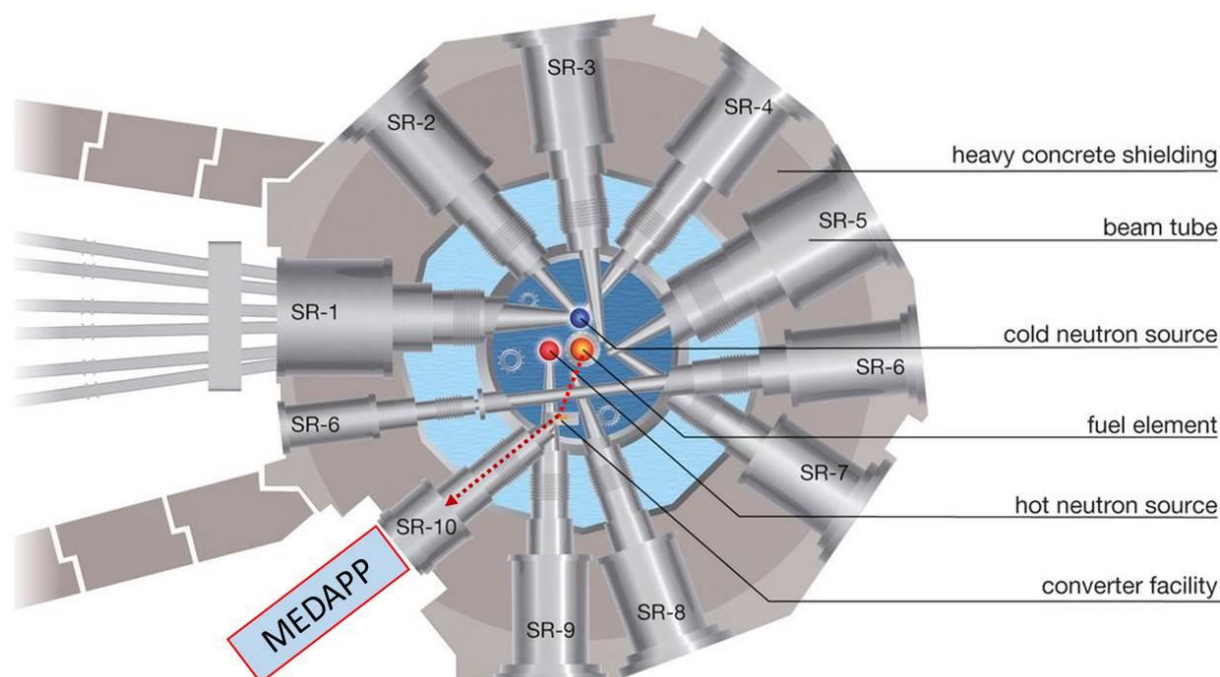
Figure 19: Schematic view of the FRM II reactor core and the adjacent beam tubes to various experimental sites, such as the MEDAPP at SR-10 used in this work. (FRMII, 2017a)

In total three experiments with microalgae could be carried out in the nuclear research reactor. The experiments are labeled "neutron mutagenesis 1 - 3" (NM1 – NM3) and the setup parameters are displayed in Table 14. The distance of the converter plate (neutron source) to the biological samples was 5.92 m, respective 5.33 m for the last experiment to maintain high neutron fluxes. One lead filter with 6 cm thickness was used to reduce gamma radiation and obtain a neutron-to-gamma ratio of 2 – 2.7 and total dosages of 0.45 – 0.60 Gy min^{-1}. The ratio was dependent on the installed converter plate and collimator that had to be changed in between reactor cycles. Shorter distance to the source allowed higher irradiation dosage at NM3. For all three experiments *Picochlorum* sp. was used with a dosage range of 0 up to 150 Gy and 0 to 500 Gy at NM2. An additional experiment with the improved dosage breakdown of 0 up to 500 Gy (see Table 14) was also performed.

Table 14: Settings for fast neutron radiation experiments, neutron mutagenesis experiments 1, 2 and 3 (NM1 –NM3)

Setup	NM1	NM2	NM3
Distance to converter plate	5.92 m (0.99 m)	5.92 m (0.99 m)	5.33 m (0.40 m)
Lead filter thickness	6 cm	6 cm	6 cm
D_n [Gy min^{-1}]	0.340	0.332	0.4028
D_γ [Gy min^{-1}]	0.126	0.121	0.1840
Cummulative dose [Gy min^{-1}]	0.466	0.453	0.5868
Ratio $D_n\ D_\gamma^{-1}$	2.70	2.74	2.189
Strain	*Picochlorum* sp.	*Picochlorum* sp.	*Picochlorum* sp.
Dosage steps [Gy]	0, 1, 6, 12, 19, 26, 35, 50, 70, 100, 150	0, 12, 50, 100, 150, 175, 200, 225, 250, 275, 300, 350, 400, 450, 500	0, 50, 100, 150, 200, 250, 300, 350, 400, 450, 500

Microalgae samples were placed horizontally within the beam in a custom made rack (3D-printed polylactic acid) for 2 mL eppendorf tubes which were completely filled with 2.1 mL cell solution. A total number of 54 tubes could be placed within the beam area simultaneously.

For the mutagenic treatment of microalgae with fast neutrons exponentially grown cells were set to 10^7 cells mL^{-1} via FACS counting in a KCl-media (see section 5.1) to reduce the formation of long lasting radioactive isotopes such as sodium isotopes with a half-time $t_{1/2}{}^{24}$Na = 14,96 h. Thus decay times of 24 hours were enough to obtain non-critical residual activation levels as the decay of radioactive isotopes was ensured. Additionally this dark storage was used to prevent photo repair. After the beam was shut down sampling was possible, as a safe access to the radiation chamber was ensured. The tubes of the predefined-triplicates were removed from the rack and the empty slots filled with dH$_2$O water tubes. The tubes were stored in darkness at room temperature. With radiation clearance the treated samples were transferred in fresh media (dilution factor 1:10) and screened for survival rate and fast growth in 24-well plates at 150 rpm, 50 µmol m^{-2} s^{-1} and 25°C.

5.11.5 Screening methods

Screening of mutagenically altered microalgae cells was performed in 24-well plate dimensions. Via Enspire plate reader measurements the optical density OD^{PR}_{750nm} and the fluorescence was measured once a day. Cellcount analysis was also possible with the drawback of a minimum sample consumption of 50 µL for each measurement. In order to obtain timely cellcounts a total number of 2 plates (48 samples at single measurement) could not be exceeded as the cell sorter needed manual feeding of each sample volume with an analytical timespan of up to 2 minutes per sample.

Obtained cultivation data was analyzed considering survival rate in the first screening and growth rate in repeated screenings afterwards up to 100 days per mutation step.

A cell staining with SYTOX® orange or SYTOX® green as reported (Sato *et al.*, 2004; Doan and Obbard, 2012; Zetsche and Meysman, 2012) did not provide reliable results for *Picochlorum* sp. and could therefore not be applied.

6 Results illumination effects

Light experiments were performed in three stages. As shown in Table 15 stage 1 experiments were conducted with three strains, *Picochlorum* sp., *Dunaliella* sp. and *M. salina* in shake flask dimensions. The illumination colors used for growth were white, green, blue and red with irradiation levels set to 150, 100 and 50 µmol m^{-2} s^{-1}. The scope of these experiments was to investigate growth under varying illumination colors and observe if light limitation due to reduced irradiation levels have an impact on growth or pigment composition. All possible combinations of color, strains and irradiation level were carried out in triplicate, resulting in 108 individual shake flask experiments.

Table 15: Overview of light effect-experiments within this work.

Setup	Stage 1	Stage 2			Stage 3
Platform	Shake flask	Shake flask			Bioreactor
Colors	White, Green, Blue, Red	White, Green, Blue, Red	White, Green, Green+BPF Green+LPF	White, Green, Green+BPF+LPF	White Green
Irradiation [µmol m^{-2} s^{-1}]	150, 100, 50	200	200	75	150
Strains	*Picochlorum* sp., *Dunaliella* sp., *M salina*,	*Picochlorum* sp.			*Picochlorum* sp.
Replicates	3	4	3	3	2

Stage 2 experiments were continued with only one strain, *Picochlorum* sp. to investigate the findings of the previous set of experiments with the main focus on pigment composition and identification of newly found pigment peaks at the green color illumination setup. Therefore, in a first experiment the setup of stage one was expanded to 200 µmol m^{-2} s^{-1} irradiation level with 4 replicates. In the following experiments, white and green light was kept as reference to compare results with the modified illumination setup with green light LEDs equipped with long pass filters (LPF) and band pass filter (BPF) as described in detail in section 5.6.3. A third experiment with green illumination combined with BPF and LPF was carried out to complete the filter setup-combination. Here the irradiation levels had to be reduced to 75 µmol m^{-2} s^{-1} due to the low filter permeability of the combined BPF and LPF as shown in Table 6 d. To conclude the experiments on light color illumination a scale up of *Picochlorum* sp. cultivation to bench-top bioreactor scale (2.3 L working volume) in stage 3 enabled ongoing pigment sampling in order to investigate pigment formation as a function of time and growth status respectively. These experiments were reduced to white and green illumination and carried out at 150 µmol m^{-2} s^{-1} irradiation levels.

6.1 Stage 1 Experiments

The results of stage 1 experiments are subsequently strain specifically discussed with the main focus on the 150 µmol m^{-2} s^{-1} irradiation experiments.

6.1.1 Illumination experiments: *Picochlorum* sp.

Picochlorum sp. was grown in triplicate shake flask experiments at irradiation levels of 150, 100 and 50 µmol m^{-2} s^{-1} at white, blue, green and red colored LED-illumination over the course of 18 days. Figure 20 displays the growth curves of *Picochlorum* sp. at varying illumination. It is visible that all three irradiation levels are sufficient for growth. Maximum growth rates calculated over the course of 3 time points (or a minimum range of 60 h) are reached after ca. day 7. For 150 µmol m^{-2} s^{-1} irradiation maximum growth rates µ$_{max}$ are significantly different according to students t-test with a *p*-values (*p* < 0.005) of *p* = 0.00047 between white and blue illumination. Significant differences with a *p*-value lower than p < 0.05 at 0.039, 0.034 and 0.015 between green vs. blue, blue vs. red and green vs. white illumination. Nevertheless, all four colored settings provide high maximum growth rates at values between 0.8 d^{-1} and 1.1 d^{-1}. Interestingly the blue light illuminated *Picochlorum* sp. strains achieved the stationary growth phase approximately at half of the cell dry weight concentration (0.4 g$_{DW}$ L^{-1}) than white, green and red illuminated strains (0.8 - 0.9 g$_{DW}$ L^{-1}). Similar growth behavior can be seen at 100 µmol m^{-2} s^{-1}. At low irradiation levels of just 50 µmol m^{-2} s^{-1} maximum growth rates µ$_{max}$ remain in the same range than higher irradiation levels but even with the bottom-lit shake flasks light limitation comes in place at cell densities of around 0.2 g$_{DW}$ L^{-1}. Thus reduces the growth rates and maximum biomass yield. Consumption of phosphate and nitrate show similar trends for all three irradiation experiments with almost double phosphate and nitrate consumption rates Y [mg g$_{DW}$$^{-1}$] at blue light (Figure 20). Samples for HPLC pigment analysis were taken at late exponential growth phase (day 9), at stationary phase (day 11) and at the end of the cultivation at phosphate and nitrate starvation (day 17). The results are shown in Figure 21 for each color. For all illumination setups the major pigments neoxanthin, violaxanthin, lutein, canthaxanthin, chlorophyll *b*, chlorohyll *a* and beta carotene could be detected. The sequence in which they are listed represents the retention time on the column (see section 5.7) and was kept that way for the course of this work. For all color settings the relative distribution and concentrations are similar with chlorophyll *a* having the highest occurrence with up to 110 mg g$_{DW}$$^{-1}$ at exponential growth in blue light. All pigment titer decline to about 20 % in concentration towards the end of the cultivation (day 9 compared to day 17) except canthaxanthin which increases the pigment content up to 2.6 fold.

a

Picochlorum sp. 150 µmol m^{-2} s^{-1}

b

Picochlorum sp. 150 µmol m^{-2} s^{-1}

color illumination	μ_{max} [d^{-1}]	$Y_{PO_4^{3-}}$ [mg g$_{DW}^{-1}$]	$Y_{NO_3^{-}}$ [mg g$_{DW}^{-1}$]
white	1.077	73.1	500.0
blue	0.813	132.1	903.0
green	0.923	74.4	508.7
red	1.145	74.7	510.6

c

Picochlorum sp. 100 µmol m^{-2} s^{-1}

d

Picochlorum sp. 100 µmol m^{-2} s^{-1}

color illumination	μ_{max} [d^{-1}]	$Y_{PO_4^{3-}}$ [mg g$_{DW}^{-1}$]	$Y_{NO_3^{-}}$ [mg g$_{DW}^{-1}$]
white	1.135	68.7	353.3
blue	1.124	132.5	635.6
green	1.007	62.7	359.8
red	1.109	70.2	361.2

e

Picochlorum sp. 50 µmol m^{-2} s^{-1}

f

Picochlorum sp. 50 µmol m^{-2} s^{-1}

color illumination	μ_{max} [d^{-1}]	$Y_{PO_4^{3-}}$ [mg g$_{DW}^{-1}$]	$Y_{NO_3^{-}}$ [mg g$_{DW}^{-1}$]
white	0.848	56.7	668.7
blue	1.249	103.6	973.8
green	1.032	74.6	724.1
red	0.879	62.6	544.4

Figure 20: Shake flask cultivations with *Picochlorum* sp. at irradiation levels of 150, 100 and 50 µmol m^{-2} s^{-1}, 120 rpm, aeration 1.8 nL h^{-1} per flask (1 % CO$_2$-enriched air) at the colors white, blue, green and red. The growth curves are shown in a), c) and e) with the corresponding cultivation characteristics max growth rate μ_{max}, and phosphate and nitrate consumption rates.

The total pigment content varies between the different illumination settings, having approximately doubled the content in blue light compared to white and green such as 0.5 fold the content at red illumination.
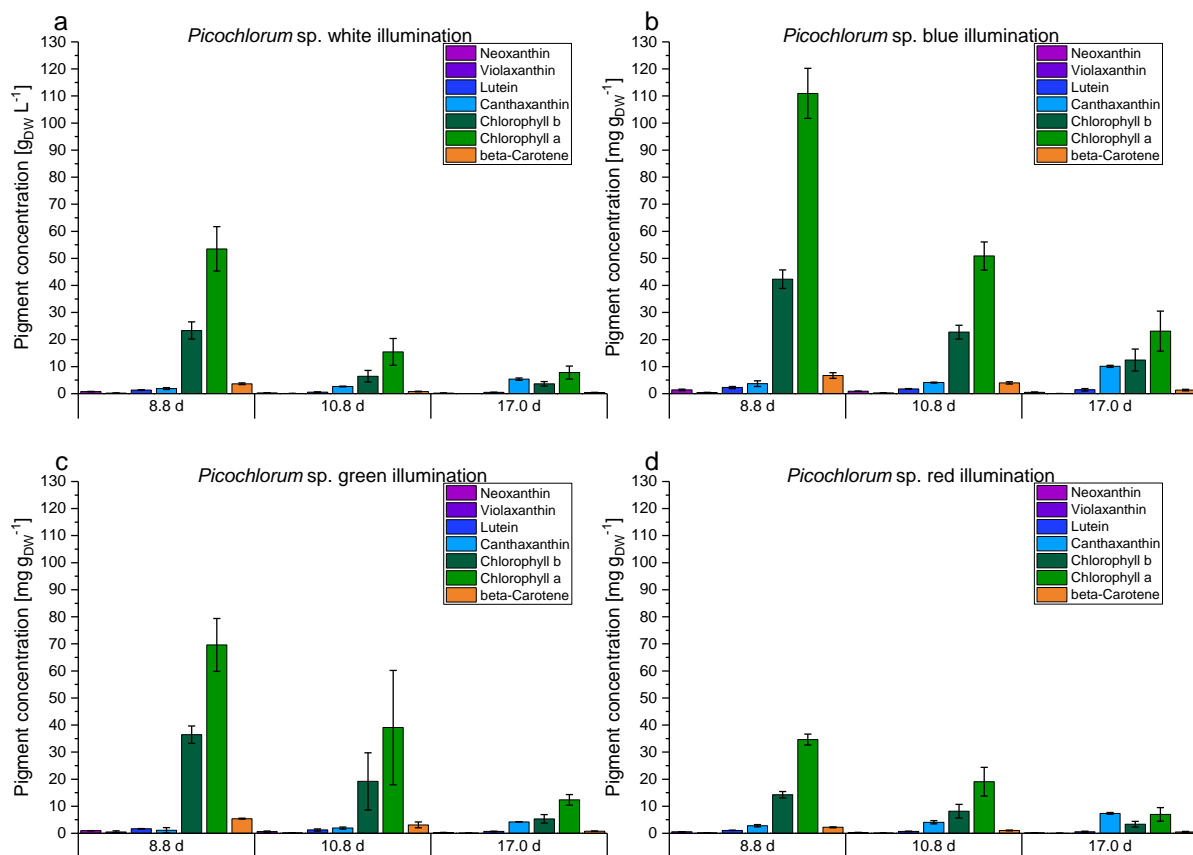
Figure 21: Display of pigment concentrations of *Picochlorum* sp. grown under different colored illumination in stage 1 experiments (150 µmol m^{-2} s^{-1} irradiation level). Pigment identification achieved via comparison with reference standards.

The HPLC plot of *Picochlorum* sp. growing at the four colors is displayed in Figure 22. The predominate peak for all HPLC plots (including the plots of *Dunaliella* sp. and *M. salina*) is always the lutein peak (4) at a retention time of 14 min. Actual lutein concentrations per dry weight [mg g_{DW}^{-1}] were usually lower compared to the second most dominant peak, the chlorophyll *a* (7) at around 20 min retention time. This results in the difference between HPLC plot (Figure 22) and the calculated pigment contents displayed in Figure 21. The raw data shown in the HPLC plot shows peaks that were not within the common and expected pigments described above. In all lines peak number 3 occurred as unknown peak. Additionally, for the green illuminated cultures three unique peaks were detected (Figure 22 c peaks labeled **a**, **b**, and **c**). For the further cause of discussion these peaks were labeled unknown 1 (U1) (peak number 3 in Figure 22 c), unknown 2 (U2), unknown 3 (U3) and unknown 4 (U4) (peaks a, b and c in Figure 22 c).
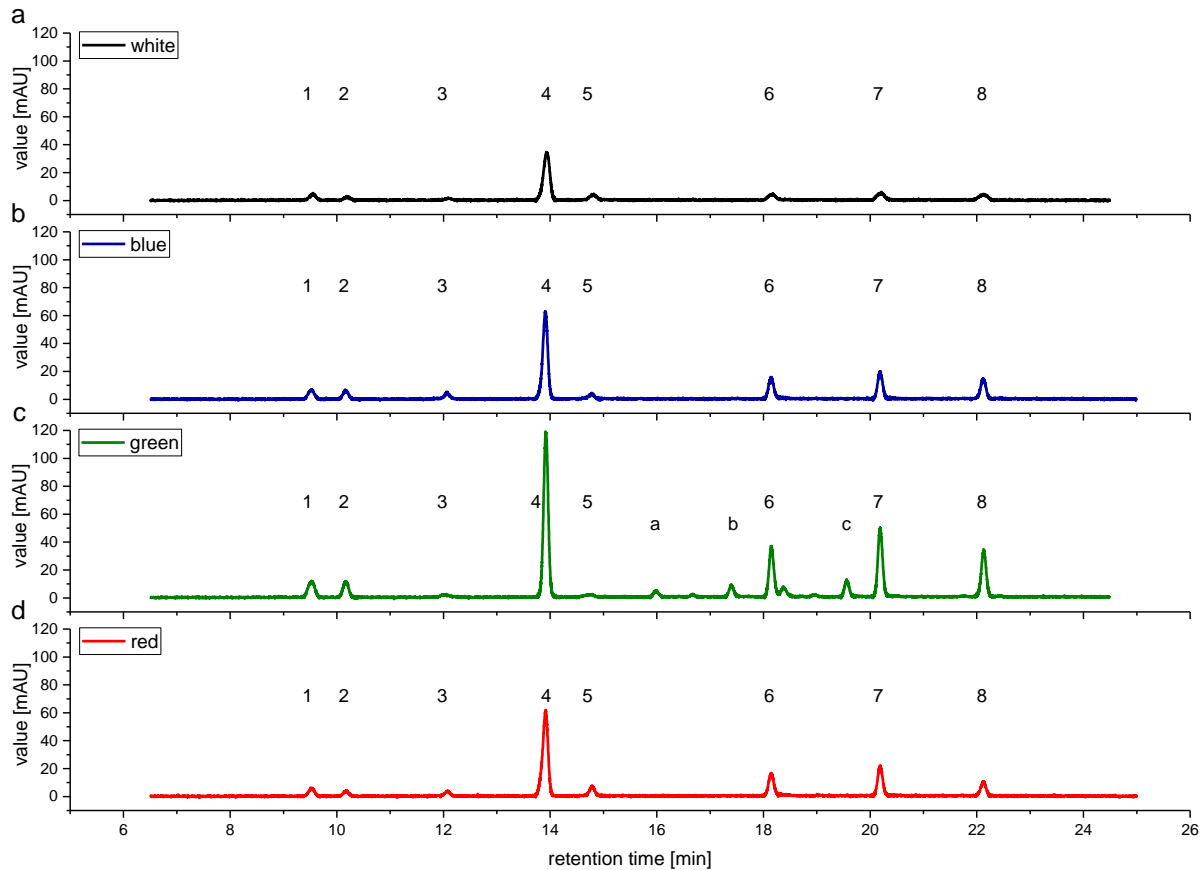
Figure 22: HPLC plots of _Picochlorum_ sp. grown at white, blue, green and red light, day 11. In stage 1 experiments (150 µmol m^{-2} s^{-1} irradiation level) Peaks: 1 all-trans Neoxanthin, 2 Violaxanthin, 3 unknown, 4 Lutein, 5 Canthaxanthin, 6 Chlorophyll _b_, 7 Chlorophyll _a_, 8 β-Carotene, a/b/c unknown (only occurring with green light). Measured on Kinetex 5 µm C8 column (150 mm * 4.6 mm), detection at λ = 450 nm. Known substances were identified in comparison to commercial standards.

For a better peak separation the initial Kinetex 5 µm C8 column (150 mm * 4.6mm) was switched after stage 1 experiments (Figure 22) with the longer YMC-Pack Pro C8 column (250 mm * 4.6 mm I.D.), 5 µm particle size which is described in detail in section 5.7.3. The retention times therefore proportionally increased but sequence and peak occurrence remained unchained. Pigment standards were reanalyzed and correlations were adapted accordingly.

6.1.2 Illumination experiments: *M. salina*.

Illumination experiments with varying light irradiations were conducted equivalent with the previous experiments with *M. salina* at different illumination setups. Cells were grown up to a total cell dry weight of 1.5 g_{DW} L^{-1}. Differing to *Picochlorum* sp., the growth of *M. salina* was inhibited at 150 µmol m^{-2} s^{-1} irradiation compared to the 100 µmol m^{-2} s^{-1} setup (see Figure 23 a-f). As seen before, the 50 µmol m^{-2} s^{-1} irradiance was insufficient to provide unlimited lighting after a certain cell density (ca. 0.2 g_{DW} L^{-1}) was reached. Maximum growth rates were lower at 150 µmol m^{-2} s^{-1} and showed significant ($p < 0.05$) differences between blue and red illumination ($p = 0.0088$) as well as blue and white illumination ($p = 0.027$). After the initial growth phase with a max growth rate of 0.566 d^{-1} the blue color illumination did not grow above cell dry weights of 0.04 g_{DW} L^{-1} in the high irradiation setup. At 100 µmol m^{-2} s^{-1} the cell growth of the blue color illumination (up to 0.6 g_{DW} L^{-1}) showed approximately the half max-value of white (1.4 g_{DW} L^{-1}), green (1.4 g_{DW} L^{-1}) and red (1.7 g_{DW} L^{-1}), which correspond to the findings for *Picochlorum* sp.. Green illumination showed slightly delayed growth compared to white illumination. Due to slow growth at the 150 µmol m^{-2} s^{-1} setup a pigment analysis was not possible and the consumption rates of nitrate and phosphate were not determined. The lower irradiated experiments showed similar consumption rates with higher values at blue and green illumination for phosphate and increased nitrate consumption at blue illumination.

Pigment analysis via HPLC as shown in Figure 24 was performed in late exponential (day 8), early stationary (day 11) and nitrate/- phosphate limitation phase at the end of the cultivation (day17). Detectable were the pigments neoxanthin, violaxanthin, lutein, canthaxanthin, chlorophyll *a*, and β-carotene (succession order according RT) and the unknown peak U1 in between violaxanthin and lutein. Aside of these the unknown peaks for U2, U3 and U4 were also visible in *M. salina*, but only as small irregularities in the baseline (data not shown) and therefore not further investigated. Highest pigment concentrations of up to 40 mg g_{DW}^{-1} were gained with chlorophyll *a* at green illumination. As before all pigment concentrations declined over the cultivation time except for of canthaxanthin. Red illumination yielded similar pigment concentrations than the white light reference.
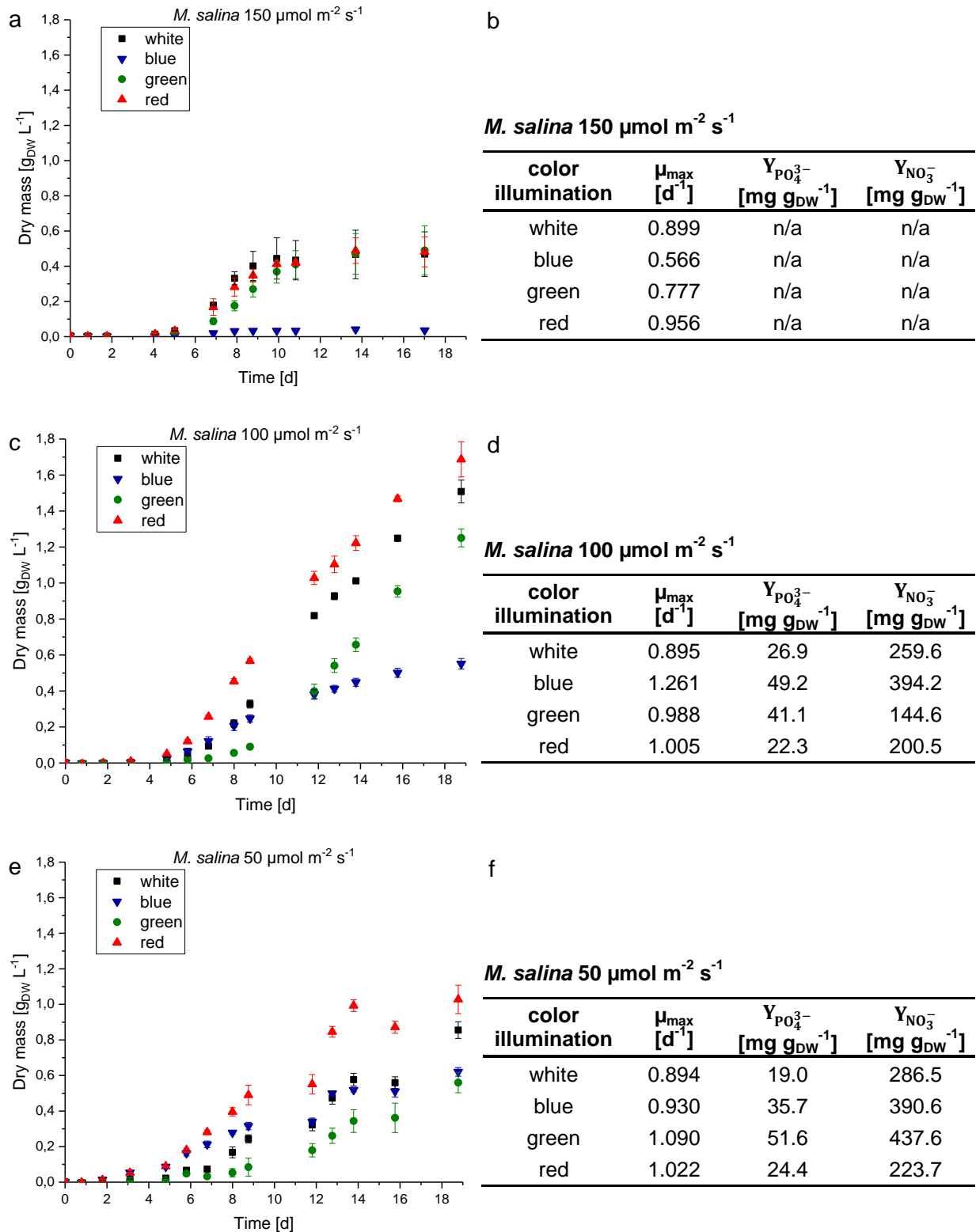
Figure 23: Shake flask cultivations of *M. salina* at irradiation levels of 150, 100 and 50 µmol m^{-2} s^{-1}, 120 rpm, aeration 1.8 nL h^{-1} per flask (1 % CO$_2$-enriched air) at the colors white, blue, green and red. The growth curves are shown in a), c) and e) with the corresponding cultivation characteristics max growth rate µ$_{max}$, and phosphate and nitrate consumption rates in b), d), and f). (nitrate/phosphate analysis carried out on one shake flask of each triplicate).

b

***M. salina* 150 µmol m^{-2} s^{-1}**

color illumination	µ$_{max}$ [d^{-1}]	Y$_{PO_4^{3-}}$ [mg g$_{DW}$$^{-1}$]	Y$_{NO_3^-}$ [mg g$_{DW}$$^{-1}$]
white	0.899	n/a	n/a
blue	0.566	n/a	n/a
green	0.777	n/a	n/a
red	0.956	n/a	n/a

d

***M. salina* 100 µmol m^{-2} s^{-1}**

color illumination	µ$_{max}$ [d^{-1}]	Y$_{PO_4^{3-}}$ [mg g$_{DW}$$^{-1}$]	Y$_{NO_3^-}$ [mg g$_{DW}$$^{-1}$]
white	0.895	26.9	259.6
blue	1.261	49.2	394.2
green	0.988	41.1	144.6
red	1.005	22.3	200.5

f

***M. salina* 50 µmol m^{-2} s^{-1}**

color illumination	µ$_{max}$ [d^{-1}]	Y$_{PO_4^{3-}}$ [mg g$_{DW}$$^{-1}$]	Y$_{NO_3^-}$ [mg g$_{DW}$$^{-1}$]
white	0.894	19.0	286.5
blue	0.930	35.7	390.6
green	1.090	51.6	437.6
red	1.022	24.4	223.7

Figure 24: Pigment content of _M. salina_ grown at different colored illumination in stage 1 experiments (150 µmol m^{-2} s^{-1} irradiation level). Pigment identification done via comparison with reference standards.

6.1.3 Illumination experiments: _Dunaliella_ sp.

Previously described experiments were also conducted with _Dunaliella_ sp. in order to monitor cell growth at white, blue, green and red illumination in bottom-lit shake flasks. Irradiation of 50 µmol m^{-2} s^{-1} was insufficient to provide growth beyond a dry mass of 0.4 g$_{DW}$ L^{-1} for all tested color setups, although the maximum growth rates were quite high at the initial growth in exponential phase. Higher irradiation levels resulted in cell growth up to 1.6 g$_{DW}$ L^{-1}, but the blue illumination with irradiation of 150 µmol m^{-2} s^{-1} yielded just 0.8 g$_{DW}$ L^{-1} maximum dry mass (Figure 25). Maximum growth rates µ$_{max}$ did not differ with statistical relevance according to students t-test (all values above $p > 0.05$) throughout all tested color illuminations and as growth continued linear without much decline for over two weeks a undetected limitation factor might be present. Phosphate and nitrate consumption rates differed significantly between the 50 and 100 µmol m^{-2} s^{-1} setups.
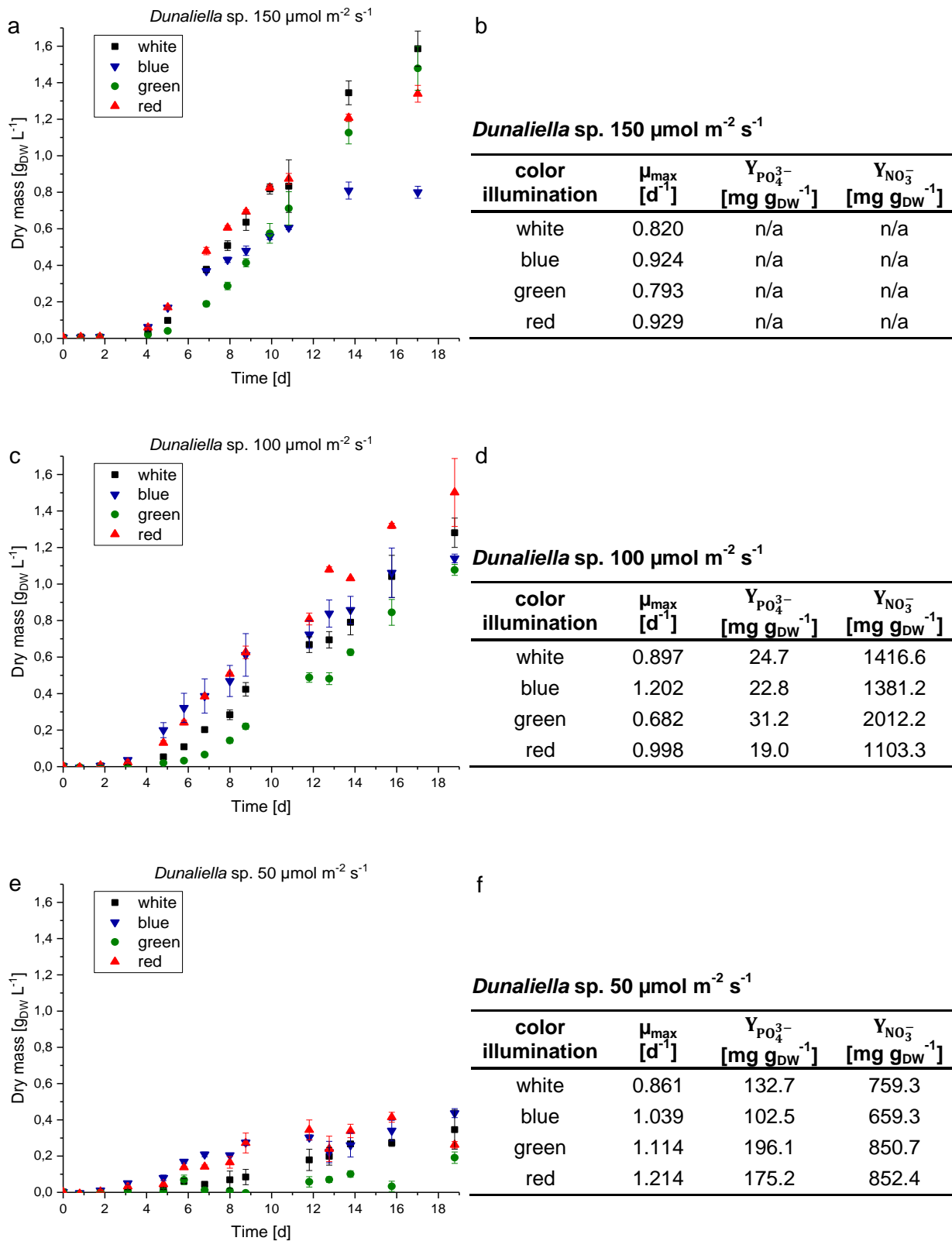
Figure 25: Shake flask cultivations of *Dunaliella* sp. at irradiation levels of 150, 100 and 50 µmol m⁻² s⁻¹, 120 rpm, aeration 1.8 nL h⁻¹ per flask (1 % CO₂-enriched air) at the colors white, blue, green and red. The growth curves are shown in a), c) and e) with the corresponding cultivation characteristics max growth rate µ_max, and phosphate and nitrate consumption rates in b), d), and f). (nitrate/phosphate analysis was done on one shake flask of each triplicate).

Dunaliella sp. 150 µmol m⁻² s⁻¹

color illumination	μ_{max} [d⁻¹]	$Y_{PO_4^{3-}}$ [mg g_DW⁻¹]	$Y_{NO_3^-}$ [mg g_DW⁻¹]
white	0.820	n/a	n/a
blue	0.924	n/a	n/a
green	0.793	n/a	n/a
red	0.929	n/a	n/a

Dunaliella sp. 100 µmol m⁻² s⁻¹

color illumination	μ_{max} [d⁻¹]	$Y_{PO_4^{3-}}$ [mg g_DW⁻¹]	$Y_{NO_3^-}$ [mg g_DW⁻¹]
white	0.897	24.7	1416.6
blue	1.202	22.8	1381.2
green	0.682	31.2	2012.2
red	0.998	19.0	1103.3

Dunaliella sp. 50 µmol m⁻² s⁻¹

color illumination	μ_{max} [d⁻¹]	$Y_{PO_4^{3-}}$ [mg g_DW⁻¹]	$Y_{NO_3^-}$ [mg g_DW⁻¹]
white	0.861	132.7	759.3
blue	1.039	102.5	659.3
green	1.114	196.1	850.7
red	1.214	175.2	852.4

HPLC analysis of pigment samples at late exponential phase, stationary phase and phosphate and nitrate limiting phase at the end of the cultivation (day 9, 11 and 17) showed a predominate occurrence of chlorophyll *a* and *b* with constant high levels throughout the samples as displayed in Figure 26. Other pigments occurred just within trace levels. White illumination yielded an average value of 50 mg g_{DW}^{-1} chlorophyll *a* and 25 mg g_{DW}^{-1} chlorophyll *b*. No other pigment peaks could be detected in *Dunaliella* sp. with the experimental setup.
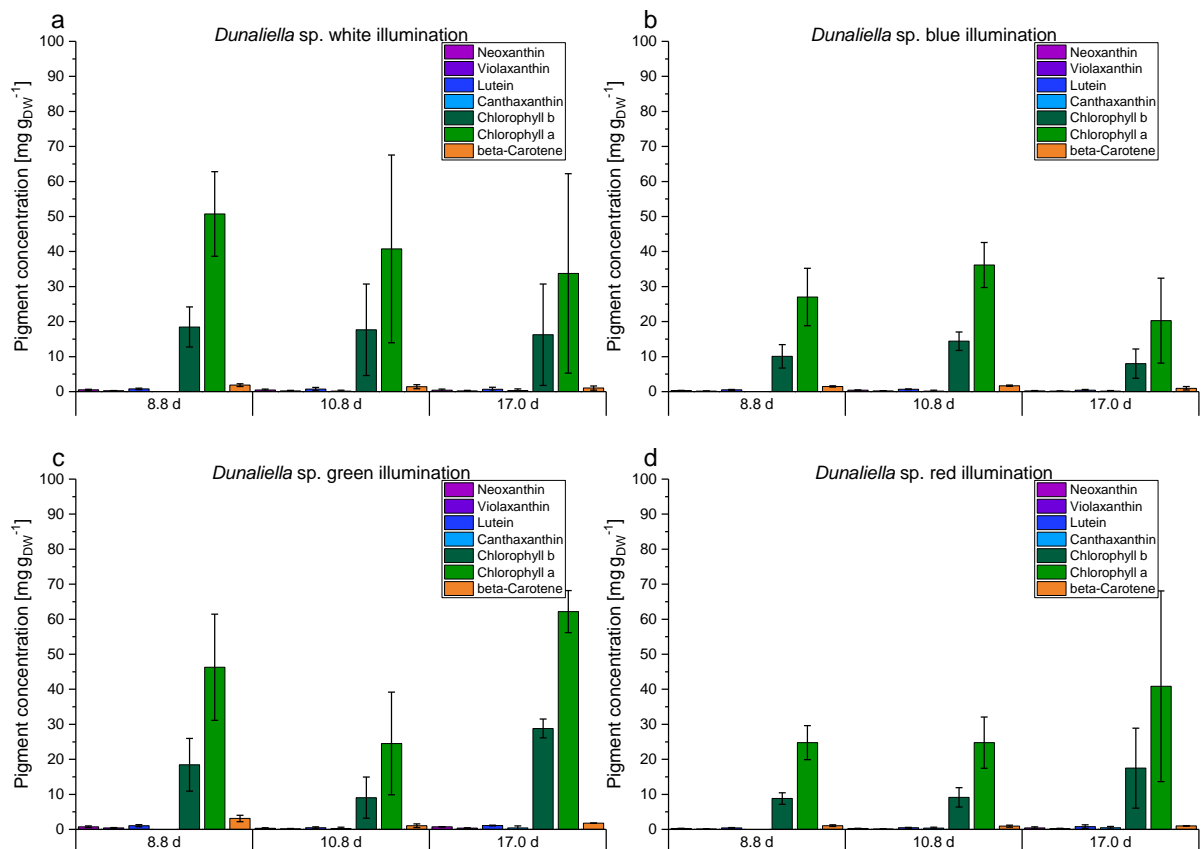
Figure 26 Pigment analysis of *Dunaliella* sp. grown at different colored light at 150 µmol m^{-2} s^{-1} irradiation. Pigment identification done via comparison with reference standards.

6.1.4 Lipid Analysis
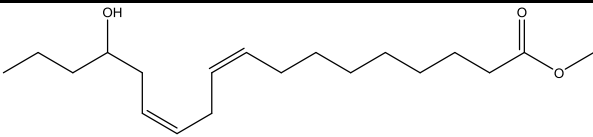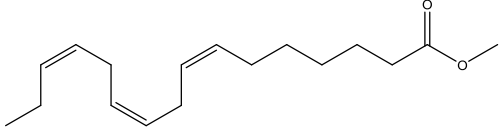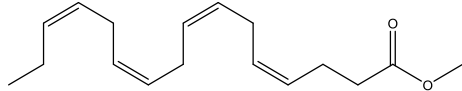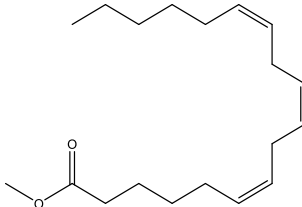
Qualitative GC-MS analysis was applied to investigate potential illumination effects on lipid formation by *Picochlorum* sp., *Dunaliella* sp. and *M. salina*. Biomass samples for lipid extraction (see section 5.9) were obtained during the stage 1 experiments in nitrate and phosphate limitation phase. Altered illumination of white, blue, green and red light of the microalgae strains did not lead to any differences in lipid production. Therefore Table 16 does not list any illumination colors but just the identified fatty acid methyl esters (FAMEs).

Table 16: GC-MS lipid analysis of *Picochlorum* sp., *Dunaliella* sp. and *M. salina.* Details of unknown FAMES A, B, C and D listed in Table 17.

RT [min]	Conformity [%]	formula	CAS-number	name	marine Oil Mix	*Picochlorum sp.*	*Dunaliella* sp.	*M. salina*
22.25	64.75	$C_{13}H_{26}O_2$	111-82-0	C12:0	x	x	x	x
27.51	71.15	$C_{15}H_{30}O_2$	124-10-7	C14:0	x	x	x	x
28.36	86.98	$C_{15}H_{28}O_2$	56219-06-8	C14:1	x			
28.81	14.53	$C_{19}H_{34}O_3$		*A*			x	
32.35	72.91	$C_{17}H_{34}O_2$	112-39-0	C16:0	x	x	x	x
32.72	33.86	$C_{17}H_{32}O_2$	1120-25-8	C16:1		x	x	x
32.87	40.81	$C_{17}H_{32}O_2$	1120-25-8	C16:1	x			
33.73	31.01	$C_{17}H_{30}O_2$	16106-03-9	C16:2		x	x	x
34.37	35.63	$C_{17}H_{28}O_2$	17364-31-7	C16:3			x	
35.15	35.46	$C_{17}H_{28}O_2$		*B*		x	x	x
35.80	39.49	$C_{17}H_{26}O_2$		*C*			x	
36.79	61.19	$C_{19}H_{38}O_2$	112-61-8	C18:0	x	x	x	x
37.18	9.99	$C_{19}H_{36}O_2$	112-62-9	C18:1 (trans-9)	x	x	x	x
37.31	11.08	$C_{19}H_{36}O_2$		C18:1 (trans-9)	x	x	x	x
38.11	18.28	$C_{19}H_{34}O_2$	112-63-0	C18:2	x	x	x	x
38.75	56.36	$C_{19}H_{32}O_2$		*D*			x	
38.88	74.00	$C_{19}H_{40}O_2$		C19 Std.		x	x	x
39.45	41.55	$C_{19}H_{32}O_2$	301-00-8	C18:3	x	x	x	x
40.89	45.59	$C_{21}H_{42}O_2$	1120-28-1	C20:0	x	x	x	x
41.28	27.41	$C_{21}H_{40}O_2$		C20:1	x	x		x
42.19	29.99	$C_{21}H_{38}O_2$		C20:2	x			
43.16	49.10	$C_{21}H_{34}O_2$	2566-89-4	C20:4	x			
43.47	29.97	$C_{21}H_{36}O_2$		C20:3	x	x	x	x
44.44	27.25	$C_{21}H_{32}O_2$		C20:5	x			
44.75	64.63	$C_{23}H_{46}O_2$	929-77-1	C22:0	x		x	
45.13	49.10	$C_{23}H_{44}O_2$		C22:1	x			x
48.36	79.72	$C_{25}H_{50}O_2$	2442-49-1	C24:0	x			x
48.72	33.30	$C_{23}H_{34}O_2$		C22:6	x			

In Table 17 the names and chemical formulas of the GC-identified FAMEs without CAS number are shown with chemical formula and name in Table 16

Table 17: Identified FAMEs with names and chemical formulas found in *Picochlorum* sp., *Dunaliella* sp. and *M. salina*.

#	Name	Chemical formula
A	methyl (9Z, 12Z)-15-hydroxyoctadeca-9,12-dienoate	
B	methyl (7Z,10Z,13Z)-hexadeca-7,10,13-trienoate	
C	methyl (4Z,7Z,10Z,13Z)-hexadeca-4,7,10,13-tetraenoate	
D	methyl (6Z,9Z,12Z)-octadeca-9,9,12-trienoate	

Total Lipid content of color illuminated strains was analyzed using GC-FID (see section 5.9.2). Table 18 displays percentages of total lipids per dry weight for the three strains tested within stage 1 experiments. In general, a maximum total lipid content of 23.90 % ± 0.28 % was obtained with *Picochlorum sp.* at green light. White light resulted in just 1.3 % less lipids than green light, whilst red and blue illumination were significantly lower in lipid yield with 16,6 % at blue light. The lowest lipid content was obtained from blue and red illuminated *M. salina* cells. In *Dunaliella* sp. highest lipid contents at 21.74 % ± 0.29 % were reached at green light illumination. White, blue and red light illumination yielded with this unlimited growth conditions all similar at around 19.5 % In *M. salina* the lipid yield was similar distributed than in *Picochlorum sp.* but a lower level of approximately 15 % and 13,4 %). In both strains blue and red illumination yielded less total lipids (approximately 2 % in *M. salina* and 6 % in *Picochlorum sp.*) than growth at white and green light.

Table 18: Total Lipid content of *Picochlorum* sp., *Dunaliella* sp. and *M. salina* at colour illumination obtained via GC-FID at unlimited growth conditions. All results displayed in percentage of dry weight.

Illumination color	*Picochlorum* sp.	*Dunaliella* sp.	*M. salina*
white	22.60 % ± 0.07 %	19.98 % ± 0.76 %	15.40 % ± 0.13 %
blue	16.66 % ± 1.07 %	19.29 % ± 0.35 %	13.42 % ± 0.12 %
green	23.90 % ± 0.28 %	21.74 % ± 0.29 %	15.07 % ± 1.16 %
red	18.89 % ± 0.41 %	19.34 % ± 0.01 %	13.40 % ± 0.12 %

6.1.5 Summarized results of stage 1 illumination experiment

Illumination was performed with the inbuilt LEDs on the shaker platform with the colors warm-white, blue, green and red. Three irradiation levels, 150, 100 and 50 µmol m^{-2} s^{-1} were chosen to investigate the effect on cell growth and pigment composition.

All strains were light limited within one week of growth at 50 µmol m^{-2} s^{-1} resulting in linear growth after cell densities of approximately 0.2 g$_{DW}$ L^{-1} were exceeded.

Pigment analysis discovered higher total pigment contents at blue and green illumination for *Picochlorum sp.* with a similar pigment distribution throughout the identified pigments. Chlorophyll *a* was the predominant pigment in all experiments.

Pigment levels were at highest concentrations during exponential growth phase and declined with ongoing cultivation or starting light limitation.

Aside known pigments one unknown pigment peak was found in all *Picochlorum sp.* setups. Three additional peaks were only identified at green light cultivations.

In *Dunaliella* sp. the total lipid content is not affected by illumination color and was detected at around 20 %. White and green illumination yield higher lipid contents in *M. salina*. (maximum yield 15.40 % ± 0.13 % per dry weight at white illumination) and *Picochlorum* sp. (maximum yields 23.90 % ± 0.28 % per dry weight at green illumination)

6.2 Stage 2 experiments – *Picochlorum* sp.

To investigate the formation of the unknown pigment peaks at green illuminated *Picochlorum* sp. cultures stage 2 experiments were performed with a modified illumination system. An overview of the experiments is shown in Table 15. With the addition of colored filter plates described in section 5.6.3 mounted on the glass surface of the LED sockets the bandwidth of the green 510 nm LED could be reduced.

6.2.1 Increase in irradiation level

As irradiance levels could be crucial for the formation of these pigments the previous experiments were initially repeated with increased irradiance level up to 200 µmol m^{-2} s^{-1} for *Picochlorum* sp. in order to extend exponential growth phase and yield higher pigment levels. The experimental setup was identical than before, experiments were performed in quadruplicate with one replicate per color used for dry mass determination, whereas the other three replicates were twice sampled for pigment content, at exponential phase (day 4) and stationary phase (day 11). With higher irradiation levels the maximum dry mass yield increased up to 5 g_{DW} L^{-1} (see Figure 27) and unlimited growth was possible until day 6. *Picochlorum* sp. grown at white and red light showed similar maximum growth rates at around 0.80 d^{-1} whereas blue and green illuminated cells grew significantly faster ($p < 0.005$) with around μ_{max} = 0.89 d^{-1}.

Picochlorum sp. 200 µmol m^{-2} s^{-1}

color illumination	μ_{max} [d^{-1}]
white	0.801 ± 0.012
blue	0.898 ± 0.026
green	0.888 ± 0.012
red	0.791 ± 0.011
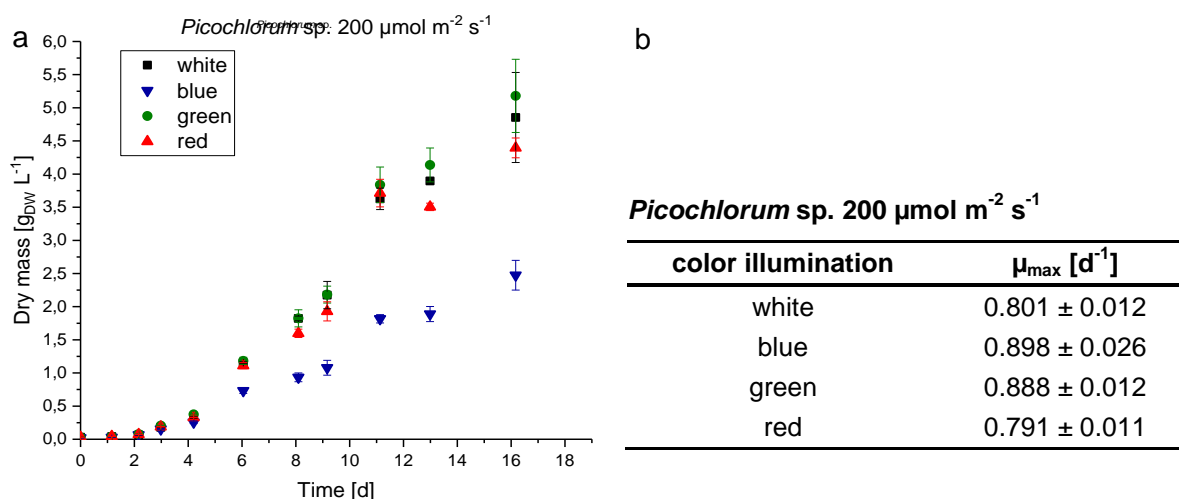
Figure 27: a) *Picochlorum* **sp. growth at 200 µmol m^{-2} s^{-1}irradiance at white, blue, green and red illumination (n = 4). b) Maximum growth rates µ$_{max}$**

Growth with blue light showed the same characteristics than previous experiments with declining growth rates and a maximum biomass yield of around 50% of the white biomass yield. Pigment quantification was executed as before but now extended to the unknown peaks (Figure 28). The correlation between peak area [mAU] at the HPLC plot and actual pigment content [mg$_{Pigment}$ g$_{DW}$$^{-1}$] will be described in section 6.3.2. Aside the unknown peak

U1, which was previously seen in traces at the HPLC plots of all colors (see Figure 22), the peaks U2, U3 and U4 were also only detected at green illumination. A fifth unknown peak, labeled U5 was also detected in stage 3 experiments, which were done simultaneously, is thus already included in the plot. The detailed description of this pigment will be in section 6.3.1. At 200 µmol m^{-2} s^{-1} irradiation *Picochlorum* sp. shows almost identical pigment distribution at white, blue and red color illumination. The sampling time at day 4 in the exponential phase was selected to see if in early exponential phase a pigment shifts towards unknown pigments occurred, which was not the case. The early sample time required a larger sample volume as very little biomass was build up yet. This led to a thinner culture volume in the shake flask and thus to increased illumination per cell and the rise in pigment concentration at day 11. Green illumination showed noticeable concentrations of U2, U3, U5 and U4 pigments at both sample points.

Figure 28: Pigment content of *Picochlorum* sp. grown at different colored illumination at 200 µmol m^{-2} s^{-1} irradiation level.

In order to analyze pigment absorption and potential growth advantages through altered pigment composition the absorption spectra of all cultures were measured. A sample of each illumination setup was taken and directly transferred in a MTP-Plate. The spectrum scan was done with the vital cells fresh out of the original culture volume. Figure 29 shows the

absorption between 350 nm and 800 nm. The values were all normed to the 750 nm-value in order to see any phase shifts especially in the green-light section between 500 and 650 nm. The green light curve shows slightly higher absorption values but no defined phase-shift towards the green light spectrum. In case of a drastically altered absorption spectra the full spectrum scan would show an distinctive difference. As all four curves are just vertically shifted no difference in absorption is detectable.

Figure 29 Spectrum scan 350 – 800 nm of *Picochlorum* sp*.* grown at white, blue, green and red light with 200 µmol m^{-2} s^{-1} irradiation, scan at day 11, absorption normed to 750 nm value. Measurement of vital cells with the plate reader.

6.2.2 LED bandwidth diminishment

After ensuring that the unknown pigment peaks of *Picochlorum* sp. grown at green illumination also occur at 200 µmol m^{-2} s^{-1} irradiation the bandwidth of the green LED was reduced to the short wavelength (green + BPF) and to the long wavelength area (green + LPF) as shown in Figure 12. Growth of white and green illuminated *Picochlorum* sp. cells was implemented only as reference cultivation. Figure 30 shows the dry mass increase for the illumination setups. Growth rates and cultivation course are quite identical for all setups with only significant difference in μ_{max} ($p = 0.029$) between white and green + LPF.

In order to analyze the pigment distribution and the buildup of pigments sampling volume was reduced, allowing five sample-points throughout the shake-flask cultivation. The time points were set at exponential- until stationary growth phase (see Figure 31) White illumination pigment distribution confirmed previous findings with a maximum content of 35 mg$_{chlorophyll\ a}$ g$_{DW}$$^{-1}$. In all green illuminated shake flasks the unknown pigments occur in concentrations up to 5 - 10 mg g$_{DW}$$^{-1}$ at green illumination and 3 - 7.5 mg g$_{DW}$$^{-1}$ at the two filter plate-modified green illumination setups. Predominant pigments were as before the two chlorophylls followed by the unknown pigments U5, U4, U2 and U3.
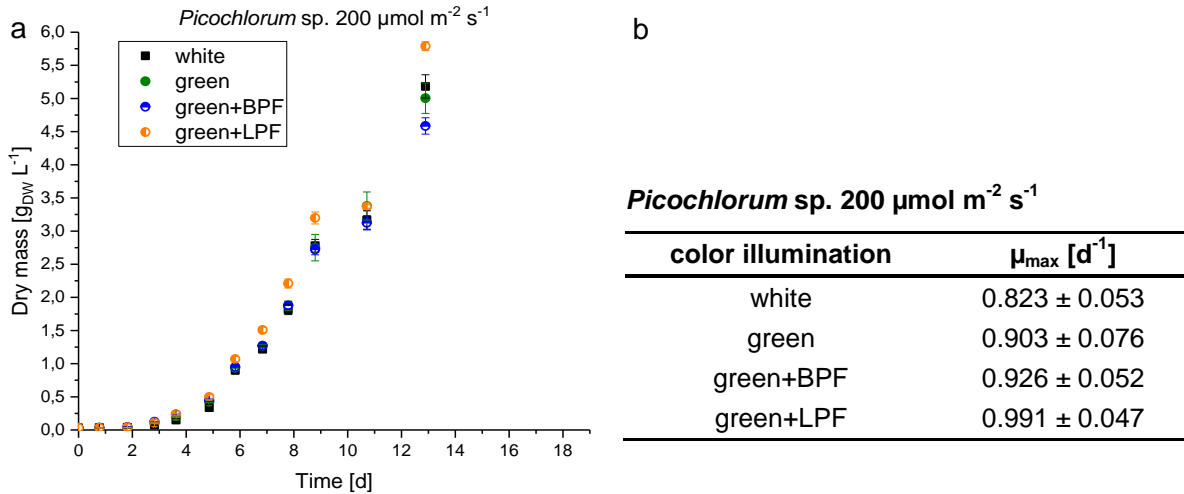
Figure 30: a) *Picochlorum* sp. growth at 200 µmol m^{-2} s^{-1} irradiance with white and green illumination compared to green LED-illumination modified via glass filter plates (green+BPF, green+LPF) (n = 3), b) maximum growth rates µ$_{max}$
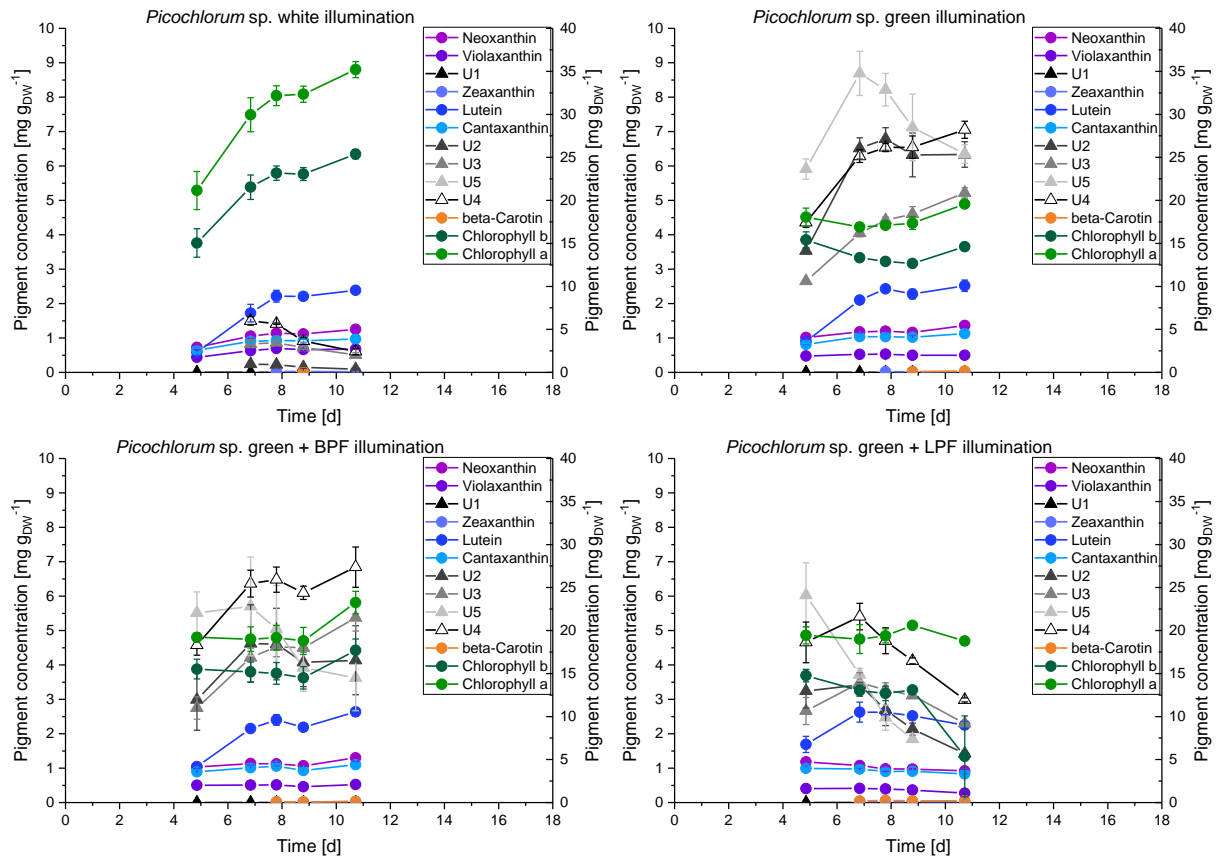
Figure 31: HPLC Analysis of *Picochlorum* sp.pigments grown at 200 µmol m^{-2} s^{-1} irradiation with white, green, green + BPF and green + LPF colors. Right side axis for Chlorophyll *a* and *b*. Experiments done in triplicates, Analysis of each point additionally done in duplicate.

Aside the pigment analysis a full spectrum scan was conducted on the plate reader in order to monitor potential absorption shifts caused by the unknown pigments. The spectrum scan was performed at every sample time point. Figure 32 a) shows the wavelength spectra of the

white (SWW) and green (510 nm) LED with the green LED modified with the band-pass filter (BPF) and long-pass filter (LPF). The spectrum was shifted accordingly and the power settings of the green LED were adapted to achieve a 200 µmol m^{-2} s^{-1} irradiance output throughout all four settings. As the bandwidth of the LED with the mounted filter plates were reduced the irradiation peaks increased consequently.
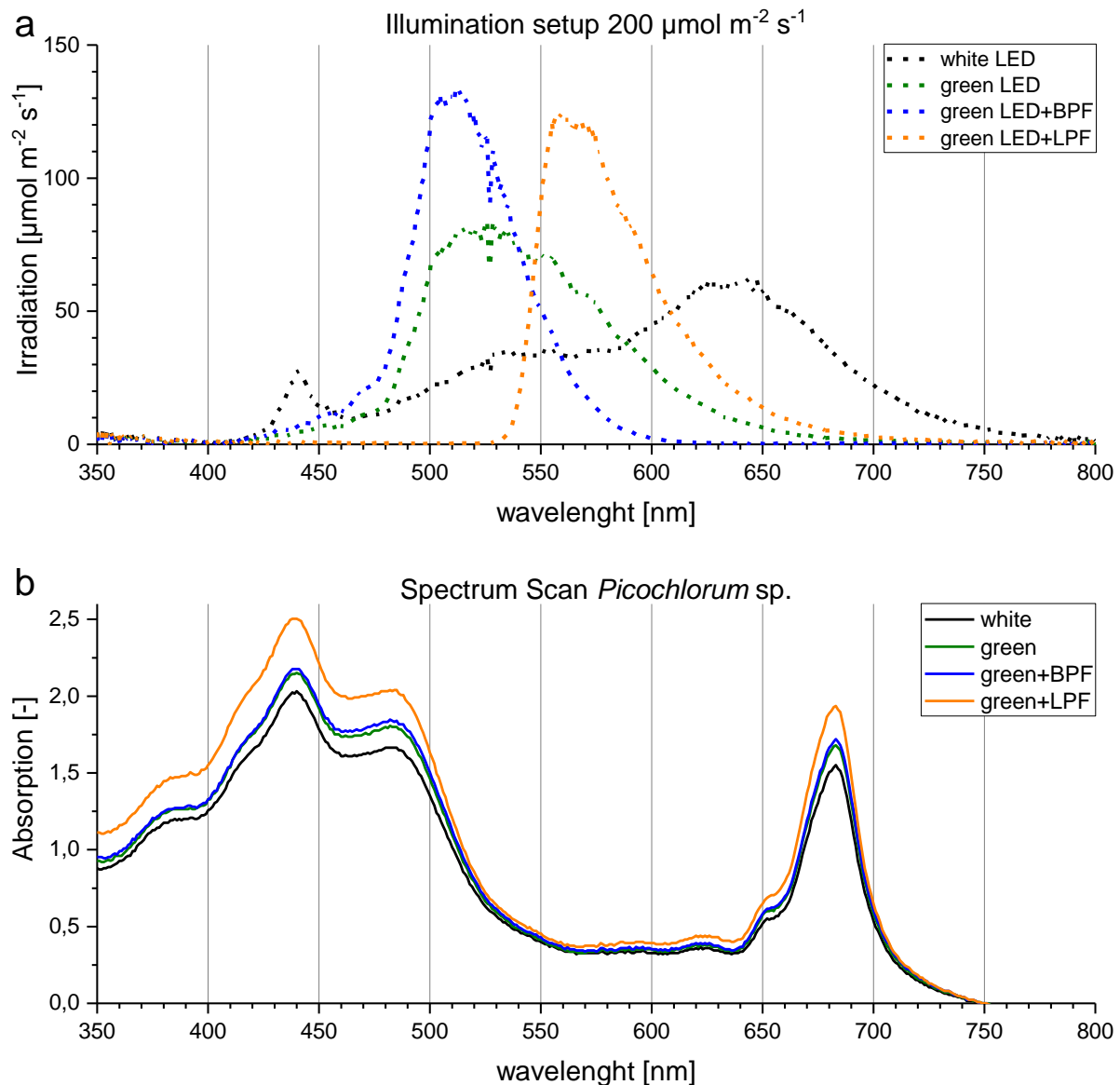
Figure 32: a) Illumination setup at 200 µmol m^{-2} s^{-1} with the glass filter plates installed on the LED-shaker platform. b) Spectrum scan 350 – 800 nm of vital *Picochlorum sp.* grown at white and green light illumination as well as green+LPF and green+BPF modified light illumination with 200 µmol m^{-2} s^{-1} irradiation, scan at day 8, absorption normed to 750 nm value. Measurement performed via plate reader.

The spectrum scan of *Picochlorum sp.* is displayed in Figure 32 b). The absorption for each strain grown with the four colors can be compared to the corresponding irradiation value in

part a) via the gridlines. The displayed spectrum scan of day 8 did not differ from the previous or later days except in total absorbance. Green light modified with the long pass filter (green+LPF) did grow slightly faster (see Figure 30) resulting in higher biomass concentration and thus a higher absorption curve. Apart from that no significant difference in wavelength-absorbance correlation can be seen throughout the four color illumination setups A normation of the absorption on biomass yield was deliberately refrained from at this experiment as optical densities of growth curves were quite similar and a biomass determination would have terminated the experiment due to the consumed culture volume of the sampling.

6.2.3 Double bandwidth diminishment

After the illumination bandwidth of the green 510 nm LED was limited on each side separately, as described in the previous section, a simultaneous reduction on both sides of the wavelength spectrum was put in place by stacking both glass filter plates on one LED-socket. Due to the barely overlapping transmission-areas of the filter plates a more narrow green illumination becomes possible (described and shown in Figure 12 b)) The green LED did not provide enough power to reach irradiation levels of 200 µmol m^{-2} s^{-1}. So even with the combination of the warm white LED (SWW), the 510 nm green LED and a green-yellow 565 nm LED, all set to 100% power, only an output of 75 µmol m^{-2} s^{-1} averaged over all 5 calibration points could be reached. Compared to stage 1 experiments the CO_2-concentration in the aeration was doubled to 2%, which led to higher biomass yields. With this the pigment sample volume could be reduced (biomass per sample approximately10 mg$_{DW}$) enabling 4 sample points for white and green and 3 for the green+BPF+LPF setup.
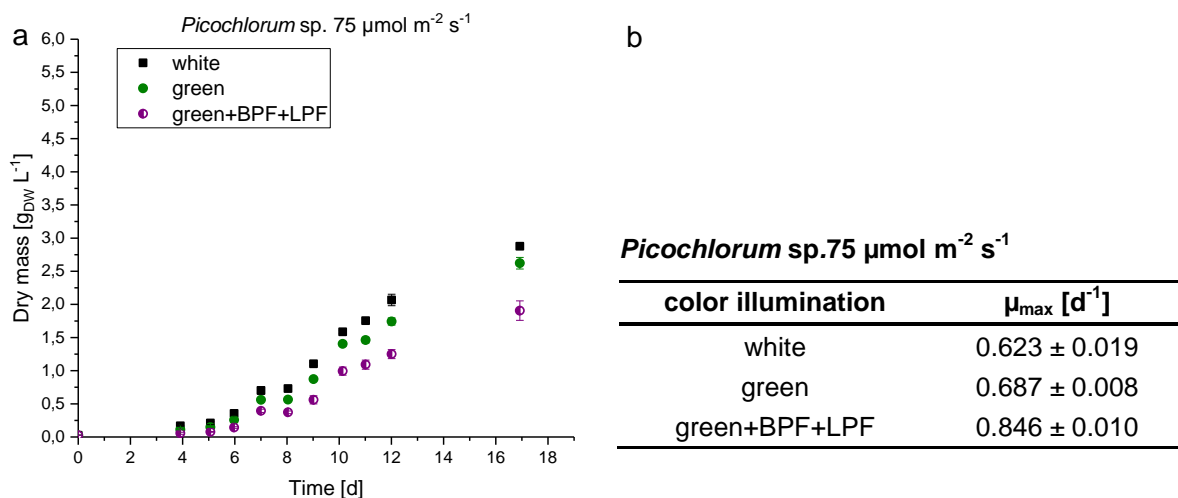
Figure 33: a) *Picochlorum* sp.growth at 75 µmol m^{-2} s^{-1} irradiance with white and green light compared to modified green+BPF+LPF LED-illumination (n = 3), b) maximum growth rates µ$_{max}$

Picochlorum sp.75 µmol m^{-2} s^{-1}

color illumination	µ$_{max}$ [d^{-1}]
white	0.623 ± 0.019
green	0.687 ± 0.008
green+BPF+LPF	0.846 ± 0.010

As expected, cell growth was reduced compared to the 200 µmol m^{-2} s^{-1} illumination described before. White and green illumination yielded similar biomasses with similar maximum growth rates. Illumination with the double-mounted glass filter plates led to statistically significant (p = 0.0062) slower growth and less total biomass. Pigment analysis results are shown in Figure 34. Concentration of chlorophyll *a* and *b*, the two dominant pigments, are similar to the values previously reported. At green illumination the unknown peaks U2 - U5 occur in concentration between 5 and 10 mg g$_{DW}$$^{-1}$. Due to the slow growth only 3 pigment samples could be obtained at the double filter setup. Interestingly, chlorophyll contents seem unchanged but the unknown peaks occur with less intensity in two out of three sample points.
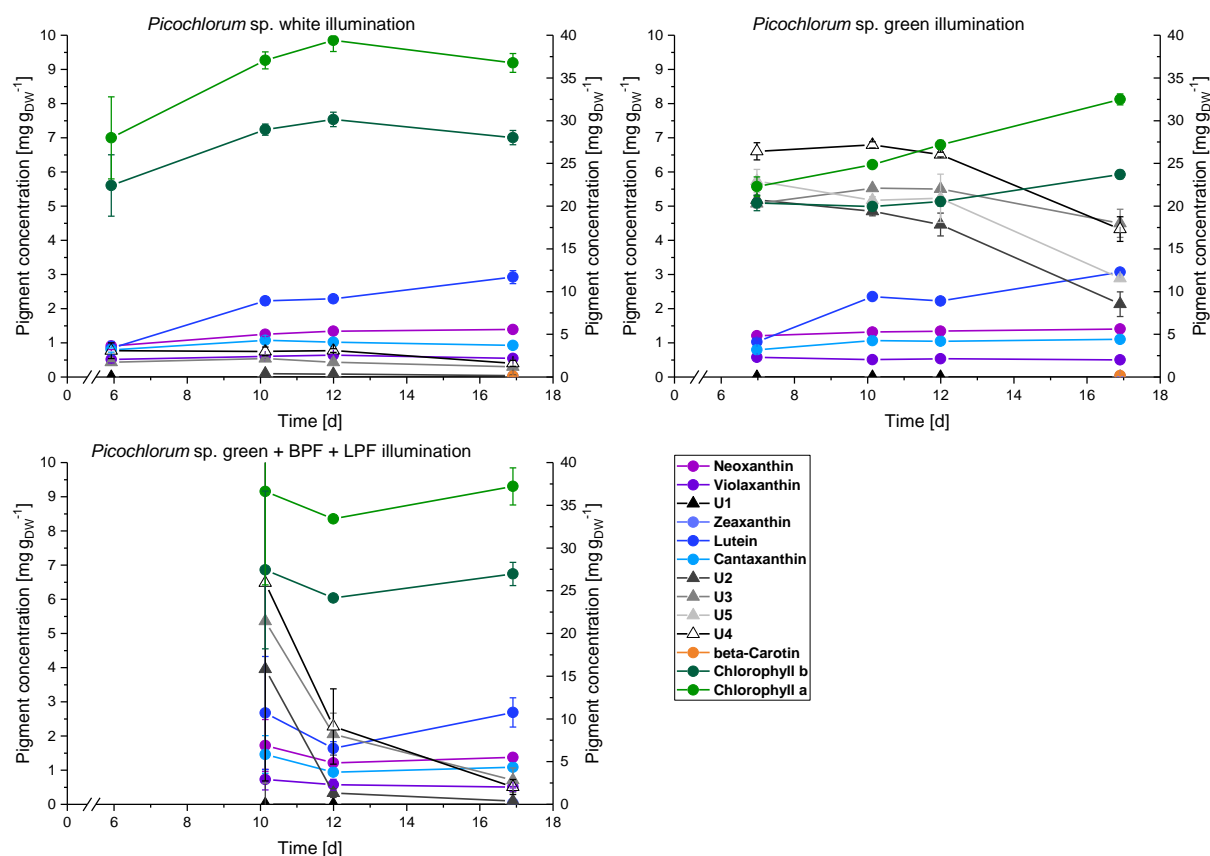
Figure 34: Pigment HPLC analysis of *Picochlorum* sp. grown at 75 µmol m^{-2} s^{-1} irradiation with white, green and green+BPF+LPF illumination. Right side axis for Chlorophyll *a* and *b*. Experiments were done in triplicate, Analysis of each point additionally done in duplicate.

A comparison of illumination bandwidth and spectrum scan of *Picochlorum* sp. at day 10 is shown in Figure 35. The green+BPF+LPF setup grew significantly slower and the difference between the three absorption curves represent the difference in cell dry weight as shown in Figure 33 a). The slow growth can be explained with the almost non-overlapping absorption and irradiation curves of the double filter-illumination setup (see Figure 35 a) and b)).

Nonetheless this overlap, combined with a base-absorption seems sufficient for *Picochlorum* sp. for a slow cell growth. Cross illumination via neighboring flasks or scatter light through the shaker front-door can be neglected as each flask was carefully shaded with a black plastic sheath. Sampling was undertaken at a sterile hood with switched off lights.
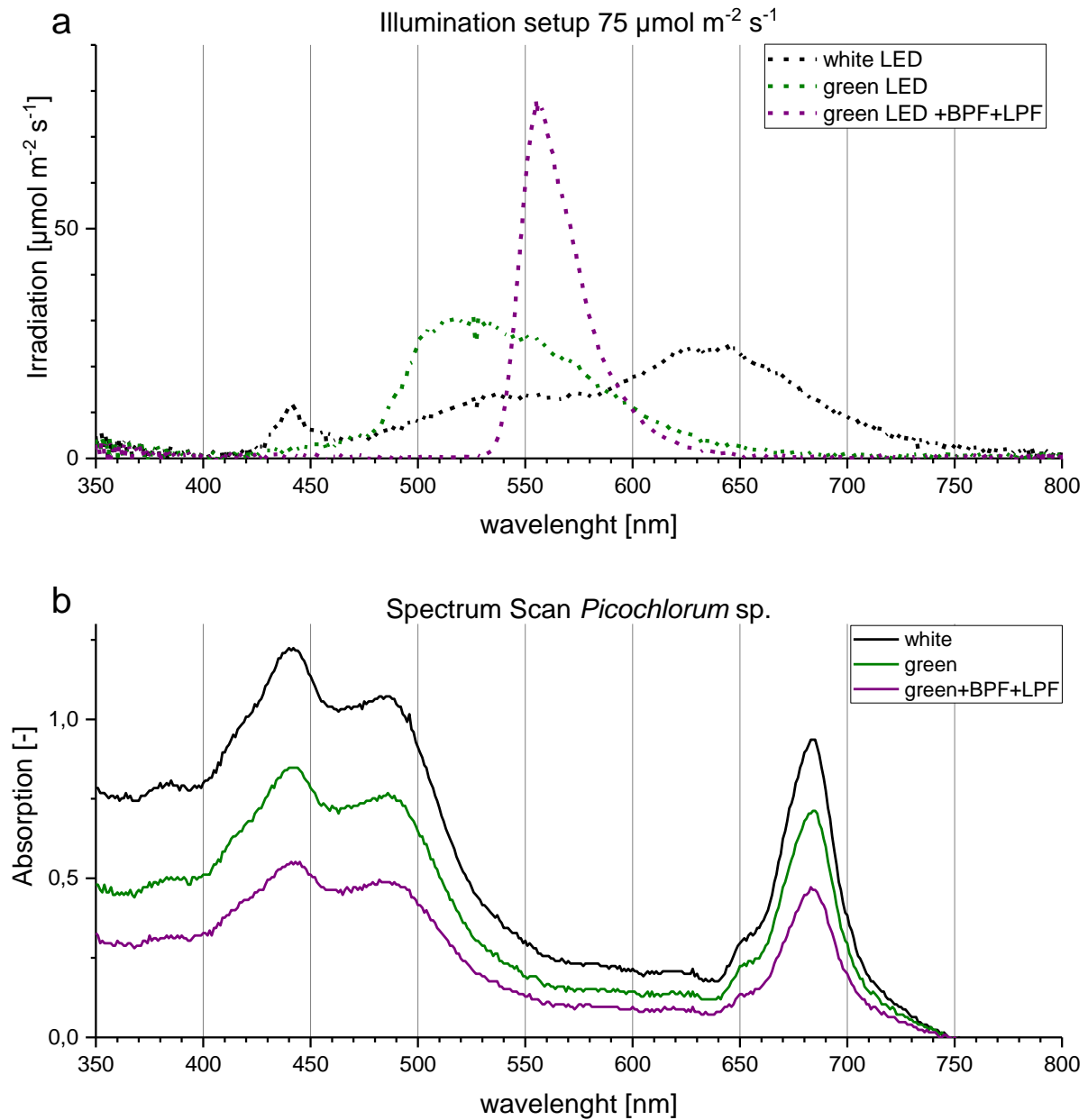
Figure 35: a) Illumination setup at 75 µmol m^{-2} s^{-1} with the glass filter plates installed on the LED-shaker platform. b) Spectrum scan 350 – 800 nm of *Picochlorum* sp., scan at day 10, absorption normed to 750 nm value. Measurement of live cells performed via plate reader.

6.2.4 Summarized results of stage 2 experiments

With the increase of irradiance level up to 200 µmol m^{-2} s^{-1} and the rise of CO_2 to 2% in the aeration biomass yields up to 5 g$_{DW}$ L^{-1} were obtained. *Picochlorum* sp. cells grew with less difference concerning the illumination color. Only at blue illumination the biomass gain was less as observed in previous experiments.

Pigment analysis replicated previous results showing increased levels of unidentified pigments at green light with reduced pigment concentration of the two dominant pigments chlorophyll *a* and *b*.

A bandwidth reduction towards the blue spectrum (green+BPF) or the red spectrum (green+LPF) did not alter the pigment spectrum. Spectrum scans did not show any difference in absorption.

A double bandwidth reduction to the central green of the 510 nm LED resulted in less growth than the parallel cultivated white or green light cultivations. Pigment formation showed less unknown pigments in two out of three samples. The spectrum scan did not show any absorbance shifts though.

6.3 Stage 3 experiments – *Picochlorum* sp. Scale up and pigment analysis

Modification of illumination bandwidth was one approach to tackle the accumulation of the observed unknown pigments. In a parallel approach the pigment formation was targeted differently. In stage 3 experiments a scale up to 2.5 L photo-bioreactor dimension was implemented. Having more working volume allowed for a higher quantity of pigment samples even at the start of the fermentation with still low biomasses.

The Infors bioreactor system (section 5.6.4) combined with the illumination system described in section 5.6.5 was set to comparably settings than the shake flasks. Thus an irradiance of 150 µmol m^{-2} s^{-1} with constant illumination was chosen. The white and green LEDs were identical to the ones used in the LED-shaker unit. pH was set to be regulated at pH = 8.2 via stepwise addition of CO_2 to the usual airflow of 0.5 vvm process air. Agitation was set at 150 rpm and temperature set to 25°C. The working volume was 2.3 L.

Cell dry mass of the cultivations with white and green light are shown in Figure 36 a) along a sigmoidal curve fit according the SGompertz model (Karkach, 2006).

	white	green
model	SGompertz	
equation	$y = a * e^{-e^{-k*(x-xc)}}$	
a	4.4929 ± 0.0813	5.1694 ± 0.0749
xc	6.6443 ± 0.1067	6.4290 ± 0.0866
k	0.2698 ± 0.0109	0.2671 ± 0.0088
Chi-Sq	0.00401	0.00354
RSQ	0.99861	0.99907
cor. RSQ	0.99838	0.99892
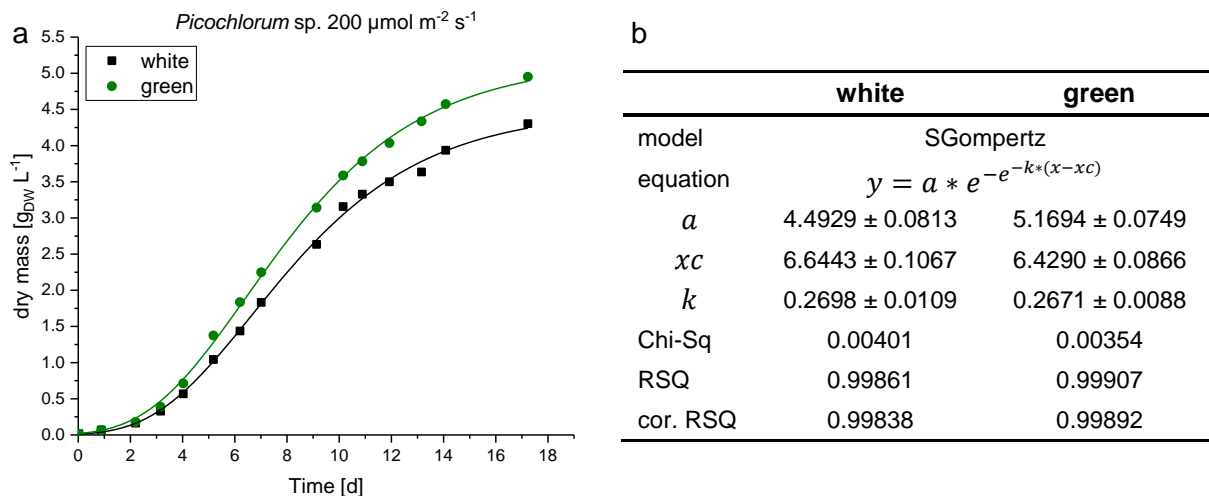
Figure 36: a) Fermentation of *Picochlorum* sp. with green and white illumination at 150 µmol m^{-2} s^{-1}. b) data of fitting SGompertz model curve for the cultivations.

Unlimited growth up to day 4-5 did slow down at dry masses of approximately 1 g_{DW} L^{-1} due to the irradiance of only 150 µmol m^{-2} s^{-1} and the culture depth at the stirred tank bioreactor. The cultivation was kept throughout the 18 days just like in the shake flasks. Total biomass of around 5 g_{DW} L^{-1} represented results obtained with the shake flask setup at 200 µmol m^{-2} s^{-1}. The analysis of pigments is shown in Figure 37 split in white and green illumination. Dry mass accumulations displayed with triangles on the right side axis. The axis was set to logarithmic scale in order to evaluate the state of cultivation. Maximum growth rates up to day 4 turn to limited growth up to day 8 and almost stationary phase until the end of

cultivation. Circles display the known pigments, most notably chlorophyll *a* and *b*, triangles display the unknown pigments occurring at green illumination.
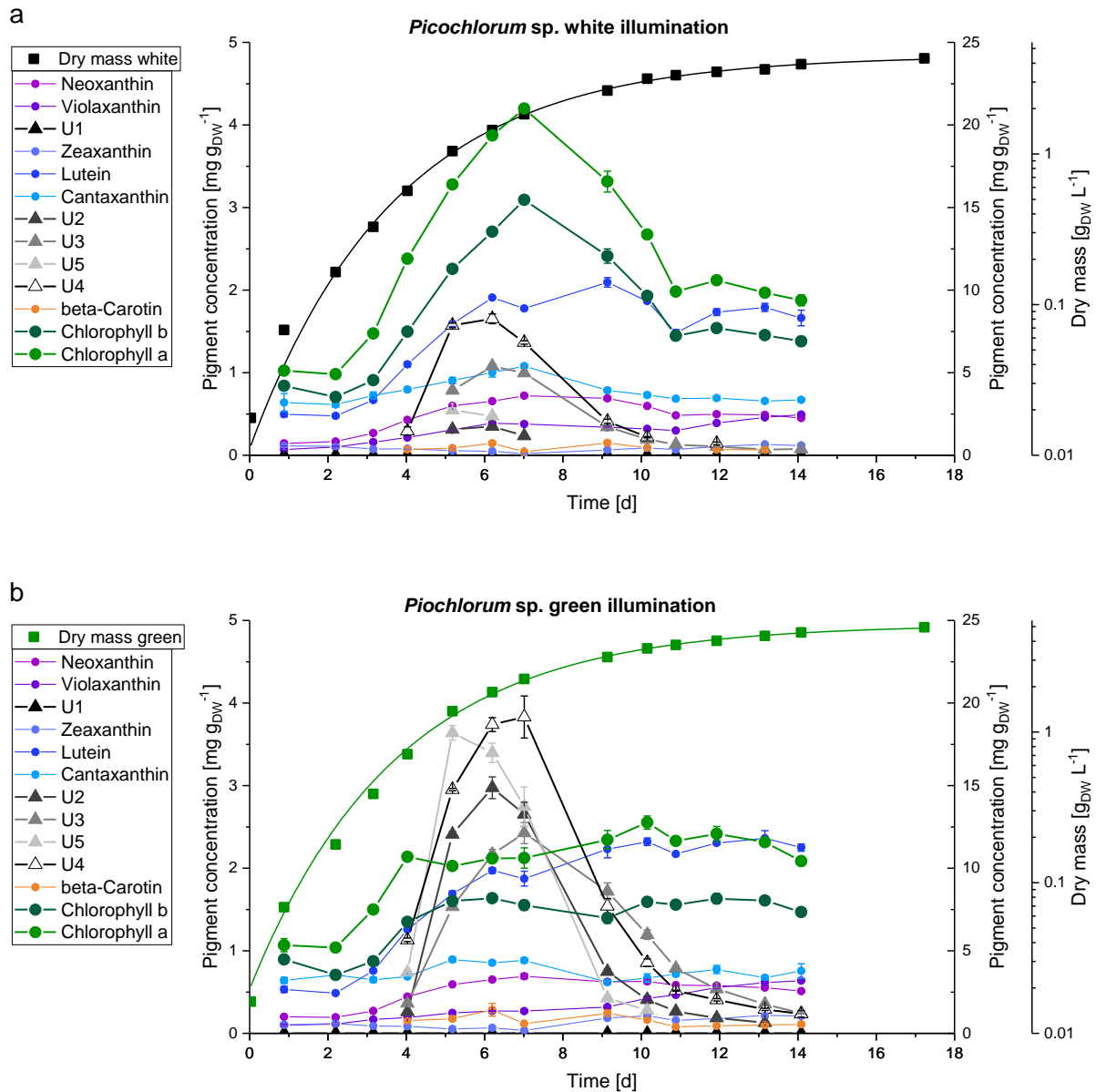
Figure 37: HPLC analysis of pigments of a) white and b) green illuminated *Picochlorum* sp. cultivation. Dry mass values (squares) are displayed on the far right logarithmic axis, pigments (known pigments in circles and unknown pigments in triangles) development on left side axis, chlorophyll *a* and *b* (green, dark green) on the right side pigment axis.

On first sight it is visible that at white light chlorophyll *a* and *b* concentrations rise during exponential and linear growth phase whereas the pigment titer [$mg_{Pigment}$ g_{DW}^{-1}] decline in the stationary phase. With green light the pigment distribution is identical for the first 4 days of unlimited cell growth. At day 4 pigment levels of the chlorophylls stagnate at half max value of the white illumination and the unknown pigments U2 - U5 accumulate. Towards the end of the linear growth phase these unknown pigments decline and the total pigment distributions match to the white illumination setup again. The different levels of pigment occurrence are shown in Figure 38 at selected time points of day 2 (early growth phase), day 6 (end of

exponential growth phase) and at day 11 (stationary phase).As the overall concentrations of Neoxanthin, Violaxanthin, Zeaxanthin, Lutein, Cantaxanthin and beta-Carotene show no major differences in the two illumination setups they were not included in this graph.
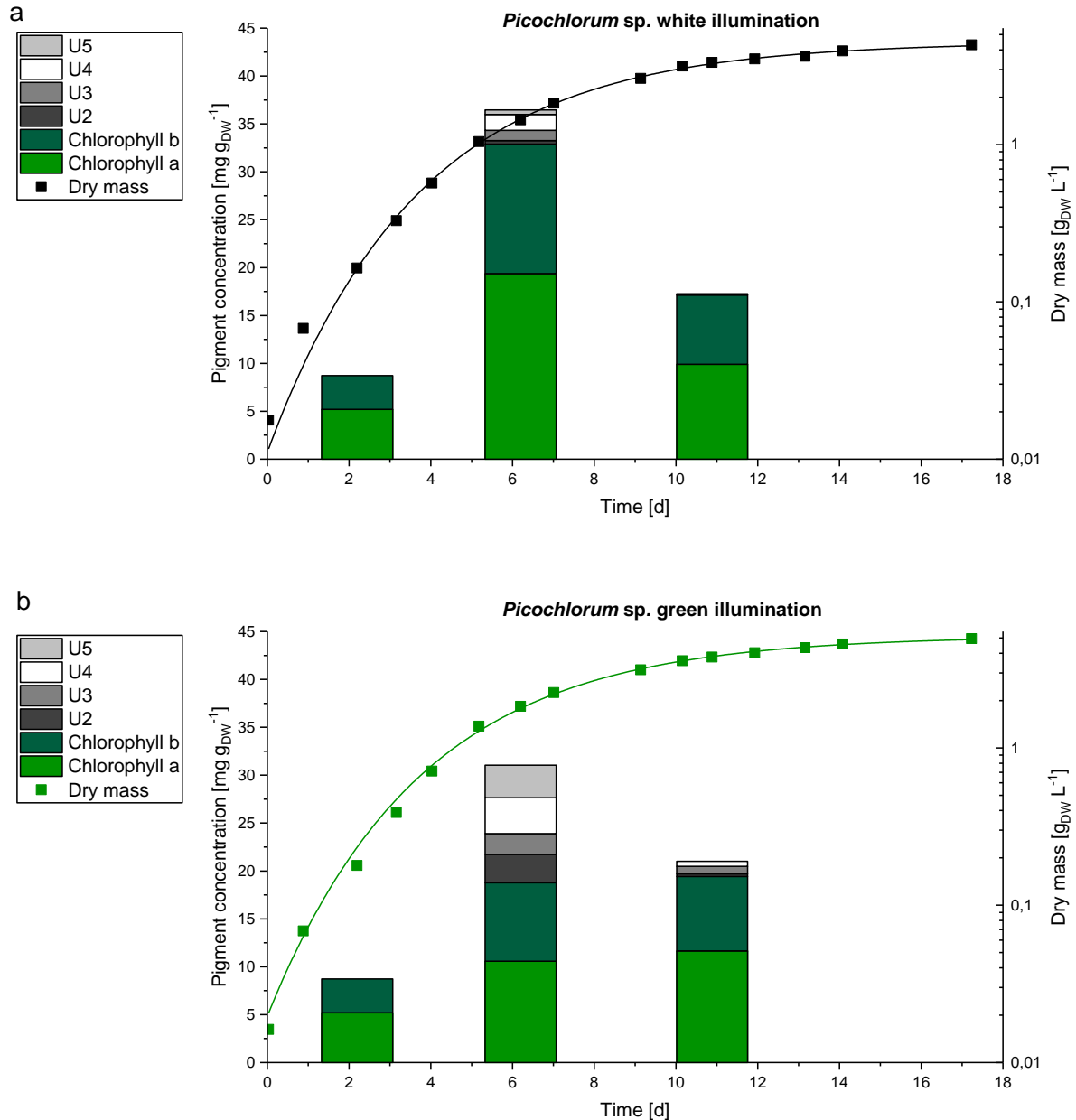
Figure 38: HPLC analysis of pigments of a) white and b) green illuminated *Picochlorum* sp. cultivation. Pigment concentration of Chl *a* and *b*, and unknown pigments U2, U3, U4 and U5 at day 2, 6 and 11 of the cultivation are shown.

As already seen in Figure 37, the formation of the unknown pigments is strongly promoted at the exponential growth phase. At day 6 the unknown peaks (see Figure 38) at green light make up 34.9 % of all detected pigments (8.7 % at white), the portion Chl *a* and *b* combined drops to 53.4 % (compared to 81.0 %) whereas the other detected pigments are stable at 11.7 % (green illumination) and 10.3 % (white illumination).

6.3.1 UV-VIS HPLC analysis

Having multiple samples of green illuminated *Picochlorum* sp. cells of exponential and linear growth phase containing the unknown pigments allowed for pooling. The samples were vacuum dried in darkness and resuspended in 5 times less volume of glacial acetonitrile. The stability of the extracted samples was monitored in a HPLC control run all of the resuspended samples. As all unknown pigment peaks were stable and unchanged (data not shown) unaffected further experiments could be performed. With these highly concentrated pigment solutions a UV-VIS analysis using the DAD was carried out. Figure 39 shows the UV-VIS spectra of chlorophyll b. Window a) represents a section of the actual HPLC chromatogram in this case from retention time = 25.49 – 27.01 min with the peak of chlorophyll b at 450 nm. Window b) shows the spectrograph at the position of the cursor line in the 3D overlay in window c), which contains the color-coded peak-intensities.
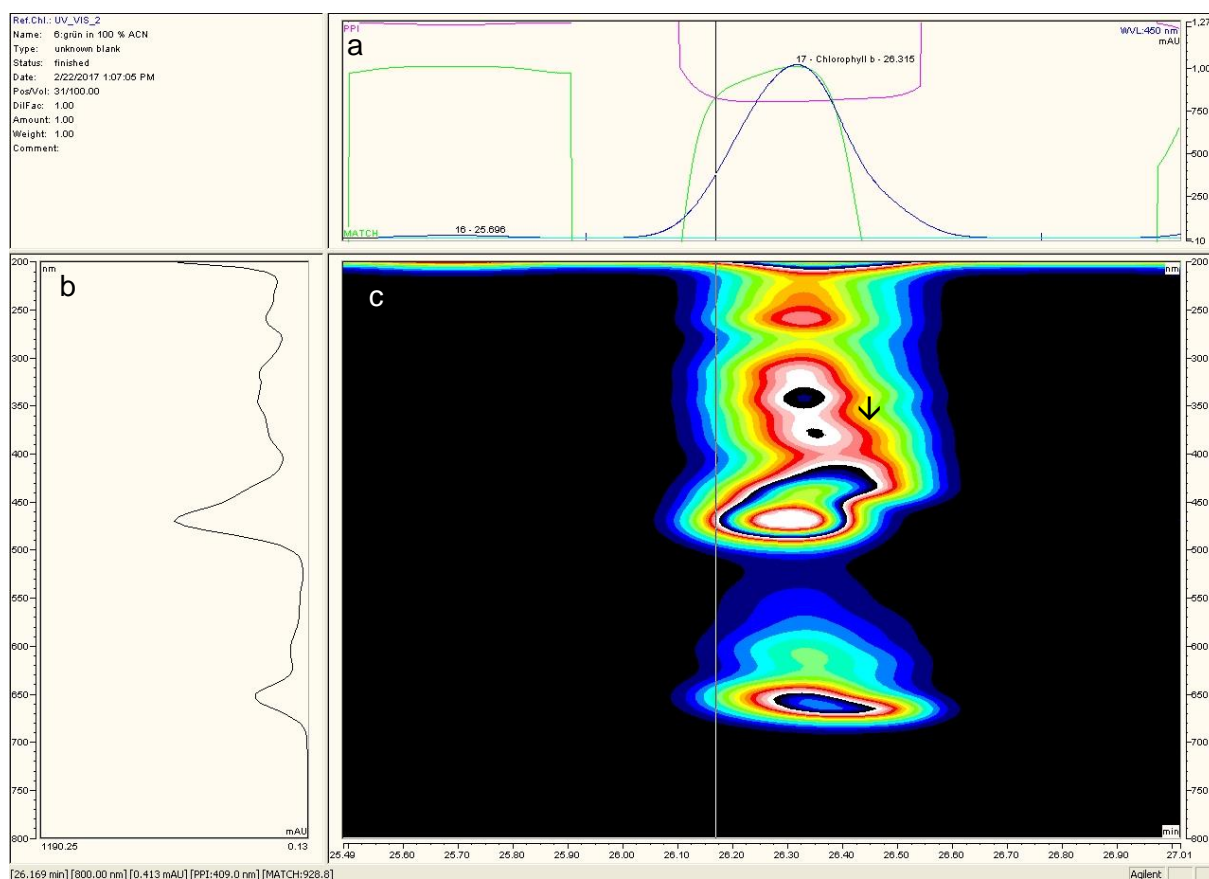
Figure 39: UV-VIS Spectra of Chlorophyll b extracted from *Picochlorum* sp. grown at green light. a) chromatogram b) spectrograph c) 3D display. Black arrow signaling occurrence of unknown pigment in the bulge of the 3d display of chlorophyll b

In case the HPLC separation on the column is working and no peaks elute at the same retention time than the 3D plots should be symmetrical with a Gaussian-style distribution curve. As seen in Figure 39 this was not the case for chlorophyll b, which showed a shift at

retention time 26.5 min (displayed with the arrow) with a barely visible shoulder on the right side of the peak in window a). The spectrograph (window b in Figure 39) set to this point (at RT 26.45 min) showed a typical chlorophyll *a* distribution within the chlorophyll *b* (RT 26.169 min, shown by the white line in the 3D overlay in Figure 39 c). The unknown chlorophyll *a*-style pigment was therefore named U5 and further considered in all experiments.
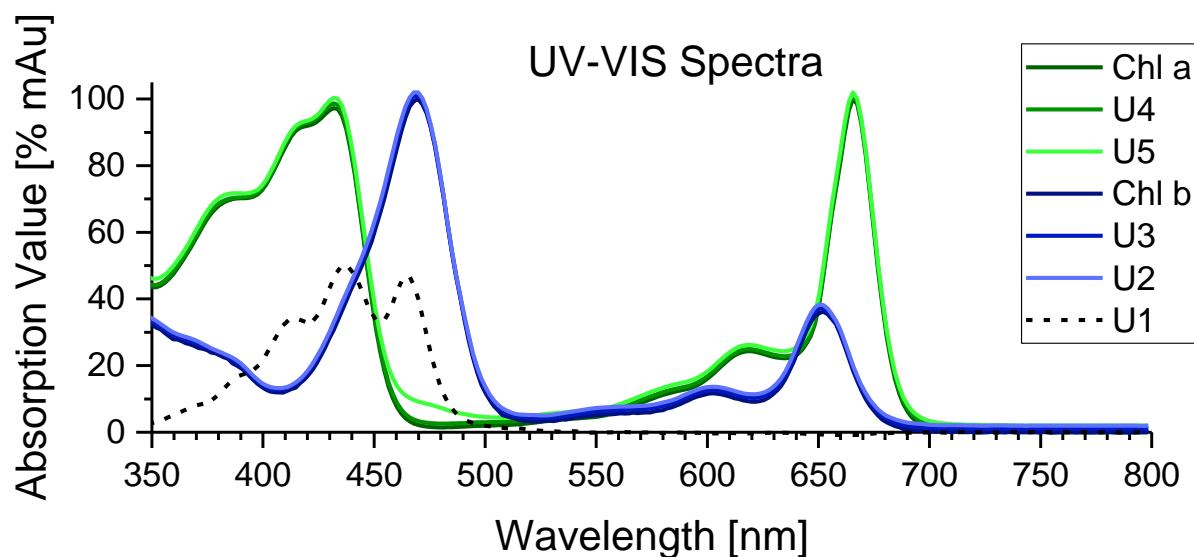
Figure 40: Spectrograph data of UV-VIS data analysis. All values normed to 100% of max value (chlorophyll a and b), 100% of max value + 1 % offset (U4 and U3), 100% of max value + 2 % offset (U5 and U2) and 50% of max value (U1)

The data obtained from the spectrograph window of each pigment is displayed in Figure 40. Spectrograph data did vary a lot in total value [mAu] depending on the position of the cursor in the overlay display. The spectrograms of U4 appeared also very similar to the Chlorophyll *a* spectra. The spectrograms of the unknown peaks U3 and U2 showed a high similarity to Chlorophyll *b*. To compare datasets and enable an overlay with the known spectral data of Chlorophyll *a* and *b* the raw data was normed to 100% of the maximum value. To display this overlay was difficult as the absorption spectra of the unknown peaks U2 and U3 were completely identical with chlorophyll *a*. Therefore, the U3 values were normed to 100% and displayed with an offset of +1 %, U2 normed to 100% and displayed with an offset of +2 % of the respective maximum value. The same findings could be seen with chlorophyll *b*, U4 (offset + 1 %) and U5 (offset + 2 %) respectively. U5 did show a slightly different curve between 460 and 500 nm compared to chlorophyll *a*. As this is in the main absorption area of chlorophyll *b* this could be a residual chlorophyll *b* effect due to the overlapping retention times. The absorption spectra of U1 pigment differed completely but show strong similarity with neoxanthin or violaxanthin of the xanthophyll class.

For further analysis, the concentrated pigment solution was separated via HPLC and fractionated manually. Aside the unknown pigment peaks, chlorophyll *a* and *b* were also pooled and fractioned and used as known reference for the analytical procedures.

6.3.2 High resolution HPLC-MS

The methods of high resolution HPLC mass spectrometry were described in section 5.8.1 and carried out for chlorophyll *a*, the mixed sample of chlorophyll *b* and U5 and the unknown pigments U1, U2, U3 and U4. Additionally, a blank sample of the preparative HPLC step was taken and analyzed to find potential contaminations or column residues. Figure 41 shows the MS- full scan of U4 in the top part a) with peaks at mass to charge ratios of 376, 398, 773, 869 and 891. The first three peaks could be assigned as impurities as they also occurred in the blank sample, as well as in all other samples. Full scans of all unknown peaks, as well as the blank sample are attached in section VII Appendix 3.
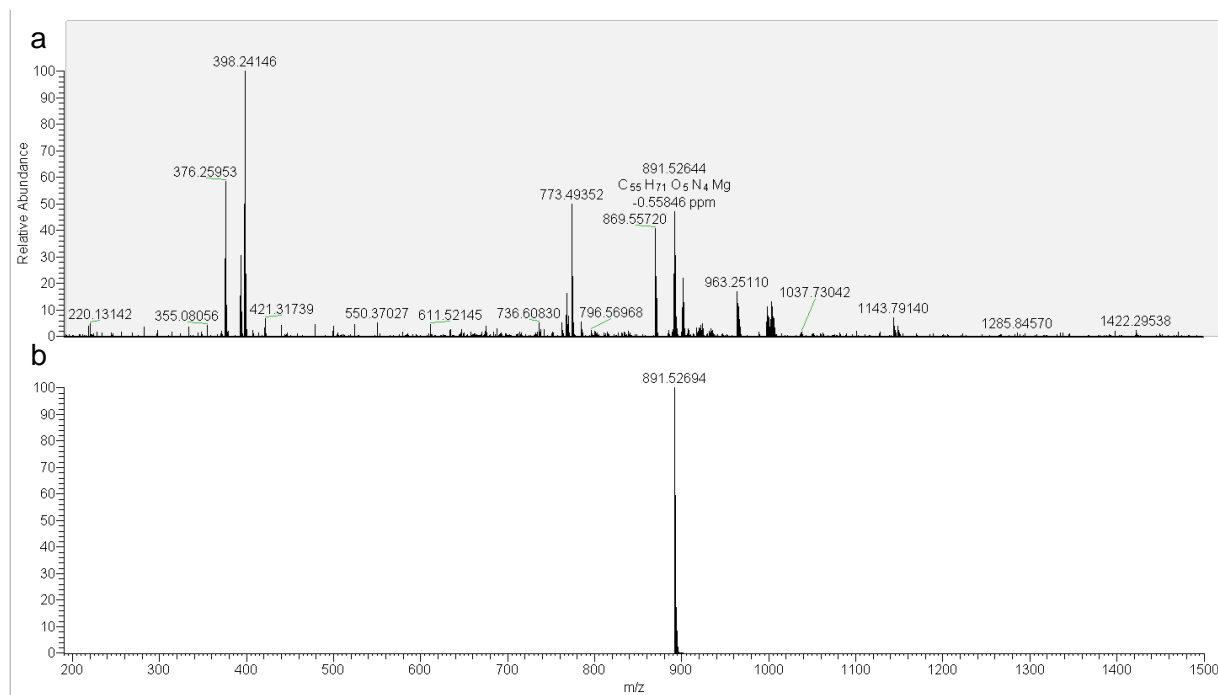
Figure 41: high resolution MS Full scan of U4 pigment in positive mode. a) MS-data relative abundance over m/z distribution. b) simulated mass distribution of $C_{55}H_{71}O_5N_4Mg$

The Peak with m/z 891.52644 matches to the simulated charge/-mass ratio of a molecule with the chemical formula $C_{55}H_{71}O_5N_4Mg$ with a confidential value of -0.55846 ppm. All conformities below 1 ppm can be considered positive. This mass formula represents the MH$^+$ ion of chlorophyll *a* ($C_{55}H_{73}O_5N_4Mg$) with a loss of two hydrogen atoms as it would occur if a single carbon bond is turned into a double carbon bond. The charge-mass ratio of 869.55720

is most likely the same U4 pigment with a loss of the magnesium ion (-23.985) and the addition of two hydrogen atoms (+1.008) at the binding position of the double positive magnesium-ion resulting in: 891.52644 -23.985 + 2*1.008 = 869.55744 m/z peak.

All analyzed pigment peaks were treated as demonstrated above with pigment peak U4 and the simulated matching molecular formula confirmed with a conformity value below 1 ppm are listed in Table 19. To keep track of the unknown pigment peaks and the simulated molecular formulas the peaks are already put in logical order. The MH$^+$ ion of chlorophyll *a* with its 73 hydrogen atoms is the base for the unknown pigments U4 and U5 which have one additional (U4) and three additional (U5) carbon double bonds resulting in 71 and 67 hydrogen atoms respectively.

Chlorophyll *b* seems to be the base-structure of the unknown pigments U3 and U2 where the same double-bond-pattern can be observed. The charge/mass ratio of U3 matches to chlorophyll *b*-MH$^+$ ion with a loss of 2 hydrogen atoms, or the addition of one carbon -double bond. U2 seems to have three additional double bonds on the chlorophyll *b* structure.

The pigment U1 has a matching molecular formula of $C_{40}H_{57}O_4$, which is the exact m/z of neoxanthin and violaxanthin MH$^+$ ion. A structural isoform could be a possible explanation for this match.

Table 19: Results of high resolution HPLC-MS analysis of Chlorophyll *a* and *b* and unknown pigment peaks U1-U5.

Pigment	actual MH$^+$ ion [m/z]	simulated matching MH$^+$ ion formula	simulated matching MH$^+$ ion [m/z]	conformity value [ppm]	Potential construct
Chl *a*	893.54219	$C_{55}H_{73}O_5N_4Mg$	893.54259	-0.44315	Chlorophyll *a*
U4	891.52644	$C_{55}H_{71}O_5N_4Mg$	891.52694	-0.55846	Chl *a* + 1 DB
U5	887.49532	$C_{55}H_{67}O_5N_4Mg$	887.49564	-0.35664	Chl *a* + 3 DB
Chl *b*	907.52182	$C_{55}H_{71}O_6N_4Mg$	907.52185	-0.04237	Chlorophyll *b*
U3	905.06698	$C_{55}H_{69}O_6N_4Mg$	905.50620	-0.24781	Chl *b* + 1 DB
U2	901.47479	$C_{55}H_{65}O_6N_4Mg$	901.47490	-0.12793	Chl *b* + 3 DB
U1	601.42519	$C_{40}H_{57}O_4$	601.42514	0.08528	cis/trans version of neoxanthin/violaxanthin

These results for the U2 - U5 pigments also correlate with the previously discovered absorbance pattern of the UV-VIS spectra displayed in Figure 40. A structural alteration of the two chlorophylls seems to be the cause of these pigment peaks occurring at green light. Nevertheless, these unknown pigments do not seem to alter the absorption spectra as it might have seemed logical. The double bonds must therefore occur in an area of the

molecule that is not directly involved in the photonic absorbance system. Similar sized MS/MS fragments (CID CE 35 %) found in all chlorophyll-altered samples could be the fragments of the same, unchanged porphyrin backbone, which would confirm that the double bonds are located somewhere in the phytol-side chain. The m/z for the phytol side chain could not be detected, because of its instability at the chosen collision energy.

The comparison of possible structural alterations and the retention time on the HPLC column (Table 19) show the same pattern: Chlorophyll *a*-altered pigments U4 (one double bond, retention time 28.84 min) and U5 (three double bonds, RT = 26.32 min) shifted in retention time from the chlorophyll peak at RT = 30.17 min forwards.

The Chlorophyll *b*-altered pigments shifted from Chlorophyll *b* (RT = 26.32 min) to U3 (RT = 24.76 min) to U2 (RT = 21.96 min).

Due to these findings pigment analysis could be extended to the unknown peaks, as a correlation factor as listed in Table 11 could previously only be established with known pigment standards. Now the correlation factor of Chlorophyll *a* was used for calculation of pigment content for U4 and U5 and the correlation factor of chlorophyll *b* correspondingly for U2 and U3. The unknown pigment U1 was correlated with the factor for neoxanthin.

6.3.3 NMR Analysis

The fractionated samples used for high resolution-MS analysis were used for NMR spectroscopy in order to resolve the double-bond theory established with the previous results.

One-dimensional ^{1}H-NMR spectra were obtained from all pigments. The ^{1}H signals are labeled according the IUPAC numbering system of the corresponding carbon number. As seen in Figure 42 the low-field signals make a differentiation of Chlorophyll *a* and *b* easy by the formyl part at the 7^1- carbon atom (see Figure 17, b) occurring at 11.25 ppm and is very characteristic for chlorophyll *b* spectra. The other characteristic low-field signals, the protons at 10, 5 and 20, as well as the 3^1 proton were detectable and could be matched according literature data (Kobayashi *et al.*, 2013). The P2-peak at 5 ppm represents the proton signal, with the influence of the double-bond between P2 and P3 (See Figure 17) and was used as indicator of additional double-bond insertions within the unknown pigments.
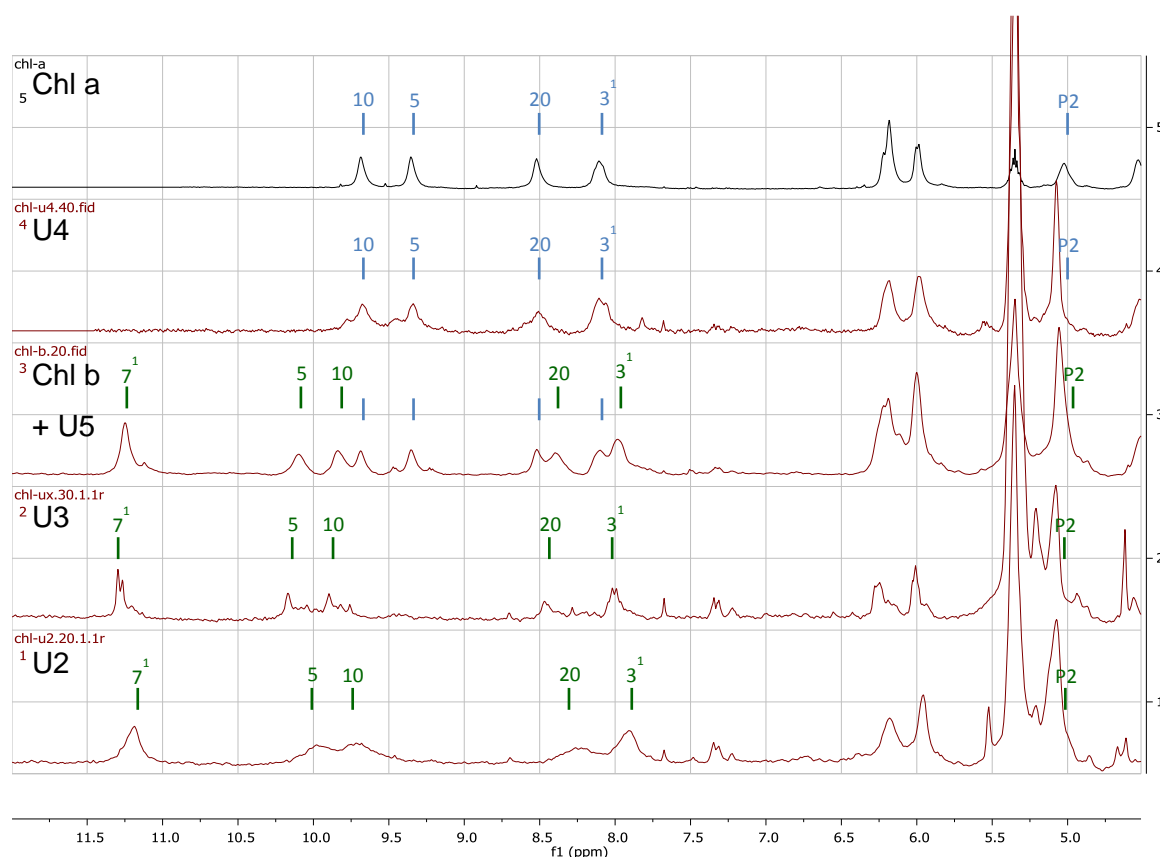
Figure 42: Low-field ^{1}H-NMR spectra and signals of IUPAC atoms 10, 5, 20, 3^1 and P2 of Chl a, U4 and U5, Chl b with signals of IUPAC atoms 7^1, 5, 10, 20, 3^1, and P2

In the mixed sample of Chlorophyll *b* the unknown U5-pigment could be seen via the different low-field shifts of the Chlorophylls *a* and *b* (labeled in blue and green at Figure 42). High field signal identification was not as clearly possible, as for the low-field signals.
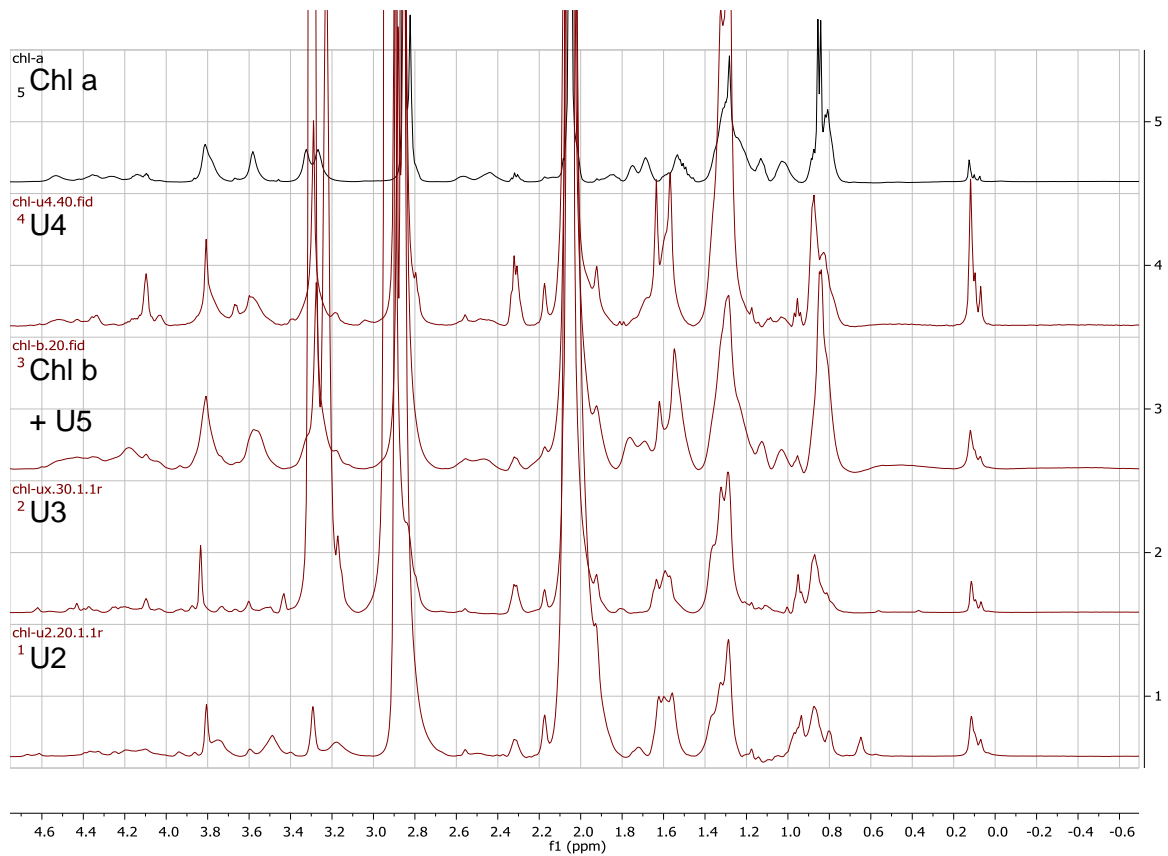
Figure 43: High-field ^{1}H-NMR spectra of Chl a, U4, Chl b and U5, U3 and U2 pigments. Acetone peak at 2.05 ppm
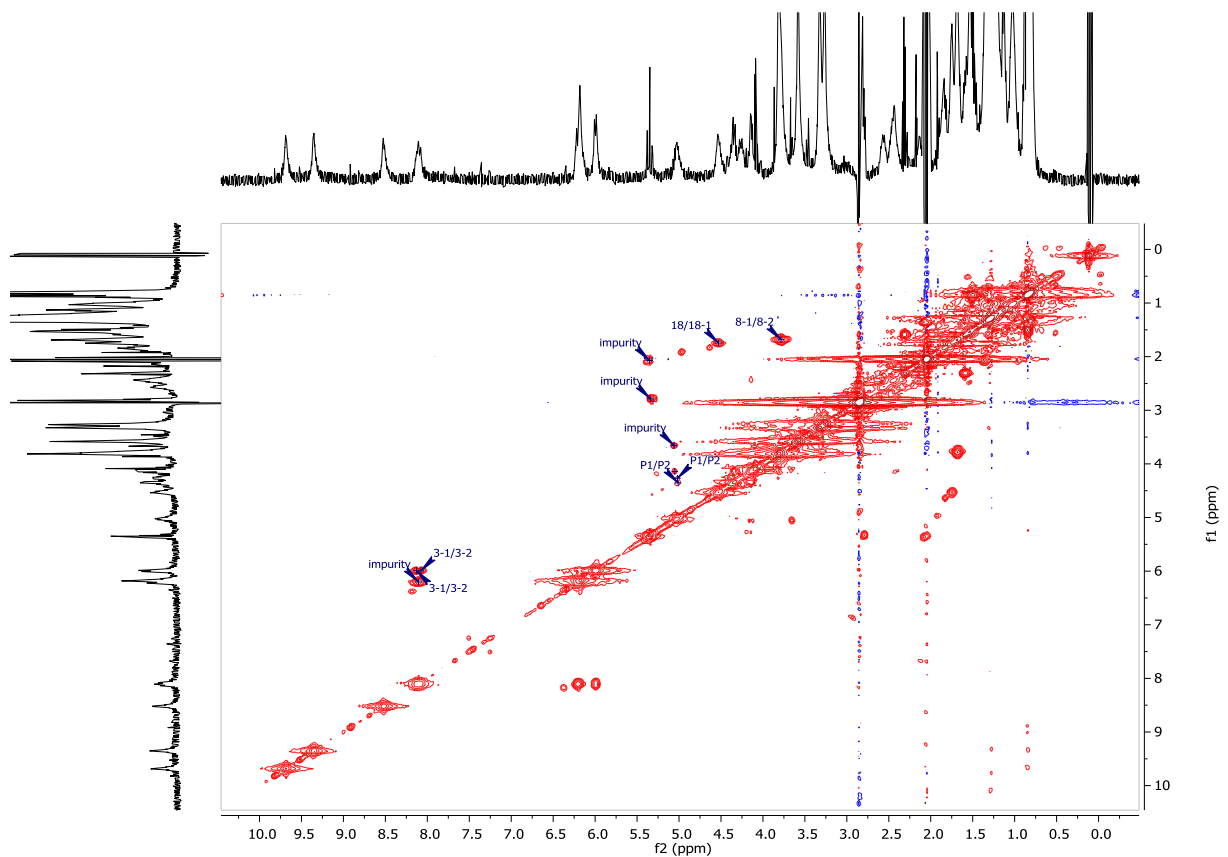
Figure 44: Chlorophyll *a* ^{1}H-^{1}H-COSY-NMR in acetone-d$_6$ at 293 K

In Figure 43 the high field ^{1}H-NMR shifts can be seen. Even with baseline correction the signals did not clearly stand out, which made an identification of all proton shifts difficult. Correlation spectroscopy (COSY) was used to identify protons interacting with neighboring proton signals such as the 3^1-3^2 interaction the P1-P2 or 8^1-8^2 signal of the ethyl-side chain (Figure 44). It also showed a number of impurities within the pigment solution that occurred as sharp signals. High-field signal assignment was also difficult to apply. With the help of the hetero nuclear single quantum coherence experiment (HSQC) the ^{1}H-signal assignment in the high-field area of the ^{1}H-spectra could be completed via linking the signals to the adjacent carbon ^{13}C-shifts on the f1-axis in Figure 45 atoms (^{1}H-^{13}C-HSQC). Through the distortionless enhancement by polarization transfer (DEPT) method the single protons (such as the proton at carbon atom 10 for example) and methyl-side chains (such as the 12^1 – methyl group) generate a positive signal (displayed in red), whereas ethyl-groups (such as 3^2) generate negative signals, denoted in blue.
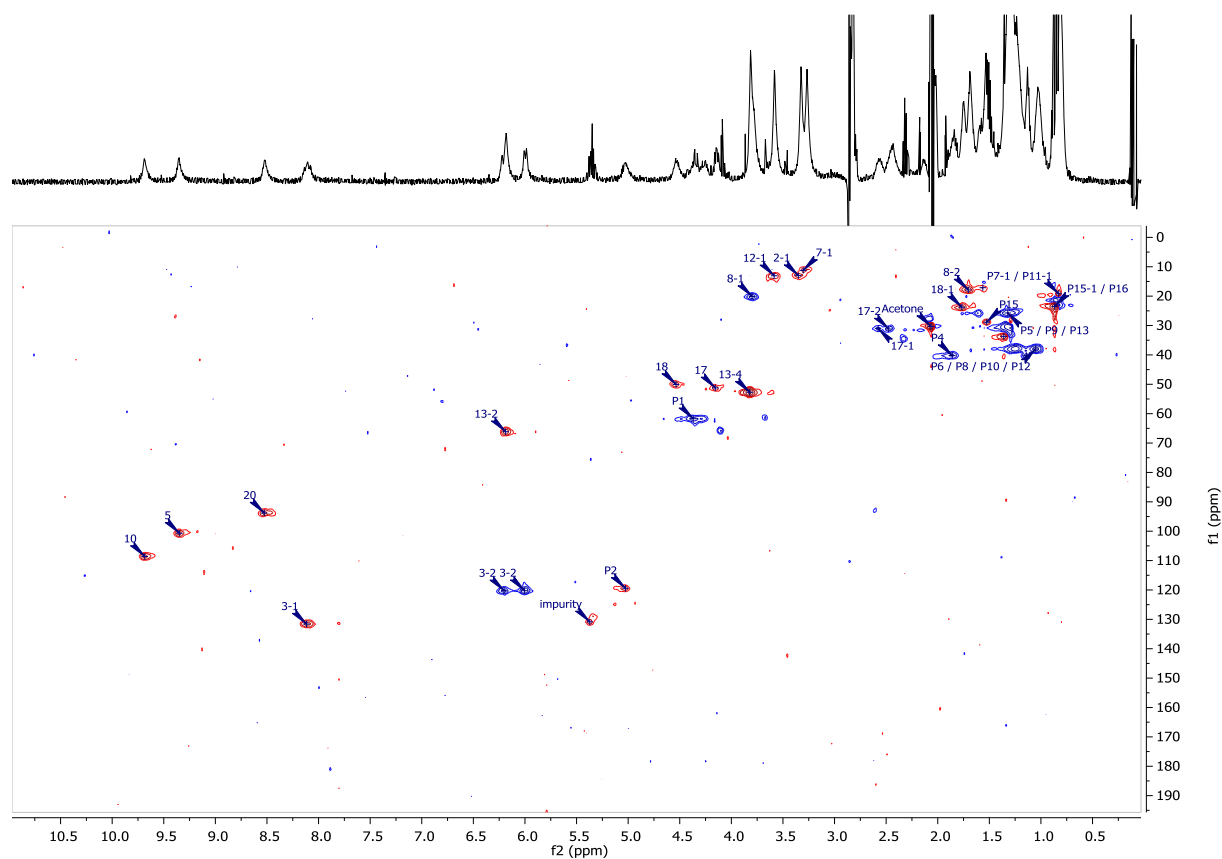
Figure 45: Chlorophyll *a* HSQC-NMR spectra in acetone-d₆ at 293K.

The complete list of identified ^{1}H chemical shifts is listed in Table 20 together with the reference shifts of Chlorophyll *a* and *b* used for identification (Kobayashi *et al.*, 2013). U5 being mixed up within the Chlorophyll *b* peak could not completely been identified.

Table 20: [1]H-chemical shifts of Chls a, b, unknowns U2 – U5 in acetone-d$_6$ at 293K. [#](Kobayashi *et al.*, 2013)

IUPAC no. of carbon atom	Chl a [#]	Chl b [#]	Chl a	Chl b	U5	U4	U3	U2
2[1]	3.343	3.316	3.32	3.32	3.32	3.39	3.30	3.29
3	-	-	-	-	-	-	-	-
3[1]	8.162	8.043	8.11	7.98	8.10	8.11	8.02	7.91
3[2]	6.242	6.302	6.22, 6.01	6.22, 6.00	6.19	6.21, 5.98	6.25, 6.01	6.18, 5.96
4	-	-	-	-	-	-	-	-
5	9.41	10.192	9.35	10.09	9.35	9.34	10.17	9.98
7[1]	3.3	11.305	3.27	11.25	3.28	3.29	11.29	11.19
8	-	-	-	-	-	-	-	-
8[1]	3.817	4.243	3.80	4.18		3.79	4.24	4.20
8[2]	1.696	1.815	1.69	1.82	1.69	1.64	1.81	
10	9.749	9.934	9.69	9.84	9.69	9.68	9.90	9.72
11	-	-	-	-	-	-	-	-
12	-	-	-	-	-	-	-	-
12[1]	3.619	3.606	3.58	3.58		3.59	3.60	3.49
13	-	-	-	-	-	-	-	-
13[2]	6.234	6.189	6.19	6.11		6.18	6.19	
13[3]	-	-	-	-	-	-	-	-
13[4]	3.829	3.842	3.81	3.81		3.81	3.83	3.81
17	4.175	4.128	n/a	4.10		4.13	4.10	4.10
17[1]	2.589	2.430	2.57	2.46	2.55	2.56	2.08	
17[2]	2.431	2.080	2.44	2.08	2.46	2.48		
18	4.572	4.524	4.53	4.43		4.51	4.43	4.37
18[1]	1.772	1.768	1.75	1.76				1.72
20	8.582	8.480	8.52	8.40	8.52	8.51	8.47	8.26
P1	4.342	4.364	4.34, 4.14	4.35		4.36, 4.25	4.37	4.33
P2	4.955	4.980	5.02	5.06	5.06	5.07	5.08	5.07
P3	-	-	-	-	-	-	-	-
P3[1]	1.509	1.519	1.58	1.55	1.50	1.57		1.56
P4	1.822	1.845	1.85					
P5	1.31	1.330	1.30	1.32	1.30	1.31	1.36	1.32
P6	0.97	0.980	1.03	0.98			1.00	n/a
P7	1.31	1.330	1.31	1.32	1.30	1.33	1.36	1.32
P7[1]	0.811	0.785	0.82, 0.81	0.78			0.79	0.80
P8	1.01	1.020	1.03	1.03				
P9	1.28	1.280	1.28	1.28		1.28	1.29	1.29
P10	1.01	1.020	1.03	1.03				
P11	1.31	1.320	1.31	1.32	1.30	1.33	1.32	1.32
P11[1]	0.783	0.809	0.82, 0.81	0.81			0.81	0.80
P12	1.01	1.020	1.03	1.03				
P13	1.28	1.280	1.28	1.28		1.28	1.29	1.29
P14	1.12	1.120	1.13	1.13				1.18
P15	1.5	1.489	1.53	1.49				
P15[1]	0.854	0.851	0.85, 0.84	0.85, 0.84			0.86, 0.84	0.87
P16	0.854	0.851	0.85, 0.84	0.85, 0.84			0.86, 0.84	0.87

In order to identify potentially new double bonds in the chlorophyll structure a change in the chemical [1]H-shifts should be detectable. As all shifts of the phytol sidechain are located in the high-field area between 0.8 and 2 ppm a loss of signal was undetectable. However, the formation of a double bond results in a downfield shift and should give a similar signal than the P2-signal at 5 ppm. So with the previous assumption of double bond insertion in the unidentified pigments summed up in Table 19 and a peak comparison of the P2 peak was conducted. The identified signals of the low-field ^{1}H spectra (Figure 42) were used as reference because each proton generates a distinct signal area and compared to the P2-area at 5 ppm. The peak integrals of the 10, 5, 20 and 3[1] signals (for Chlorophyll *b* also the 7[1] signal) were averaged and multiplied with the number of expected double bonds, which was then set into ratio with the actual P2-area to confirm the assumed double bond count (Figure 46).
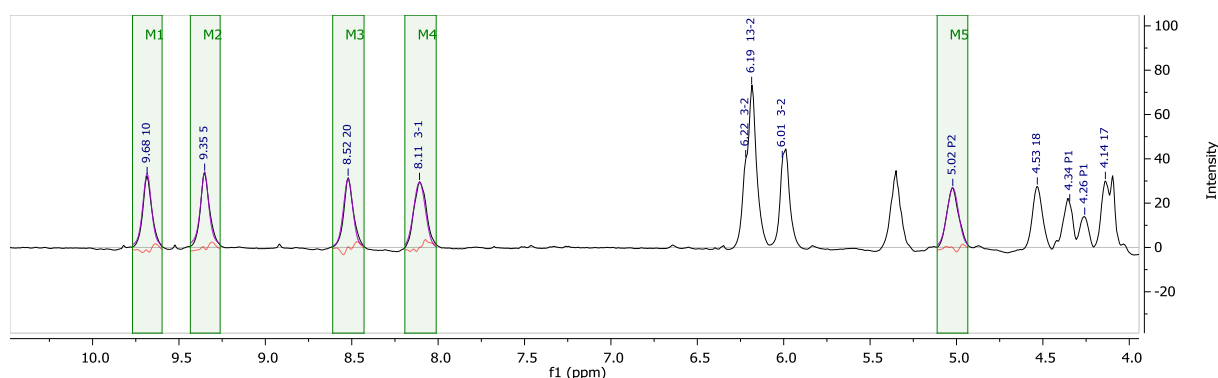
Figure 46: Peak area integrals (M1- M4) of Chlorophyll *a* (10, 5, 20 and 3[1] versus P2) for estimation of P2 area (M5).

For Chlorophyll *a* with no additional double bonds at the phytol side chain the P2 area should be at the same size than the average low-field shift peak. The ratio calculates as followed:

$$ratio = \frac{P2_{area}}{P2_{expected}} = \frac{7434.1}{7556.3} = 98.4\ \%$$ (7)

In the case of the mixed Chlorophyll *b* with the U5 pigment it is a little bit more difficult, as both P2-peaks have the same chemical shift and are thus adding up to each other: The P2 area of the Chl b should be the averaged Chl b peak with 2762.8. Adding up to this the P2 peak of the U5 pigment plus three additional averaged P2 peaks of U5, resulting in:

$$ratio = \frac{P2_{area}^{Chl\ b+U5}}{P2_{expected}^{Chl\ b} + P2_{expected}^{Chl\ b}} = \frac{11602.7}{2762.8 + (2096.7 + 3*2096.7)} = 104.1\ \%$$ (8)

The expected ratios of U4 and U3 (one extra double bonds each) and U2 with three additional double bonds were calculated accordingly.

Table 21: Peak area calculation and conformity ratio

Peak	Average peak area	P2 area	P2 expectation	ratio
Chl a	7556.3 ± 327.2	7434.1	7556.3	98.4%
Chl b +	2762.8 ± 41.6			
U5	2096.7 ± 118.8	11602.7	11149.5	104.1%
U4	4392.0 ± 97.0	8529.7	8784.1	97.1%
U3	2.21E+08 ± 6.54E+06	4.96E+08	4.42E+08	112.1%
U2	5.29E+08 ± 1.07E+08	2.31E+09	2.12E+09	109.1%

Table 21 displays the averages low-field-peak area and the P2-area of the ^{1}H-NMR spectra. The expected P2 area is calculated as shown in equation (7) and (8). With a ration of < 5 % deviation the additional double bond in U4 and the three additional double bonds of U5 in comparison to the Chlorophyll *a* structure are confirmed. With a deviation of around 10 % the Chlorophyll *b* derivatives U3 (with one additional double bond) and U2 (plus 3 double bonds) are also strongly supported.

6.3.4 Stage 3 summary

Stage 3 experiments carried out in photo bioreactor dimensions enabled closer sample frequency and higher sample quantities for pigment analysis. The unknown pigments were observed to occur in exponential and linear growth phase but decline towards stationary phase. A fifth unidentified pigment, named chronologically U5, (although having a shorter RT than U4), was identified via UV-VIS analysis and elute very close to Chlorophyll *b*. U2 and U3 shows identical absorbance than Chlorophyll *b*, whereas the spectra of U4 and U5 are identical to Chlorophyll *a*.

Via high resolution LC-MS the structural similarities of the unknown pigments to chlorophyll *a* and *b* are confirmed with potential additional double bonds (+1 and +3) at the phytol side-chain. U1 pigment is confirmed as a potential isoform of violaxanthin or neoxanthin.

NMR analysis was completed for U2 - U5 and the ^{1}H chemical shifts were obtained. The change of peak-area at the P2-shift compared to the chlorophylls confirms the double bond insertion and their position on the phytol side chain via a second method.

7 Results Mutagenic Procedures

All mutagenic procedures were carried out with the scope of producing and finding fast growing microalgae mutant strains. *Picochlorum* sp. was the strain of interest within the framework of this dissertation and therefore all new mutagenic procedures were carried out with this strain.

Previous *Picochlorum* sp. tests growing on agar or gelrite plates with various salt-media did not deliver any good and reliable growth with the additional problem of proper growth assessment. 96-well plates were the smallest liquid-handling possibility to grow algae on a shaker platform. With small volumes of just 200 - 300 µL the evaporation rates had a tremendous effect on cultivation and daily evaporation adjustments (such as automated volume control with refill) would be needed. Additionally, growth rates were also quite low. The 24-well-plate shaker platform with 1 mL culture volume seemed a good approach with a reasonable amount of wells per plate and thus a high number of parallel feasible assays. With an initial growth analysis, the range of possible cultivations in 24-well plates with *Picochlorum* sp. was assessed.
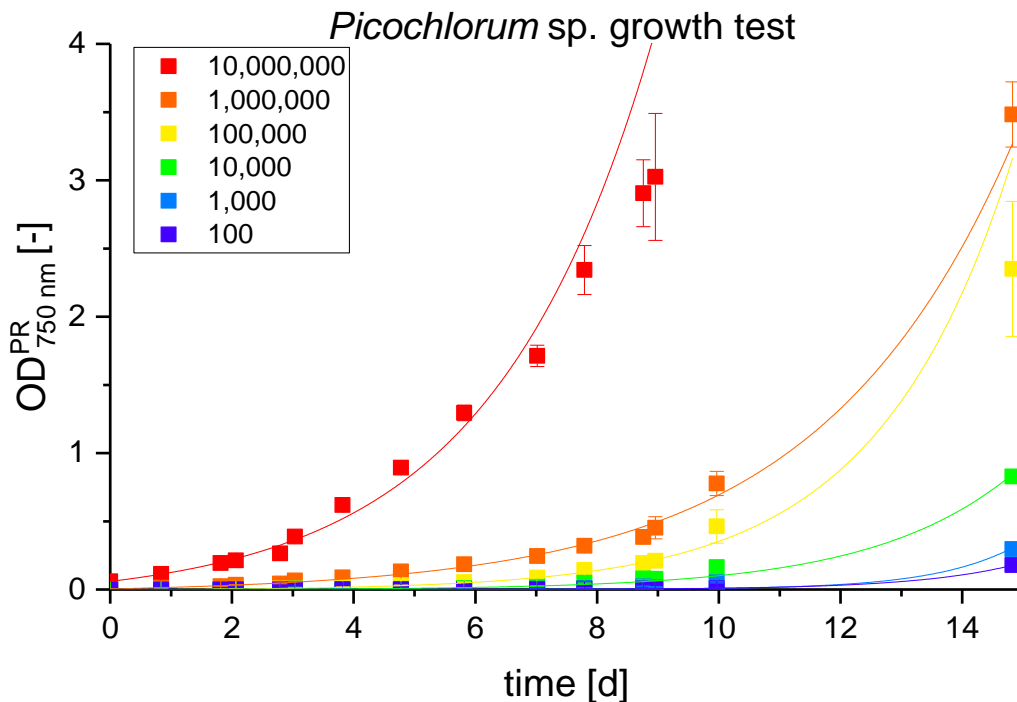
Figure 47: Growth test of *Picochlorum* sp. grown in 24 well plates, 150 rpm and 50 µmol m^{-2} s^{-1} irradiation at 25°C with aeration every 48 h. Initial cellcounts 100 – 10,000,000 cells mL^{-1} (n=4)

Cultivations with 150 rpm at 25°C and with 50 µmol m^{-2} s^{-1} irradiation showed a stable and repeatable growth pattern. To prevent evaporation, the 24-well plates need to be sealed with Parafilm otherwise the plate will dry out, starting from the 4 corner wells, within 7 days. Through the sealing an evaporation of the plate every 48 hours was required (at high cell

densities every 24 hours) via placing the plates in a sterile environment and lifting the lid for 2 minutes. Growth analytics with optical density measurement did work for cell densities up to 0.5 at the EnSpire Plate reader. Higher densities exceeded the linear phase and wells have to be diluted with fresh media accordingly. Figure 47 shows an initial growth test with *Picochlorum* sp. grown in 24-well plates. Exponentially grown cells were diluted to cell concentrations from 10^7 cells mL^{-1} till 100 cells mL^{-1} by using the S3 cell sorter (Biorad) and aliquoted in a 24-well plate in quadruplicates. Cell growth was monitored and wells were diluted once they reached optical densities of OD$^{PR}_{750\,nm}$ > 0.5. In Table 22 the values of an exponential curve fit (OriginPro 2017G software b9.4.0.220) of the growth curves shown in Figure 47 is presented. With overall growth rates from 0.37 d^{-1} to 0.45 d^{-1} (start cellcounts 10,000,000 till 10,000) the growth is slower than in shake flasks but still at reasonable speed. The growth rates of the 1,000 cell approach with 0.75 d^{-1} are within the range seen in shake flasks at unlimited growth and at 1000 cells starting with 0.61 d^{-1} just in between the observed ranges.

Table 22: Curve fitting values of exponential growth of *Picochlorum* sp. in 24-well plates with varying starting cellcounts of 100 up to 10^7 cells ml^{-1}

	10,000,000	1,000,000	100,000	10,000	1,000	100
model			exponential			
equation			$y = y0 + A * e^{(R0*x)}$			
$y0$	-0.08327	-0.02634	-0.00573	-0.00262	0.00132	2.776E-4
A	0.14278	0.03079	0.00393	0.00134	3.927E-6	2.031E-5
$R0$	0.37704	0.31524	0.45140	0.43533	0.75956	0.61222
Chi-Sq	24.27539	3.99249	1.63777	5.07427	23.0065	0.88065
RSQ	0.97067	0.97823	0.97335	0.95908	0.77537	0.96617
cor. RSQ	0.96480	0.97460	0.96891	0.95226	0.73793	0.96053

With these settings a screening of mutant cells seemed reliable in 24-well plate-dimensions and was thus used for all following screening procedures. Cultivations were carried out with a maximum duration of 2 weeks as afterwards evaporation effects generating a false-positive growth appearance. Cell densities of just 100 cells mL^{-1} are thus set as the lower detection boarder within one cultivation cycle. For initial survival tests after mutagenic treatment, a dilution step of 2 (500 µL well volume filled up with 500 µL fresh media) was implemented to prolong the initial screening and enable single cell mutation strains to grow up to detection range.

7.1 ARTP Plasma mutation

Plasma treatment of microalgae with atmospheric and room temperature plasma (ARTP) was carried out as described in section 5.11.3 with the flow settings shown in Table 13. 1 mL cell solution with 10 Mio. cells ml^{-1} was treated in each experiment. After treatment the remaining cell volume was collected and stored in darkness for 24 h and then 100 µL were aliquoted in 24-well plates and filled up with 900 µL fresh media. In the first screening the survival rate was determined. Whereas the following screenings had the focus of finding fast growing *Picochlorum* sp. mutant strains. After the initial dilution step with fresh media the 24-well plates were shaken at 150 rpm and illuminated with 50 µmol m^{-2} s^{-1}. The sealed plate (to prevent evaporation) was aerated at least every 48 hours and cell growth was monitored via measurement of optical density and cellcounting on the sorter.

7.1.1 Plasma kill rate

Figure 48 displays the optical density OD$^{PR}_{750\ nm}$ at day 10 of the initial growth check. Each data point represents one well containing a potential mutant strain.
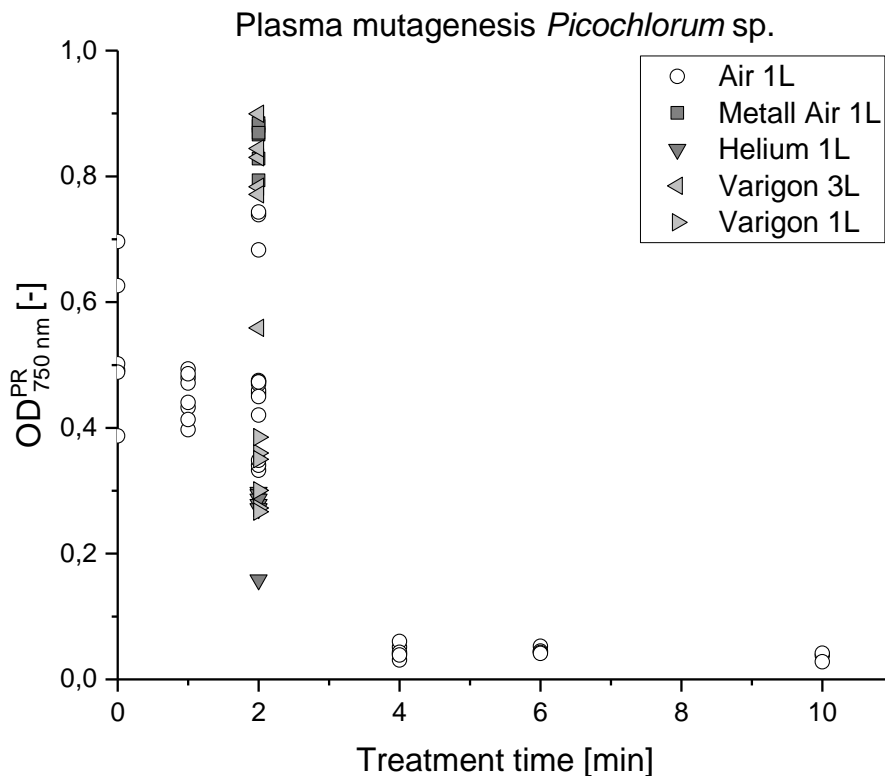
Figure 48: Plasma mutagenesis with *Picochlorum* sp. Initial growth 10 days after treatment. Plasma with air as carrier gas, plasma on metal plate, helium as carrier gas, varigon with 3L min^{-1} and 1L min^{-1}

The untreated control strains (0 min treatment) started growth with a cellcount of 10^6 cells mL^{-1}. For all treated strains the number of surviving cells should be lower or ideally close to zero. In circles the standard plasma treated cells with air as carrier gas are shown with treatment durations up to 10 minutes. At that time more than half of the initial 1 mL was

evaporated through the plasma-flame. After 15 minutes treatment the petridish was completely dried out and no sample could be recovered. No cell growth was detectable beyond 4 minutes of plasma treatment. The initial screening was carried out for 17 days and the samples with treatment for 4 - 10 minutes did not show any growth after that time. So the 100% kill point was set between 2 and 4 minutes. The substitution of the carrier gas to Helium (downwards triangles in Figure 48) did result in similar growth than the untreated cells but with less total biomass yield. The varigon®H2 carrier gas (98 % Argon and 2% Helium) with a flow rate of 1L min^{-1} did also result in less biomass than the air plasma. Varigon®H2 with 3 nL min^{-1} flow did show a higher biomass production in the initial screening, which might be due to the fact that the higher flow rate caused a higher evaporation leading towards a concentration effect and thus a higher biomass start-concentration at the screening. Still the growth rate of varigon®H2 with 3 nL min^{-1} is significantly higher (p = 0.033) than the 0 min treatment control group (see Table 23 b). The metal-approach, a 1 mL of cell suspension was placed on a brass plate instead of a petridish and was plasma-treated for 2 min with air as carrier gas, did generate higher biomass and significantly higher growth rates than the comparative 2 min treatment in a petridish.

Table 23: plasma treatment a) display of maximum growth rates in initial survival test of *Picochlorum* sp. b) *p*-values of students t-test correlation between µmax growth rates of plasma experiments

a

b	0 min	1 min	2 min	metal	helium	var 3L	var 1L
0 min	---	0.176	0.319	**0.008**	0.677	**0.033**	0.109
1 min		---	**0.030**	8.8E-13	0.0059	5.3E-9	5.1E-04
2 min			---	**0.043**	0.416	0.311	0.813
metal				---	**0.016**	1.8E-04	2.3E-03
helium					---	**0.035**	0.085
var 3L						---	**0.049**
var 1L							---
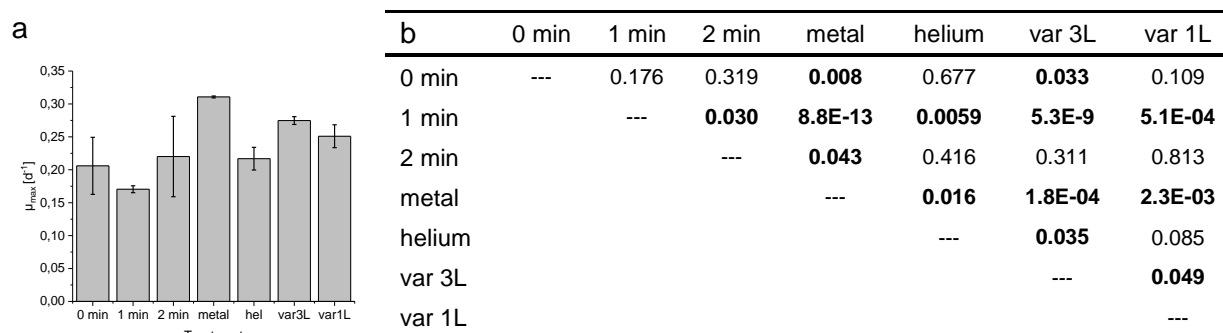
7.1.2 Mutant screening

Following the initial screening for survivability the wells were set into 10 groups of similar optical densities and less than 5 % deviation, the cellcount for each group was analyzed with the cell sorter. The screening cycle was started with individual dilution for each well (according to the group-cellcount) with fresh media and a cellcount of 10^6 cells well^{-1} or cells mL^{-1}. The first screening was carried out for 14 days. The 4, 6 and 10 min samples were recultivated as well in case very little cells did survive the initial plasma treatment and to enable cell growth from less than 100 cells, which was not detectable within the first screening. For to wells of the 4 - 10 min treatment range growth and build-up of biomass were detected, one from the 4 and one from the 6 min treatment group. All other potential

mutant strains did grow which was monitored via $OD^{PR}_{750\,nm}$ analysis and cellcounting via cell sorting. Due to the tremendous time-effort cellcounting could only be carried out four times within the two weeks giving exact cell numbers with the drawback of just four sample points over the 14 day cultivation. With comparison of the data obtaining from these cellcountings and the data obtained via plate reader measurement further cellcount-analysis was suspended.

For all mutant and untreated cells the maximum growth rate was determined over 4 sample points (minimum 60 hours) and a RSQ > 0.95 (see section 5.3.3). The max growth rate of the untreated cells (for screening 1: $\mu_{max} = 0.328 \pm 0.036$ d^{-1}) was set as benchmark for potential mutant cells. Table 24 provides an overview of the 3 subsequent screenings. In Screening 1 which lasted 14 days, out of 82 assays 57 mutant strains did grow and 33 were monitored with higher growth rates than the benchmark value. These strains were equally distributed over all treatment variations. The best mutant strain out of the 2 min treatment group did show a maximum growth rate of $\mu_{max} = 0.401$ d^{-1}. Nonetheless the average maximum growth rate of all faster-than-untreated-strain growing mutants did not differ significantly (*p*-value of students t-test: *p* = 0.076).

Table 24: Screening of plasma treated *Picochlorum* sp. Number of positive screened, fast growing mutants and their distribution throughout the treatment.

Plasma treatment	Screening 1	Screening 2	Screening 3
Screening duration	14 days	17 days	12 days
Treatment			
1 min	3	4	3
2 min	9	5	2
4 min	1	0	1
6 min	1	1	0
metal	5	1	3
helium	3	3	3
var3L	6	3	4
var1L	5	5	4
total/grown/positive	82/57/33	72/59/22	72/60/20
μ_{max} [d^{-1}] best mutant	0.401	0.315	0.368
μ_{max} [d^{-1}] control	0.328 ± 0.036	0.204 ± 0.008	0.310 ± 0.061
μ_{max} [d^{-1}] average mutants	0.355 ± 0.021	0.227 ± 0.027	0.328 ± 0.015
p-value	0.076	0.022	0.655

After screening 1 the mutant strains were rearranged for screening 2 and screening 3 leaving out those wells (mostly with 4, 6 and 10 min treatment strains) which did not show any kind of growth. Screening 2 and 3 were executed for 17 and 12 days. Overall approximately a third of the grown strains had growth rates higher than the average of the untreated control. In Screening 2 the average of the faster growing mutants did differ significantly (*p* = 0.022) if

compared to the average growth rate of the untreated cells. The maximum detected growth rate was μ_{max} = 0.315 d^{-1} of one strain still growing after 6 minutes treatment. With screening 3 the difference between faster growing mutant strains and control did decrease again with a maximum growth rate detected of μ_{max} = 0.368 d^{-1} of a strain with 2 min plasma treatment time. The control averages were a bit faster as well with μ_{max} = 0.310 ± 0.061 d^{-1}.

Of 22 positively screened strains in the second screening, 10 were also positive screened in the first screening. 7 out of 20 in the third screening did match with screening 2 and 10 matched positive strains of the first screening. In total only 2 strains were amongst the positive screened strains throughout all three screenings.

The best 9 mutant strains from the previous screenings were selected for ongoing screenings with 3 reference strains. Screening 4 was carried out in 100 mL shake flasks for 9 days in order to build-up biomass.

The final screening 5 was again carried out in 24-well plates. The selected 12 strains (9 mutant and 3 control strains) were grown in quadruplicate for 14 days. The results of growth analysis are listed in Figure 49 a) where the maximum growth rates with standard deviation are shown compared to the control column at the end. The origin of the mutant strains is listed in Figure 49 b) together with the p-value compared to the controls. The highest growth rate with μ_{max} = 0.323 ± 0.019 d^{-1} was significant higher (p = 0.016) than the control (μ_{max} = 0.273 ± 0.046 d^{-1}) and was achieved with mutant strain number 9, originated from the varigon®H2 plasma treatment with 3 nL min^{-1} airflow. In screening 3 this strain was already among the best growing strains.

The other significantly faster strain (p = 0.042) with a growth rate of μ_{max} = 0.309 ± 0.014 d^{-1} was mutant 1, originated from the 2 min plasma treatment and was among the fastest growing strains in screening 2 and 3.

a

b

strain	origin	p-value
1	2 min	**0.042**
2	4 min	0.760
3	2 min	0.142
4	1 min	0.452
5	var 3nL	0.249
6	var 1nL	0.184
7	1 min	0.954
8	2 min	0.703
9	var 3nL	**0.016**
control	0 min	
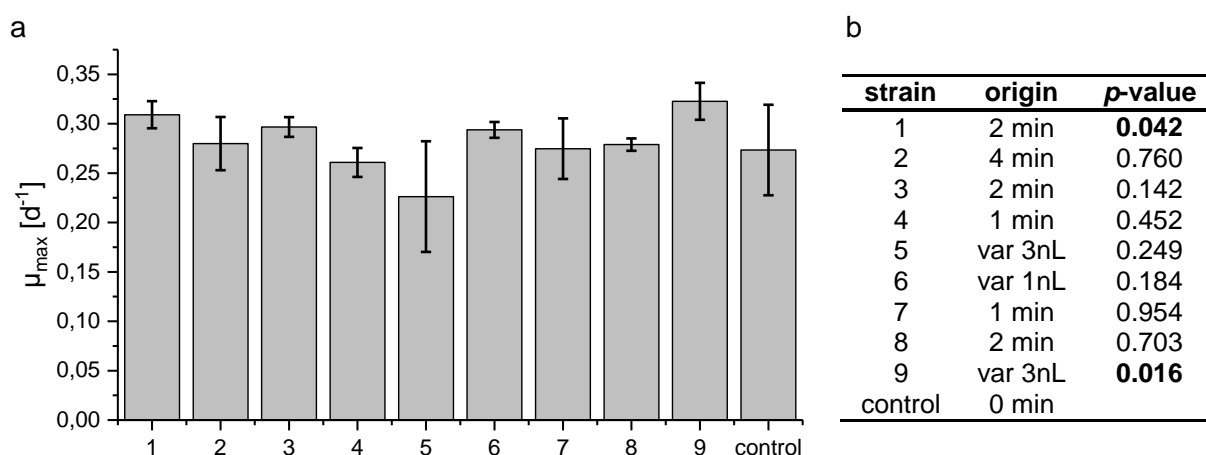
Figure 49: Screening 5 results a) maximum growth rates μ_{max} of the 9 best *Picochlorum* sp. mutant strains after plasma treatment (n=4) and untreated control strains (n=12). b) strain origin and *p*-value according t-test compared to control.

7.2 Fast neutron radiation

Fast Neutron mutagenesis was performed at the Research Neutron Source Heinz Maier-Leibnitz (FRM II) as described in section 5.11.4. The treatment was tested for the microalgae *Picochlorum* sp. in two experiments and was then repeated at slightly changed lead filter setup at the latest experiment (see Table 14). With regard on published data for mutagenic procedures with *Arabidiopsis* sp. (Koornneef *et al.*, 1982) and heavy ion radiation with *Arabidopsis* sp. und *N. oceanica* (Kazama *et al.*, 2011; Ma *et al.*, 2013) the dose range of applied radiation was between 20 and 160 Gy for heavy ions at *N. oceanica* and 20 - 60 Gy with *Arabidopsis* seeds. A recent paper working with fast neutrons on *Chlorella* sp. (S. Liu *et al.*, 2016) did not provide clear radiation values.

7.2.1 Fast neutron mutagenesis with *Picochlorum* sp.

For the first experiment a radiation range with dosage steps from 1 Gy to 150 Gy (see Table 14) was set. Exponentially grown *Picochlorum* sp. cells were set in a special KCl-media where NaCl was swapped. The cell growth in this KCl-media was tested beforehand and did not affect *Picochlorum* sp. if exposed for 3 days before transferring the cells back to the standard NaCl-based media (Table 3). The cell concentration of 10^7 cells mL^{-1} was implemented via cell sorting. To achieve a homogenous exposure of all cells 2 mL Eppendorf tubes completely filled up with cell suspension (2.1 mL per tube), were placed in a custom made rack horizontally within the fast neutron beam. Application of a 6 cm lead filter plate provided a neutron dose $D_n = 0.340$ Gy min^{-1} and a gamma radiation dose of $D_\gamma = 0.126$ Gy min^{-1}. The total dose was therefore $D_{total} = 0.466$ Gy min^{-1} with ratio of $D_n\ D_\gamma^{-1} = 2.7$. For 1 Gy dose the tubes had an exposure time of 142 seconds.

For the screening process eight 24-well plates with a total amount of 192 wells were used for the first screening and cultivated in parallel. For each radiation step (including non-radiated reference strains) 16 replicates were screened. A distribution of the replicates over all eight plates ensured statistical balancing and prevented data loss in case of one plate should be spoiled during the screening (for instance due to evaporation or manual errors). To prevent screening errors via manual handling of the plates only two plates were removed from the shaker at once and put in the plate reader for measurement. Each plate was also shaken directly prior to the measurement to avoid settling of cells.

The first screening for survival strains was carried out for 10 days. Figure 50 a) shows the growth curves for all 11 strains treated with different radiation doses with 16 replicates for each. The control strains (0 Gy) grow fastest together with the 1 Gy and 6 Gy treated cells. With increasing radiation dose a decline in biomass build-up is seen. However, even the 150 Gy irradiated mutants start growing, signaling that the kill point was not reached with this first experiment and that the reported doses could not directly be transferred to the microalgae

Picochlorum sp.. A calculation of survival rate is shown in Figure 50 b) where the growth of the control group was set as 100 % and the radiation treated mutant strains were set in relation according to their biomass gain. A logistic model fit with the equation

$$y = A_2 + \frac{A_1 - A_2}{(1 + (x/x_0)^p}$$
(9)

and the parameters A_1 = 101.230 ± 2.230, A_2 = 8.957 ± 18.226, x_0 = 70.041 ± 23.418 and p = 1.306 ± 0.282 was fitted with an RSQ of 0.98811 describing the function.
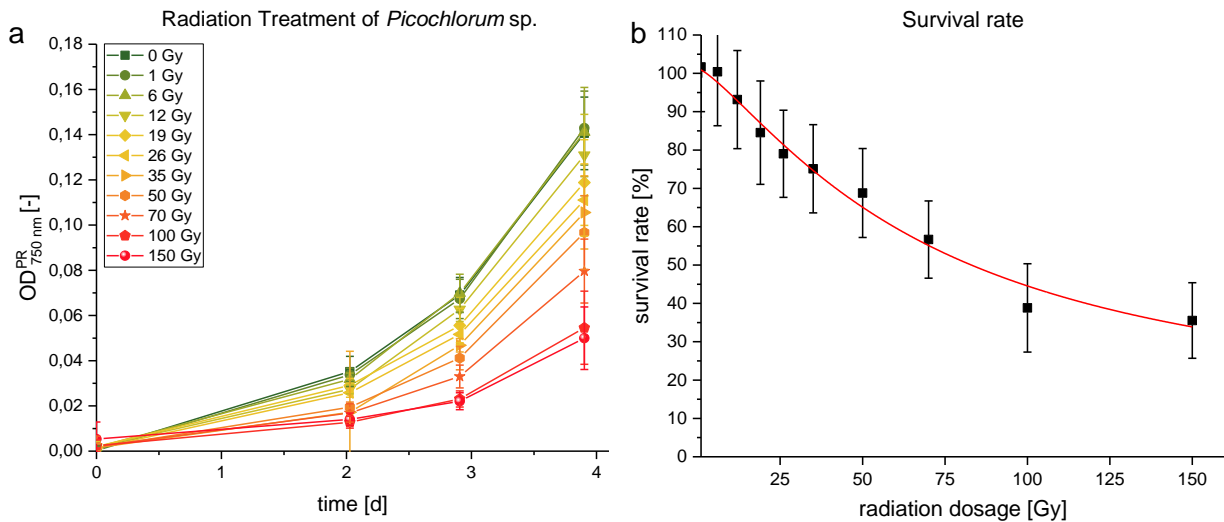
Figure 50 a) Initial survival screening of NM1 experiments with *Picochlorum* sp. (n=16) b) calculation of survival rate of *Picochlorum* sp. via growth during the first days after treatment with fast neutron radiation.

Based on these first results a new mutation experiment was planned with an increased irradiation range up to 500 Gy. Nonetheless, the screening for potential fast growing strains was carried out even though the kill point was not reached. For a total of 80 days the cells were grown with an average cultivation time of 10 days and eight recultivation steps in between. Fresh plates were used for the strain recultivation to prevent clouding of the surface due to salt crystals or scratches which might interfere with the OD-measurement. Fresh media was prepared and the wells were diluted individually according to their current OD^{PR}_{750nm} value to a new start concentration of OD^{PR}_{750nm} = 0.025. In Table 25, the results of the first screening with *Picochlorum* sp. for fast growing mutant strains after fast neutron radiation treatment is listed.

Table 25: Summary of NM1 screening. Total screening duration, μ_{max} of control strains, amount of faster growing mutant strains (out of 160 total) and average μ_{max} of fast growing mutant strains

Fast neutron radiation	Screen 1	Screen 2	Screen 3	Screen 4	Screen 5	Screen 6	Screen 7	Screen 8
Screening duration [days]	10	6	10	11	12	16	8	6
μ_{max} [d^{-1}] control	0.779 ± 0.239	0.404 ± 0.082	0.471 ± 0.041	0.607 ± 0.121	0.564 ± 0.093	0.512 ± 0.165	0.470 ± 0.124	0.745 ± 0.088
mutant count	68	65	28	72	94	37	45	52
Fast mutant count	28	36	5	18	31	14	0	21
μ_{max} [d^{-1}] average best mutants	1.042 ± 0.183	0.521 ± 0.105	0.497 ± 0.018	0.715 ± 0.113	0.653 ± 0.084	0.670 ± 0.114	0.505 ± 0.027	0.841 ± 0.071

A wide scatter in standard deviation of the reference strains indicated an unstable growth with maximum growth values ranging between $\mu_{max} = 0.404$ d^{-1} up to $\mu_{max} = 0.779$ d^{-1} and relative standard deviation up to 25 %. Mutant strains did also show a wide spread in maximum growth. The number of mutant strains which showed higher maximum growth rates than the average growth rate of the control strains were listed in the "mutant count" column. The "fast mutant count" column lists the number of mutant strains that showed faster growth than the average growth rate plus the respective standard deviation. For instance in screening 1 a total number of 68 strains (out of the 160 screened) had higher growth rates than $\mu_{max} = 0.779$ and from this 28 did even grow faster than $\mu_{max} = 0.779 + 0.239 = 1.018$ d^{-1}. In order to compensate high standard deviations and possible unstable growth in each screening the fast growing strains were marked and compared in the next screening. With this method a constantly faster growing strain can be detected even though the total growth rate is changing from screening to screening. With the first growth criteria (faster than the average control strains) 11 mutant strains did grow faster in 5 out of 8 screenings and one strain even 6 out of 8 times. With regard to the wide range of standard deviation of the controls this was considered as a potentially false positive result and the harsher criteria (mutant strains > standard growth rate + standard deviation) was applied resulting in a maximum positive hit number of just 9 mutant strains that grew faster just 3 times within the 8 screening rounds.

7.2.2 Extended fast neutron mutagenesis

With the second mutagenesis for *Picochlorum* sp. the fast neutron radiation treatment was increased up to a radiation dosage of 500 Gy. With similar settings of the lead filter and the distance to the uranium source providing the fast neutrons (see Table 14) the experiment duration increased up to 18.5 hours of exposure time. Sample treatment was as described before. A total count of 252 mutant strains was spread on twelve 24-well plates with additional 18 reference strains (without neutron radiation) and blank samples. The initial

screening for survival of the radiation treatment was carried out for 13 days. Figure 51 displays the initial growth with a clear split of untreated cells and a lessen cell response with increasing radiation dosage. The survival rate was calculated according equation (9) with the parameters A_1 = 96.612 ± 1.456, A_2 = 1.053 ± 0.934, x_0 = 67.569 ± 2.113 and p = 2.726 ± 0.188 was fitted with an RSQ of 0.99741. The kill curve was slightly steeper as seen in the first screening with a survival rate of less than 10% at 150 Gy and less than 5% at 200 Gy. Increasing radiation treatment beyond 300 Gy resulted in no cell growth.
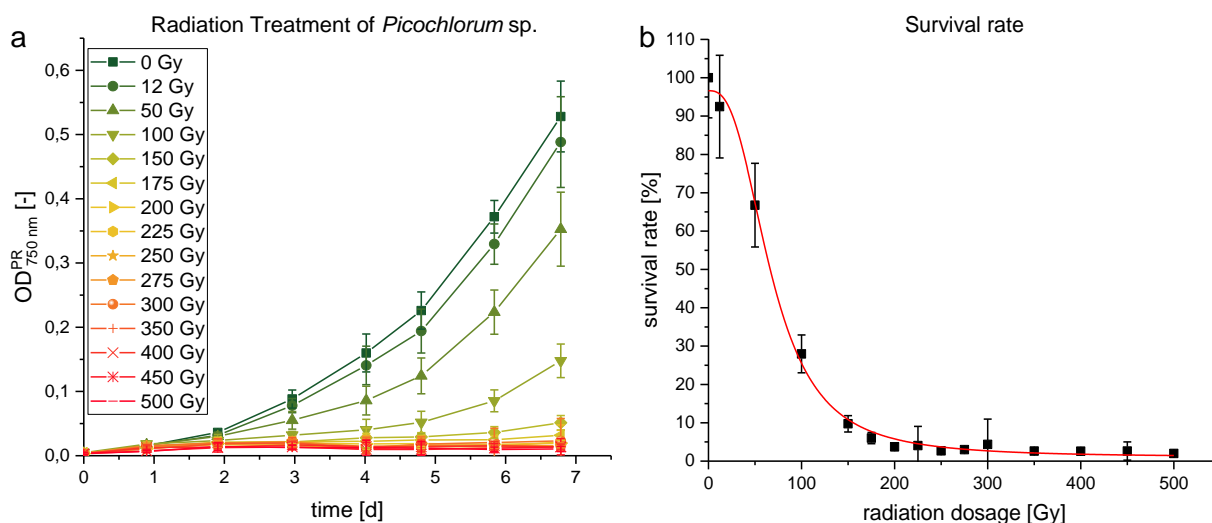
Figure 51: Initial survival screening of second fast neutron mutagenesis experiment with *Picochlorum* sp. a) Growth within the first 7 days, b) Survival rate

In order to increase the possibility of finding a positive hit (a fast growing *Picochlorum* sp. mutant strain) within the second screening the replicates (18 of each radiation step) of the highly irradiated cells were discarded and replaced with mutant strains out of the zone with just 1 -10% survival rate (150 – 250 Gy). The samples with 275 Gy, 350 Gy, 400 Gy, 450 Gy and 500 Gy treatment were replaced with 150 Gy, 175 Gy, 200 Gy, 225 Gy and 250 Gy samples forthe first recultivation screening.

The screening was carried out as previously described, but with an increased sampling frequency and plate aeration. The almost daily aeration resulted in higher total growth rates for all strains. With a total duration of 106 days split up in 13 individual screenings the twelve 24-well plates underwent a very extensive screening procedure. Due to the large sample number the recultivation steps were simplified with a two-step 1:100 dilution in the new plate: A 1:10 dilution plus final plate reader analysis and a second 1:10 dilution in the new screening plate. Every third recultivation, an exact calculation was carried out with individual dilutions for each well to level out faster growing strains in order to keep the average growth range as close as possible. To avert a too wide gap between slower growing strains and fast growing mutant strains this synchronization was necessary and prevented an early drop out of the linear range on the plate reader measurement of the faster growing strains. An

overview of the 13 screening rounds is displayed in Table 26. Due to the large data volume only a brief summary of the characteristic figures can be displayed. Aside the individual screening duration the averaged μ_{max} of the control strains (n=18) is shown. The mutant count represents for the number of mutants in the respective screening (out of 252 mutant strains) that had a higher maximum growth rate than the averaged control strains. The fast mutant count in the fourth row shows the amount of mutant strains which had a faster growth than the averaged control strains plus their standard deviation, setting a higher benchmark value to overcome. The last row displays the averaged growth rate of these best and fastest growing mutant strains.

Table 26: Summary of NM2 screening. Total screening duration, μ_{max} of control strains, amount of faster growing mutant strains (out of 252 total) and average μ_{max} of fast growing mutant strains

Fast neutron radiation	#1	#2	#3	#4	#5	#6	#7
Screening duration [days]	5	10	6	6	7	9	6
μ_{max} [d^{-1}] control	0.551 ± 0.059	0.958 ± 0.054	0,729 ± 0.284	0.384 ± 0.080	0.279 ± 0.121	0.769 ± 0.121	0.912 ± 0.091
mutant count	133	47	105	104	83	129	128
fast mutant count	95	27	68	39	60	55	56
μ_{max} [d^{-1}] average fast mutants	0.733 ± 0.098	1.096 ± 0.099	1.052 ± 0.039	0.597 ± 0.119	0.337 ± 0.039	0.922 ± 0.029	1.112 ± 0.108
	#8	**#9**	**#10**	**#11**	**#12**	**#13**	
Screening duration [days]	8	11	7	10	11	10	
μ_{max} [d^{-1}] control	0.557 ± 0.106	0.887 ± 0.165	1.002 ± 0.126	0.676 ± 0.130	0.797 ± 0.229	0.906 ± 0.196	
mutant count	104	127	104	115	153	131	
fast mutant count	29	25	36	37	45	56	
μ_{max} [d^{-1}] average best mutants	0.742 ± 0.073	1.157 ± 0.101	1.250 ± 0.134	0.889 ± 0.097	1.180 ± 0.152	1.297 ± 0.184	

Screening number 4 and number 5 show slower growth rates than the other 11 screenings, which is due to the fact that these cultivations were carried out during the holiday season with limited access to the lab and thus a reduced air exchange and CO_2 limitation.

As before the standard deviation of the control strains was high (averaged 18 % relative standard deviation). An evaluation of potential mutant strains was therefore carried out only with the fast mutant count strains. Out of the 13 screenings (11 without the 2 limited screenings #4 and #5) four strains had repeatedly high growth rates and were present in the fast group for a minimum of six times. An overview of the four fast growing mutants and the averaged control group is shown in Figure 52. The strain abbreviation is put together with the experiment abbreviation (nM2 – neutron mutagenesis #2) the plate number (i.e. 11) with the well (D01) and the applied radiation dosage (50 Gy). Interestingly, one strain was only

treated with 50 Gy radiation, whereas the other three are from the high-potent range of the 150 – 250 Gy zone.
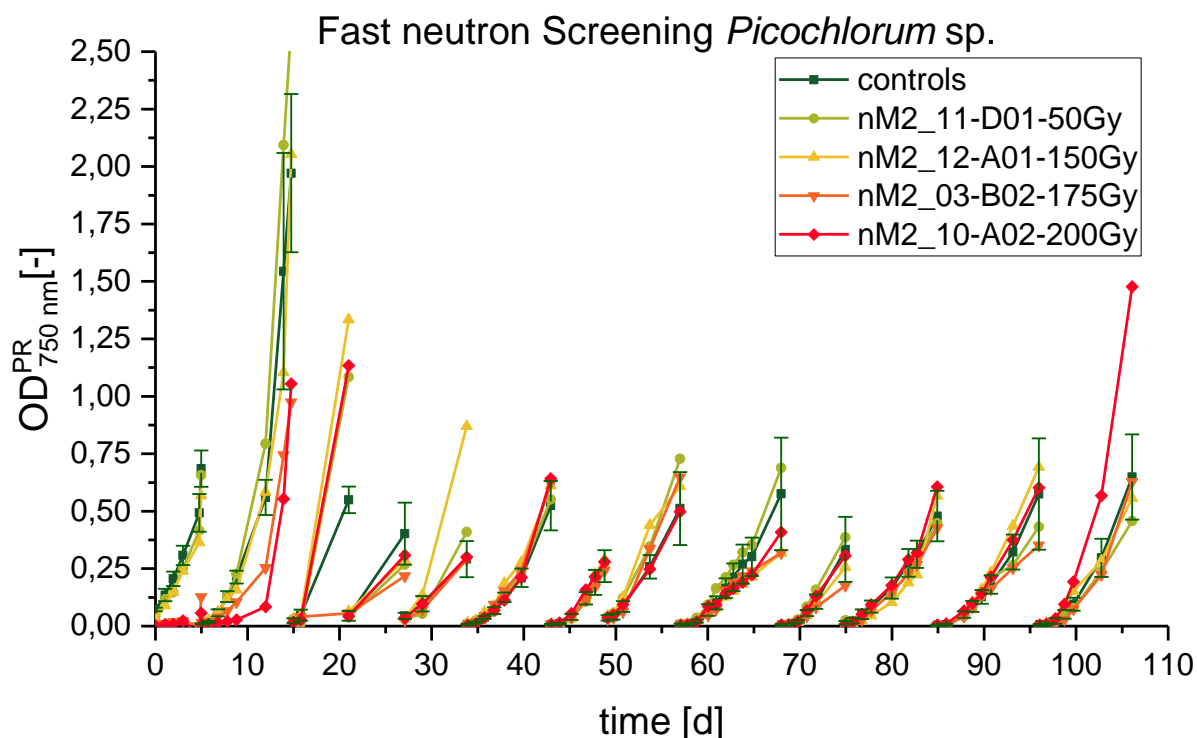
Figure 52: Second fast neutron mutagenesis screening with *Picochlorum* sp. Green: untreated control strains (n=18), best mutant strains.

In Table 27, the four mutants were listed with their occurrence in the mutant group (faster growth compared to averaged controls), the fast mutant group (faster growth compared averaged controls with added standard deviation) and their averaged relative maximum growth rate. The average relative maximum growth rate was calculated using the relative growth rates (calculated with the actual growth rate normed to the average control growth rate) of the mutant count.

Table 27: Positive screening mutants after fast neutron radiation of *Picochlorum* sp.

Fast neutron mutants	Mutant count	Fast mutant count	average rel. μ_{max} [%]	total average rel. μ_{max} [%]
nM2_11-D01-50Gy	6	6	149.07 ± 17.80	115.88 ± 30.80
nM2_12-A01-150Gy	9	6	129.50 ± 13.53	114.38 ± 24.08
nM2_03-B02-175Gy	8	6	122.34 ± 9.39	101.38 ± 27.95
nM2_10-A02-200Gy	11	8	120.58 ± 13.54	115.75 ± 23.39

While this system is useful to find fast growing mutants for the characterization of the fast growing mutant strains all relative growth rates have to be considered. The last row in Table 27, the total average relative μ_{max} represents the averaged maximum growth rate over all 13 screening cultivations (each compared to the control growth rate, thus in relative

percentage). With these numbers the best mutant strain has a growth rate of 116 % with a standard deviation of 23 %.

A third round of fast neutron mutagenesis was performed with *Picochlorum* sp. The settings of the third irradiation process were changed a bit, mostly to increase the dosage per minute by reducing the distance to the radiation source by half a meter (see Table 14). The dosage range was kept, from 0 Gy up to 500 Gy. Initial survival screening was carried out as previously described, Figure 53 shows the results. The calculation of the survival rate was fitted with the same equation than before (equation (9)) with the parameters $A_1 = 99.725 \pm 1.643$, $A_2 = -0.714 \pm 0.854$, $x_0 = 66.054 \pm 1.814$ and $p = 2.574 \pm 0.151$ resulting in a RSQ of 0.99830.
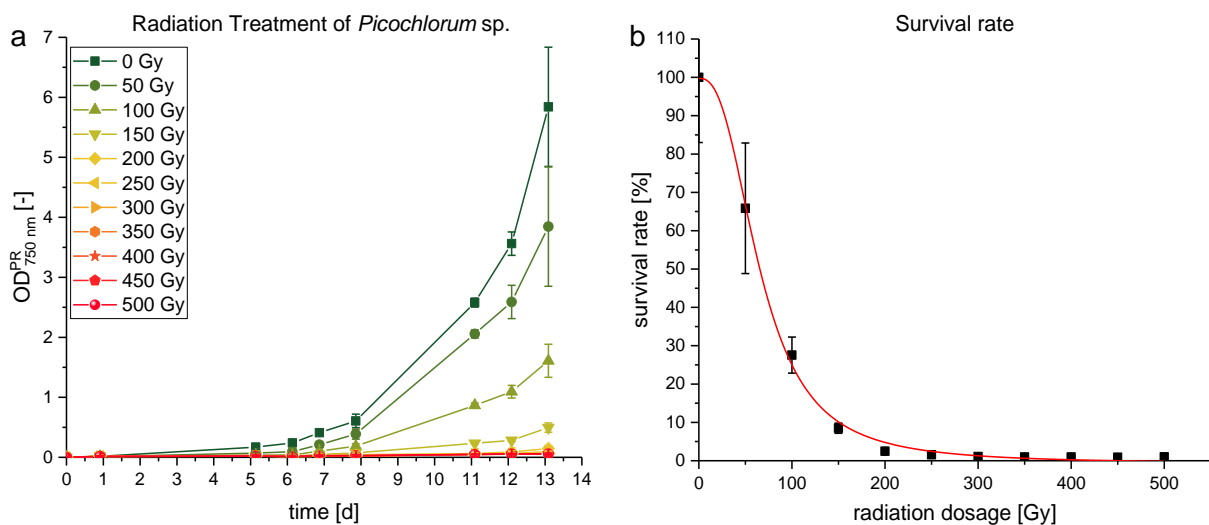
Figure 53: Initial survival screening of third fast neutron mutagenesis with *Picochlorum* sp.. a) Growth within the first 13 days, b) Survival rate

Due to the large standard deviations of the previous screening an extensive screening was aborted after the first two recultivations to obtain the data for the survival rate.

7.2.3 Fast neutron mutagenesis summary

Fast neutron irradiation as a source of mutagenizing radiation for microalgae has been tested with *Picochlorum* sp. in the Research Neutron Source Heinz Maier-Leibnitz (FRM II). Three mutation rounds were carried out, the first one closely related to the scarce data obtained from literature. With ten dosage steps ranging from 1 Gy up to a total dosage of 150 Gy the kill rate of 90% or more was not reached for *Picochlorum* sp., setting up the maximum dosage to 500 Gy for the following treatments. With the second and third experiment *Picochlorum* sp. was within the intended kill rate. Both experiments showed a very similar

survival rate as presented in Figure 54. Dosage levels of 150 Gy up to 250 Gy enabled less than 10% of the strains to survive and potentially damaged the remaining survivors heavily.
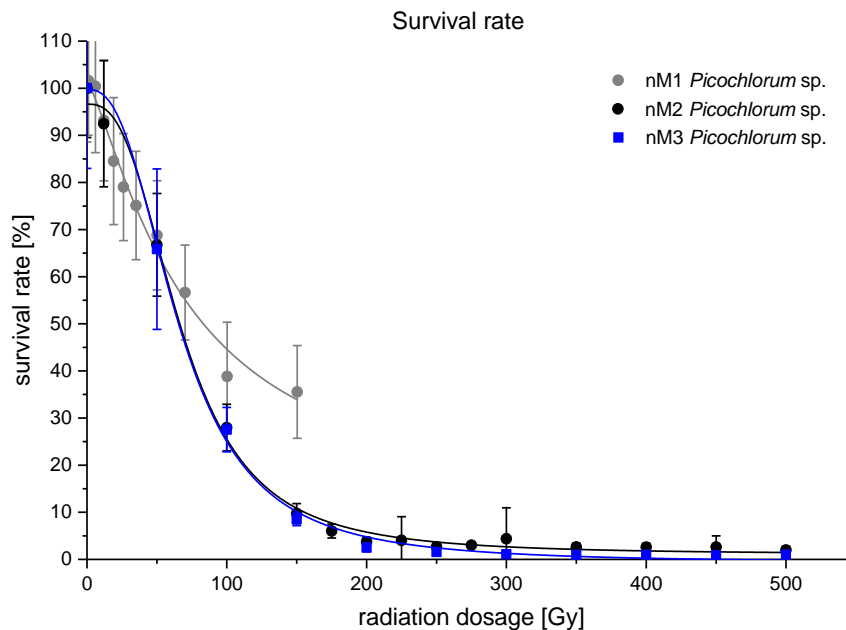
Figure 54: Survival rates of *Picochlorum* sp. at fast neutron radiation treatment

The first and second mutagenesis round with *Picochlorum* sp. were subjected to a thorough screening with 79 and 106 days. A total amount of 160 and 252 potential mutant strains were screened with the objective to find a fast growing mutant strain of *Picochlorum* sp.. Several potential mutant strains were identified, which indicated higher maximum growth rates compared to the control strains without radiation exposation. Unfortunately, the screening itself had a very high scatter in the control group, which made it very difficult to identify a positive mutant confidentially. Several mutants strains grew up to 15 % faster but showed also a high standard deviation of up to 20 %.

7.3 UV and EMS mutation

UV radiation as mutagenic treatment for microalgae is one of the common and easy applicable methods to obtain random mutant strains. (Lanfaloni *et al.*, 1991; Doan and Obbard, 2012; Manandhar-Shrestha and Hildebrand, 2013; Zayadan *et al.*, 2014) and was therefore set as reference method for the new mutagenesis treatments with cold atmospheric plasma and fast neutron radiation. *Picochlorum* sp. cells were treated as described in section 5.11.1 and screened for survival rate and fast growth in a subsequent screening for 79 days. The screening was carried out alongside the first fast neutron radiation screening with similar results concerning the high standard deviation of the controls. No mutant strain was found that showed a repeating higher growth rate than the corresponding control strain. The kill rate was obtained from the first screening displayed in Figure 55 a) and is shown in Figure 56 c). Surprisingly, a strong decline in survival rate was observed even with just short irradiation exposures. This is represented in the slow growth compared to the untreated control group, as seen in the growth curve in Figure 55 a).
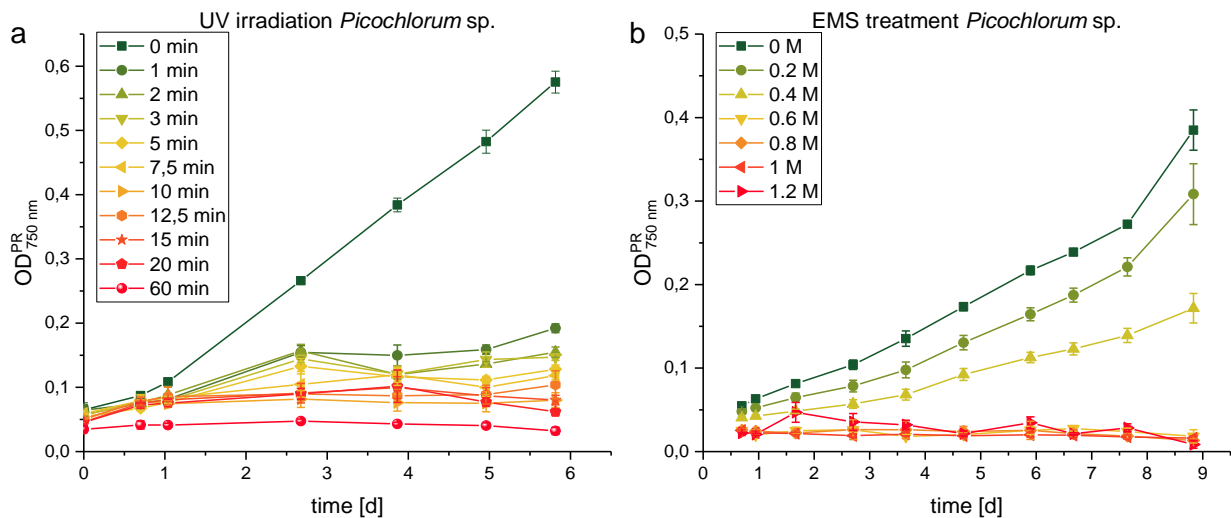
Figure 55: a) initial growth of *Picochlorum* sp. after UV irradiation for up to 60 minutes (n=4). b) EMS treatment of *Picochlorum* sp. and initial growth (n=9)

Random mutagenesis via EMS was selected as second standard mutation procedure to compare the effects with *Picochlorum* sp. The procedure was performed accordingly to Doan and Obbard (Doan and Obbard, 2012) and is described in section 5.11.2. The EMS range was extended up to 1.2 M. The growth response after the chemical treatment is shown in Figure 55 b) and the survival rate calculation is displayed in Figure 56 d). With EMS an initial screening with just two rescreenings was carried out in order to obtain the survival rates.

7.4 Summary of mutagenic procedures

In this work four random mutagenesis procedures were tested for their suitability for microalgae application with the strain *Picochlorum* sp.. The novel procedures with cold and room temperature plasma (ARTP) and fast neutron radiation were developed and tried with this strain for the first time. To compare the results an UV irradiation and EMS exposure was carried out to obtain comparably data for the survival rate.
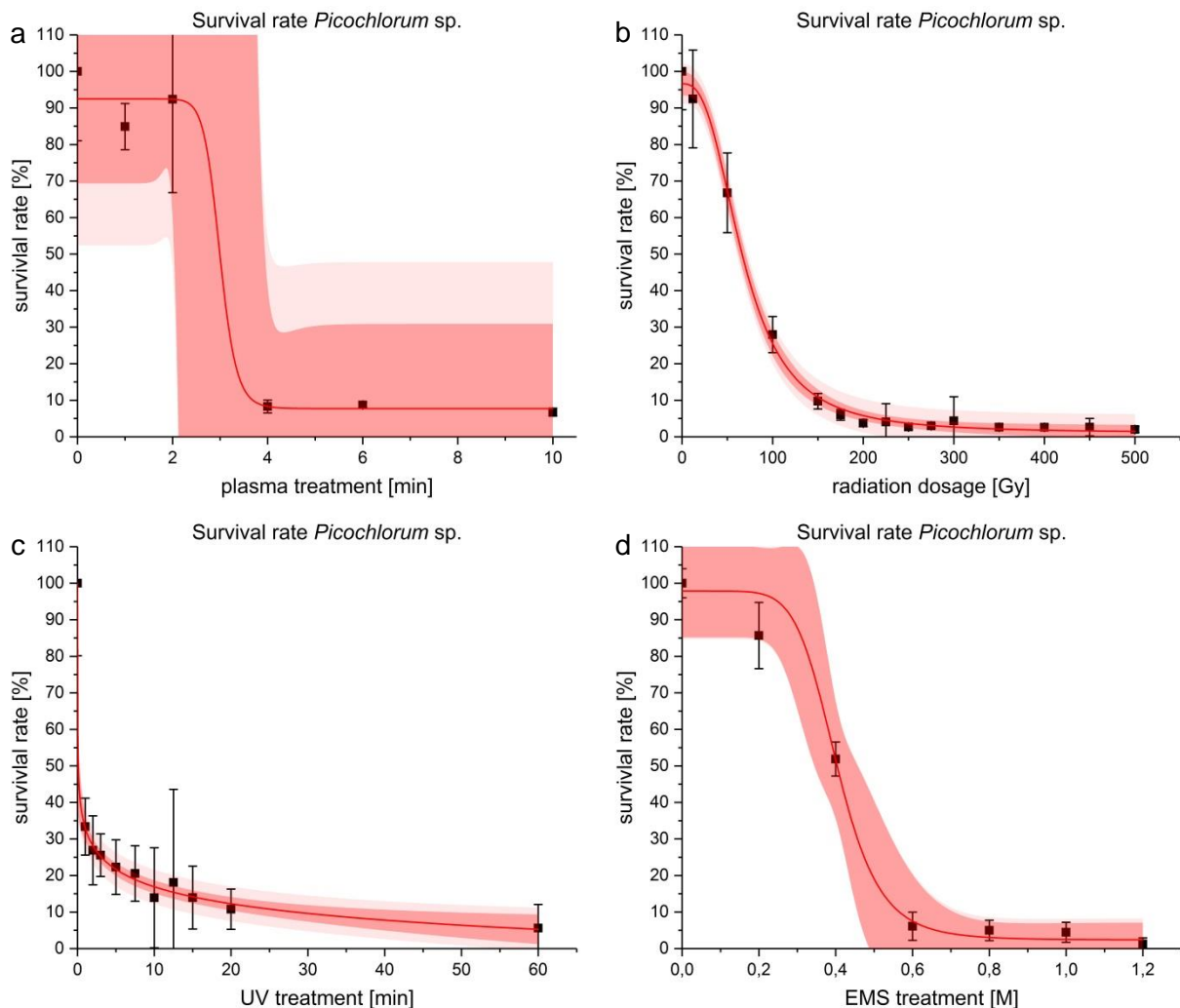
Figure 56: Overview of determined survival rates for *Picochlorum* sp. mutagenesis procedures at a) plasma treatment, b) fast neutron radiation s) UV radiation and d) EMS treatment. In red fitted curve, dark red confidence band (95%), light red prediction band (95%).

In Figure 56 the results of the survivability of *Picochlorum* sp. after each mutation treatment are presented. The red curve is a logistic fit to the data to calculate 50 %, 10 % and 2 % survival rate values. The dark red area represents the confidence band, which is proportional to the standard error and signals the area which contains 95 % of all fitted curves. The light red area represents the prediction band depicting, with 95 % accuracy, the area of possible additional sample points within the plot. The tighter these areas occur, the better and accurate the data basis for the fitted curve. Table 28 displays a sum up of the data obtained with the four tested mutation procedures. The 50 % and 10 % survival rate could be

determined for all methods. The 2 % survival values for ARTP and EMS were not predictable with the current fit model.

Table 28: Summary of all tested mutagenesis procedures with curve fit models and survival rates.

	ARTP plasma treatment	fast neutron radiation	UV radiation	EMS treatment
Logistic curve fit		$y = A_2 + \dfrac{A_1 - A_2}{(1 + (^X/_{x_0})^p)}$		
RSQ	0.98932	0.99741	0.99643	0.99479
A1	92.461 ± 5.377	96.612 ± 1.456	99.999 ± 1.831	97.842 ± 3.984
A2	7.72 ± 5.381	1.053 ± 0.934	-38.925 ± 54.15	2.382 ± 1.507
x0	2.993 ± 8.384	67.569 ± 67.569	1.422 ± 5.345	0.403 ± 0.013
p	17.191 ± 164.525	2.722 ± 2.722	0.204 ± 0.113	7.220 ± 2.316
50 % survival rate	2 min 59 sec	66.4 Gy	5.0 sec	0.404 M
10 % survival rate	3 min 40 sec	155.6 Gy	28 min 18 sec	0.566 M
2 % survival rate	n/a	366.8 Gy	102 min 42 sec	n/a

Additional to the survival rate data extensive screenings were conducted for the plasma and fast neutron mutant strains in order to obtain a fast growing *Picochlorum* sp. mutant strain. Although several mutant strains have been repeatedly identified a stable faster growing mutant strain could not be obtained. This might be caused through suboptimal screening conditions with the 24-well plate screening applied. Large standard deviations in the non-treated control groups indicated problems with the screening system, that could not be resolved satisfactorily until the end of the screening phases, making a certain statement concerning faster growing mutant strains difficult.

8 Discussion chapter

8.1 Pigments discussion

The discussion of pigment experiments is split in the general growth and lipid screening of *Picochlorum* sp*., Dunaliella* sp. and *M. salina* and the observations targeting of the new pigments in *Picochlorum* sp.*.*

8.1.1 Growth experiments with colored LED illumination

The experiments labelled as stage 1 experiments (see Table 8) were conducted in shake flask dimensions on the novel LED shaking platform with three strains, *Picochlorum* sp*., Dunaliella* sp. and *M. salina*. The outline of these experiments was to investigate the effect of different colored light illumination on growth, pigment composition and lipid formation. The colors selected were a warm white LED illumination, blue, red and as negative control a green colored LED light. The available spectrum range of the inbuilt LEDs are shown in Figure 9.

The three illumination intensities 50, 100 and 150 µmol m^{-2}s^{-1} affected growth of *Picochlorum* sp.. Low irradiance levels of just 50 µmol m^{-2}s^{-1} lead to light limited growth at a very early stage. The slower growth under green light, as seen in the 150 µmol m^{-2}s^{-1} approach, resulted at this low level irradiance in a prolonged lag phase. Blue light illumination lead to reduced maximum growth and a potential morphology change of the *Picochlorum* sp. cells. This could not be statistically confirmed via FACS counting or light microscopy, but was reported for blue illumination of *Chlorella kessleri* that resulted in larger cell sizes (Koc, Anderson and Kommareddy, 2013). Linear growth following cell densities exceeding 0.2 g$_{DW}$ L^{-1} at the second week of cultivation is caused by self-shading of the biosuspension. Even though the bottom lit shake flasks offer a good surface per volume ratio, a 200 mL culture volume in a 500 mL shake flask, the culture depth is still ca. 2 cm. The algae suspension is well mixed by agitation at 120 rpm and the culture depth constantly changes between 0.5 cm and approximately 4 cm. *Picochlorum sp.* is an isolate from the Bahamas region with daily high irradiances. and is also reported as potential candidate for lipid production in open pond systems with robustness towards high irradiance levels (de la Vega *et al.*, 2011; M. Huesemann *et al.*, 2013; Dahmen *et al.*, 2014).

For *Dunaliella sp.* the illumination with 50 µmol m^{-2}s^{-1} was light limited. At higher irradiance levels no statistically significant difference throughout the four tested color illuminations was observed. The growth of *M. salina* at different illumination and irradiation levels was unexpected as the high irradiance experiments resulted in very limited growth compared to the 100 µmol m^{-2}s^{-1} setup. As this limited growth occurred at all replicates of this experiment only an unfortunately undetected outside effect (such as discontinuous CO_2 aeration) can be

the cause for this growth response.

The overall growth rates of *M. salina* are within ranges reported in literature with $\mu max = 1 - 1.1\ d^{-1}$ at 150 µmol m^{-2}s^{-1}.(Sforza *et al.*, 2012)(M. H. Huesemann *et al.*, 2013). In literature the illumination of *Nannochloropsis* sp. with different colored LEDs was reported and resulted for phototrophic growth of μ_{max} in blue (0.64 d^{-1}) > white (0.58 d^{-1}) > green (0.54 d^{-1}) > red (0.51 d^{-1}) contradicting the results of this work (Das *et al.*, 2011). Unfortunately, the authors do only state the peak wavelength of the used LEDs (Green λ_{max} = 550 nm, Red λ_{max} = 680 nm and Blue λ_{max} = 470 nm) and not their wavelength range. The irradiance is also just listed as light intensities at steps between 400 and 1200 lux, making a comparison to the used units µmol m^{-2}s^{-1} or µE and thus an evaluation of the illumination results impossible. Considering the 100 µmol m^{-2}s^{-1} experiments, a similar growth pattern as seen with *Picochlorum* sp. appears. Blue illumination resulted in reduced total biomass and green light shows slower initial growth rates than red light illumination.

The cellular response of microalgae to wavelength specific illumination is strongly affected by the pigment composition of the microalgae. Therefore, it is not surprising that for various species different growth reactions are documented. *B. braunii* was reported to grow 1.26 fold faster with blue-green LED illumination compared to red-green-blue and blue LED (Okumura *et al.*, 2015). *Chlorella vulgaris* strains showed higher biomass production with yellow, red and white light compared to blue, green and purple irradiation (Xu *et al.*, 2013; Hultberg *et al.*, 2014). These finding were confirmed by Yan *et al.* showing dry weight reproduction correlating to illumination from red > white > yellow > purple > blue > green (Yan *et al.*, 2013). In the studies of Rendon *et al. C. vulgaris* also showed better growth when being exposed to white (1.59 g$_{DW}$ L^{-1}) and blue (1.53 g$_{DW}$ L^{-1}) light compared to blue-red (1.27 g$_{DW}$ L^{-1}) and just red light (0.45 g$_{DW}$ L^{-1}) (Rendón, Roldan and Voroney, 2013). Red and pink LED illuminations promoted fastest growth of *Arthrospira. platensis* whereas green LEDs showed almost similar growth response than white light. Slowest growth was monitored at blue LED illumination (Markou, 2014). For *Spirulina platensis* red light was also reported to generate fastest growth followed by yellow, green and white and blue LED light. (Chen *et al.*, 2010). Biomass productivity of *Tetraselmis suecia* is reduced to less than half at blue and green color illuminations compared to growth at white and red LEDs (Abiusi *et al.*, 2014). Red and blue illumination of *Chlorella kessleri* cells resulted in larger cell size at blue illumination and faster growth at red illumination (Koc, Anderson and Kommareddy, 2013). Green LEDs (430 – 610 nm, λ_{max} = 525 nm) were inefficient to promote comparable growth (μ_{max} = 0.384 d^{-1} compared to 0.552 – 0.648 d^{-1} with purple, blue-purple, blue, red LEDs and fluorescent lamps) in *Haematococcus pluvialis* caused by the inefficiency of chlorophyll for this wavelength region (Katsuda *et al.*, 2004). Nevertheless, in reported work with colored LEDs for numerous strains blue light irradiance often resulted in lower or reduced growth as

seen in this work.

Aside blue illumination the red light is the other, most common used color for artificial lighting. This is not surprising as these two colors match the main absorbance region of chlorophyll as described in section 3.1.1. The use of green light is often combined with other colors as pink, far-red or yellow in a wholescale approach. The little usage of green light in the spectra between of 530 - 600 nm (see Figure 29) might be caused by the poor absorption capabilities of plants and in classes of green algae.

Microalgae cultivation of the cyanobacteria *Synechococcus elongatus* with green light illumination however outperformed other wavelengths (blue, red and yellow light) in terms of both productivity and efficiency at high light condition (Ooms *et al.*, 2017).As cyanobacteria contain Phycocyanin, a blue light-harvesting pigment absorbing well in the 500 – 700 nm region (Eriksen, 2008) this should be considered when comparing these results to green algae.

The good growth observed could be caused by the fact that green light is less absorbed by a single cell (due to the lower absorbance bands) and therefore has a higher culture depth penetration compared to highly absorbed red light for instance. In high density cultures or low-light limited cultures this could lead to an overall less light limited culture and therefore to an increased overall cell growth. This might be an additional reason for the good cell growth at green light observed in this work.

The observed growth at green light for all three strains was still somewhat unexpected. A comparison of the green LED bandwidth used in the shaker platform and chlorophyll absorption spectra (see Figure 32) shows that the broad baseline of the inbuilt LED is stretching into the blue and red absorbance region of chlorophyll and thus allowing absorption of sufficient photons for photosynthesis. Therefore a detailed description of the LED properties used in the respective work (see Table 7 and Figure 9) is crucial for discussion and evaluation of other work in this field. Most reports in literature working with different colored LEDs have little information on the actual irradiance put on the algae. Concerning the LEDs there is often a reference to the manufacturer and /or the peak wavelength and the range and the set maximum irradiance [$\mu mol\ m^{-2}s^{-1}$] but then it is not stated how it was analyzed or set for the experiments.

8.1.2 Lipid formation of microalgae with multicolor illumination

The lipid composition of the three tested microalgae was investigated in order to see a potential impact of blue, white, green or red color illumination on the lipid formation. The sampling for the lipid analysis was performed once at the end of each cultivation (at around day 18). As the lipid formation was not the main objective of the experiments the optimum

sample time was probably not achieved as nitrate and phosphate starvation usually occurred much earlier in the cultivation between day 8 and 11. With these non-optimum sample times the maximum potential lipid content was certainly missed. Total lipid content was calculated as displayed in Table 18 with levels between 19.34 % for red and 21.74 % for green illumination in *Dunaliella* sp.*,* 13.4 % for blue and red and around 15.2 % for white and green illumination in *M. salina* and 16.66 % for blue, 18.89 % for red and around 23.0 % for white and green illumination in *Picochlorum* sp.*.* These findings are within range of literature data in which the total FAME content (in % of dry weight) of *Nannochloropsis* sp. was reported with green light (15.11 %) > blue (14.78 %) > white (14.32 %) > red (14.26 %) and slightly differing lipid composition throughout the different color illuminations (Das *et al.*, 2011). The total lipid content in literature for *Nannochloropsis* sp. ranges between 10 % at 150 µmol m^{-2}s^{-1} irradiance level (Sforza *et al.*, 2012) up to 52.0% lipid accumulation in a two-phase green LED light stress system (Ra *et al.*, 2016). In other microalgae a changing color illumination does effect the lipid formation as the highest lipid content in *A. platensis* was obtained with blue LED illumination (up to 6%) compared to green light (4.8 %) and red, white and yellow (ca. 4.2%) (Markou, 2014). Interestingly, lower lipid content in *Chlorella vulgaris* at green light illumination was reported compared to white illumination (Hultberg *et al.*, 2014). With better timed sampling a difference in lipid formation might also been observable within the used strains of this work.

The qualitative GC-MS analysis revealed that for the three strains at hand and with the sampling conducted in these experiments no differences was observable. The identified FAMEs in Table 16 correlate with the most common lipids present in the standard solution marine oil mix from Restek. *Dunaliella* sp. shows unique FAMEs that are not present in the other two strains, a C16:3, C16:4, C18:3 and C22:0 fatty acid and *M.salina* possesses two long chain fatty acids with C22:1 and C24:0.

8.1.3 Pigment formation effected by colored illumination

In the early experiments of stage 1 pigment sampling was carried out three times over the course of the cultivation, twice in late exponential phase once enough biomass was build-up and again at the end of the cultivation. In *Picochlorum* sp. and *M. salina* the pigment content was decreasing over the course of these three sample points caused by the limited growth and stationary phase towards the end of the cultivation. As shown in Figure 25 a) *Dunaliella* sp. at 150 µmol m^{-2}s^{-1} irradiation rate was still growing slowly at the end of the cultivation resulting in almost stable pigment concentrations. The two major pigments observed were chlorophyll *a* and with approximately half the concentration chlorophyll *b*. Traces of beta-Carotene and Lutein and Canthaxanthin were also observed and within literature values (Singh, 1975; Fisher, Minnaard and Dubinsky, 1996; Abiusi *et al.*, 2014). The different color illumination resulted in *Picochlorum* sp. with increased (2–fold) pigment

content at blue compared to white illumination. Green illumination yielded similar amounts than the white and at red illumination pigment formation was decreased to approximately 65 % compared to white light. This effect with reduced chlorophyll content at red LED illumination and enhanced content with blue light has also been described for *T. suecica* (Abiusi *et al.*, 2014). At *M. salina* green light increased pigment formation 1.6-fold compared to white and red illumination. The growth under blue light was massively reduced as previously described preventing accurate growth analysis and pigment sampling due to shortage of available biomass.

The linear growing *Dunaliella* sp. did not differ much in pigment yield at the four colors of illumination. In general mechanism for photo adaption and chromatic acclimation in response to different irradiance and spectrum are known for microalgae species. This way the pigment concentration can be raised in light-limiting conditions (Kandilian, Lee and Pilon, 2013). Effects like this are highly strain specific and can even differ within the same species as shown for *Nannochloropsis* sp. (Fisher, Minnaard and Dubinsky, 1996; L. L. Lubián *et al.*, 2000; Gentile and Blanch, 2001). *A. platensis* on the other hand does seems not to be effected by illumination color with a slight increase at blue LED illumination as maximum difference (Markou, 2014). In total not much work has been published with multicolor illumination of microalgae. Astaxanthin production with *H. pluvialis* can be increased with a change in illumination from red LEDs to blue LEDs (Katsuda *et al.*, 2004). In the review of LEDs usage for microalgae cultivation of 2015 some articles using green LED light were listed (Glemser *et al.*, 2015).

8.1.4 Unknown pigments in *Picochlorum* sp.

During the HPLC analysis of the first experiments in stage 1 an abnormality in the chromatogram of the green illuminated *Picochlorum* sp. strains was observed. With an initial growth experiment, the increase of the irradiation spectrum up to 200 µmol m^{-2} s^{-1} and an increase of the CO_2 content in the aeration of up to 2 % was tested. Improved cell growth was observed with up to 5 g_{DW} L^{-1} indicating that the previous cultivations were CO_2 limited. After the initial exponential growth phase with very little differences in maximum growth rates between the four illumination colors blue > green > white > red (0.898 d^{-1} > 0.888 d^{-1} > 0.801 d^{-1} > 0.791 d^{-1}) (see Figure 27) a linear growth was observed for all four colors from 1 g_{DW} L^{-1} up to 5 g_{DW} L^{-1}. The pigment samples were obtained earlier than in previous experiments at early exponential phase (day 4) and early linear phase (day 11). Compared to the results of the less illuminated experiments an increase in pigment content was observed. At green color illumination the additional peaks U2, U3, U4 and U5 could be found. Nevertheless, these experiments pointed out a correlation of cultivation state and pigment (including unknown pigments at green color) occurrence. The pigment distribution matched reported pigments in literature (de la Vega *et al.*, 2011).

In order to investigate these unknown peaks a two-route strategy was applied. First, in order to increase sampling number throughout the whole cultivation an upscale to photo bioreactor dimensions was implemented for green color illumination and white color, which was used as reference. This also enabled the accumulation of sufficient amounts of unknown pigment sample for further analysis. In a second approach, a possible correlation of the green LED bandwidth and the unknown pigment formation was investigated. This was achieved via the addition of glass filter plates (Longpass filter and bandpass filters) to potentially see an impact on pigment formation. As different colored illumination effects the pigment formation in various microalgae (L. Lubián *et al.*, 2000; Mohsenpour, Richards and Willoughby, 2012; Markou, 2014; Schulze *et al.*, 2014; Glemser *et al.*, 2015) the idea behind this experimental approach was that the microalgae cells might be triggered to produce other pigments for the adaption to the non-optimal green illumination.

The first spectrum scan of white, blue, green and red illuminated cells grown at the 200 µmol m^{-2} s^{-1} setup did not show much difference in the absorbance spectrum obtained from the live culture thus showing the significant green light peaks at the chromatograph of the HPLC analysis. In the following experiments different bandwidths of green light were used to grow *Picochlorum* sp.. The bandwidth diminishment via colored glass filters worked as intended and limited the wide green LED band as shown in Figure 12. Growth of the green + LPF and green + BPF illuminated microalgae cells was very similar compared to the white light control strains. The pigment distribution (Figure 31) showed the highest levels of U5 of up to 9 mg g$_{DW}^{-1}$ at day 7. This was a little bit more than half the of chlorophyll *a* and *b* (17 and 14 mg g$_{DW}^{-1}$) concentration at the same time point. U2, U3 and U4 levels were constantly rising through the analyzed timeframe between day 5 and 11. This is in contrast to the pigment spectrum of the green + LPF setup in which all unknown pigments decreased throughout the monitored timeframe correlating with the Chl *b* drop. In the green + BPF setup the pigment levels were more or less constant. The initially surprising similar growth of the strains illuminated with a narrowed bandwidth band compared to the green and broadband white LED can be simply explained. These results were caused by the calibration itself, having a setup with identically photon flux densities the bandwidths of the green + LPF and green + BPF filters were pushed to the longer and shorter edges of the spectra. By reducing the width of the spectra with the LPF filter an increased number of photons was observed in the 550 nm- 600 nm region with approximately 1.5-fold at 550 nm and 2-fold at 525 nm and 550 nm. Unfortunately, this doubled photon intensity was also still in place at 650 nm. In this region the lower bandwidth absorbance peak of *Picochlorum* sp. (mostly Chl *a* and *b*) is already in place (compare Figure 32 a and b). The same effect goes with the BPF filter varied green LED on the short wavelength spectrum of the LED. No observable difference in the absorbance of the spectrum scan amongst the white, green, green + LPF and green +

BPF setups was therefore not surprising.

The double bandwidth diminishment in the further experiment canceled out these border-illumination effects and should expose any differences in absorbance. Due to the very narrow overlap in transmission of the two filters of just over 30 nm FWHM the peak intensity was approximately tripled compared to the non-filter photon emission of the green LED. Due to power limitations of the used LED illumination system a maximum irradiance of just 75 µmol m^{-2} s^{-1} could not exceeded even with switching all available LEDs to maximum output. The reduced growth of the control illumination setup with white and green light was therefore expected. Nonetheless, the double-filter setup showed a further reduced growth, lowering the possibility of good pigment sampling to a late sample point after 10 days, as an earlier sampling would have depleted the culture volume completely. The missing sample point of day 8 of the green+ LPF + BPF setup might have been crucial for an assuming of the trend curve, as the concentration of unknown peaks U4, U5 and U2 drastically drop down between day 10 and day 12. Therefore, no clear finding could be observed with this experiment. The spectrum scans showed different maximum absorbance due to the different cell concentrations, but no shift within the wavelength spectrum of the absorbance.

This experimental approach indicates that the observed new pigment peaks do not increase the absorbance range in *Picochlorum* sp. when illuminated and growing with green light. The observed growth in the early experiments with the green LED must therefore be caused by absorbance overlap of LED spectra and cell absorbance. This finding correlates with the observed reduced growth at the narrow bandwidth illumination with the double-filter setup in stage 2. The cause of the formation of the unknown pigment peaks must therefore be triggered by the green illumination but does not directly correlate with absorbance or growth of the *Picochlorum* sp. cells. It is also possible that the potential differences in the spectrum scan obtained with the MTP reader were simply too weak to detect with the applied scanning method. As the cell suspension was analyzed fresh out of the culture volume only the total absorption of the whole culture is detectable. With the dispersion of the unfiltered cell suspension and without any pigment extraction steps sensitivity of the detection could be reduced. Nonetheless with an abundance of 34.9 % unknown pigments (see Figure 38) a change in the absorption spectra should have been detectable if existing.

Aside the experimental approach to identify the possible cause or effects of these unknown peaks with the variation of culturing conditions in the light spectra the second approach was the scale-up, continuous sampling and sample analysis (stage 3 experiments, section 6.3) as well as further analytical methods such as high resolution HPLC-MS and NMR identification. The two fermentations at green and white light illumination were performed with the same spectral properties than the initial illumination (without any filter plates) while using the shaker platform. Similar growth was obtained that just differed in higher dry weight yield after

18 days at green light with 4.95 g_{DW} L^{-1} compared to 4.0 g_{DW} L^{-1} at white illumination. In the shake flask experiments, the difference in biomass yield was smaller, which could be caused by a differing LED calibration of either the shake flasks or the fermenter setup. All cultivations with differing illumination setups were always performed originating from the same preculture.

With the increased cultivation volume, a sampling for pigment analysis could be performed once a day for the first two weeks of cultivation. The pigment concentrations rise up to 21.0 mg g_{DW}^{-1} Chl *a* and 15.5 mg g_{DW}^{-1} Chl *b* at day 7 of the cultivation, which also marks the end of the exponential growth phase and decline towards a base level of approximately 10 mg g_{DW}^{-1} (Chl *a*) and 7.5 mg g_{DW}^{-1} (Chl *b*) towards the end of the cultivation. Compared to this the Chl *a* and *b* content in the green illuminated *Picochlorum* sp. cells level at approximately 12 mg g_{DW}^{-1} (Chl *a*) and 8 mg g_{DW}^{-1} (Chl *b*) throughout the whole cultivation, including the exponential growth phase. In this phase between day 4 and 9 of the cultivation (peak levels around days 5 till 7) the period with the fastest growth the unknown peaks U4, U5, as well as U2 and U3 occurred significantly with up to 4 mg g_{DW}^{-1} (U4). At day 6 the pigment content of U4 (3.7 mg g_{DW}^{-1}) and U5 (3.4 mg g_{DW}^{-1}) of the green illuminated cells almost make up the difference of Chl *a* at white illumination (19.4 mg g_{DW}^{-1}) and Chl *a* at green illumination (10.6 mg g_{DW}^{-1}). In total the unknown peaks made up 34.9 % of all extracted pigments, reducing the Chlorophylls ratio during the exponential growth phase from 81.0 % to 53.4 % at green light. The occurrence of the unknown pigments is limited to the exponential growth phase and declines afterwards in the stationary phase. This implies that the formation of the unknown pigments provide *Picochlorum* sp. a benefit for fast growth at uninhibited conditions. A better light utilization seems the most likely reason here.

The pooling and concentration of pigment samples of the green illuminated experiments originating from the exponential growth phase enabled a HPLC analysis with better resolution as overall pigment concentrations were much higher. After the discovery of the unknown pigment U5 almost within the Chl *b* peak the spectrograph analysis of the UV-VIS data (see Figure 40) revealed that there is a change in absorption with the unknown pigment U5. Compared to the spectral absorption of Chl *a,* the difference occurs in the region between 460 nm and 500 nm in which U5 shows higher absorption levels, enabling a potential photon usage within this bandwidth band. As U5 was overlapping with Chl *b*, which has its absorption peak exactly in this region this could be an artefact of Chl *b*. Further experiments with a better HPLC peak separation will be needed to resolve this finding.

No literature reference or report was found for these kinds of specially occurring pigment peaks at green light illumination in *Picochlorum* sp..

The structural finding in the HPLC-MS analysis of the one - and three double bond gaps in charge/-mass ratio of the unknown peaks compared to their chlorophyll reference revealed

important structural information. The hypothesis of the inserted double bonds in the phytol side chain explains the absence of a change in the absorption region. As the phytol chain is commonly considered not to be part of the chromophore structure in chlorophylls it is therefore spectroscopically silent (Deisenhofer *et al.*, 1995; Fiedor *et al.*, 2008) explaining the identical absorption scans of the unknown pigments compared to the chlorophylls. The unknown pigment U1 was not further investigated as isolation quantities were very low and occurrence at the green light exponential phase was also notable but still not very high.

The chlorophyll *a* and *b* concentration in the fractioned samples for NMR analysis were high enough to perform ^{1}H-^{1}H-COSY-NMR and HSQC-NMR aside the ^{1}H NMR analysis. This allowed for a complete peak identification of all chemical shifts of the analytes dissolved in acetone-d$_6$. The ^{1}H-chemical shifts could be correlated with literature data (Abraham and Rowan, 1991; Valverde and This, 2008; Kobayashi *et al.*, 2013) as shown in Table 20. Even though the chemical shifts of the unknown pigments were difficult to identify in the high-field region of the individual ^{1}H spectra, the peak intensity in the low-field region was sufficient to calculate the integrals of the peak area. In that way a second independent analysis confirmed the double bond hypothesis of the unknown pigments established via the HPLC-MS dataset.

In bacteriochlorophyll (BChl) biosynthesis the final steps of the phytyl-group formation were discussed (Mizoguchi, Harada and Tamiaki, 2006). In this work the position of the C=C double bond and their stepwise reduction originating from geranylgeranyl (GG) residue to the phytyl group is explained.
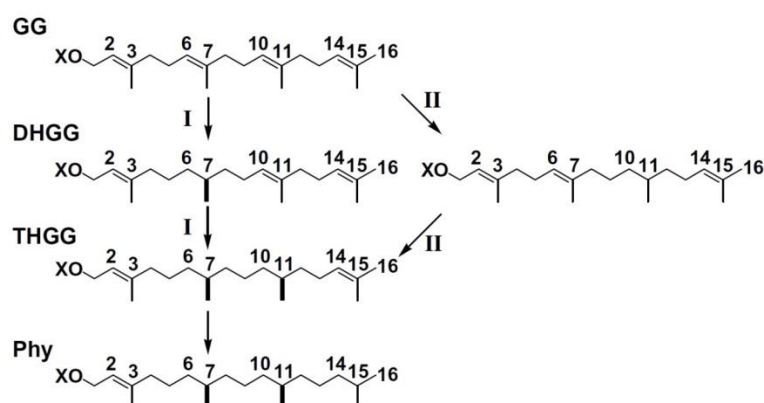
Figure 57: Reduction of geranylgeranyl to phytyl group at final bChl biosynthesis step. XO = chlorophyllide-*a*, GG = geranylgeranyl, DHGG = dihydrogeranylgeranyl, THGG = tetrahydrogeranyl-geranyl, Phy = phytyl (Mizoguchi, Harada and Tamiaki, 2006)

As displayed in Figure 57 the reduction of double bonds in the formation of the bacteriochlorophyll from GG to Phy is reached in three steps via the intermediates dihydrogeranylgeranyl (DHGG) in two possible chemical structures and tetrahydrogeranyl-geranyl (THGG). As final step the last double bond at carbon atom P[14] and P[15] (see IUPAC

numbering in Figure 17) is reduced. The difference in the chemical shifts of GG, DHGG, THGG and Phy are located in the high-field region between 2.0 and 0.8 ppm of the ^{1}H spectra (in chlorophorm-*d*-pyridine-*d_5* solvent system). Unfortunately, the NMR signals obtained for the unknown pigments are too weak in this region for a substantial comparison to the literature data.

Yet this pathway is a solid base for the estimation of the position of the observed double bonds, indicating that they are indeed at position P^6-P^7, P^{10}-P^{11} and P^{14}-P^{15} in the unknown pigments U5 and U2 with three extra double bonds and at position P^{14}-P^{15} for pigments U4 and U3.

Even though the phytyl residue is considered to be not involved in the spectral properties of the chlorophyll it indirectly affects the electronic absorption as the interactions of the molecule with the hydrophobic environment is affiliated by the phytyl-residue (Fiedor *et al.*, 2003). The insertion of additional double bonds in the phytyl-residue of the chlorophylls *a* and *b* could therefore have a beneficial effect for *Picochlorum* sp. in means of lipid solubility within the thylakoid membrane of the photosystems at green light illumination. As the two photosystems are finely tuned to respond to changing light qualities, the phosphorylation of the LHCII antenna complexes have been observed in *Arabidopsis thaliana* (Wunder *et al.*, 2013; Longoni *et al.*, 2015) and *Chlamydomonas* sp. (Bellaflore *et al.*, 2005; Frenkel *et al.*, 2007; Goldschmidt-Clermont and Bassi, 2015). The antenna complexes in the photosystem can be adapted for optimum response to changing light qualities and quantities by repositioning and rearrangement of antenna chromophores. The observed formation of the new pigments of *Picochlorum* sp. in the exponential growth phase under green light illumination could be caused by a similar regulation system. The additional double bonds in the phytol side chain turn the chlorophylls more mobile within the hydrophobic membranes. With this enhanced mobility a better regulation between the photosystems could be enabled in order to adapt to the unusual green light illumination. The interaction with other proteins in the thylakoid membrane could also be affected through the altered side-chain and have a positive impact on the structures of the antenna chromophores within the light harvesting complex of *Picochlorum* sp..

8.2 Mutagenesis Experiments

In this work four mutagenesis methods were developed and adapted to the microalgae *Picochlorum* sp.. Two new methods, an ARTP plasma mutation and a fast neutron radiation procedure were established and compared to UV and EMS methods.

8.2.1 Plasma discussion

The novel use of atmospheric and room temperature plasma as mutagenic agent has gained rising interest in recent years (Zhang *et al.*, 2014). The particles produced in the plasma interact with and change the cell wall and cell membrane causing the SOS repair mechanism to come in place. High error levels produce mismatches in the DNA repair process provoking a high number of random mutation events. These effects combined with a simple and non-toxic process makes this new technology highly promising for the generation of biological mutants or mutation breeding (Zhang *et al.*, 2014; Cao *et al.*, 2017).

With only one experiment run, which was possible with the ARTP plasma tool, and no reference data for the estimation of the impact of the plasma-carrier gas combinations the experimental setup was set wide to evaluate several influencing variables (see Table 13).

In order to compare the results and methods established for *Picochlorum* sp. a recent literature research of ARTP applications published from 2014 till 2017 is presented in Table 29. The focus of this listing is on the plasma methods and screening procedures applied. Additionally, the mini-review by Zhang et al. (Zhang *et al.*, 2014) provides a broad overview of plasma mutation procedures towards bacteria, fungi, yeast, actinomycetes and microalgae till 2014. A comparison of ARTP methods revealed that almost all of these publications were affiliated with the Biological Technology Laboratory, Department of Chemical Engineering of the Tsinghua University in Beijing, China. This is due to the fact that reported by early publications (Li *et al.*, 2008, 2012; Lu *et al.*, 2011) this department developed the ARTP device (see Figure 8), which is now marketed as ARTP (Atmospheric Room Temperature Plasma) Mutagenesis Breeding Machine by the Si Qing Yuan Bio-technology Co. Ltd.. These works are marked as „Tsinghua–System" in Table 29 and all have used helium as carrier gas. In every case, the distance between the sample on a steel plate (stainless steel) with 10 – 50 µL sample volume and the plasma nozzle was set to 2 mm. Maximum treatment durations were between 1 and 3 minutes. The work published by Gao, Yang and Liu (Gao, Yang and Liu, 2017) did not state what kind of system or carrier gas was used for the ARTP treatment. Jinghua Liu et al. (J. Liu *et al.*, 2016) working with *Haematococcus pluvialis* used an atmospheric pressure argon dielectric barrier discharge (DBD) as sole working with argon as carrier gas. The work published by Jing Liu et al.(J. Liu *et al.*, 2017) used a system provided by Yuanqing tianmu Biotechnol Inc with helium as carrier gas which was also not further specified.

Table 29: Recent studies working with ARTP mutagenesis methods, separated in organism kingdoms. Methods with volume used, surface for plasma sample, distance to nozzle and treatment duration. System: Tsinghua = Si Qing Yuan Bio-technology Co. Ltd., DBD = atmospheric pressure argon dielectric barrier discharge, Yuanqing = Yuanqing tianmu Biotechnol Inc.,

Type	Microorganism	Methods	Carrier gas	System	reference
	Mini-Review covering microalgae/fungi/bacteria			Tsinghua	(Zhang *et al.*, 2014)
bacteria	*Enterobacter aerogenes*	50 µL, steel plate, up to 3 min	helium	Tsinghua	(Lu *et al.*, 2011)
	Methylosinus trichosporium	stainless steel plate	helium	Tsinghua	(Li *et al.*, 2012)
	Bacillus subtilis	10 µL, steel plate, 2 mm	helium	Tsinghua	(Ma *et al.*, 2016)
	Streptomyces mobaraensis	10 µL, 4 mm, up to 60 sec,	helium	Tsinghua	(Jiang *et al.*, 2017)
	Actinomyces JN537	2 mm, up to 180s	helium	Tsinghua	(Ren, Chen and Tong, 2017)
	Lactobazillus sp.	10 µL, iron plate, up to 240 sec	n/a	n/a	(Gao, Yang and Liu, 2017)
	Symbiotic system TSH06	10 µL, metal slide	helium	Tsinghua	(Gu *et al.*, 2017)
fungi	*Yarrowia lipolytica*	10 µL, steel plate, 2 mm	helium	Tsinghua	(Zeng *et al.*, 2015)
	Mortierella alpina	10^6 cells mL^{-1}, 20 µL steel plate, 2 mm, up to 225 sec	helium	Tsinghua	(Li *et al.*, 2015)
	Yarrowia lipolytica	10 µL, steel plate, 2 mm	helium	Tsinghua	(X. Liu *et al.*, 2017)
micoalgae	*Spirulina platensis*	10 µL, stainless steel, 2 mm, up to 80 sec	helium	Tsinghua	(Fang *et al.*, 2013)
	Crypthecodinium cohnii	50000 cells in 20 µL, steel disc, 2 mm, up to 120 sec	helium	Tsinghua	(Liu *et al.*, 2015)
	Spirulina platensis	10 µL, steel plate, 2 mm	helium	Tsinghua	(Tan *et al.*, 2015)
	Haematococcus pluvialis	$7*10^4$ cells mL^{-1}	argon	DBD	(J. Liu *et al.*, 2016)
	Crypthecodinium cohnii	10^6 - 10^7 cells mL^{-1} + 10 % glycerol, 10 µL	helium	Yuanqing	(J. Liu *et al.*, 2017)
	Spirulina platensis	100 µL, 2 mm, up to 80 sec	helium	Tsinghua	(An *et al.*, 2017)
	Chlorella pyrenoidosa	10 µL, 2 mm	helium	Tsinghua	(Cao *et al.*, 2017)
yeast	*Rhodosporidium toruloides*	10 µL, iron plate, 2 mm	helium	Tsinghua	(Kitahara *et al.*, 2014)
	Rhodotorula mucilaginosa	108 cells mL-1,2 mm, 120 sec	helium	Tsinghua	(Wang et al., 2017)

Focusing on the work dealing with microalgae seven recent publications were found. Three worked with the cyanobacteria *Spirulina platensis* (listed here in the microalgae section) in order to generate mutants with increased carbohydrate content and growth rate (Fang *et al.*, 2013; Tan *et al.*, 2015). Dead or Alive screening was carried out utilizing the unique multicellular spiral structure of *Spirulina platensis,* which was destroyed via ARTP treatment. The filament fragments could be counted and split in 96-well plates. Surviving and growing fragments were then selected for high throughput screening in 48-well plates. The third work with *S. platensis* aimed to enhance astaxanthin production (An *et al.*, 2017). Treatment was carried out at the Tsinghua University using the β-ionone treatment was performed to screen for high yields of astaxanthin among mutant strains.

Higher levels of extracellular polysaccharides (EPS) were achieved with ARTP mutant

strains of *Crypthecodinium cohnii* (Liu *et al.*, 2015). Dead or alive screening was carried out on solid agar plates for 14 days. The EPS production was then correlated via enhanced glucose consumption of the heterotrophic dinoflagellate. High growth and lipid content was the screening goal for *C. cohnii* mutants as reported by Jing Liu et al. (J. Liu *et al.*, 2017). Dead or alive screening was also carried out on agar plates. The screening for fast growth was conducted via the acetyl-CoA carboxylase (ACCase) inhibitor sethoxydim. ACCase is a key enzyme catalyzing the first reaction in fatty acid synthesis (Hu *et al.*, 2008). An overexpression (triggered by random mutagenesis for instance) of the ACCase coding gene in *Solanum tuberosum* (potato) resulted in higher lipid content (Klaus *et al.*, 2004). Jing Liu et al. identified faster growing mutant strains with upregulated ACCase coding gene able to grow on sethoxydim plates under limiting of the fatty acid synthesis.

The DBD plasma treatment is very similar to the ARTP treatment with the difference that the biological sample is placed in between two electrodes which generates the plasma field. Just as the ARTP it produces charged particles, reactive species, UV radiation and energetic ions and electrons (Li *et al.*, 2008) and is therefore comparable to ARTP methods. Jinghua Liu *et al.* used argon as carrier gas, with the same reactive species, for the mutation of *Haematococcus pluvialis* in order to generate hyperproducing astaxanthin mutant strains (J. Liu *et al.*, 2016). The dead or alive screening was evaluating the efficiency of the mutation procedure by colony counting on agar plates. Growth rate was later determined via cellcount using a haemacytometer via two-point determination.

Agar plate based dead or alive determination was also chosen for the screening of ARTP mutated *Chlorella pyrenoidosa* (Cao *et al.*, 2017). The survival rate (in %) was determined like in the previous publications through the fraction of treated samples and control samples times 100. The lipid production screening was carried out via Nile-Red staining after 7 days of growth in shake flasks. The stability of the strains was subsequently screened for 6 recultivation times.

Compared to these findings the plasma torch system used for this work was much smaller but very easy to handle. As treated volume a 1 mL cell suspension with 10^7 cell mL^{-1} was used. The plasma nozzle was evenly moved above the thinly spread cell droplet on the pretreated petri dish. The treatment distance to the nozzle was approximately 1 cm. This is certainly a critical point to assess in further work to implement a mounting and automated moving system over the sample in order to reduce manual handling impact on the samples. The treatment duration was extended up to 10 minutes, resulting in a strong evaporation rate. In order to increase the effect of the plasma DMSO could be added to get higher permeability's of the cell walls as reported for *C. cohnii,* which approximately doubled the lethal rate from 43.5 % up to 90.7 % (Liu *et al.*, 2015) at the same plasma treatment duration. This would also benefit the evaporation rate as shorter treatment results in less sample

evaporation through the helium plasma flow. An addition of 10 % (v/v) glycerol solution could also be added to prevent evaporation as reported by Liu et al (J. Liu *et al.*, 2017).

With the selected setting (process air flow of 1 L min^{-1}) a kill curve (see Figure 56 a)) could be calculated with a 10% survival rate after 220 seconds of treatment. The wide spread prediction bands of *Picochlorum* sp. for this first experiment are not surprising and could certainly be narrowed down to obtain improved prediction values with further experiments. The critical time for further consideration is between 2 and 4 minutes of treatment. Due to the widespread of the 2 min samples a better prediction was unfortunately not possible for this first set of data points. The short treatment time is also comparable with the reported values in recent literature as shown in Table 29.

Additional to the varying treatment durations other carrier gas systems have been tested. For these experiments only a treatment time of 2 minutes was possible within the first experiment. Helium and varigon®H2 as carrier gas, both with an air flow of 1 L min^{-1}, resulted in slower biomass gain throughout the initial screening of 10 days. This indicates a higher initial kill rate and thus less surviving cells to start with as the maximum growth rates are similar to the control group (see Table 23). The use of varigon®H2 with 3 L min^{-1} gas flow resulted in higher cell growth after 10 days of initial cultivation. The growth rate was also significantly higher compared to the non-treated control group (p = 0.033). Here two effects seem to correlate positively. With the increased carrier gas flow a higher evaporation rate was monitored resulting in a higher cell concentration of the treated sample. The remaining sample volume after the treatment with initially 10^7 cells mL^{-1} was diluted at factor 10 and screened for growth. The evaporation rate with varigon®H2 (3 L min^{-1}) was comparabe with the evaporation level of 6 min treatment with air as carrier gas suggesting, that in the initial dilution for the screening the cell concentration was higher than in the other 2 minute treatment experiments. The higher maximum growth rate indicates that helium as carrier gas seemed indeed promoting the generation of mutants that did grow faster than the control group. The highest maximum growth rates (significantly faster than the control group with p = 0.008 and also significantly faster than the group with 2 min treatment time on petri dish p = 0.043) were observed with the samples placed on the brass metal plate instead on the plastic petri dish for treatment. For this experimental setup air was used as carrier gas with the normal gas flow of 1 L min^{-1}. The higher maximum growth rates and the gain of biomass production within the first 10 days of screening indicate towards the successful generation of faster growing mutant strains. The metal plate, working as a conduction electrode, could have the effect that the plasma penetrated better through the sample film than on the isolating plastic petri dishes, thus having a better impact and effect on the biological tissue. This theory is supported by the fact that the ARTP plasma tool developed at the Tsinghua

University is also using a stainless steel plate for thetreatment (see Table 29) (Li *et al.*, 2008; Lu *et al.*, 2011).

8.2.2 Fast neutron mutagenesis discussion

Most work with fast neutron radiation for mutagenesis has been reported with plants (see section 3.4.3).

Fast neutron irradiation of microalgae has been reported only once up to now (S. Liu *et al.*, 2016). The *Chlorella* sp. strains irradiated by Liu et al were treated with 2.45 MeV neutron energy for 125 minutes at three different distances (15, 16 and 18 cm) to the neutron source. The dosage was stated as $8.14*10^9$ n cm^{-2} at 15 cm distance, $5.64*10^8$ n cm^{-2} at 16 cm distance and $9.42*10^7$ n cm^{-2} at 18 cm distance. Unfortunately, these specifications are not sufficient to calculate the radiation dosage per minute [Gy min^{-1}] or total radiation [Gy]. Reported dosages of plants were in the range of 60 Gy for *Arabidopsis* sp. (Koornneef *et al.*, 1982), and 18 – 33 Gy for rice (Bruggemann *et al.*, 1996; Li, Lassner and Zhang, 2002; Wu *et al.*, 2005). Therefore, the first experiment (nM1, see section 7.2.1) conducted with the microalgae *Picochlorum* sp. was set with a dosage range of 1 Gy up to 150 Gy (see Table 14). Growth was observed at all irradiated levels as shown in Figure 50. The cells irradiated with 150 Gy had a survival probability of 35.5 ± 9.8 %.

With the second experiment the irradiation dosage was increased up to 500 Gy in order to achieve a kill rate of 100 %. This was succeeded as displayed in Figure 53. Cells irradiated with 300 Gy and higher did not show detectable growth within the first two weeks of screening. From the initial 10^7 cells mL^{-1} of each replicate a 1 to 10 dilution was performed for the screening, resulting in 10^6 cells mL^{-1} irradiated cells at the start of the screening. With the initial growth experiment for screening of *Picochlorum* sp. in 24-well plates (see section 7) a dilution of 100 cells mL^{-1} was detectable within 14 days of cultivation. This indicates that out of 10^6 cells mL^{-1} (100 %) a minimum of 100 cells would have needed to survive the treatment to be still detectable. This equals 0.01 % of the treated cells and signals the lower detection limit of this screening method.

At the irradiance dosage of 300 Gy upwards no cell growth was detectable. The survival rate calculation is shown in Figure 56 b) with very narrow confidence and prediction bands and a RSQ of 0.996. A calculated 50 % survival rate could therefore be reached at a fast neutron dosage of 66.4 Gy, 10 % at 155.6 Gy and 2% at 366.8 Gy (see Table 28) with the cumulative dosage of 0.466 Gy min^{-1} consisting of a neutron radiation to gamma radiation ratio of $D_n D_\gamma^{-1} = 2.70$. (see Table 14).

During the third irradiation experiment (see section **Fehler! Verweisquelle konnte nicht gefunden werden.**) the fast neutron mutagenesis was repeated with *Picochlorum* sp.. A

comparison of the two kill rates of *Picochlorum* sp of experiment 2 and 3 is displayed in Figure 54. There is almost no detectable difference between the two slightly changed experimental setups concerning the survivability after fast neutron irradiation. The first experiment nM1 with *Picochlorum* sp. is also displayed in Figure 54. Here the curve of the survival rate flattens slower than at the following experiment nM2. This could be due to the fact that this experiment was performed within an earlier operating phase of the FRM II research reactor. With the periodically change of the fuel element of the reactor core a new collimator element was installed between nM1 and nM2 experiments. Nevertheless, the output dosage and neutron to gamma ratio was set similar for each experiment as stated in Table 14. The change of the collimator should therefore not interfere with the neutron dosage. In experiment nM3 the cumulative dosage was increased by reduction of the sample-distance to the neutron source. The reduction of irradiation dosage with increased distance is the outcome of the not vacuum channeled fast neutron beam, which enabled the neutrons to interact with the nitrogen, oxygen, argon and carbon dioxide atoms in the air and thus reduced the total amount of neutrons in the beam.

The screening for fast growing *Picochlorum* sp. mutant strains after fast neutron mutagenesis was carried out as described before in 24-well plates. In the first screening of the nM1 experiment a widespread deviation of the control strains was observed. The maximum growth rate of the control strains (and therefore also the growth rate of the mutant strains) fluctuated between μ_{max} = 0.404 d^{-1} (screening #2) and μ_{max} = 0.779 d^{-1} (screening #1). The criteria for a positive screening hit have to be extended (averaged growth rate + standard deviation as minimum benchmark). Out of the 160 mutant strains screened within the first experiment only 9 strains showed enhanced growth. However, the 9 strains did each excel the extended control benchmark in just 3 screening cycles out of the performed 8 cycles. With this unstable growth the screening was therefore aborted after the screening cycle 8. In the second experiment nM2 the total number of screened mutants and the screening duration was extended to 252 strains and 106 days of screening, split in 13 subsequent cycles. The screening was conducted with all grown mutant strains that were irradiated up to 300 Gy. The samples which did not show growth in the initial screen were replaced with samples of the 1 - 10% survival rate irradiation range (150 – 275 Gy) to increase the possibility of identifying a fast growing mutant strain. Because of the high standard deviation, the enhanced mutant growth benchmark was chosen as before. The best four mutant strains (growth shown in Figure 52, growth data in Table 27) identified in the screenings had an individual maximum growth rate of 120 – 149 %. Taking the growth rates of all 13 cycles into account, the average growth rate was at 116 ± 23 % for the best mutant strain "nM2_10-A02-200Gy".

8.2.3 Screening discussion

Dead or alive screening

Growth on agar plates with a follow up colony count as often described in Literature (Fang *et al.*, 2013; Tan *et al.*, 2015; Gu *et al.*, 2017) was not applicable for *Picochlorum* sp. as this strain did barely grow at all on solid agar plates. Growth could be monitored after 3 weeks and ongoing. Cultivations on agar plates longer than 3 weeks led to the problem of drying plates and this method could therefore not be used for *Picochlorum* sp..

The dead or alive-staining with SYTOX® Green nucleic acid or SYTOX® orange staining was reported to work for *Nannochloropsis* sp., phytoplankton as well as zooplankton and *Chlamydomonas reinhardtii*. It functions via penetration of damaged cell membranes allowing the discrimination of live and dead cells if compared to auto-fluorescence. (Sato *et al.*, 2004; Doan and Obbard, 2012; Zetsche and Meysman, 2012). Despite the drawback of the consumption of cell volume (e.g. in case of 24-well screening with just 1 mL culture volume) this method was tested for *Picochlorum* sp. with various concentrations and addition of DMSO but no staining procedure delivered satisfying results and was thus not applied in the screening of mutated cells.

Dead or alive screening was thus performed as described in section 5.3.4 via the $OD^{PR}_{750\,nm}$ optical density measurement with the plate reader. This system was tested beforehand in a comparative experiment with FACS cellcount analysis. The advantages of the purely optical analysis were that no cell volume was wasted for the measurements. The time consuming cellcounts were performed with a minimum volume of 50 µL in triplicates, losing 150 µL for each measurement. This was considered too much of a loss and as the results could be correlated with the optical analysis this method was preferred.

Screening for fast growing mutant strains

The initial growth test with the sequentially diluted *Picochlorum* sp. inoculum (see section 7) was successful. Screening in 24-well plates with regular aeration and plate reader analysis works sufficiently for 7 up to 10 days until the cell density exceeds the linear range of the multi plate reader. Unfortunately, the screening setup itself did not provide continuously equal conditions resulting in a widespread deviation of the control group, permitting to question the results of the mutant strains.

Main influencing factor on the screening in 24-well plates was the aeration difficulties caused by the sealed lids (to prevent evaporation) and the manual air exchange during measurement intervals. This was clearly visible in the neutron screening nM2 #4 and #5 (see Table 26) during the holiday season. Here the limited access to the lab prevented regular aeration, which resulted in reduced growth rates for all strains. An effect of the plate position at the shaker platform in the nM2 screening with a total of 12 plates was also observed, generated by a smaller lamp and a wider spread area of the plates underneath. This caused

the corner plates to get less illumination and also diagonal illumination so that the wells were not completely illuminated from directly above. A systematic rotation of the plates, which was implemented after discovery of this effect in the middle of screening period 2, could compensate this effect. Additionally, inaccuracies in handling can occur at any time during the daily measurements or recultivation steps.

9 Conclusion and outlook

Using different colored LED illumination setups and intensities the growth characteristics of *Picochlorum* sp., *Dunaliella* sp. and *M. salina* have been determined. Pigment formation and lipid content have been investigated. The formation of pigments of *Picochlorum* sp. has been studied extensively with the discovery of novel pigment peaks occurring at green light illumination. Through experimental setup changes via the use of chromatic filter plates the irradiation spectra has been clearly focused to the green light region (550 nm till 590 nm) to investigate the cause of the pigment formation. The scale-up to bioreactor dimensions enabled continuous sampling and revealed that the new pigments occurred in exponential growth phase and declined at stationary growth. With the increased sample volume HR LC-MS and NMR analysis were applied to discover the structural composition of the unknown pigments. Chlorophyll *a* and *b* variation with one and three additional double bindings in the phytol-residue of the chlorophylls could be identified. In order to further investigate these findings and the potential benefit for the microalgae an improved pooling and fractionating procedure is needed in order to increase purified sample volumes and thus generate higher resolution in NMR analysis.

As it could not be finally resolved if the newly identified pigments originate from an incomplete biosynthesis, that occurred intentionally or were caused by an altered cell metabolism of the green illuminated *Picochlorum* sp. cells further metabolomic studies could provide new answers to these findings. A combination of analytical and metabolic work and an alteration of the illumination setup seems a promising approach. Here the spectral properties of the used LEDs such as bandwidth, peak intensity, FWHM and overall illumination intensity should be closely monitored and considered for analysis. The use of pulse-amplitude-modulated (PAM) fluorescence could also lead to new insights on the status of the photosystems at different color illumination (Cosgrove and Borowitzka, 2006; White, Anandraj and Bux, 2011). With this fast and non-invasive technique an online monitoring of the PS II reaction centers would be possible to observe potential changes in the composition and organization of the photosynthesis in green illuminated *Picochlorum* sp. cultures.

Four mutation methods have been tested and adapted to the microalgae *Picochlorum* sp.. The novel method of ARTP plasma treatment was developed with a new plasma generator tool opposed to the work in recent literature that was all performed on the same plasma instrument (Zhang *et al.*, 2014) The Plasma mutation trial with the handheld plasma torch showed promising first results. Despite the problems during the screening and no clear positively identified mutant strain the method itself worked well. The theoretical effects of plasma are superior to just UV or EMS treatment and therefore endorse this new mutagenic procedure. In order to set up a reliable plasma mutation method with the tested device further experiments would be required. For the new approach, helium as carrier gas seems

to deliver the best results, corresponding with literature data. A sample plate switch to the used brass plate or stainless steel plate according to literature results seems favorable. Via the addition of DMSO plasma permeability on the cells could be extended, thus reducing treatment duration. A 100 % kill rate is probably accomplishable within 5 minutes of treatment. This short exposure time would also reduce the evaporation effects making smaller sample volumes possible.

Fast neutron bombardment as mutagenesis tool for microalgae was successfully established for the microalgae *Picochlorum* sp.. The calculation of irradiation time and survival rate was very accurate with narrow confidence bands. With an improved screening system this data provides a reliable experiment as basis for further fast neutron irradiations on microalgae.

For future screenings a semi or fully automated screening mechanism is strongly recommended, as conventional screening methods such as for instance phenotypic screening proofed to be time and lab consuming. This becomes more significant when working with more than 4 plates simultaneously. Bottom lit 24-well plates would reduce an angling effect of lamps installed at the top of the shaker with a certain distance to the plates. Aeration or venting of the plates could be neglected in a shaker platform with complete CO_2 regulation and humidity control.

10 Bibliography

Abiusi, F. *et al.* (2014) 'Growth, photosynthetic efficiency, and biochemical composition of Tetraselmis suecica F&M-M33 grown with LEDs of different colors', *Biotechnol Bioeng.* 2013/08/02, 111(5), pp. 956–964. doi: 10.1002/bit.25014.

Abraham, R. J. and Rowan, A. E. (1991) 'Nuclear Magnetic Resonance Spectroscopy of Chlorophyll', in Scheer, H. (ed.) *Chlorophylls.* CRC Press, pp. 797–834. doi: epub2343.

Ahmad, M., Lin, C. and Cashmore, A. R. (1995) 'Mutations throughout an Arabidopsis blue-light photoreceptor impair blue-light-responsive anthocyanin accumulation and inhibition of hypocotyl elongation', *The Plant Journal*, pp. 653–658. doi: 10.1046/j.1365-313X.1995.08050653.x.

Akiyama, M. *et al.* (2001) 'Detection of chlorophyll d' and pheophytin a in a chlorophyll d-dominating oxygenic photosynthetic prokaryote Acaryochloris marina.', *Analytical sciences : the international journal of the Japan Society for Analytical Chemistry*, 17(1), pp. 205–208. doi: 10.2116/analsci.17.205.

An, J. *et al.* (2017) 'Screening for enhanced astaxanthin accumulation among Spirulina platensis mutants generated by atmospheric and room temperature plasmas', *Algal Research*. Elsevier, 25(January), pp. 464–472. doi: 10.1016/j.algal.2017.06.006.

Arunyanart, S. and Soontronyatara, S. (2002) 'Mutation induction by gamma and X-ray irradiation in tissue cultured lotus', *Plant Cell, Tissue and Organ Culture*, 70(1), pp. 119–122. doi: 10.1023/A:1016021627832.

Bellaflore, S. *et al.* (2005) 'State transitions and light adaptation require chloroplast thylakoid protein kinase STN7', *Nature*, 433(7028), pp. 892–895. doi: 10.1038/nature03286.

BIOspec GmbH (2017) *LED Retrofit Reactor*. Available at: https://biospec.de/index.php/led-retrofit-reactor.html (Accessed: 12 June 2017).

Bolon, Y.-T. *et al.* (2011) 'Phenotypic and Genomic Analyses of a Fast Neutron Mutant Population Resource in Soybean', *Plant Physiology*, 156(1), pp. 240–253. doi: 10.1104/pp.110.170811.

Bonardi, V. *et al.* (2005) 'Photosystem II core phosphorylation and photosynthetic acclimation require two different protein kinases', *Nature*, 437(7062), pp. 1179–1182. doi: 10.1038/nature04016.

Borowitzka, M. A. (2013) 'High-value products from microalgae—their development and commercialisation', *Journal of Applied Phycology*, 25(3), pp. 743–756. doi: 10.1007/s10811-013-9983-9.

Bruggemann, W. *et al.* (1996) 'Analysis of fast neutron-generated mutants at the Arabidopsis thaliana HY4 locus', *Plant Journal*, pp. 755–760. doi: 10.1046/j.1365-313X.1996.10040755.x.

Brzezowski, P., Richter, A. S. and Grimm, B. (2015) 'Regulation and function of tetrapyrrole biosynthesis in plants and algae', *Biochimica et biophysica acta*. Elsevier B.V., 1847(9), pp. 968–985.

doi: 10.1016/j.bbabio.2015.05.007.

Del Campo, J. A. *et al.* (2000) 'Carotenoid content of chlorophycean microalgae: factors determining lutein accumulation in Muriellopsis sp. (Chlorophyta)', *Journal of Biotechnology*, 76(1), pp. 51–59. doi: 10.1016/S0168-1656(99)00178-9.

Cao, S. *et al.* (2017) 'Improving of lipid productivity of the oleaginous microalgae Chlorella pyrenoidosa via atmospheric and room temperature plasma (ARTP)', *Bioresource Technology*. doi: 10.1016/j.biortech.2017.05.039.

Chen, H.-B. *et al.* (2010) 'Modeling on chlorophyll a and phycocyanin production by Spirulina platensis under various light-emitting diodes', *Biochemical Engineering Journal*, 53(1), pp. 52–56. doi: http://dx.doi.org/10.1016/j.bej.2010.09.004.

Chen, M. *et al.* (2012) 'A cyanobacterium that contains chlorophyll f – a red-absorbing photopigment', *FEBS Letters*, 586(19), pp. 3249–3254. doi: http://dx.doi.org/10.1016/j.febslet.2012.06.045.

Chisti, Y. (2007) 'Biodiesel from microalgae', *Biotechnology Advances*. Elsevier Inc., 25(3), pp. 294–306. doi: 10.1016/j.biotechadv.2007.02.001.

Cosgrove, J. and Borowitzka, M. (2006) 'Applying Pulse Amplitude Modulation (PAM) fluorometry to microalgae suspensions: Stirring potentially impacts fluorescence', *Photosynthesis Research*, 88(3), pp. 343–350. doi: 10.1007/s11120-006-9063-y.

Dahmen, I. *et al.* (2014) 'Optimisation of the critical medium components for better growth of Picochlorum sp. and the role of stressful environments for higher lipid production', *Journal of the Science of Food and Agriculture*. John Wiley & Sons, Ltd, 94(8), pp. 1628–1638. doi: 10.1002/jsfa.6470.

Das, N. and Das, D. (2013) 'Recovery of rare earth metals through biosorption: An overview', *Journal of Rare Earths*. The Chinese Society of Rare Earths, 31(10), pp. 933–943. doi: 10.1016/S1002-0721(13)60009-5.

Das, P. *et al.* (2011) 'Enhanced algae growth in both phototrophic and mixotrophic culture under blue light', *Bioresource Technology*. Elsevier Ltd, 102(4), pp. 3883–3887. doi: 10.1016/j.biortech.2010.11.102.

Deisenhofer, J. *et al.* (1995) 'Crystallographic Refinement at 2.3\,\AA Resolution and Refined Model of the Photosynthetic Reaction Centre from Rhodopseudomonas viridis', *J. Mol. Biol.*, 246, pp. 429–457. Available at: citeulike-article-id:240311.

Doan, T. T. Y. and Obbard, J. P. (2012) 'Enhanced intracellular lipid in Nannochloropsis sp. via random mutagenesis and flow cytometric cell sorting', *Algal Research*, 1(1), pp. 17–21. doi: http://dx.doi.org/10.1016/j.algal.2012.03.001.

Dor, E. *et al.* (2010) 'Characterization of a novel tomato mutant resistant to the weedy parasites

Orobanche and Phelipanche spp', *Euphytica*, 171(3), pp. 371–380. doi: 10.1007/s10681-009-0041-2.

Einstein, A. and Infeld, L. (1938) 'The Evolution of Physics', *The Cambridge Library of Modern Science*. doi: 10.1119/1.1987055.

Eriksen, N. T. (2008) 'Production of phycocyanin - A pigment with applications in biology, biotechnology, foods and medicine', *Applied Microbiology and Biotechnology*, 80(1), pp. 1–14. doi: 10.1007/s00253-008-1542-y.

Fang, M. Y. *et al.* (2013) 'Rapid Mutation of Spirulina platensis by a New Mutagenesis System of Atmospheric and Room Temperature Plasmas (ARTP) and Generation of a Mutant Library with Diverse Phenotypes', *Plos One*, 8(10), p. 12. doi: 10.1371/journal.pone.0077046.

Farhi, E. *et al.* (2008) 'Spectroscopic investigation of ionizing-radiation tolerance of a Chlorophyceae green micro-alga', *Journal of Physics: Condensed Matter*, 20(10), p. 104216. doi: 10.1088/0953-8984/20/10/104216.

Fawley, M. W., Jameson, I. and Fawley, K. P. (2015) 'The phylogeny of the genus Nannochloropsis (Monodopsidaceae, Eustigmatophyceae), with descriptions of N. australis sp. nov. and Microchloropsis gen. nov.', *Phycologia*. Taylor & Francis, 54(5), pp. 545–552. doi: 10.2216/15-60.1.

Fiedor, L. *et al.* (2003) 'Phytol as one of the determinants of chlorophyll interactions in solution', *Photosynthesis Research*, 78(1), pp. 47–57. doi: 10.1023/A:1026042005536.

Fiedor, L. *et al.* (2008) 'Understanding chlorophylls: Central magnesium ion and phytyl as structural determinants', *Biochimica et Biophysica Acta - Bioenergetics*, 1777(12), pp. 1491–1500. doi: 10.1016/j.bbabio.2008.09.005.

Fisher, T., Minnaard, J. and Dubinsky, Z. (1996) 'Photoacclimation in the marine alga Nannochloropsis sp. (Eustigmatophyte): A kinetic study', *Journal of Plankton Research*, 18(10), pp. 1797–1818. doi: 10.1093/plankt/18.10.1797.

Frenkel, M. *et al.* (2007) 'Hierarchy amongst photosynthetic acclimation responses for plant fitness', *Physiologia Plantarum*, 129(2), pp. 455–459. doi: 10.1111/j.1399-3054.2006.00831.x.

Fridman, G. *et al.* (2007) 'Comparison of direct and indirect effects of non-thermal atmospheric-pressure plasma on bacteria', *Plasma Processes and Polymers*, 4(4), pp. 370–375. doi: 10.1002/ppap.200600217.

FRMII (2017) *MEDAPP Irradiation facility*. Available at: http://www.frm2.tum.de/en/the-neutron-source/irradiation-facilities/irradiation-with-fast-neutrons/ (Accessed: 10 August 2017).

Gao, C., Yang, F. and Liu, Y. (2017) 'Plasma Mutation Breeding of High Yield γ-Aminobutyric Acid Lactic Acid Bacteria', *Gene Science and Engineering*, 1(1), pp. 8–18.

Garrido, J. L. and Zapata, M. (1998) 'Detection of new pigments from Emiliania huxleyi (Prymnesiophyceae) by high-performance liquid chromatography, liquid chromatography-mass

spectrometry, visible spectroscopy, and fast atom bombardment mass spectrometry', *Journal of Phycology*, 34(1), pp. 70–78. doi: 10.1046/j.1529-8817.1998.340070.x.

Gentile, M. P. and Blanch, H. W. (2001) 'Physiology and xanthophyll cycle activity of Nannochloropsis gaditana', *Biotechnology and Bioengineering*, 75(1), pp. 1–12. doi: 10.1002/bit.1158.

Glemser, M. *et al.* (2015) 'Application of light-emitting diodes (LEDs) in cultivation of phototrophic microalgae: current state and perspectives', *Applied Microbiology and Biotechnology*, 100(3), pp. 1077–1088. doi: 10.1007/s00253-015-7144-6.

Goldschmidt-Clermont, M. and Bassi, R. (2015) 'Sharing light between two photosystems: Mechanism of state transitions', *Current Opinion in Plant Biology*. Elsevier Ltd, 25, pp. 71–78. doi: 10.1016/j.pbi.2015.04.009.

Griffiths, M. J., van Hille, R. P. and Harrison, S. T. L. (2010) 'Selection of Direct Transesterification as the Preferred Method for Assay of Fatty Acid Content of Microalgae', *Lipids*, 45(11), pp. 1053–1060. doi: 10.1007/s11745-010-3468-2.

Gu, C. *et al.* (2017) 'ARTP mutation and genome shuffling of ABE fermentation symbiotic system for improvement of butanol production', *Applied Microbiology and Biotechnology*. Applied Microbiology and Biotechnology, 101(5), pp. 2189–2199. doi: 10.1007/s00253-017-8093-z.

Gueymard, C. A., Myers, D. and Emery, K. (2002) 'Proposed reference irradiance spectra for solar energy systems testing', *Solar Energy*, 73(6), pp. 443–467. doi: 10.1016/S0038-092X(03)00005-7.

Guihéneuf, F. *et al.* (2010) 'Effect of UV stress on the fatty acid and lipid class composition in two marine microalgae Pavlova lutheri (Pavlovophyceae) and Odontella aurita (Bacillariophyceae)', *Journal of Applied Phycology*, 22(5), pp. 629–638. doi: 10.1007/s10811-010-9503-0.

Henley, W. J. *et al.* (2004) 'Phylogenetic analysis of the "Nannochloris-like" algae and diagnoses of Picochlorum oklahomensis gen. et sp. nov. (Trebouxiophyceae, Chlorophyta)', *Phycologia*, 43(6), pp. 641–652. doi: 10.2216/i0031-8884-43-6-641.1.

Hessen, D. O., De Lange, H. J. and van Donk, E. (1997) 'UV-induced changes in phytoplankton cells and its effects on grazers', *Freshwater Biology*, 38, pp. 513–524.

Van Heukelem, L. and Thomas, C. S. (2001) 'Computer-assisted high-performance liquid chromatography method development with applications to the isolation and analysis of phytoplankton pigments', *Journal of Chromatography A*, 910(1), pp. 31–49. doi: http://dx.doi.org/10.1016/S0378-4347(00)00603-4.

Hoffmann, D. *et al.* (2007) 'Nodulation deficiency caused by fast neutron mutagenesis of the model legume Lotus japonicus', *Journal of Plant Physiology*, 164(4), pp. 460–469. doi: 10.1016/j.jplph.2006.12.005.

Hooker, S. B. *et al.* (2005) 'The Second SeaWiFS HPLC analysis Round-Robin experiment

(SeaHARRE-2)', *NASA Tech. Memo,Goddard Space Flight Center*, 2005–21278(August), p. 112pp. Available at: http://hdl.handle.net/2060/20110008482.

Hu, Q. *et al.* (2008) 'Microalgal triacylglycerols as feedstocks for biofuel production: Perspectives and advances', *Plant Journal*, 54(4), pp. 621–639. doi: 10.1111/j.1365-313X.2008.03492.x.

Huesemann, M. *et al.* (2013) 'Simulation of Outdoor Pond Cultures Using Indoor LED-lighted and Temperature-Controlled Raceway Ponds'. Available at: http://www.google.de/url?sa=t&rct=j&q=&esrc=s&source=web&cd=1&ved=0CCIQFjAA&url=http%3A%2F%2Fwww.algaebiomass.org%2Fwp-content%2Fgallery%2F2012-algae-biomass-summit%2F2010%2F06%2FHuesemann-Michael1.pdf&ei=WP2LVZuWNoizUfLQgiA&usg=AFQjCNHlVqpZ2zGcXo66CEYUSZ.

Huesemann, M. H. *et al.* (2013) 'A screening model to predict microalgae biomass growth in photobioreactors and raceway ponds', *Biotechnology and Bioengineering*. Wiley Subscription Services, Inc., A Wiley Company, 110(6), pp. 1583–1594. doi: 10.1002/bit.24814.

Hultberg, M. *et al.* (2014) 'Impact of light quality on biomass production and fatty acid content in the microalga Chlorella vulgaris', *Bioresource Technology*, 159, pp. 465–467. doi: 10.1016/j.biortech.2014.03.092.

Hwang, W. J. *et al.* (2015) 'Genome-wide analysis of mutations in a dwarf soybean mutant induced by fast neutron bombardment', *Euphytica*, 203(2), pp. 399–408. doi: 10.1007/s10681-014-1295-x.

Infors AG (2017) *Labfors 5 Lux*. Available at: http://www.infors-ht.com/index.php/de/produkte/bioreaktoren/tischbioreaktoren/labfors-5-lux (Accessed: 15 June 2017).

Jiang, Y. *et al.* (2017) 'Enhancing transglutaminase production of Streptomyces mobaraensis by iterative mutagenesis breeding with atmospheric and room-temperature plasma (ARTP)', *Bioresources and Bioprocessing*. Springer Berlin Heidelberg, 4(1), p. 37. doi: 10.1186/s40643-017-0168-2.

Kalin, M., Wheeler, W. N. and Meinrath, G. (2004) 'The removal of uranium from mining waste water using algal/microbial biomass', *Journal of Environmental Radioactivity*, 78(2), pp. 151–177. doi: 10.1016/j.jenvrad.2004.05.002.

Kandilian, R., Lee, E. and Pilon, L. (2013) 'Radiation and optical properties of Nannochloropsis oculata grown under different irradiances and spectra', *Bioresource Technology*. Elsevier Ltd, 137, pp. 63–73. doi: 10.1016/j.biortech.2013.03.058.

Karkach, A. S. (2006) 'Trajectories and models of individual growth', *Demographic Research*, 15. doi: 10.4054/DemRes.2006.15.12.

Katsuda, T. *et al.* (2004) 'Astaxanthin production by Haematococcus pluvialis under illumination with LEDs', *Enzyme and Microbial Technology*, 35(1), pp. 81–86. doi: http://dx.doi.org/10.1016/j.enzmictec.2004.03.016.

Kazama, Y. *et al.* (2011) 'Characterization of highly efficient heavy-ion mutagenesis in Arabidopsis thaliana', *BMC plant biology.* BioMed Central, 11, p. 161. doi: 10.1186/1471-2229-11-161.

Kitahara, Y. *et al.* (2014) 'Isolation of oleaginous yeast (Rhodosporidium toruloides) mutants tolerant of sugarcane bagasse hydrolysate', *Bioscience, Biotechnology and Biochemistry*. Taylor & Francis, 78(2), pp. 336–342. doi: 10.1080/09168451.2014.882746.

Klaus, D. *et al.* (2004) 'Increased fatty acid production in potato by engineering of acetyl-CoA carboxylase', *Planta*, 219(3), pp. 389–396. doi: 10.1007/s00425-004-1236-3.

Kobayashi, M. *et al.* (1998) 'Light-independent isomerization of bacteriochlorophyll g to chlorophyll a catalyzed by weak acid in vitro', *Analytica Chimica Acta*, 365(1–3), pp. 199–203. doi: 10.1016/S0003-2670(98)00088-9.

Kobayashi, M. *et al.* (2013) 'Physicochemical properties of chlorophylls in oxygenic photosynthesis—succession of co-factors from anoxygenic to oxygenic photosynthesis', in *Photosynthesis. InTech*, pp. 47–90.

Koc, C., Anderson, G. A. and Kommareddy, A. (2013) 'Use of Red and Blue Light-Emitting Diodes (LED) and Fluorescent Lamps to Grow Microalgae in a Photobioreactor', *Israeli Journal of Aquaculture-Bamidgeh*, 65(8), p. 8.

Koornneef, M. *et al.* (1982) 'EMS- and relation-induced mutation frequencies at individual loci in Arabidopsis thaliana (L.) Heynh', *Mutation Research/Fundamental and Molecular Mechanisms of Mutagenesis*, 93(1), pp. 109–123. doi: http://dx.doi.org/10.1016/0027-5107(82)90129-4.

de la Vega, M. *et al.* (2011) 'Isolation of a new strain of Picochlorum sp and characterization of its potential biotechnological applications', *Biotechnology Progress*, 27(6), pp. 1535–1543. doi: 10.1002/btpr.686.

Lanfaloni, L. *et al.* (1991) 'Mutagenesis of the cyanobacterium Spirulina platensis by UV and nitrosoguanidine treatment', *FEMS Microbiology Letters*, 83(1), pp. 85–90. Available at: http://www.sciencedirect.com/science/article/pii/037810979190449K.

Laroussi, M. and Leipold, F. (2004) 'Evaluation of the roles of reactive species, heat, and UV radiation in the inactivation of bacterial cells by air plasmas at atmospheric pressure', *International Journal of Mass Spectrometry*, 233(1–3), pp. 81–86. doi: 10.1016/j.ijms.2003.11.016.

LASER COMPONENTS GmbH (2017) *Colored Glass Filter*. Available at: http://www.lasercomponents.com/de-en/product/colored-glass/ (Accessed: 29 July 2017).

Li, G. *et al.* (2008) 'Genetic effects of radio-frequency, atmospheric-pressure glow discharges with helium', *Applied Physics Letters*, 92(22), pp. 2006–2009. doi: 10.1063/1.2938692.

Li, H. P. *et al.* (2012) 'Studies on the physical characteristics of the radio-frequency atmospheric-pressure glow discharge plasmas for the genome mutation of methylosinus trichosporium', *IEEE*

Transactions on Plasma Science, 40(11 PART1), pp. 2853–2860. doi: 10.1109/TPS.2012.2213274.

Li, X. *et al.* (2001) 'A fast neutron deletion mutagenesis-based reverse genetics system for plants', *Plant Journal*, 27(3), pp. 235–242. doi: 10.1046/j.1365-313X.2001.01084.x.

Li, X. *et al.* (2015) 'Enhanced arachidonic acid production from Mortierella alpina combining atmospheric and room temperature plasma (ARTP) and diethyl sulfate treatments', *Bioresource Technology*. Elsevier Ltd, 177, pp. 134–140. doi: 10.1016/j.biortech.2014.11.051.

Li, X., Lassner, M. and Zhang, Y. (2002) 'Deleteagene: A fast neutron deletion mutagenesis-based gene knockout system for plants', *Comparative and Functional Genomics*, 3(2), pp. 158–160. doi: 10.1002/cfg.148.

Li, X. and Zhang, Y. (2002) 'Reverse genetics by fast neutron mutagenesis in higher plants', *Functional and Integrative Genomics*, 2(6), pp. 254–258. doi: 10.1007/s10142-002-0076-0.

Lim, D. K. Y. *et al.* (2015) 'Isolation of High-Lipid Tetraselmis suecica Strains Following Repeated UV-C Mutagenesis, FACS, and High-Throughput Growth Selection', *Bioenergy Research*, 8(2), pp. 750–759. doi: 10.1007/s12155-014-9553-2.

Liu, B. *et al.* (2015) 'Mutation breeding of extracellular polysaccharide-producing microalga Crypthecodinium cohnii by a novel mutagenesis with atmospheric and room temperature plasma', *International Journal of Molecular Sciences*, 16(4), pp. 8201–8212. doi: 10.3390/ijms16048201.

Liu, J. *et al.* (2016) 'Isolation and characterization of astaxanthin-hyperproducing mutants of Haematococcus pluvialis (Chlorophyceae) produced by dielectric barrier discharge plasma', *Phycologia*, 55(August), pp. 650–658. doi: 10.2216/16-14.1.

Liu, J. *et al.* (2017) 'Screening and transcriptomic analysis of Crypthecodinium cohnii mutants with high growth and lipid content using the acetyl-CoA carboxylase inhibitor sethoxydim', *Applied Microbiology and Biotechnology*. Applied Microbiology and Biotechnology, 101(15), pp. 6179–6191. doi: 10.1007/s00253-017-8397-z.

Liu, S. *et al.* (2016) 'Enhancement of lipid productivity in green microalgae Chlorella sp. via fast neutron irradiation', *Biomass and Bioenergy*, 91, pp. 196–203. doi: http://dx.doi.org/10.1016/j.biombioe.2016.05.013.

Liu, X. *et al.* (2017) 'Erythritol production by Yarrowia lipolytica mutant strain M53 generated through atmospheric and room temperature plasma mutagenesis', *Food Science and Biotechnology*. The Korean Society of Food Science and Technology, 26(4), pp. 979–986. doi: 10.1007/s10068-017-0116-0.

Longoni, P. *et al.* (2015) 'Phosphorylation of the Lhcb2 isoform of Light Harvesting Complex II is central to state transitions', *Plant Physiology*, 169(December), p. pp.01498.2015. doi: 10.1104/pp.15.01498.

López-Rosales, L. *et al.* (2016) 'Pilot-scale bubble column photobioreactor culture of a marine dinoflagellate microalga illuminated with light emission diodes', *Bioresource Technology*, 216, pp. 845–855. doi: 10.1016/j.biortech.2016.06.027.

Lorenz, R. T. and Cysewski, G. R. (2000) 'Commercial potential for Haematococcus microalgae as a natural source of astaxanthin', *Trends in Biotechnology*, 18(April), pp. 160–167.

Lu, Y. *et al.* (2011) 'Characteristics of hydrogen production of an Enterobacter aerogenes mutant generated by a new atmospheric and room temperature plasma (ARTP)', *Biochemical Engineering Journal*. Elsevier B.V., 55(1), pp. 17–22. doi: 10.1016/j.bej.2011.02.020.

Lubián, L. *et al.* (2000) 'Nannochloropsis (Eustigmatophyceae) as source of commercially valuable pigments', *Journal of Applied Phycology*, 12, pp. 249–255. doi: 10.1023/A:1008170915932.

Lubián, L. L. *et al.* (2000) 'Nannochloropsis (Eustigmatophyceae) as source of commercially valuable pigments', *Journal of Applied Phycology*, 12(3–5), pp. 249–255. doi: 10.1023/a:1008170915932.

Ma, Y. *et al.* (2016) 'Significantly enhancing recombinant alkaline amylase production in Bacillus subtilis by integration of a novel mutagenesis-screening strategy with systems-level fermentation optimization', *Journal of Biological Engineering*. Journal of Biological Engineering, 10(1), p. 13. doi: 10.1186/s13036-016-0035-2.

Ma, Y. B. *et al.* (2013) 'Increased lipid productivity and TAG content in Nannochloropsis by heavy-ion irradiation mutagenesis', *Bioresource Technology*. Elsevier Ltd, 136, pp. 360–367. doi: http://dx.doi.org/10.1016/j.biortech.2013.03.020.

Manandhar-Shrestha, K. and Hildebrand, M. (2013) 'Development of flow cytometric procedures for the efficient isolation of improved lipid accumulation mutants in a Chlorella sp. microalga', *Journal of Applied Phycology*, 25(6), pp. 1643–1651. doi: 10.1007/s10811-013-0021-8 M4 - Citavi.

Maness, P.-C. *et al.* (2009) 'Photobiological hydrogen production - prospects and challenges', *Microbe*, 4(6), pp. 275–280. doi: 10.1016/j.tibtech.2010.01.007.

Markou, G. (2014) 'Effect of various colors of light-emitting diodes (LEDs) on the biomass composition of Arthrospira platensis cultivated in semi-continuous mode', *Appl Biochem Biotechnol*. 2014/01/18, 172(5), pp. 2758–2768. doi: 10.1007/s12010-014-0727-3.

Masojidek, J. *et al.* (2013) 'Photosynthesis in Microalgae', in Richmond, A. and Hu, Q. (eds) *Handbook of Microalgal Culture.* 2nd edn. Blackwell Publishing Ltd, pp. 20–39. doi: 10.1002/9780470995280.ch2.

Masojídek, J., Koblížek, M. and Torzillo, G. (2003) 'Photosynthesis in Microalgae', in *Handbook of Microalgal Culture.* Blackwell Publishing Ltd, pp. 20–39. doi: 10.1002/9780470995280.ch2.

Masters, B. R. (2014) 'Paths to Förster's resonance energy transfer (FRET) theory', *European Physical Journal H*, 39(1), pp. 87–139. doi: 10.1140/epjh/e2013-40007-9.

Mata, T. M., Martins, A. A. and Caetano, N. S. (2010) 'Microalgae for biodiesel production and other applications: A review', *Renewable and Sustainable Energy Reviews*, 14(1), pp. 217–232. doi: http://dx.doi.org/10.1016/j.rser.2009.07.020.

Meinke, D., Sweeney, C. and Muralla, R. (2009) 'Integrating the genetic and physical maps of Arabidopsis thaliana: Identification of mapped alleles of cloned essential (EMB) genes', *PLoS ONE*, 4(10). doi: 10.1371/journal.pone.0007386.

Melih, Ş. *et al.* (2011) 'Förster Energy Transfer Theory as Reflected in the Structures of Photosynthetic Light-Harvesting Systems', *ChemPhysChem*. Wiley-Blackwell, 12(3), pp. 518–531. doi: 10.1002/cphc.201000944.

Milledge, J. J. (2011) 'Commercial application of microalgae other than as biofuels: A brief review', *Reviews in Environmental Science and Biotechnology*, 10(1), pp. 31–41. doi: 10.1007/s11157-010-9214-7.

Mizoguchi, T., Harada, J. and Tamiaki, H. (2006) 'Structural determination of dihydro- and tetrahydrogeranylgeranyl groups at the 17-propionate of bacteriochlorophylls-a', *FEBS Letters*, 580(28–29), pp. 6644–6648. doi: 10.1016/j.febslet.2006.11.020.

Mohsenpour, S. F., Richards, B. and Willoughby, N. (2012) 'Spectral conversion of light for enhanced microalgae growth rates and photosynthetic pigment production', *Bioresource Technology*. Elsevier Ltd, 125, pp. 75–81. doi: 10.1016/j.biortech.2012.08.072.

Morfill, G. E., Kong, M. G. and Zimmermann, J. L. (2009) 'Focus on plasma medicine', *New Journal of Physics*, 11. doi: 10.1088/1367-2630/11/11/115011.

Muñoz, R. and Guieysse, B. (2006) 'Algal-bacterial processes for the treatment of hazardous contaminants: A review', *Water Research*, 40(15), pp. 2799–2815. doi: 10.1016/j.watres.2006.06.011.

NASA (2014) *The Electromagnetic Spectrum*. Available at: https://imagine.gsfc.nasa.gov/science/toolbox/emspectrum1.html (Accessed: 11 June 2017).

Netravali, A. N. and Chabba, S. (2003) 'Composites get greener', *Materials Today*, 9(7–8), p. 13. doi: 10.1016/S1369-7021(06)71564-4.

Newton, J., Tyler, D. and Slodki, M. (1979) 'Effect of Ultraviolet-B (280-320nm) radiation on blue-green algae (cyanobacteria), possible biological indicators of stratospheric ozone depletion', *Applied and Environmental Microbiology*, 37(6), pp. 1137–1141.

Ohashi, S. *et al.* (2010) 'An overview on chlorophylls and quinones in the photosystem I-type reaction centers', *Photosynthesis Research*, 104(2), pp. 305–319. doi: 10.1007/s11120-010-9530-3.

Okumura, C. *et al.* (2015) 'Economic efficiency of different light wavelengths and intensities using LEDs for the cultivation of green microalga Botryococcus braunii (NIES-836) for biofuel production', *Environmental Progress & Sustainable Energy*, 34(1), pp. 269–275. doi: 10.1002/ep.11951.

Oldroyd, G. E. D. and Long, S. R. (2003) 'Identification and Characterization of Nodulation- Signaling Pathway 2 , a Gene of Medicago truncatula Involved in Nod Factor Signaling', *Plant Physiology*, 131(March), pp. 1027–1032. doi: 10.1104/pp.102.010710.ence.

Ooms, M. D. *et al.* (2017) 'Light dilution via wavelength management for efficient high-density photobioreactors', *Biotechnology and Bioengineering*, 114(6), pp. 1160–1169. doi: 10.1002/bit.26261.

Palmieri, M. C., Garcia, O. and Melnikov, P. (2000) 'Neodymium biosorption from acidic solutions in batch system', *Process Biochemistry*, 36(5), pp. 441–444. doi: 10.1016/S0032-9592(00)00236-3.

Peiffer, S. and Pecher, K. (1997) *Experimentelle Aquatische Chemie*. Spektrum Akademischer Verlag, Heidelberg, Berlin.

Phytoplankton Pigments: Characterization, Chemotaxonomy and Applications in Oceanography (2011) *Cambridge Environmental Chemistry Series*. Cambridge: Cambridge University Press. doi: 10.1017/CBO9780511732263.

Pilon, L., Berberoĝlu, H. and Kandilian, R. (2011) 'Radiation transfer in photobiological carbon dioxide fixation and fuel production by microalgae', *Journal of Quantitative Spectroscopy and Radiative Transfer*, 112(17), pp. 2639–2660. doi: 10.1016/j.jqsrt.2011.07.004.

Posten, C. and Walter, C. (2013) *Microalgal Biotechnology: Potential and Production*. De Gruyter. Available at: https://books.google.de/books?id=vtx8R2MFD3kC.

Prasanna, R. *et al.* (2009) 'Cyanobacterial diversity in the rhizosphere of rice and its ecological significance', *Indian Journal of Microbiology*, 49(1), pp. 89–97. doi: 10.1007/s12088-009-0009-x.

Ra, C. H. *et al.* (2016) 'Effects of light-emitting diodes (LEDs) on the accumulation of lipid content using a two-phase culture process with three microalgae', *Bioresource Technology*. Elsevier Ltd, 212, pp. 254–261. doi: 10.1016/j.biortech.2016.04.059.

Raheem, A. *et al.* (2018) 'A review on sustainable microalgae based biofuel and bioenergy production: recent developments', *Journal of Cleaner Production*. Elsevier Ltd. doi: 10.1016/j.jclepro.2018.01.125.

Raven, P. H. *et al.* (2013) 'Photosynthesis', in *Biology*. 6th edn. McGraw-Hill, Boston, MA, pp. 183–204.

Relyon Plasma GmbH (2017) *piezobrush PZ2*. Available at: https://www.relyon-plasma.com/relyon-plasma-produkte/piezobrush-pz2/piezobrush-pz2-i/ (Accessed: 9 August 2017).

Ren, F., Chen, L. and Tong, Q. (2017) 'Highly improved acarbose production of Actinomyces through the combination of ARTP and penicillin susceptible mutant screening', *World Journal of Microbiology and Biotechnology*. Springer Netherlands, 33(1). doi: 10.1007/s11274-016-2156-7.

Rendón, S. M., Roldan, G. J. C. and Voroney, R. P. (2013) 'Effect of Carbon Dioxide Concentration on the Growth Response of Chlorella vulgaris Under Four Different Led Illumination', *International Journal of Biotechnology for Wellness Industries*, 2(3), pp. 125–131.

Sánchez Mirón, A. *et al.* (2003) 'Shear stress tolerance and biochemical characterization of Phaeodactylum tricornutum in quasi steady-state continuous culture in outdoor photobioreactors', *Biochemical Engineering Journal*, 16(3), pp. 287–297. doi: 10.1016/S1369-703X(03)00072-X.

Sato, M. *et al.* (2004) 'A simple and rapid dual-fluorescence viability assay for microalgae', *Microbiol Cult Coll*, 20(2), pp. 53–59. Available at: http://www.jscc-home.jp/journal/No20_2/No20_2_53.pdf.

Satyanarayana, K. G., Mariano, A. B. and Vargas, J. V. C. (2010) 'A review on microalgae, a versatile source for sustainable energy and materials', *International journal of energy research*, 35(August 2007), pp. 291–311. doi: 10.1002/er.1695.

Schneider, J. C. *et al.* (1995) 'A mutant of Nannochloropsis deficient in eicosapentaenoic acid production', *Phytochemistry*, 40(3), pp. 807–814. doi: https://doi.org/10.1016/0031-9422(95)00365-E.

Schulze, P. S. C. *et al.* (2014) 'Light emitting diodes (LEDs) applied to microalgal production', *Trends in Biotechnology*, 32(8), pp. 422–430. doi: 10.1016/j.tibtech.2014.06.001.

Schumann (2013) *Photometrische Bestimmung von Phosphat, Biologische Station Zingst, Universität Rostock.* Available at: https://www.bsz.uni-rostock.de/fileadmin/uni-rostock/Alle_MNF/Bio_Zingt/Dokumente/Lehrmaterial/An_Phosp.pdf (Accessed: 19 November 2015).

Sforza, E. *et al.* (2012) 'Adjusted Light and Dark Cycles Can Optimize Photosynthetic Efficiency in Algae Growing in Photobioreactors', *Plos One*, 7(6), p. e38975. doi: 10.1371/journal.pone.0038975.

Sharma, K., Li, Y. and Schenk, P. M. (2014) 'UV-C-mediated lipid induction and settling, a step change towards economical microalgal biodiesel production', *Green Chem.*, 16(7), pp. 3539–3548. doi: 10.1039/C4GC00552J.

Shuba, E. S. and Kifle, D. (2018) 'Microalgae to biofuels: "Promising" alternative and renewable energy, review', *Renewable and Sustainable Energy Reviews*, 81(August 2017), pp. 743–755. doi: 10.1016/j.rser.2017.08.042.

Singh, P. K. (1975) 'Photoreactivation of UV-irradiated blue-green algae and algal virus LPP-1', *Archives of Microbiology*, 103(3), pp. 297–302. doi: 10.1007/BF00436364.

Sivaramakrishnan, R. and Incharoensakdi, A. (2017) 'Enhancement of lipid production in Scenedesmus sp. by UV mutagenesis and hydrogen peroxide treatment', *Bioresource Technology*. Elsevier Ltd, 235, pp. 366–370. doi: 10.1016/j.biortech.2017.03.102.

Spolaore, P. *et al.* (2006) 'Commercial applications of microalgae', *Journal of Bioscience and Bioengineering*, 101(2), pp. 87–96. doi: 10.1263/jbb.101.87.

Stern, D. P. (2006) *Sunlight and the Earth, Sunlight and the Earth*. Available at: http://www-spof.gsfc.nasa.gov/stargaze/Sun1lite.htm (Accessed: 10 June 2017).

Taiz, L. and Zeiger, E. (2010) *Plant Physiology, Annals of Botany*. doi: 10.1104/pp.900074.

Tan, Y. *et al.* (2015) 'Culture characteristics of the atmospheric and room temperature plasma-mutated Spirulina platensis mutants in CO2 aeration culture system for biomass production', *Journal of Bioscience and Bioengineering*. Elsevier Ltd, 120(4), pp. 438–443. doi: 10.1016/j.jbiosc.2015.02.012.

Valverde, J. and This, H. (2008) '1 H NMR Quantitative Determination of Photosynthetic Pigments from Green Beans (Phaseolus vulgaris L.)', *Journal of Agricultural and Food Chemistry*, 56(2), pp. 314–320. doi: 10.1021/jf070277j.

Vaulot, D. *et al.* (2008) 'The diversity of small eukaryotic phytoplankton (≤3 μm) in marine ecosystems', *FEMS Microbiology Reviews*, 32(5), pp. 795–820. doi: 10.1111/j.1574-6976.2008.00121.x.

Wang, B. *et al.* (2008) 'CO2 bio-mitigation using microalgae', *Applied Microbiology and Biotechnology*, 79(5), pp. 707–718. doi: 10.1007/s00253-008-1518-y.

Wang, J. S. *et al.* (2015) 'Generation of peanut mutants by fast neutron irradiation combined with in vitro culture', *J Radiat Res*. 2015/02/06, 56(3), pp. 437–445. doi: 10.1093/jrr/rru121.

Wang, Q. *et al.* (2017) 'Enhancing carotenoid production in Rhodotorula mucilaginosa KC8 by combining mutation and metabolic engineering', *Annals of Microbiology*. Annals of Microbiology, 67(6), pp. 425–431. doi: 10.1007/s13213-017-1274-2.

Wang, X. *et al.* (2014) 'The atmospheric and room-temperature plasma (ARTP) method on the dextranase activity and structure', *International Journal of Biological Macromolecules*. Elsevier B.V., 70, pp. 284–291. doi: 10.1016/j.ijbiomac.2014.07.006.

Von Wettstein, D., Gough, S. and Kannangara, C. G. (2010) 'Chlorophyll Biosynthesis.', *The Plant cell*, 285(7), pp. 8268–8277. doi: 10.1105/tpc.7.7.1039.

White, S., Anandraj, A. and Bux, F. (2011) 'PAM fluorometry as a tool to assess microalgal nutrient stress and monitor cellular neutral lipids', *Bioresource Technology*. Elsevier Ltd, 102(2), pp. 1675–1682. doi: 10.1016/j.biortech.2010.09.097.

Wu, J. *et al.* (2005) 'Chemical- and irradiation-induced mutants of indica rice IR64 for forward and reverse genetics', *Plant Molecular Biology*, 59, pp. 85–97. doi: 10.1007/s11103-004-5112-0.

Wunder, T. *et al.* (2013) 'The major thylakoid protein kinases STN7 and STN8 revisited: effects of altered STN8 levels and regulatory specificities of the STN kinases', *Frontiers in Plant Science*, 4(October), pp. 1–15. doi: 10.3389/fpls.2013.00417.

Xu, B. *et al.* (2013) 'The effect of varying LED light sources and influent carbon/nitrogen ratios on treatment of synthetic sanitary sewage using Chlorella vulgaris', *World Journal of Microbiology & Biotechnology*, 29(7), pp. 1289–1300. doi: 10.1007/s11274-013-1292-6.

Yan, C. *et al.* (2013) 'Effects of various LED light wavelengths and light intensity supply strategies on synthetic high-strength wastewater purification by Chlorella vulgaris', *Biodegradation*, 24(5), pp. 721–

732. doi: 10.1007/s10532-013-9620-y.

Zayadan, B. K. *et al.* (2014) 'Isolation, mutagenesis, and optimization of cultivation conditions of microalgal strains for biodiesel production', *Russian Journal of Plant Physiology*, 61(1), pp. 124–130. doi: 10.1134/s102144371401018x.

Zeng, W. *et al.* (2015) 'A high-throughput screening procedure for enhancing α-ketoglutaric acid production in Yarrowia lipolytica by random mutagenesis', *Process Biochemistry*, 50(10), pp. 1516–1522. doi: https://doi.org/10.1016/j.procbio.2015.06.011.

Zetsche, E.-M. and Meysman, F. J. R. (2012) 'Dead or alive? Viability assessment of micro- and mesoplankton', *Journal of Plankton Research*, 34(6), pp. 493–509. doi: 10.1093/plankt/fbs018.

Zhang, L. *et al.* (2006) 'Rpr1, a gene required for Rpg1-dependent resistance to stem rust in barley', *Theoretical and Applied Genetics*, 113(5), pp. 847–855. doi: 10.1007/s00122-006-0342-y.

Zhang, X. *et al.* (2014) 'Atmospheric and room temperature plasma (ARTP) as a new powerful mutagenesis tool', *Applied Microbiology and Biotechnology*, 98(12), pp. 5387–5396. doi: 10.1007/s00253-014-5755-y.

Zhu, X. G., Long, S. P. and Ort, D. R. (2008) 'What is the maximum efficiency with which photosynthesis can convert solar energy into biomass?', *Current Opinion in Biotechnology*, 19(2), pp. 153–159. doi: 10.1016/j.copbio.2008.02.004.

V. Appendix 1

Table 30: OD$^{PR}_{750\,nm}$ values of stage 1-2 light color experiment. Values with subtracted blank-value and multiplied with dilution factor. Cultivation at constant illumination with colored LEDs (white SSW, blue 425 nm, green 510 nm and red 680 nm) at 150 µmol m^{-2} s^{-1} and 1.8 nL h^{-1} aeration with 1% (v/v) CO$_2$ enriched air, 120 rpm and 25°C. Experiments done in triplicate.

Strain	color	0.00 d	0.84 d	1.76 d	4.07 d	5.02 d	6.87 d	7.89 d	8.77 d	9.91 d	10.82 d	13.70 d	17.01 d
Dunaliella sp.													
	blue	0.0037	0.0037	0.0087	0.0483	0.1343	0.2978	0.3621	0.4158	0.4690	0.5030	0.7088	0.6788
		0.0037	0.0032	0.0047	0.0488	0.1318	0.2998	0.3336	0.3658	0.4450	0.4890	0.6238	0.6513
		0.0037	0.0052	0.0067	0.0553	0.1428	0.2978	0.3493	0.3842	0.4390	0.4810	0.6338	0.6138
	green	0.0037	0.0057	0.0052	0.0168	0.0343	0.1468	0.2136	0.3158	0.4250	0.4810	0.8588	1.0813
		0.0037	0.0013	0.0032	0.0143	0.0323	0.1483	0.2436	0.3575	0.4670	0.6370	0.9713	1.2913
		0.0037	0.0042	0.0082	0.0208	0.0353	0.1728	0.2536	0.3525	0.5330	0.6450	0.9613	1.2913
	red	0.0037	0.0052	0.0062	0.0438	0.1303	0.3308	0.4421	0.4942	0.5970	0.6090	0.8963	0.9513
		0.0037	0.0047	0.0042	0.0418	0.1203	0.3478	0.4307	0.5075	0.5910	0.6410	0.8613	0.9538
		0.0037	0.0057	0.0072	0.0443	0.1208	0.3673	0.4521	0.5142	0.6170	0.6610	0.8838	1.0238
	white	0.0037	0.0052	0.0047	0.0278	0.0783	0.3078	0.4179	0.5325	0.6630	0.5030	1.1188	1.2538
		0.0037	0.0062	0.0062	0.0318	0.0853	0.3018	0.4079	0.5125	0.6510	0.7750	1.0513	1.3313
		0.0037	0.0052	0.0062	0.0263	0.0673	0.2778	0.3693	0.4508	0.6110	0.6830	0.9938	1.1463
Picochlorum sp.													
	blue	0.0023	0.0023	0.0038	0.0158	0.0293	0.1368	0.2450	0.3908	0.5490	0.5870	0.6988	0.7288
		0.0023	0.0053	0.0028	0.0138	0.0263	0.1318	0.2464	0.3808	0.5410	0.5990	0.7188	0.7188
		0.0023	0.0048	0.0028	0.0168	0.0318	0.1723	0.3079	0.4275	0.5870	0.6430	0.6913	0.6988
	green	0.0023	0.0000	0.0008	0.0058	0.0123	0.0783	0.1964	0.3275	0.6310	0.8470	0.9888	0.9938
		0.0023	0.0033	0.0023	0.0123	0.0148	0.0858	0.2093	0.3692	0.6750	0.8990	0.9588	0.9663
		0.0023	0.0023	0.0018	0.0073	0.0158	0.0398	0.0964	0.2092	0.4510	0.7170	0.9413	0.9488
	red	0.0023	0.0023	0.0063	0.0173	0.0443	0.3203	0.6279	0.7942	0.8810	0.8230	1.0138	1.0113
		0.0023	0.0003	0.0013	0.0173	0.0533	0.3763	0.7107	0.8242	0.9110	0.9670	1.0563	1.0938
		0.0023	0.0018	0.0013	0.0123	0.0318	0.2688	0.5464	0.7492	0.8490	0.9310	0.9913	1.0138
	white	0.0023	0.0018	0.0018	0.0098	0.0238	0.1783	0.4179	0.6875	0.9450	0.8810	0.9688	1.0163
		0.0023	0.0013	0.0018	0.0108	0.0293	0.2233	0.4907	0.7708	0.9450	0.9070	0.9738	0.9513
		0.0023	0.0008	0.0013	0.0093	0.0288	0.2068	0.4707	0.7292	0.9210	0.9470	0.9313	0.9838
M. salina													
	blue	0.0071	0.0030	0.0015	0.0075	0.0075	0.0175	0.0514	0.0567	0.0580	0.0560	0.0850	0.0625
		0.0071	0.0050	0.0040	0.0100	0.0125	0.0510	0.0657	0.0617	0.0640	0.0580	0.0650	0.0625
		0.0071	0.0020	0.0010	0.0035	0.0040	0.0295	0.0400	0.0467	0.0460	0.0520	0.0550	0.0525
	green	0.0071	0.0035	0.0035	0.0135	0.0330	0.1220	0.2500	0.3950	0.5940	0.6740	0.8150	0.8875
		0.0071	0.0035	0.0040	0.0260	0.0335	0.0810	0.1743	0.2683	0.4020	0.4640	0.5400	0.5325
		0.0071	0.0035	0.0005	0.0115	0.0295	0.1365	0.2571	0.3850	0.4360	0.4520	0.4675	0.4825
	red	0.0071	0.0015	0.0040	0.0250	0.0425	0.1330	0.2686	0.3833	0.5400	0.5660	0.7550	0.7725
		0.0071	0.0040	0.0035	0.0155	0.0550	0.2755	0.4129	0.4967	0.5540	0.5400	0.6025	0.5700
		0.0071	0.0040	0.0035	0.0165	0.0315	0.2395	0.4071	0.4617	0.5020	0.5160	0.5300	0.5175
	white	0.0071	0.0060	0.0035	0.0200	0.0405	0.2265	0.4757	0.6383	0.7540	0.7260	0.8150	0.8100
		0.0071	0.0050	0.0040	0.0180	0.0455	0.2330	0.4543	0.5517	0.5980	0.5960	0.6300	0.6150
		0.0071	0.0045	0.0035	0.0185	0.0450	0.2390	0.3643	0.3783	0.3820	0.3740	0.3775	0.4050

VI. Appendix 2: Pigment standards

Table 31: List of all used pigment standards

| Name	Semi-systematic name	Formula	Molecular weight (g mol^{-1})	manufacturer
Neoxanthin	(9'Z,3S,5R,6R,3'S,5'R,6'S)-5',6'-Epoxy-6,7-didehydro-5,6,5',6'-tetrahydro-β,β-carotene-3,5,3'-triol	$C_{40}H_{56}O_4$	600.89	Carote*Nature* GmbH, Ostermundigen, Switzerland
Violaxanthin	(3S,5R,6S,3'S,5'R,6'S)-5,6,5',6'-Diepoxy-5,6,5',6'-tetrahydro-β,β-carotene-3,3'-diol	$C_{40}H_{56}O_4$	600.89	Carote*Nature* GmbH, Ostermundigen, Switzerland
(rac./meso)-Astaxanthin	(3RS,3'RS)-3,3'-Dihydroxy-β,β-carotene-4,4'-dione	$C_{40}H_{52}O_4$	596.86	Carote*Nature* GmbH, Ostermundigen, Switzerland
Zeaxanthin	(3R,3'R)-β,β-Carotene-3,3'-diol	$C_{40}H_{56}O_2$	568.89	Carote*Nature* GmbH, Ostermundigen, Switzerland
Lutein	(3R,3'R,6'R)-β,ε-Carotene-3,3'-diol	$C_{40}H_{56}O_2$	568.89	Carote*Nature* GmbH, Ostermundigen, Switzerland
Cantaxanthin	β,β-Carotene-4,4'dione	$C_{40}H_{52}O_2$	564.86	Carote*Nature* GmbH, Ostermundigen, Switzerland
Chlorophyll *b*		$C_{55}H_{70}MgN_4O_6$	900.47	Sigma-Aldrich Chemie GmbH Munich, Germany
Chlorophyll *a*		$C_{55}H_{72}MgN_4O_5$	893.49	Sigma-Aldrich Chemie GmbH Munich, Germany
γ-Carotene	β, ψ-Carotene	$C_{40}H_{56}$	536.89	Carote*Nature* GmbH, Ostermundigen, Switzerland
β-Carotene	β,β-Carotene	$C_{40}H_{56}$	536.89	Carote*Nature* GmbH, Ostermundigen, Switzerland

VII.   Appendix 3: HPLC-MS Data
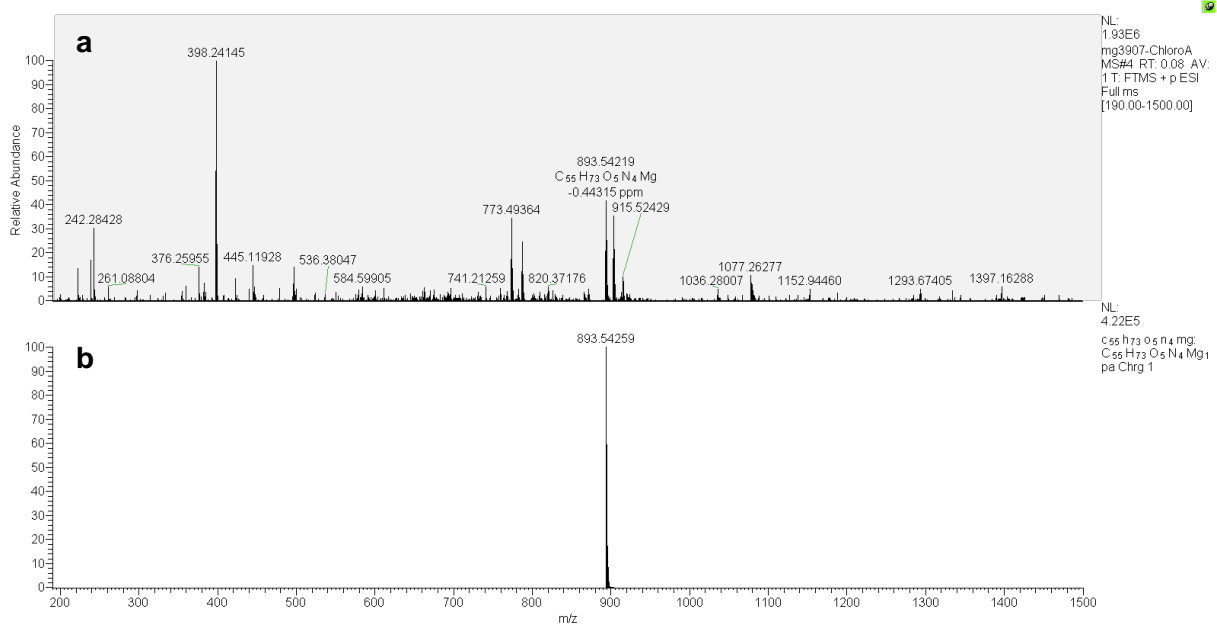
Figure 58: High resolution MS Full scan of Chl *a* in positive mode. a) MS-data relative abundance over m/z distribution. b) Simulated mass distribution of $C_{55}H_{73}O_5N_4Mg$
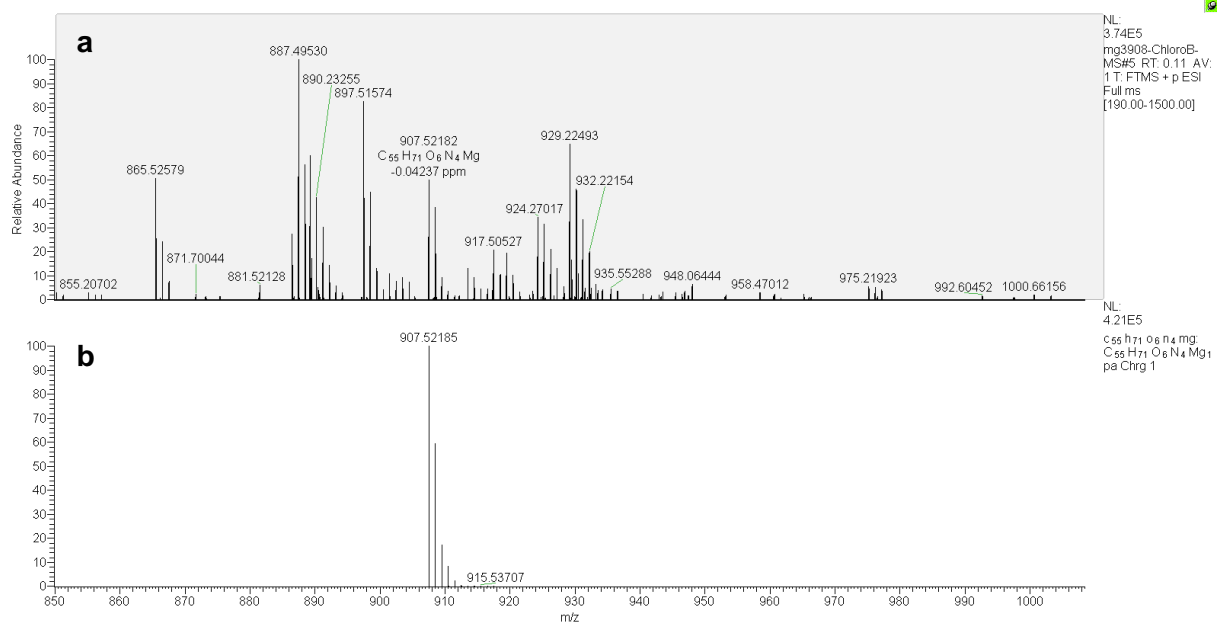

Figure 59: High resolution MS Full scan of Chl *b* (including U5) in positive mode. a) MS-data relative abundance over m/z distribution. b) Simulated mass distribution of $C_{55}H_{71}O_6N_4Mg$
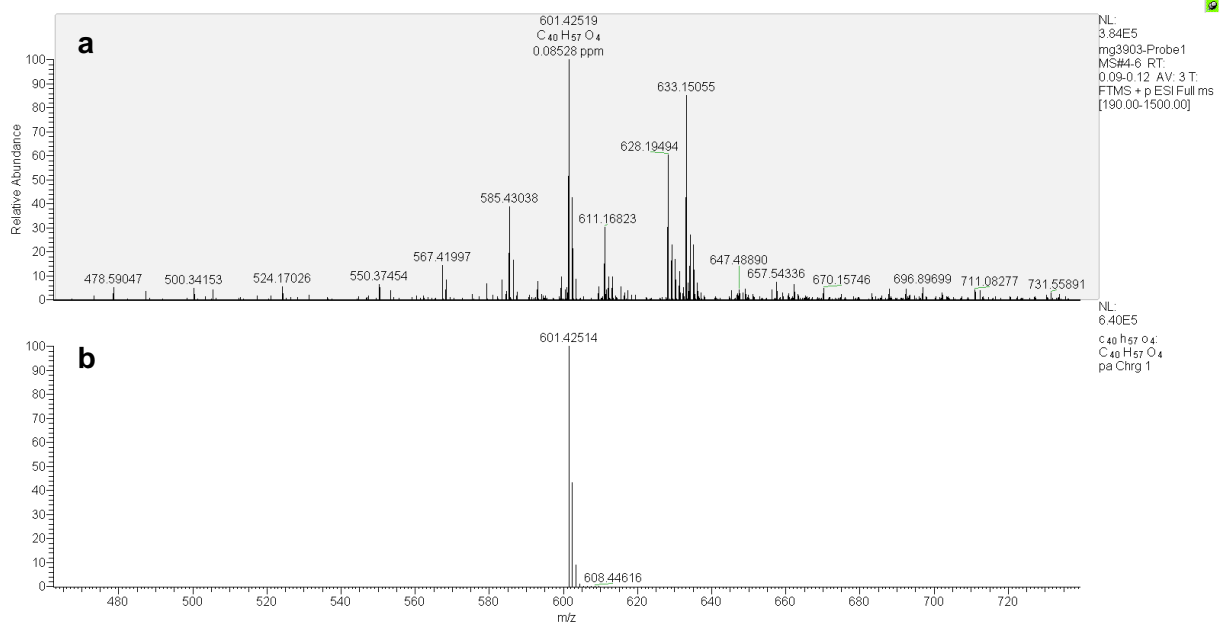
Figure 60: High resolution MS Full scan of U1 in positive mode. a) MS-data relative abundance over m/z distribution. b) Simulated mass distribution of $C_{40}H_{57}O_4$
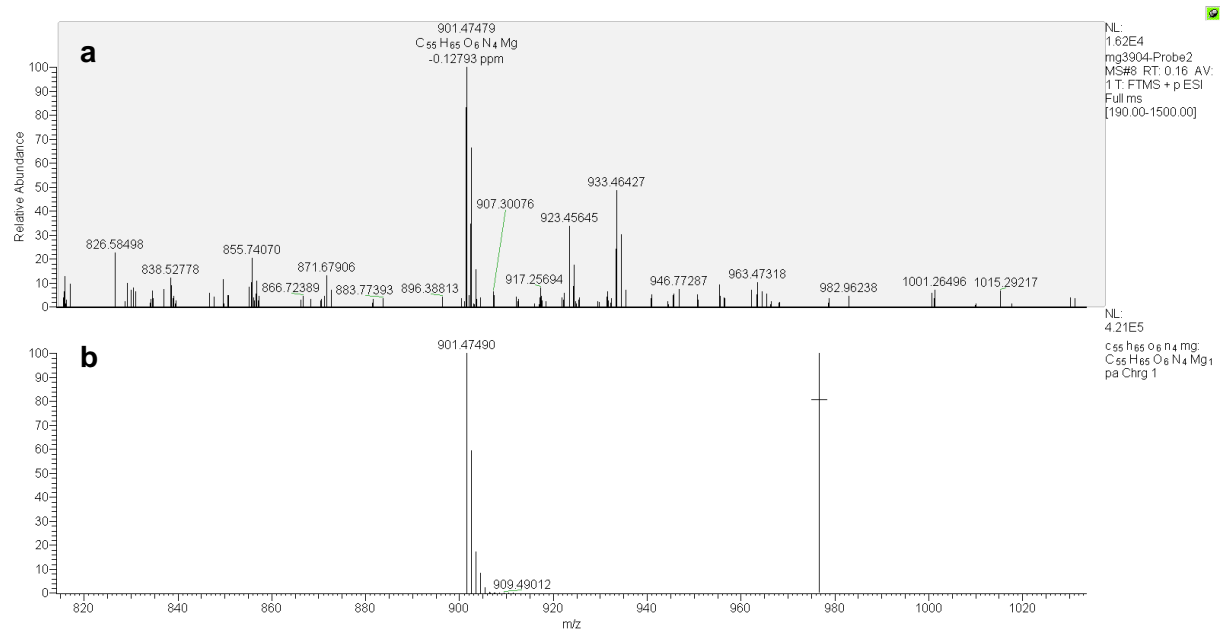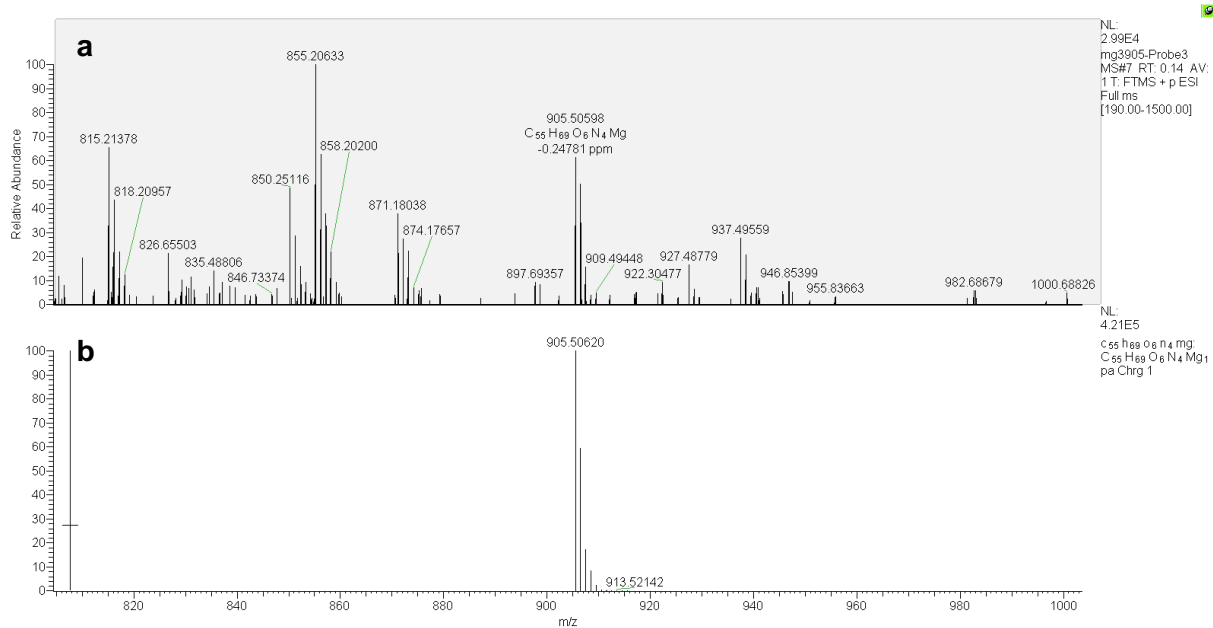

Figure 61: High resolution MS Full scan of unknown pigment U2 in positive mode. a) MS-data relative abundance over m/z distribution. b) Simulated mass distribution of $C_{55}H_{65}O_6N_4Mg$

Figure 62: High resolution MS Full scan of unknown pigment U3 in positive mode. a) MS-data relative abundance over m/z distribution. b) Simulated mass distribution of $C_{55}H_{69}O_6N_4Mg$
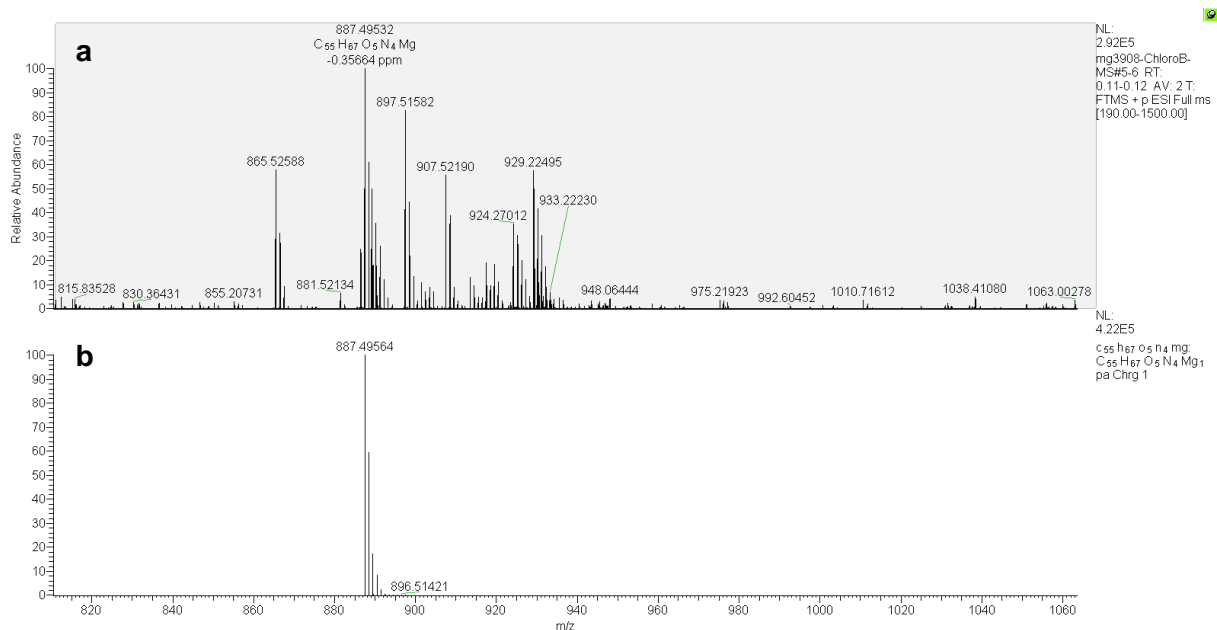

Figure 63: High resolution MS Full scan of unknown pigment U5 contained in Chl *b* in positive mode. a) MS-data relative abundance over m/z distribution. b) Simulated mass distribution of $C_{55}H_{67}O_5N_4Mg$
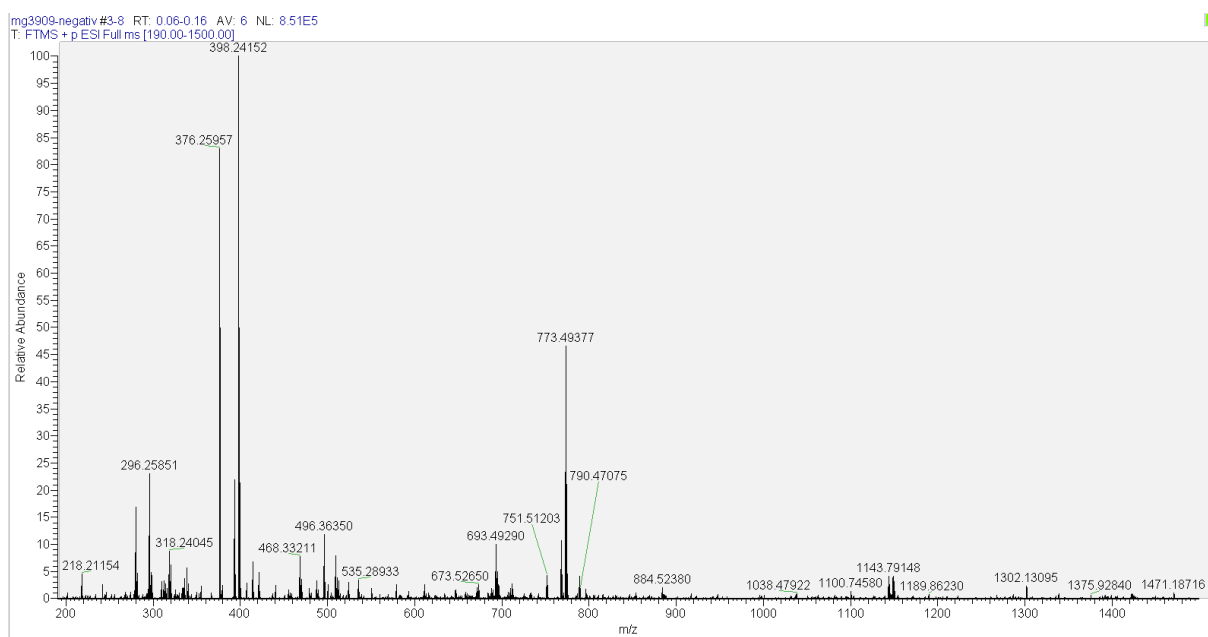
Figure 64: High resolution MS Full scan of background residues of the column in positive mode.